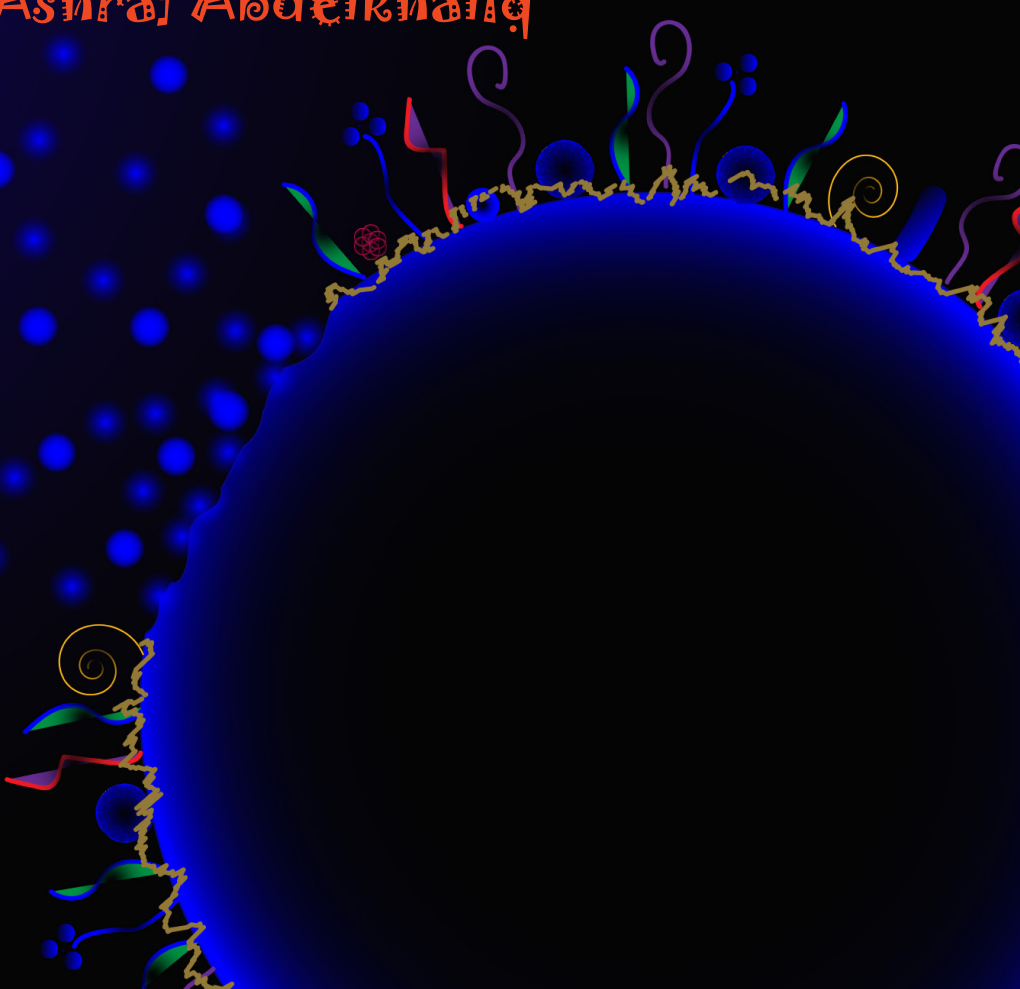




In vitro testing
strategies for hazard
assessment of
nanoparticles

Ashraf Abdelkhalig



Propositions

1. Combining toxicological *in vitro* models with advanced analytical techniques provides a competent approach for the hazard characterization of nanoparticles.
(this thesis)
2. The *de novo* silver nanoparticles formed intracellularly contribute substantially to internal nanoparticle exposure levels.
(this thesis)
3. The powers of artificial intelligence and supercomputers are revolutionizing and enabling outstanding discoveries in different scientific fields.
4. Robogamis are expanding the capabilities of current robotics beyond imagination.
5. Revolutions are planned by the smart, done by the brave and won by the cravens.
(based on the Egyptian novel "*Adrift from the Nile*" by Naguib Mahfouz)
6. Refusing to be vaccinated and sharing the world with little kids is irresponsible.

Propositions belonging to the thesis, entitled:

In vitro testing strategies for hazard assessment of nanoparticles

Ashraf Abdelkhalik

Wageningen, 9th June 2020

***In vitro* testing strategies for hazard
assessment of nanoparticles**

Ashraf Abdelkhalig

Thesis committee

Promotor

Prof. Dr. I.M.C.M. Rietjens
Professor of Toxicology
Wageningen University & Research

Co-promotors

Dr. H. Bouwmeester
Associate Professor of Toxicology
Wageningen University & Research

Dr. M. van der Zande
Scientist
Wageningen Food Safety Research

Other members

Prof. Dr. HJ Wichers, Wageningen University & Research

Prof. Dr. F.R. Cassee, National Institute of Public Health and the Environment (RIVM),
Bilthoven and Utrecht University

Dr. A. Salvati, University of Groningen

Dr. H.A. Leslie, Vrije Universiteit Amsterdam

This research was conducted under the auspices of the Graduate School VLAG (Advanced studies in Food Technology, Agrobiotechnology, Nutrition and Health Sciences).

***In vitro* testing strategies for hazard
assessment of nanoparticles**

Ashraf Abdelkhaliq

Thesis

submitted in fulfilment of the requirements for the degree of doctor
at Wageningen University
by the authority of the Rector Magnificus
Prof. Dr. A.P.J. Mol,
in the presence of the
Thesis Committee appointed by the Academic Board
to be defended in public
on Tuesday 9th June 2020
at 11 a.m. in the Aula.

Ashraf Abdelkhaliq

In vitro testing strategies for hazard assessment of nanoparticles, 218 pages.

PhD thesis, Wageningen University, Wageningen, The Netherlands (2020)

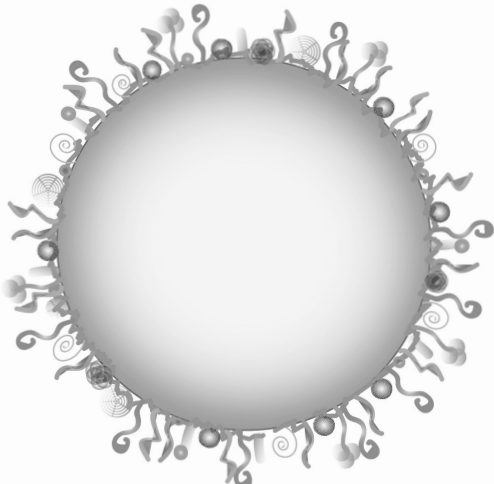
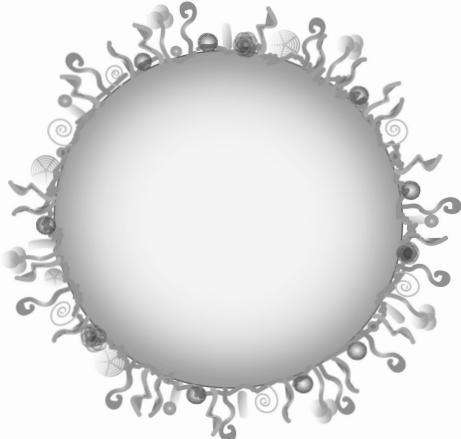
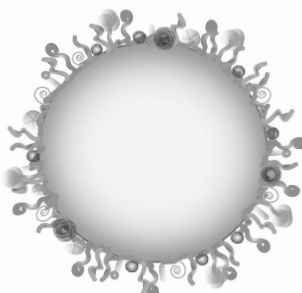
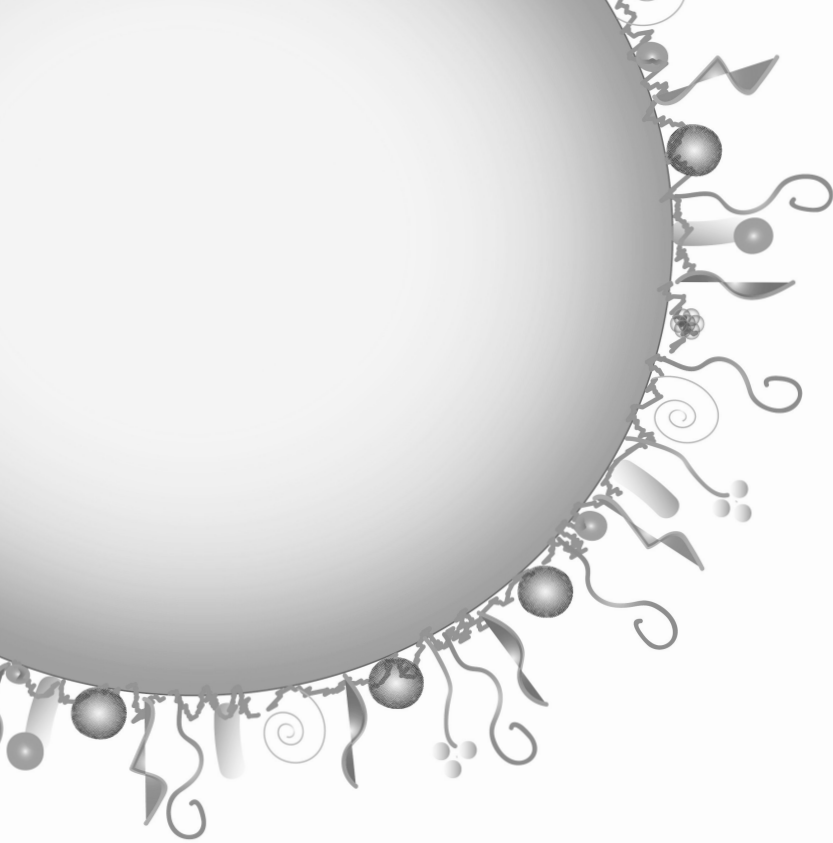
With references, with summary in English

ISBN: 978-94-6395-390-0

DOI: <https://doi.org/10.18174/520489>

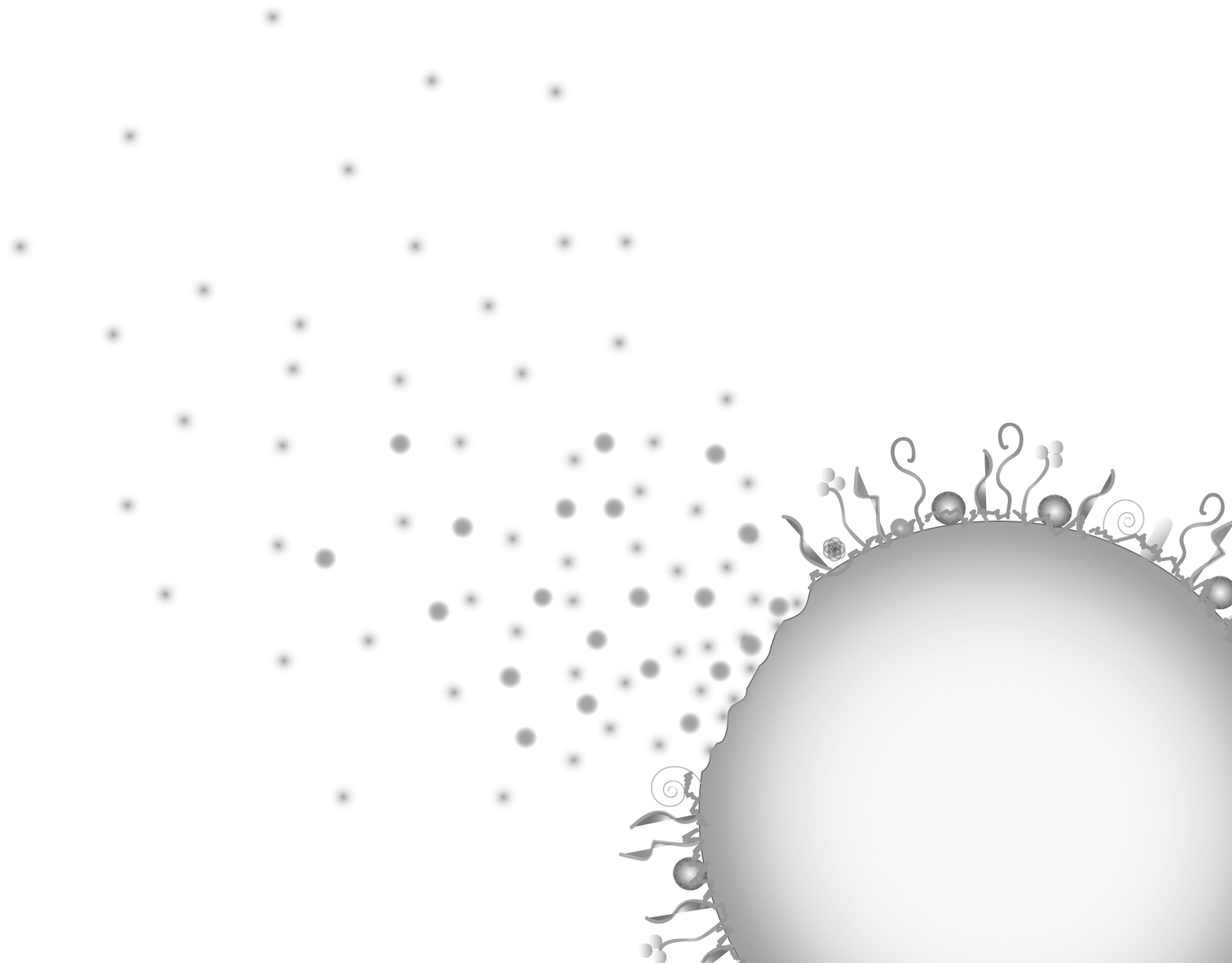
Table of contents

Chapter 1	General introduction	7
Chapter 2	Impact of nanoparticle surface functionalization on the protein corona and cellular adhesion, uptake and transport	43
Chapter 3	Impact of <i>in vitro</i> digestion on gastrointestinal fate and uptake of silver nanoparticles with different surface modifications	73
Chapter 4	Combination of the BeWo b30 placental transport model and the embryonic stem cell test to assess the potential developmental toxicity of silver nanoparticles	107
Chapter 5	Induction of γ -H ₂ AX lesions and cytotoxicity in HepG2 cells by silver nanoparticles.	145
Chapter 6	General discussion, future perspectives and overall conclusions	173
Chapter 7	Summary	201
Appendices		209
	Acknowledgments	211
	About the author	215
	List of publications	216
	Overview of completed training activities	217



1

General Introduction





NANOTECHNOLOGY AND NANOMATERIALS: DEFINITIONS

Nanotechnology is an emerging technology that rapidly evolved in the past decades. It includes the synthesis, production and utilization of materials, devices and systems in the nanometre range (Prajitha *et al.* 2019; Benelmekki 2015; Vance *et al.* 2015; Bouwmeester *et al.* 2009). Manipulations and size reductions of materials into the nano-scale (10^{-9} m), created materials with novel physicochemical properties that are called nanomaterials which are further developed into new and diverse applications (Benelmekki 2015; Chaudhry *et al.* 2008). **Nanomaterials (NMs)** are defined as “*a natural, incidental or manufactured material containing particles, in an unbound or aggregate or agglomerate state and where, for 50% or more of the particles in the number size distribution, one or more external dimensions is in the size range of 1 nm to 100 nm*” (EU 1169/2011). The particles in a nanomaterial with one or more external dimensions in the size range of 1 nm to 100 nm are referred to as **nanoparticles (NPs)**. The implementation of these definitions into practice remains challenging where competent analytical and detection methods are required to identify and quantify the NMs and NPs (Rasmussen *et al.* 2019; Boverhof *et al.* 2015; Bleeker *et al.* 2013).

SAFETY CONSIDERATIONS OF NPS

It is most likely that most human exposure to NPs results from unintentional exposure. A common route of human exposure to NPs is the presence of the NPs in the food production chain (Jeevanandam *et al.* 2018). For example, the study of Gatti *et al.* in which 86 wheat breads and 49 wheat biscuits from 14 different countries were analysed, revealed that 40% of the samples analysed contained micro- and nanoparticulate contaminants of several elements including silver (Gatti *et al.* 2008). Besides, there is an increasing number of commercially available products that contain NPs intentionally *e.g.* clothing, textiles, cosmetics, electronics and food packaging which adds up to the total human exposure to NPs (Bouwmeester *et al.* 2014; Durán and Marcato 2013; Chaudhry *et al.* 2008). In food related applications, NPs like Ag, zinc oxide (ZnO) and magnesium oxide (MnO) NPs are used in packaging materials because of their antimicrobial properties (Cao *et al.* 2016; Chaudhry *et al.* 2008). While titanium dioxide (TiO₂) and silica (SiO₂) NPs, registered food additives in the EU under E numbers E171 and E551, respectively, are used as colorants, thickeners, anticaking agents and carriers for

fragrances and flavours (Peters *et al.* 2020; McClements and Xiao 2017; Higashisaka *et al.* 2015).

The utilization and inclusion of NPs in different products and applications that are used daily by the consumers have increased the concerns over the safety of the NPs and their potential to induce adverse health effects (Boverhof *et al.* 2015; Drake and Hazelwood 2005; Oberdörster *et al.* 2005). Consequently, an increased number of studies and projects have commenced to study and identify the potential hazards associated with the use of NPs which became later on the core focus of the emerging field of nanotoxicology (Oberdörster 2010; Buzea *et al.* 2007).

APPROACHES TO CHARACTERIZE NPS IN TOXICOLOGICAL STUDIES

Soon it was realized that toxicological studies with NPs require a stringent characterization of the NPs that are used in the experiments. This implies a sound characterization of the NPs and consideration of this characterization in terms of the observed effects on cells and organisms. Given the diversity of NPs' properties that could be considered, several analytical techniques have been explored and developed for this purpose (López-Serrano *et al.* 2014). The suitability of different analytical approaches has been extensively studied and reviewed elsewhere (Abdolahpur Monikh *et al.* 2019a; Mattarozzi *et al.* 2017). The analytical techniques that have been used for the work described in this thesis are described briefly hereafter.

Dynamic light scattering (DLS)

DLS was developed decades ago and many DLS instruments are widely available and used nowadays for particle size and size distribution measurements as a function of light scattered by the NPs in homogeneously dispersed suspensions (Langevin *et al.* 2018; Ramos 2017). The polydispersity index (PDI) is an important output from the DLS measurement which characterizes the width of the NPs size range. The size of the NPs measured by DLS does not represent the size of the NPs core, it represents what is called the *hydrodynamic size* which reflects the size of the NPs including the core, as well as other molecules surrounding the core and that move with it (Babick 2020; Ramos 2017).

DLS seems to be a versatile method, but if it is used to measure the sizes of NPs in a suspension it must be carefully performed. Notably, applying DLS to NPs in biological media that contain complex ingredients like proteins or the presence of NPs aggregates/agglomerates in a suspension can create a measurement bias in terms of reported size distributions of the NPs. Also, DLS-based size measurements are based on the assumption that the NPs are spherical which adds complexity for analysis of non-spherical NPs (Matarozzi *et al.* 2017). Still, DLS is a sensitive and non-invasive method that offers one of the most practical and fast ways to study the size distribution of NPs of different types of materials (Babick 2020; Sakho *et al.* 2017).

Transmission electron microscopy (TEM)

TEM has evolved over many years to be one of the highly sophisticated instruments that has widespread applications in several disciplines. The capability of TEM to capture high resolution images of surfaces has been utilized in the field of nanotoxicology to determine the size, shape and morphology of the NPs even when localized and distributed within cells or tissues (Mühlfeld *et al.* 2007). Sometimes, the capability of TEM to distinguish between the NPs and cellular organelles is a challenge requiring the use of complementary methodologies such as X-ray energy dispersive spectroscopy (EDS) or electron energy-loss spectroscopy (EELS) which generate additional information on the compositional distribution of the NPs (Su 2017; Mühlfeld *et al.* 2007). TEM imaging provides high resolution characterization of NPs but at the same time requires considerable resources and experience for sample preparation and well-trained operators.

Inductively coupled plasma mass spectrometry (ICP-MS)

ICP-MS and its variants have emerged as powerful analytical approaches of high sensitivity and precision in detecting and quantifying inorganic materials and they are now being used extensively also in toxicological studies with NPs (Auffan *et al.* 2014; McTeer *et al.* 2014; Au *et al.* 2010). Among the variants of ICP-MS, the development of single particle (sp) ICP-MS was shown to be a very powerful and advantageous approach for NPs detection and measurement in toxicological studies. Using spICP-MS, the size, mass and number-based size distribution of metallic NPs can be calculated. spICP-MS can quantify NPs at low concentration

without prior separation of NPs from their dissolved ions (*e.g.* ICP-MS and atomic absorption spectroscopy) (Goenaga-Infante and Bartczak 2020; Abdolahpur Monikh *et al.* 2019b; Ding *et al.* 2018; Weigel *et al.* 2017; Hsiao *et al.* 2016; van der Zande *et al.* 2016; Peters *et al.* 2015). This analytical approach has been extensively used for the work described in this thesis on silver (Ag) NPs.

PHYSICOCHEMICAL PROPERTIES OF NPS

A solid description and characterization of the physicochemical properties of NPs are of importance to understand the toxicological behaviour of NPs. It is well established that the (biological) environment that the NPs encounter affects several of the physicochemical properties of the NPs such as surface chemistry, charge and dissolution rate (Casals *et al.* 2017; Bouwmeester *et al.* 2011a; Park *et al.* 2011; Oberdörster *et al.* 2005). A selected number of these properties that are of main importance for the work of this thesis are described briefly.

Size

The size of the NPs is considered one of the important parameters influencing the cellular uptake and internalization of the NPs (Sun *et al.* 2017; Varela *et al.* 2012). It is important to realize that NPs do not have a single size but come with a size distribution which is an inherent consequence of the synthesis of NPs. In case a material of a certain size is produced, great care is taken by manufacturers of NPs to minimize the size distribution within a batch of NPs, but some variability in NP sizes is always present.

An important question is whether the size of NPs has a consequence for their ability to be taken up by cells or not. It is suggested that the optimal particle diameter for *in vitro* cellular internalization of spherical NPs is 50 nm while NPs of smaller (15 – 30 nm) or bigger (70 – 240 nm) sizes tend to have lower cellular internalization (Foroozandeh and Aziz 2018; Wang *et al.* 2010). But no scientific consensus has been reached on this matter, as other studies estimated a different size range to be the optimum for cellular internalization. This includes for example studies exposing human cervical cancer cells to spherical gold (Au) NPs with sizes of 14, 30, 50, 74 and 100 nm reporting an optimum range for cellular uptake of 50 – 74 nm (Zhang *et al.* 2009; Chithrani *et al.* 2006). An even larger optimum size for cellular uptake has been found

following exposure of cells to polystyrene (PS) NPs with sizes of 50, 100, 200, 500 and 1000 nm which pointed towards the 100 nm PSNPs as the ones that were internalized most readily (Yin Win and Feng 2005). These discrepancies clearly illustrate that it is difficult to define a straightforward relation between size and cellular internalization. Most likely other properties of the NPs, such as the chemical composition, surface chemistry or charge, interfere with the ability of NPs to be taken up by cells.

Surface chemistry and charge

Other important properties of the NPs that influence their biological interactions are the surface chemistry and surface charge. Changing the surface charge of the NPs influences the colloidal properties of NPs, which amongst others, could result in aggregation (Kadiyala *et al.* 2010). The surface charge also influences the interaction of the NPs with other molecules and proteins in the biological fluids (Behzadi *et al.* 2017). Furthermore, several studies, using different *in vitro* cellular models, have reported that the surface charge of the NPs (positive, neutral or negative) influences their cellular internalization, toxicity and bioavailability (Nagy *et al.* 2011; Asati *et al.* 2010; He *et al.* 2010; Villanueva *et al.* 2009).

The effect of the NPs surface chemistry on toxicity can be illustrated using the example of SiO₂ NPs. The SiO₂ NPs can be relatively easily functionalized with different chemical structures. The introduction of very reactive silanol functional groups on the surface of SiO₂ NPs renders them to be very toxic to the macrophages, while this toxicity was significantly reduced when aminopropyltriethoxysilane (APTES) groups were attached on the SiO₂ NPs' surfaces (Lehman *et al.* 2016). Examples of the influence of other functional groups on the surface of NPs and the consequences for interactions with cells have been described elsewhere (Zhao *et al.* 2019).

Protein corona

An additional tier of complexity is added upon the contact of NPs with biological/physiological media where different proteins and biomolecules can be adsorbed onto the surfaces of the NPs forming a so-called *protein corona* (Riediker *et al.* 2019; Monopoli *et al.* 2012; Lesniak *et al.* 2010). It was found that the NPs protein corona can influence the biological and toxicological interactions of the NPs (Nath Roy *et al.* 2017; Pederzoli *et al.* 2017;

Mirshafiee *et al.* 2016; Pino *et al.* 2014; Lesniak *et al.* 2010; Lynch *et al.* 2009). For example, A549 lung cells exposed to SiO₂ NPs in serum-free medium (to prevent corona formation) had higher cellular internalization, association and cytotoxicity compared to exposure to the SiO₂ NPs under serum-rich conditions (Lesniak *et al.* 2012).

Not only the presence of the protein corona has an effect on the biological interactions and effects of the NPs, but also the composition of the corona affects these characteristics (Tedja *et al.* 2012). Recently, it has been shown that SiO₂ NPs with a different protein corona can be recognized by different cell receptors, resulting in different mechanisms of cellular uptake (Francia *et al.* 2019). The main protein candidates in the protein corona would be mainly lung surfactant proteins, serum proteins, or enzymes and food biomolecules depending on whether the exposure took place via the inhalation, intravenous, or oral route, respectively (Riediker *et al.* 2019).

Dissolution

The potential of part of the NPs, especially metal-based NPs, to dissolve is another property of the NPs that defines their biological interactions and influences their biopersistence and possible accumulation (Borm *et al.* 2006). Dissolution and ion release could take place before, during or after the contact of NPs with biological media, *e.g.* in stock suspensions containing NPs or in the cell culture medium used in *in vitro* cell models (Maurer *et al.* 2014; Borm *et al.* 2006). The dissolution rate of NPs differs between the NPs, as the dissolution of AuNPs was limited (0.6 -3) (Carlander *et al.* 2019) while AgNPs were found to dissolve up to 90% (Kittler *et al.* 2010) and ZnO NPs (Eixenberger *et al.* 2017) and CuO NPs (Liu *et al.* 2020) can dissolve completely.

Dissolution of NPs is a dynamic process that is influenced by intrinsic properties of the NPs like the size, surface chemistry or chemical composition and by properties of the surrounding environment like the temperature, pH, ionic strength, light and presence of organic components in the suspensions (Misra *et al.* 2012). The size of the NPs is an important factor influencing the NP dissolution, as it was found that small AgNPs with a size of 10 nm dissolved and released relatively more silver ions (Ag⁺) than the larger AgNPs (40, 50 and 75 nm) (Gluga *et al.* 2014). Furthermore, the study of Studer *et al.* demonstrated that the surface chemistry of the NPs also affects the dissolution of the NPs where coating of metal oxide NPs

with inert materials (*i.e.* carbon) reduced their dissolution (Studer *et al.* 2010). This illustrates the complexity behind the dissolution behaviour of NPs and the difficulty in identifying a key parameter ruling the process.

NPs dissolution and ion release can also take place intracellularly upon cellular internalization. This process of continuous ion release is known as the ‘*trojan horse*’ phenomenon (van der Zande *et al.* 2016; Hsiao *et al.* 2015; Maurer *et al.* 2014). Several studies have investigated this phenomenon using *in vitro* artificial lysosomal fluid, as it is assumed that the dissolution of NPs happens in the lysosomes where an acidic pH exists. Chao *et al.* reported about 90 % dissolution of ZnO NPs within 24 hr incubation in this fluid (Cho *et al.* 2011). This phenomenon was observed with several metal NPs accompanied by an increase of the cytotoxicity of these NPs upon their dissolution (van der Zande *et al.* 2016; Aueviriyavit *et al.* 2014; Beer *et al.* 2012; Vandebriel and De Jong 2012; Bouwmeester *et al.* 2011b). Obviously, the cytotoxicity of NPs upon dissolution depends also on the (intrinsic) toxicity of the ions released (Cho *et al.* 2011). Clearly, the release of ions upon the dissolution of NPs can have an important impact on the toxicity of NPs. The dissolution of NPs therefore has implications for the risk assessment where it should be considered whether the observed effects relate to the NPs themselves or to the ions released by them.

EXPOSURE TO NPS AND THEIR TOXICOLOGICAL FATE

Humans are exposed to different NPs via different routes *e.g.* inhalation, dermal and oral routes (De Matteis 2017; Bouwmeester *et al.* 2009). Assessing the potential risks associated with exposure to NPs using animal studies will require high numbers of experimental animals, especially considering the enormous diversity of NPs that are currently engineered and developed, which is highly undesirable. Alternatively, applying the principles of the ‘*3Rs*’ which stands for *reducing, refining and replacing animal in vivo models* in the field of nanotoxicology is currently reducing the number of experimental animals. This is done by the development of *in vitro* models to screen for possible adverse effects that might be induced by the wide diversity of NPs (EFSA Scientific Committee *et al.* 2018). Consequently, there is an increasing demand on developing and optimizing reliable and robust *in vitro* methods for NPs hazard identification research (Kroll *et al.* 2009).

The aim of the present thesis was to investigate the potential of different *in vitro* methods combined with advanced analytical techniques as a screening strategy to study the toxicokinetics and toxicodynamics of NPs. The work described in this thesis was focused on *in vitro* models used to study NPs following oral exposure. Several *in vitro* models have been used in the current thesis to investigate the cellular uptake and transport (toxicokinetics) of NPs through different biological barriers (intestinal and placental barriers). Also, the potential toxicity (toxicodynamics) of these NPs *e.g.* their cytotoxicity, developmental toxicity, reactive oxygen species (ROS) generation and genotoxicity were assessed using a battery of *in vitro* models combined with advanced analytical techniques. For the current studies, two different types of NPs were used as model NPs: polystyrene NPs and silver NPs with different sizes and surface chemistries.

Polystyrene nanoparticles (PSNPs)

PSNPs are polymeric NPs that have been widely utilized in food packaging to improve the properties such as barrier selectivity, mechanical strength and heat resistance and to reduce the production costs (Chiu *et al.* 2015; Lee *et al.* 2014; Arora and Padua 2010). Concerns were raised about the potential migration of these PSNPs into food or drinks, which might put the safety of the food products that are in contact with these PSNPs containing packages into question (Chaudhry *et al.* 2008). Apart from their use in packaging materials, PSNPs represent a good model for NPs because of their high commercial availability in different sizes and surface modifications, low costs and the flexibility to add fluorescent labels to facilitate their detection and quantification (Varela *et al.* 2012). In this thesis PSNPs of different sizes and surface chemistries were used to assess the importance of these NPs properties on cellular interactions and effects.

Silver nanoparticles (AgNPs)

AgNPs are among the most produced NPs worldwide and are frequently used in food related products because of their antimicrobial properties (Vance *et al.* 2015; Nowack *et al.* 2011; Bouwmeester *et al.* 2009). Additionally, the increased use of AgNPs by various other industrial sectors leads to an increased possibility for AgNPs release into the environment and subsequent entry into the food production chain where chronic exposure of human to too high levels of ionic silver might induce argyria in humans (Böhmert *et al.* 2014; Wijnhoven *et*

al. 2009). AgNPs are prone to several physicochemical processes *e.g.* dissolution, agglomeration and complexation with ligands present in their environment (Kaegi *et al.* 2011; Kim *et al.* 2010). Upon environmental release or in organisms AgNPs can thus undergo (dynamic) modifications, which is also called the aging of AgNPs. An important aging process is the sulfidation of AgNPs, resulting in the formation of silver sulphide (Ag₂S) NPs. The formation of Ag₂S NPs can take place involving the original AgNPs directly, or by precipitation of Ag ions, formed through dissolution of the AgNPs, into Ag₂S aggregates in the nano-range (Thalmann *et al.* 2014). The stability of Ag₂S NPs was found to be high with very low solubility resulting in Ag₂S NPs being the dominant silver species in the environment (He *et al.* 2019). Therefore, in this thesis we used Ag₂S NPs representing such aged AgNPs next to pristine AgNPs of different surface chemistries.

***In vitro* models of digestion**

The main physiological function of the human gastrointestinal (GI) tract is to digest food into basic components via digestion processes and facilitate the absorption of nutrients. Upon oral exposure, NPs will encounter very different environmental conditions upon moving through the GI tract. The digestion is a very dynamic process with elevated temperature, high ionic strength and varying pH along the GI tract (the mouth has neutral pH, the stomach has very low pH (ranging from 1 to 5, depending on whether the stomach is empty or full) while the small intestine has neutral pH) which can all significantly influence the dissolution and aggregation rates of the NPs (Ban *et al.* 2018; Kästner *et al.* 2018; Kästner *et al.* 2017).

In media of high ionic strength and pH close to the isoelectric point of the NPs, the net surface charge of the NPs tends to be neutral while the high ionic strength will also reduce in the influence of the repulsive electrostatic double layer (EDL) forces, together enhancing the effects of van der Waal's (vdW) attraction forces resulting in increased chances of agglomeration of the NPs. In contrast, in low ionic strength media, the EDL extends from the NPs surfaces leading to repulsion between the NPs opposing agglomeration (Muraleetharan *et al.* 2019). These factors significantly influence the colloidal stability of the NPs and are explained in the Derjaguin–Landau–Verwey–Overbeek (DLVO) theory (Muraleetharan *et al.* 2019; Bian *et al.* 2011).

In the stomach, the food content is mixed mechanically by peristalsis with gastric juices and after residing for 1-2 hr the resulting mixture is released into the duodenum where it is mixed with pancreatic digestive enzymes, bicarbonate and bile from the liver, which neutralizes the pH of the mixture. Under continuing peristalsis, the final output is pushed through the intestines and the constituents (for example sugar, amino acids or fatty acids) are absorbed through the GI epithelia to enter the portal vein and reach the systemic circulation upon passing the liver (Pindřáková *et al.* 2017; Barrett 2014; Goodman 2010). The GI epithelia also have an important gatekeeper function as the cells form a barrier that prevents and/or controls the penetration of several substances including NPs (Goodman 2010).

To emulate the *in vivo* digestive processes, various *in vitro* models have been developed with different level of complexity depending on their purpose of use (Egger *et al.* 2016). These models are utilized also to characterize the changes that NPs undergo during the digestion processes (Lefebvre *et al.* 2015). Digestion models usually include incubation of the NPs in artificial juices resembling three major steps of the digestion, including the oral, gastric and intestinal phases (EFSA Scientific Committee *et al.* 2018; Egger *et al.* 2016). Several models are simplified, some are only simulating gastric digestion using a saline buffer at low pH (Mwilu *et al.* 2013; Mahler *et al.* 2009) and others are simulating only the small intestinal conditions especially when lipid digestion processes are of interest (Li and McClements 2010). Most advanced models include dynamic digestion, where the shearing, mixing and retention times within the intact GI tract are mimicked and completely integrated including feedback controls of several parameters (*e.g.* pH and temperature) (Vardakou *et al.* 2011; Kong and Singh 2010). For a specific food ingredient or drug related research questions, these dynamic digestion models offer clear advantages, but these models require costly specialized equipment and expertise. In addition, the use of tubing raises concerns for NPs research purposes because of the potential of NPs to adhere to the tubing. Therefore, in this thesis a well described static *in vitro* digestion model has been used.

Several static *in vitro* digestion models have been described in the literature (Van de Wiele *et al.* 2015; Van de Wiele *et al.* 2007; Oomen *et al.* 2003a; Ruby *et al.* 1996). In this thesis, a model that was originally developed by Oomen *et al.* was used. It incorporates oral, gastric and small intestinal conditions (Brodkorb *et al.* 2019; Versantvoort *et al.* 2005; Oomen *et al.* 2003a). It has been used extensively in studies determining the bioaccessibility of orally

ingested substances *e.g.* heavy metals (Oomen *et al.* 2003b), aflatoxin B1 (Versantvoort *et al.* 2005) and NPs (Peters *et al.* 2012; Walczak *et al.* 2012). This static model allows easy sampling while adequately simulating the main biochemical dynamics in the human GI tract that might influence the fate of ingested NPs.

***In vitro* models of a healthy intestinal epithelial barrier**

Besides NP digestion, NP absorption through the intestinal epithelium is also a key element for the risk assessment of NPs (Lefebvre *et al.* 2015). *In vitro* cell models of the intestinal epithelium gained a lot of attention as an alternative, fast and high-throughput method for biological barrier permeability screening in studying the toxicokinetics of NPs (Lefebvre *et al.* 2015). To mimic the intestinal epithelium, several cell lines are frequently used *e.g.* Caco-2 and HT-29-MTX cell lines which form monolayers with tight junctions (Devriese *et al.* 2017; Dharmasathaphorn *et al.* 1984; Polak-Charcon *et al.* 1978). Among these different cell lines, cells from the Caco-2 line are the most commonly used intestinal *in vitro* cell model and this model is well established for toxicokinetic studies of xenobiotics (Lefebvre *et al.* 2015; Chen *et al.* 2010). However, Caco-2 cells, do not produce a mucus layer which next to its protective role for the underlying tissues, also represents an efficient acellular barrier for the oral cavity, the oesophagus, the stomach and the intestine (Fröhlich and Roblegg 2012; Hubatsch *et al.* 2007).

Therefore, it is of relevance to include a mucus layer in an *in vitro* model used to study the potential transport of NPs, which also serves to protect the Caco-2 cells against the harmful components in the digestive fluids (chyme). This is an important added functionality when combining an *in vitro* digestion model with an *in vitro* transport model as performed in this thesis. Such a protective mucus layer can be formed *in vitro* following the co-culture of Caco-2 cells with the mucus secreting HT29-MTX cells and this combined culture has been used previously to assess the permeability and transport of NPs *e.g.* TiO₂ NPs (García-Rodríguez *et al.* 2018) and Fe₂O₃ NPs (Strugari *et al.* 2018) (Table 1) and was also used in this thesis.

Table 1: Highlights on a selection of available studies on NPs using different *in vitro* models.

<i>In vitro</i> model	NPs used	Findings	Reference
Intestinal digestion <i>in vitro</i> model			
<i>In vitro</i> digestion model	≥ 8 nm surface-passivated Al ^P -core NPs and 5 – 10 nm Al ₂ O ₃ NPs	Strong agglomeration of both Al ^P and Al ₂ O ₃ NPs at low pH in gastric fluid together with an increased Al ion release. In intestinal fluid and the particles deagglomerated and the levels of free Al ions decreased.	(Sieg <i>et al.</i> 2017)
	3.6 - 16 nm AgNPs	No difference in the Caco-2 cellular uptake of pristine and digested AgNPs with food. While the cellular uptake of AgNPs digested without food was 60 % less.	(Lichtenstein <i>et al.</i> 2015)
	7 nm AgNPs	AgNPs agglomerate to a high extent during gastric passage while these aggregates break down upon moving to the intestinal compartment.	(Böhmer <i>et al.</i> 2014)
	60 nm citrate-coated AgNPs	AgNPs agglomerate to a high extent during gastric passage while these aggregates broke down upon moving to the intestinal compartment.	(Walczak <i>et al.</i> 2012)
	32 nm SiO ₂ NPs	Large clusters of SiO ₂ NPs in found the acidic gastric compartment. Smaller SiO ₂ NPs found in the intestinal compartment of higher pH.	(Peters <i>et al.</i> 2012)

Intestinal barrier *in vitro* model

Caco-2/HT29 coculture	< 25 nm TiO ₂ nanospheres, < 100 nm (diameter) TiO ₂ nanorods and < 10 nm (diameter) TiO ₂ nanowires	All three TiO ₂ nanomaterials were able to cross the mucus layer, the cell barrier model and reach the basolateral compartment. Both TiO ₂ nanospheres and nanorods were taken up faster than nanowires.	(García-Rodríguez <i>et al.</i> 2018)
Caco-2 with HT29-MTX coupled to <i>in vitro</i> digestion	50 nm, carboxylated, aminated and plain PSNPs	Incubation of the NPs in the <i>in vitro</i> digestion model resulted in increased translocation levels compared to 'nondigested' NPs.	(Walczak <i>et al.</i> 2015)
Caco-2/HT29-MTX coculture	Insulin loaded chitosan nanoparticles.	CSK peptide modification showed enhanced transport. The presence of mucus increased the translocation of both modified and unmodified NPs.	(Jin <i>et al.</i> 2012)
Caco-2 / MTX-E12 coculture	Hydrophobic polystyrene, bioadhesive chitosan and stealth PLA-PEG NPs	Mucus is presenting a major barrier for hydrophobic polystyrene NPs and chitosan. Chitosan NPs seemed to be taken up by adsorptive transcytosis and Polystyrene NPs via non-adsorptive transcytosis.	(Behrens <i>et al.</i> 2002)

Placental barrier *in vitro* model

BeWo b30 model	23-38 nm Magnetite Na-oleate-coated (OC-Fe ₃ O ₄) NPs and 25 and 50 nm Fluorescent rhodamine-labelled silica (FI-SiO ₂) NPs	All the NPs tested could transport through the placental barrier to comparable levels regardless the size or surface chemistry differences.	(Correia Carreira <i>et al.</i> 2015b)
-----------------------	----------------------------------------------------------------------------------------------------------------------------------------------------------------	---------------------------------------------------------------------------------------------------------------------------------------------	----------------------------------------

25 and 50 nm Rhodamine labelled SiO ₂ NPs	After 6 hours, a limited transport through the BeWo b30 cell layer of both NPs regardless of the NPs size	(Poulsen <i>et al.</i> 2015)
146 and 232 nm Dexamethasone loaded poly (d, l-lactide-coglycolide) (PLGA) NPs	Transport across the placental barrier of dexamethasone loaded PLGA NPs was inversely correlated with the size of the NPs.	(Ali <i>et al.</i> 2013)
50 and 100 nm PSNPs	3.5% (50 nm) and 0.6% (100 nm) of the initial amount added to the apical chamber was found in the basal chamber after 24 hr.	(Cartwright <i>et al.</i> 2012)
10 – 30 PEGylated AuNPs	The PEGylated AuNPs were taken up in BeWo cells after 48 hr after exposure.	(Myllynen <i>et al.</i> 2008)
Developmental toxicity in vitro models		
20, 80 and 113 nm AgNPs	No developmental toxicity was induced as the cytotoxicity was induced at lower or similar concentrations that induced inhibition of the differentiation of stem cells into contracting cardiomyocytes.	(Park <i>et al.</i> 2011)
17 nm aminosilane and thiolisilane coated cobalt ferrite (Si-CoFe) NPs and 17 nm aminosilane, thiolisilane and gold coated cobalt ferrite (AuSi-CoFe) NPs	There was an effect of the surface coating on the inhibition of the differentiation of stem cells into contracting cardiomyocytes. AuSi-CoFe NPs were not embryotoxic while Si-CoFe NPs were weakly embryotoxic.	(Di Guglielmo <i>et al.</i> 2010)
10, 30, 80 and 400 nm SiO ₂ NPs	10 and 30 nm SiO ₂ NPs induced inhibition of the differentiation of stem cells into contracting cardiomyocytes while the larger NPs did not.	(Park <i>et al.</i> 2009)

EST

***In vitro* placental transport models**

The transport of NPs via the placental barrier has been investigated in several studies using an *ex vivo* model of a perfused human placenta (Juch *et al.* 2013; Tina Buerki-Thurnherra 2012; Saunders 2009). Although this model maintains the complexity of intact human placenta, this model has some disadvantages as it is laborious and can only be used for short exposure conditions (Juch *et al.* 2013). Furthermore, the placental *ex vivo* model mainly corresponds to the late pregnancy stages, which results in difficulties in drawing conclusions upon early pregnancy exposure to NPs (Juch *et al.* 2013; Tina Buerki-Thurnherra 2012).

Several *in vitro* placental barrier models have been developed using human placental cells, *e.g.* BeWo, Jar and JEG-3 cells, to study placental transport of different drugs and substances including NPs (Blazquez *et al.* 2014; Ikeda *et al.* 2011; Manley *et al.* 2005). Among these different cell lines, the BeWo cells and its b30 subclone are the most commonly used cell lines to study placental transport. Culturing the BeWo b30 cells on permeable membranes in transwells where a continuous cell layer is formed results in a model where the maternal and foetal side are represented by respectively the apical and basolateral compartments of the transwells (Correia Carreira *et al.* 2015b; Correia Carreira *et al.* 2015a; Saunders 2009; Liu *et al.* 1997). This model has been used to study the transport of different NPs *e.g.* 10-30 nm PEGylated AuNPs (Myllynen *et al.* 2008), 23-28 nm iron oxide (Fe₂O₃) and SiO₂ NPs (Correia Carreira *et al.* 2015b), 50 and 100 nm PSNPs (Kloet *et al.* 2015; Cartwright *et al.* 2012), 140-289 nm dexamethasone loaded poly lactic-co-glycolic acid (PLGA) NPs (Ali *et al.* 2013) and 25 and 50 nm rhodamine labelled SiO₂ NPs (Poulsen *et al.* 2015) (Table 1). Most of these studies focused on the effect of the NPs size and material on the potential transport via the *in vitro* placental model. In this thesis the BeWo be 30 model was used to study the impact of the aged AgNPs and surface chemistries of pristine AgNPs on their potential transport via the placental barrier.

***In vitro* developmental toxicity models**

The ability of the NPs to reach and cross the placenta points towards the potential of the NPs to reach the foetus making it relevant to consider their potential to induce developmental toxicity (Riediker *et al.* 2019; Wick *et al.* 2010). The data on the potential of

NPs to induce developmental toxicity are limited and are obtained mainly from rodent *in vivo* studies (Ema *et al.* 2016; Garcia *et al.* 2016; Hougaard *et al.* 2015; Powers *et al.* 2013). One of the *in vitro* alternative assays for developmental toxicity testing is the embryonic stem cell test (EST).

The EST has an added value as it does not require pregnant animals and it has been validated for use as an *in vitro* developmental toxicity assay by the European Centre for the Validation of Alternative Methods (ECVAM) (de Jong *et al.* 2011; Seiler and Spielmann 2011; Augustine-Rauch *et al.* 2010; Genschow *et al.* 2004). In the EST, the potential developmental toxicity of substances is tested by assessing the ability of a substance to inhibit the capacity of mouse embryonic stem cells (mESCs) to differentiate into beating cardiomyocytes (Campagnolo *et al.* 2013; Buesen 2004). The test has been used previously to investigate the potential developmental toxicity of several NPs *e.g.* SiO₂ NPs (Park *et al.* 2009), AuNPs and cobalt ferrite NPs (Di Guglielmo *et al.* 2010) (Table 1). Most of these studies focused on the effect of the size and material of the NPs on the potential developmental toxicity, whereas the consequences of surface chemistry of the NPs were not studied in depth. This is therefore studied in chapter four in the current thesis using pristine and aged AgNPs.

***In vitro* genotoxicity models**

Following the increased human exposure to NPs with their highly reactive surfaces, concerns have been raised about the genotoxic potential of NPs (Petersen and Nelson 2010; Landsiedel *et al.* 2009; Singh *et al.* 2009; Gonzalez *et al.* 2008). The mechanisms behind NP induced genotoxicity remain to be elucidated. But according to the most widely accepted hypothesis, the genotoxicity mechanisms of NPs are classified into three groups, including; i) direct effects from the surface of the NPs, ii) redox mechanisms including production of ROS and/or iii) activation of membrane receptors induced upon the exposure and the intracellular diffusion of the NPs (Elespuru *et al.* 2018; Benameur *et al.* 2012; Xie *et al.* 2011; AshaRani *et al.* 2009; Landsiedel *et al.* 2009).

Several studies have reported the potential of different NPs such as AgNPs (AshaRani *et al.* 2009), TiO₂ NPs (Osman *et al.* 2010; Rahman *et al.* 2002), ZnO NPs (Osman *et al.* 2010; Gopalan *et al.* 2009) and copper oxide NPs (Karlsson *et al.* 2008) to induce genotoxic effects. For example, it was reported that TiO₂ and SiO₂ NPs could reach the cellular nucleus and

interact directly and induce physical damage to the genetic material by forming intranuclear protein aggregates (Liu *et al.* 2007; Chen and von Mikecz 2005; Geiser *et al.* 2005). While the NPs made of transition metals (*e.g.* cobalt, cadmium, chrome, titanium and zinc) were found to be able to induce generation of ROS (Singh *et al.* 2009; Brown *et al.* 2001). The ROS are highly reactive entities that could be generated at the NPs surfaces and these ROS can interact with the DNA and induce DNA damage leading to genotoxic effects (Abdal Dayem *et al.* 2017).

Different *in vitro* assays have been developed to detect and assess the genotoxicity of NPs which could measure several genotoxicity endpoints, *i.e.* primary DNA alterations, gene mutations or chromosome mutations (Benameur *et al.* 2012). The Ames (bacterial reverse mutation) test is a well-established and OECD validated assay to detect gene mutations where one or more strains of mutated bacterial strains of *Salmonella typhimurium* (*S. typhimurium*) and/or *Escherichia coli* are used (Benameur *et al.* 2012; Landsiedel *et al.* 2009; OECD 1997). However, this bacterial assay is not recommended for testing NPs genotoxicity because of the lack of the bacterial cells of any endocytic mechanism of NPs uptake which reduces the probability of the NPs to penetrate the rigid outer double membrane of the Gram negative bacteria (Elespuru *et al.* 2018; Clift *et al.* 2013). This was reported in several studies on the potential mutagenicity of several NPs *e.g.* TiO₂ and AgNPs (Butler *et al.* 2015; Butler *et al.* 2014). While other studies showed a weak potential of *S. typhimurium* to take up NPs *e.g.* TiO₂, ZnO, cerium oxide NPs and carbon nanotubes (Clift *et al.* 2013; Kumar *et al.* 2011).

Various alternative assays have been developed, like the comet assay and the γ -H₂AX assay. In this thesis, we evaluated the γ -H₂AX assay as an alternative method to detect the potential of AgNPs to induce DNA-double-strand breaks (DSBs) (Louisse *et al.* 2019; Wan *et al.* 2019; Watters *et al.* 2009; Kuo and Yang 2008). The assay was shown able to detect DNA-DSBs induction by several xenobiotics and also by different NPs *e.g.* silver, cobalt, cerium oxide and nickel oxide NPs (Åkerlund *et al.* 2018; Könen-Adıgüzel and Ergene 2018; Wan *et al.* 2017; Zhao *et al.* 2016). The sensitivity of the assay is due to the close correlation of the phosphorylation of H₂AX to each DNA-DSBs taking place (Wan *et al.* 2019; Sedelnikova *et al.* 2002). Accordingly, this assay was chosen to evaluate its capability to detect the potential of AgNPs to induce DNA-DSBs in a HepG2 liver cell *in vitro* model.

OUTLINE OF THE THESIS

The aim of the present thesis was to investigate the potential of different *in vitro* methods combined with advanced analytical techniques as a screening strategy to study the toxicokinetic and toxicodynamic properties of silver and polystyrene nanoparticles. This work is presented in **six** chapters:

The present chapter, **chapter 1**, provides an introduction and background information on nanotoxicology and presents an overview of several *in vitro* alternative models of which some were used in the present thesis.

In **chapter 2**, the influence of the size and surface chemistry of pristine PSNPs on the protein corona formation and subsequent uptake/association and transport through a Caco-2 intestinal cell model is characterized. Also, the relation between surface modification and uptake/association was studied.

In **chapter 3**, the impact of the biochemical conditions within the human digestive tract on the intestinal transport of AgNPs of different surface chemistries across an intestinal *in vitro* model of differentiated Caco-2/HT29-MTX cells was studied. An *in vitro* digestion model was used to simulate the human digestion process. AgNPs of different surface chemistries and silver nitrate (AgNO₃) as a source of ionic silver were used. Using ICP-MS and spICP-MS, the size distribution, dissolution, particle concentration (mass- and number-based) and total silver content of the AgNPs were characterized before and after digestion and in the apical, basolateral and cellular compartments of the Caco-2/HT29-MTX intestinal transport model.

In **chapter 4**, a combination of the BeWo b30 placental transport model and the EST was used to investigate the capability of pristine AgNPs of different surface chemistries and aged AgNPs (Ag₂S NPs) to cross the placental barrier and their capability for inducing *in vitro* developmental toxicity. Again, AgNO₃ as a source of ionic silver, was tested for comparison. ICP-MS and spICP-MS were used to characterize the size distribution, dissolution, particle concentration (mass- and number-based) and total silver content of the AgNPs in the apical, basolateral and cellular compartments of the BeWo b30 placental transport model at different time points.

In **chapter 5**, the In-Cell Western- γ -H₂AX assay was evaluated as an alternative *in vitro* assay to detect the potential of aged AgNPs and pristine AgNPs to induce phosphorylation of H₂AX, reflecting induction of DNA-DSBs, in HepG2 liver cells. AgNO₃ was used to quantify the effects of ionic silver. Additionally, the potential of these AgNPs to induce ROS production as a potential underlying mechanism of inducing DNA-DSBs, was assessed, both under cell-free conditions and in HepG2 cells.

In **chapter 6**, the findings described in the thesis are critically discussed and in addition, suggestions for future research are presented.

REFERENCES

- Abdal Dayem A, Hossain MK, Lee SB, Kim K, Saha SK, Yang G-M, Choi HY, Cho S-G. 2017. The Role of Reactive Oxygen Species (ROS) in the Biological Activities of Metallic Nanoparticles. *Int J Mol Sci* 18:120.
- Abdolahpur Monikh F, Chupani L, Vijver MG, Vancová M, Peijnenburg WJGM. 2019a. Analytical approaches for characterizing and quantifying engineered nanoparticles in biological matrices from an (eco)toxicological perspective: old challenges, new methods and techniques. *Science of The Total Environment* 660:1283-1293.
- Abdolahpur Monikh F, Chupani L, Zusková E, Peters R, Vancová M, Vijver MG, Porcal P, Peijnenburg WJGM. 2019b. Method for extraction and quantification of metal-based nanoparticles in biological media: number-based biodistribution and bioconcentration. *Environmental Science & Technology* 53:946-953.
- Åkerlund E, Cappellini F, Di Bucchianico S, Islam S, Skoglund S, Derr R, Odnevall Wallinder I, Hendriks G, Karlsson HL. 2018. Genotoxic and mutagenic properties of Ni and NiO nanoparticles investigated by comet assay, γ -H2AX staining, Hprt mutation assay and ToxTracker reporter cell lines. *Environmental and Molecular Mutagenesis* 59:211-222.
- Ali H, Kalashnikova I, White MA, Sherman M, Rytting E. 2013. Preparation, characterization, and transport of dexamethasone-loaded polymeric nanoparticles across a human placental in vitro model. *International Journal of Pharmaceutics* 454:149-157.
- Arora A, Padua GW. 2010. Review: Nanocomposites in Food Packaging. *Journal of Food Science* 75:R43-R49.
- Asati A, Santra S, Kaittanis C, Perez JM. 2010. Surface-charge-dependent cell localization and cytotoxicity of cerium oxide nanoparticles. *ACS nano* 4:5321-5331.
- AshaRani PV, Low Kah Mun G, Hande MP, Valiyaveetil S. 2009. Cytotoxicity and Genotoxicity of Silver Nanoparticles in Human Cells. *ACS Nano* 3:279-290.
- Au L, Zhang Q, Cobley CM, Gidding M, Schwartz AG, Chen J, Xia Y. 2010. Quantifying the cellular uptake of antibody-conjugated Au nanocages by two-photon microscopy and inductively coupled plasma mass spectrometry. *ACS nano* 4:35-42.
- Aueviriyavit S, Phummiratch D, Maniratanachote R. 2014. Mechanistic study on the biological effects of silver and gold nanoparticles in Caco-2 cells – Induction of the Nrf2/HO-1 pathway by high concentrations of silver nanoparticles. *Toxicology Letters* 224:73-83.
- Auffan M, Matson CW, Rose J, Arnold M, Proux O, Fayard B, Liu W, Chaurand P, Wiesner MR, Bottero J-Y, Di Giulio RT. 2014. Salinity-dependent silver nanoparticle uptake and transformation by Atlantic killifish (*Fundulus heteroclitus*) embryos. *Nanotoxicology* 8:167-176.
- Augustine-Rauch K, Zhang CX, Panzica-Kelly JM. 2010. In vitro developmental toxicology assays: A review of the state of the science of rodent and zebrafish whole embryo culture and embryonic stem cell assays. *Birth Defects Research Part C: Embryo Today: Reviews* 90:87-98.
- Babick F. 2020. Chapter 3.2.1 - Dynamic light scattering (DLS). In: Hodoroaba V-D, Unger WES, Shard AG, eds. *Characterization of Nanoparticles*. Elsevier, 137-172.

- Ban C, Jo M, Lim S, Choi YJ. 2018. Control of the gastrointestinal digestion of solid lipid nanoparticles using PEGylated emulsifiers. *Food Chemistry* 239:442-452.
- Barrett KE. 2014. Functional Anatomy of the GI Tract and Organs Draining into It. In: Barrett KE, ed. *Gastrointestinal Physiology*. 2nd edition. New York: McGraw-Hill.
- Beer C, Foldbjerg R, Hayashi Y, Sutherland DS, Autrup H. 2012. Toxicity of silver nanoparticles— Nanoparticle or silver ion? *Toxicology Letters* 208:286-292.
- Behrens I, Pena A, Alonso M, Kissel T. 2002. Comparative Uptake Studies of Bioadhesive and Non-Bioadhesive Nanoparticles in Human Intestinal Cell Lines and Rats: The Effect of Mucus on Particle Adsorption and Transport. *Pharmaceutical research* 19:1185-93.
- Behzadi S, Serpooshan V, Tao W, Hamaly MA, Alkawareek MY, Dreaden EC, Brown D, Alkilany AM, Farokhzad OC, Mahmoudi M. 2017. Cellular uptake of nanoparticles: journey inside the cell. *Chemical Society Reviews* 46:4218-4244.
- Benameur L, Wei L, Botta A. 2012. Genotoxicity of Nanoparticles. In: Bhushan B, ed. *Encyclopedia of Nanotechnology*. Dordrecht: Springer Netherlands, 952-962.
- Benelmekki M. 2015. An introduction to nanoparticles and nanotechnology. *Designing Hybrid Nanoparticles*. Morgan & Claypool Publishers, 1-1-1-14.
- Bian S-W, Mudunkotuwa IA, Rupasinghe T, Grassian VH. 2011. Aggregation and Dissolution of 4 nm ZnO Nanoparticles in Aqueous Environments: Influence of pH, Ionic Strength, Size, and Adsorption of Humic Acid. *Langmuir* 27:6059-6068.
- Blazquez AG, Briz O, Gonzalez-Sanchez E, Perez MJ, Ghanem CI, Marin JJG. 2014. The effect of acetaminophen on the expression of BCRP in trophoblast cells impairs the placental barrier to bile acids during maternal cholestasis. *Toxicology and Applied Pharmacology* 277:77-85.
- Bleeker EAJ, de Jong WH, Geertsma RE, Groenewold M, Heugens EHW, Koers-Jacquemijns M, van de Meent D, Popma JR, Rietveld AG, Wijnhoven SWP, Cassee FR, Oomen AG. 2013. Considerations on the EU definition of a nanomaterial: Science to support policy making. *Regulatory Toxicology and Pharmacology* 65:119-125.
- Böhmert L, Girod M, Hansen U, Maul R, Knappe P, Niemann B, Weidner SM, Thünemann AF, Lampen A. 2014. Analytically monitored digestion of silver nanoparticles and their toxicity on human intestinal cells. *Nanotoxicology* 8:631-642.
- Borm P, Klaessig FC, Landry TD, Moudgil B, Pauluhn Jr, Thomas K, Trottier R, Wood S. 2006. Research Strategies for Safety Evaluation of Nanomaterials, Part V: Role of Dissolution in Biological Fate and Effects of Nanoscale Particles. *Toxicological Sciences* 90:23-32.
- Bouwmeester H, Brandhoff P, Marvin HJP, Weigel S, Peters RJB. 2014. State of the safety assessment and current use of nanomaterials in food and food production. *Trends in Food Science & Technology* 40:200-210.
- Bouwmeester H, Dekkers S, Noordam MY, Hagens WI, Bulder AS, de Heer C, ten Voorde SECG, Wijnhoven SWP, Marvin HJP, Sips AJAM. 2009. Review of health safety aspects of nanotechnologies in food production. *Regulatory Toxicology and Pharmacology* 53:52-62.
- Bouwmeester H, Lynch I, marvin HJP, Dawson KA, Berges M, Braguer D, Byrne HJ, Casey A, Chambers G, Clift MJD, Elia G, Fernandes TF, Fjellsbø LB, Hatto P, Juillerat L, Klein C, Kreyling WG, Nickel

- C, Riediker M, Stone V. 2011a. Minimal analytical characterization of engineered nanomaterials needed for hazard assessment in biological matrices. *Nanotoxicology* 5:1-11.
- Bouwmeester H, Poortman J, Peters RJ, Wijma E, Kramer E, Makama S, Puspitaninganindita K, Marvin HJP, Peijnenburg AACM, Hendriksen PJM. 2011b. Characterization of Translocation of Silver Nanoparticles and Effects on Whole-Genome Gene Expression Using an In Vitro Intestinal Epithelium Coculture Model. *ACS Nano* 5:4091-4103.
- Boverhof DR, Bramante CM, Butala JH, Clancy SF, Lafranconi M, West J, Gordon SC. 2015. Comparative assessment of nanomaterial definitions and safety evaluation considerations. *Regulatory Toxicology and Pharmacology* 73:137-150.
- Brodkorb A, Egger L, Alminger M, Alvito P, Assunção R, Ballance S, Bohn T, Bourlieu-Lacanal C, Boutrou R, Carrière F, Clemente A, Corredig M, Dupont D, Dufour C, Edwards C, Golding M, Karakaya S, Kirkhus B, Le Feunteun S, Lesmes U, Macierzanka A, Mackie AR, Martins C, Marze S, McClements DJ, Ménard O, Minekus M, Portmann R, Santos CN, Souchon I, Singh RP, Vegarud GE, Wickham MSJ, Weitschies W, Recio I. 2019. INFOGEST static in vitro simulation of gastrointestinal food digestion. *Nature Protocols* 14:991-1014.
- Brown DM, Wilson MR, MacNee W, Stone V, Donaldson K. 2001. Size-Dependent Proinflammatory Effects of Ultrafine Polystyrene Particles: A Role for Surface Area and Oxidative Stress in the Enhanced Activity of Ultrafines. *Toxicology and Applied Pharmacology* 175:191-199.
- Buesen R, A. Visan, E. Genschow, B. Slawik, H. Spielmann and A. Seiler. 2004. Trends in improving the embryonic stem cell test (EST): an overview. *ALTEX* 21:15-22.
- Butler KS, Casey BJ, Garborcauskas GVM, Dair BJ, Elespuru RK. 2014. Assessment of titanium dioxide nanoparticle effects in bacteria: Association, uptake, mutagenicity, co-mutagenicity and DNA repair inhibition. *Mutation Research/Genetic Toxicology and Environmental Mutagenesis* 768:14-22.
- Butler KS, Peeler DJ, Casey BJ, Dair BJ, Elespuru RK. 2015. Silver nanoparticles: correlating nanoparticle size and cellular uptake with genotoxicity. *Mutagenesis* 30:577-591.
- Buzea C, Pacheco II, Robbie K. 2007. Nanomaterials and nanoparticles: Sources and toxicity. *Biointerphases* 2:MR17-MR71.
- Campagnolo L, Fenoglio I, Massimiani M, Magrini A, Pietroiusti A. 2013. Screening of Nanoparticle Embryotoxicity Using Embryonic Stem Cells. In: Turksen K, ed. *Stem Cell Nanotechnology: Methods and Protocols*. Totowa, NJ: Humana Press, 49-60.
- Cao Y, Li J, Liu F, Li X, Jiang Q, Cheng S, Gu Y. 2016. Consideration of interaction between nanoparticles and food components for the safety assessment of nanoparticles following oral exposure: A review. *Environmental Toxicology and Pharmacology* 46:206-210.
- Carlander U, Midander K, Hedberg YS, Johanson G, Bottai M, Karlsson HL. 2019. Macrophage-Assisted Dissolution of Gold Nanoparticles. *ACS Applied Bio Materials* 2:1006-1016.
- Cartwright L, Poulsen MS, Nielsen HM, Pojana G, Knudsen LE, Saunders M, Rytting E. 2012. In vitro placental model optimization for nanoparticle transport studies. *International journal of nanomedicine* 7:497-510.
- Casals E, Gusta MF, Piella J, Casals G, Jiménez W, Puentes V. 2017. Intrinsic and Extrinsic Properties Affecting Innate Immune Responses to Nanoparticles: The Case of Cerium Oxide. *Frontiers in Immunology* 8.

- Chaudhry Q, Scotter M, Blackburn J, Ross B, Boxall A, Castle L, Aitken R, Watkins R. 2008. Applications and implications of nanotechnologies for the food sector. *Food Additives & Contaminants: Part A* 25:241-258.
- Chen M, von Mikecz A. 2005. Formation of nucleoplasmic protein aggregates impairs nuclear function in response to SiO₂ nanoparticles. *Experimental Cell Research* 305:51-62.
- Chen X-M, Elisia I, Kitts DD. 2010. Defining conditions for the co-culture of Caco-2 and HT29-MTX cells using Taguchi design. *Journal of Pharmacological and Toxicological Methods* 61:334-342.
- Chithrani BD, Ghazani AA, Chan WCW. 2006. Determining the Size and Shape Dependence of Gold Nanoparticle Uptake into Mammalian Cells. *Nano Letters* 6:662-668.
- Chiu H-W, Xia T, Lee Y-H, Chen C-W, Tsai J-C, Wang Y-J. 2015. Cationic polystyrene nanospheres induce autophagic cell death through the induction of endoplasmic reticulum stress. *Nanoscale* 7:736-746.
- Cho W-S, Duffin R, Howie SEM, Scotton CJ, Wallace WAH, MacNee W, Bradley M, Megson IL, Donaldson K. 2011. Progressive severe lung injury by zinc oxide nanoparticles; the role of Zn²⁺ dissolution inside lysosomes. *Particle and Fibre Toxicology* 8:27.
- Clift MJD, Raemy DO, Endes C, Ali Z, Lehmann AD, Brandenberger C, Petri-Fink A, Wick P, Parak WJ, Gehr P, Schins RPF, Rothen-Rutishauser B. 2013. Can the Ames test provide an insight into nano-object mutagenicity? Investigating the interaction between nano-objects and bacteria. *Nanotoxicology* 7:1373-1385.
- Correia Carreira S, Walker L, Paul K, Saunders M. 2015a. In vitro models of the human placental barrier – In regione caecorum rex est luscus. *Nanotoxicology* 9:135-136.
- Correia Carreira S, Walker L, Paul K, Saunders M. 2015b. The toxicity, transport and uptake of nanoparticles in the in vitro BeWo b30 placental cell barrier model used within NanoTEST. *Nanotoxicology* 9:66-78.
- de Jong E, Barenys M, Hermsen SAB, Verhoef A, Ossendorp BC, Bessems JGM, Piersma AH. 2011. Comparison of the mouse Embryonic Stem cell Test, the rat Whole Embryo Culture and the Zebrafish Embryotoxicity Test as alternative methods for developmental toxicity testing of six 1,2,4-triazoles. *Toxicology and Applied Pharmacology* 253:103-111.
- De Matteis V. 2017. Exposure to Inorganic Nanoparticles: Routes of Entry, Immune Response, Biodistribution and In Vitro/In Vivo Toxicity Evaluation. *Toxics* 5:29.
- Devriese S, Van den Bossche L, Van Welden S, Holvoet T, Pinheiro I, Hindryckx P, De Vos M, Laukens D. 2017. T84 monolayers are superior to Caco-2 as a model system of colonocytes. *Histochemistry and Cell Biology* 148:85-93.
- Dharmasathaphorn K, McRoberts JA, Mandel KG, Tisdale LD, Masui H. 1984. A human colonic tumor cell line that maintains vectorial electrolyte transport. *American Journal of Physiology-Gastrointestinal and Liver Physiology* 246:G204-G208.
- Di Guglielmo C, López DR, De Lapuente J, Mallafre JML, Suárez MB. 2010. Embryotoxicity of cobalt ferrite and gold nanoparticles: A first in vitro approach. *Reproductive Toxicology* 30:271-276.
- Ding R, Yang P, Yang Y, Yang Z, Luo L, Li H, Wang Q. 2018. Characterisation of silver release from nanoparticle-treated baby products. *Food Additives & Contaminants: Part A* 35:2052-2061.

- Drake PL, Hazelwood KJ. 2005. Exposure-Related Health Effects of Silver and Silver Compounds: A Review. *Annals of Work Exposures and Health* 49:575-585.
- Durán N, Marcato PD. 2013. Nanobiotechnology perspectives. Role of nanotechnology in the food industry: a review. *International Journal of Food Science & Technology* 48:1127-1134.
- EFSA Scientific Committee, Hardy A, Benford D, Halldorsson T, Jeger MJ, Knutsen HK, More S, Naegeli H, Noteborn H, Ockleford C, Ricci A, Rychen G, Schlatter JR, Silano V, Solecki R, Turck D, Younes M, Chaudhry Q, Cubadda F, Gott D, Oomen A, Weigel S, Karamitrou M, Schoonjans R, Mortensen A. 2018. Guidance on risk assessment of the application of nanoscience and nanotechnologies in the food and feed chain: Part 1, human and animal health. *EFSA Journal* 16:e05327.
- Egger L, Ménard O, Delgado-Andrade C, Alvito P, Assunção R, Balance S, Barberá R, Brodkorb A, Cattenoz T, Clemente A, Comi I, Dupont D, Garcia-Llatas G, Lagarda MJ, Le Feunteun S, JanssenDuijghuijsen L, Karakaya S, Lesmes U, Mackie AR, Martins C, Meynier A, Miralles B, Murray BS, Pihlanto A, Picariello G, Santos CN, Simsek S, Recio I, Rigby N, Rioux L-E, Stoffers H, Tavares A, Tavares L, Turgeon S, Ulleberg EK, Vegarud GE, Vergères G, Portmann R. 2016. The harmonized INFOGEST in vitro digestion method: From knowledge to action. *Food Research International* 88:217-225.
- Eixenberger JE, Anders CB, Hermann RJ, Brown RJ, Reddy KM, Punnoose A, Wingett DG. 2017. Rapid Dissolution of ZnO Nanoparticles Induced by Biological Buffers Significantly Impacts Cytotoxicity. *Chemical Research in Toxicology* 30:1641-1651.
- Elespuru R, Pfuhler S, Aardema MJ, Chen T, Doak SH, Doherty A, Farabaugh CS, Kenny J, Manjanatha M, Mahadevan B, Moore MM, Ouédraogo G, Stankowski JLF, Tanir JY. 2018. Genotoxicity Assessment of Nanomaterials: Recommendations on Best Practices, Assays, and Methods. *Toxicological Sciences:kfy100-kfy100*.
- Ema M, Hougaard KS, Kishimoto A, Honda K. 2016. Reproductive and developmental toxicity of carbon-based nanomaterials: A literature review. *Nanotoxicology* 10:391-412.
- Foroozandeh P, Aziz AA. 2018. Insight into Cellular Uptake and Intracellular Trafficking of Nanoparticles. *Nanoscale Res Lett* 13:339-339.
- Francia V, Yang K, Deville S, Reker-Smit C, Nelissen I, Salvati A. 2019. Corona Composition Can Affect the Mechanisms Cells Use to Internalize Nanoparticles. *ACS Nano* 13:11107-11121.
- Fröhlich E, Roblegg E. 2012. Models for oral uptake of nanoparticles in consumer products. *Toxicology* 291:10-17.
- García-Rodríguez A, Vila L, Cortés C, Hernández A, Marcos R. 2018. Effects of differently shaped TiO₂NPs (nanospheres, nanorods and nanowires) on the in vitro model (Caco-2/HT29) of the intestinal barrier. *Particle and Fibre Toxicology* 15:33.
- Garcia T, Lafuente D, Blanco J, Sánchez DJ, Sirvent JJ, Domingo JL, Gómez M. 2016. Oral subchronic exposure to silver nanoparticles in rats. *Food and Chemical Toxicology* 92:177-187.
- Gatti AM, Tossini D, Gambarelli A, Montanari S, Capitani F. 2008. Investigation of the Presence of Inorganic Micro- and Nanosized Contaminants in Bread and Biscuits by Environmental Scanning Electron Microscopy. *Critical Reviews in Food Science and Nutrition* 49:275-282.

- Geiser M, Rothen-Rutishauser B, Kapp N, Schürch S, Kreyling W, Schulz H, Semmler M, Im Hof V, Heyder J, Gehr P. 2005. Ultrafine particles cross cellular membranes by nonphagocytic mechanisms in lungs and in cultured cells. *Environmental health perspectives* 113:1555-1560.
- Genschow E, Spielmann H, Scholz G, Pohl I, Seiler A, Clemann N, Bremer S, Becker K. 2004. Validation of the Embryonic Stem Cell Test in the International ECVAM Validation Study on Three In Vitro Embryotoxicity Tests. *Alternatives to Laboratory Animals* 32:209-244.
- Gluga AR, Skoglund S, Odnevall Wallinder I, Fadeel B, Karlsson HL. 2014. Size-dependent cytotoxicity of silver nanoparticles in human lung cells: the role of cellular uptake, agglomeration and Ag release. *Particle and Fibre Toxicology* 11:11.
- Goenaga-Infante H, Bartczak D. 2020. Chapter 3.1.1 - Single particle inductively coupled plasma mass spectrometry (spICP-MS). In: Hodoroaba V-D, Unger WES, Shard AG, eds. *Characterization of Nanoparticles*. Elsevier, 65-77.
- Gonzalez L, Lison D, Kirsch-Volders M. 2008. Genotoxicity of engineered nanomaterials: A critical review. *Nanotoxicology* 2:252-273.
- Goodman BE. 2010. Insights into digestion and absorption of major nutrients in humans. *Advances in Physiology Education* 34:44-53.
- Gopalan RC, Osman IF, Amani A, De Matas M, Anderson D. 2009. The effect of zinc oxide and titanium dioxide nanoparticles in the Comet assay with UVA photoactivation of human sperm and lymphocytes. *Nanotoxicology* 3:33-39.
- He C, Hu Y, Yin L, Tang C, Yin C. 2010. Effects of particle size and surface charge on cellular uptake and biodistribution of polymeric nanoparticles. *Biomaterials* 31:3657-3666.
- He D, Garg S, Wang Z, Li L, Rong H, Ma X, Li G, An T, Waite TD. 2019. Silver sulfide nanoparticles in aqueous environments: formation, transformation and toxicity. *Environmental Science: Nano* 6:1674-1687.
- Higashisaka K, Yoshioka Y, Tsutsumi Y. 2015. Applications and Safety of Nanomaterials Used in the Food Industry. *Food Safety* 3:39-47.
- Hougaard KS, Campagnolo L, Chavatte-Palmer P, Tarrade A, Rousseau-Ralliard D, Valentino S, Park MVDZ, de Jong WH, Wolterink G, Piersma AH, Ross BL, Hutchison GR, Hansen JS, Vogel U, Jackson P, Slama R, Pietrojusti A, Cassee FR. 2015. A perspective on the developmental toxicity of inhaled nanoparticles. *Reproductive Toxicology* 56:118-140.
- Hsiao I-L, Bierkandt FS, Reichardt P, Luch A, Huang Y-J, Jakubowski N, Tentschert J, Haase A. 2016. Quantification and visualization of cellular uptake of TiO₂ and Ag nanoparticles: comparison of different ICP-MS techniques. *Journal of Nanobiotechnology* 14:50.
- Hsiao IL, Hsieh Y-K, Wang C-F, Chen IC, Huang Y-J. 2015. Trojan-Horse Mechanism in the Cellular Uptake of Silver Nanoparticles Verified by Direct Intra- and Extracellular Silver Speciation Analysis. *Environmental Science & Technology* 49:3813-3821.
- Hubatsch I, Ragnarsson EGE, Artursson P. 2007. Determination of drug permeability and prediction of drug absorption in Caco-2 monolayers. *Nature Protocols* 2:2111.
- Ikeda K, Utoguchi N, Tsutsui H, Yamaue S, Homemoto M, Nakao E, Hukunaga Y, Yamasaki K, Myotoku M, Hirotani Y. 2011. In Vitro Approaches to Evaluate Placental Drug Transport by Using

- Differentiating JEG-3 Human Choriocarcinoma Cells. *Basic & Clinical Pharmacology & Toxicology* 108:138-145.
- Jeevanandam J, Barhoum A, Chan YS, Dufresne A, Danquah MK. 2018. Review on nanoparticles and nanostructured materials: history, sources, toxicity and regulations. *Beilstein journal of nanotechnology* 9:1050-1074.
- Jin Y, Song Y, Zhu X, Zhou D, Chen C, Zhang Z, Huang Y. 2012. Goblet cell-targeting nanoparticles for oral insulin delivery and the influence of mucus on insulin transport. *Biomaterials* 33:1573-1582.
- Juch H, Nikitina L, Debbage P, Dohr G, Gauster M. 2013. Nanomaterial interference with early human placenta: Sophisticated matter meets sophisticated tissues. *Reproductive Toxicology* 41:73-79.
- Kadiyala I, Loo Y, Roy K, Rice J, Leong KW. 2010. Transport of chitosan–DNA nanoparticles in human intestinal M-cell model versus normal intestinal enterocytes. *European Journal of Pharmaceutical Sciences* 39:103-109.
- Kaegi R, Voegelin A, Sinnet B, Zuleeg S, Hagendorfer H, Burkhardt M, Siegrist H. 2011. Behavior of Metallic Silver Nanoparticles in a Pilot Wastewater Treatment Plant. *Environmental Science & Technology* 45:3902-3908.
- Karlsson HL, Cronholm P, Gustafsson J, Möller L. 2008. Copper Oxide Nanoparticles Are Highly Toxic: A Comparison between Metal Oxide Nanoparticles and Carbon Nanotubes. *Chemical Research in Toxicology* 21:1726-1732.
- Kästner C, Lampen A, Thünemann AF. 2018. What happens to the silver ions? – Silver thiocyanate nanoparticle formation in an artificial digestion. *Nanoscale* 10:3650-3653.
- Kästner C, Lichtenstein D, Lampen A, Thünemann AF. 2017. Monitoring the fate of small silver nanoparticles during artificial digestion. *Colloids and Surfaces A: Physicochemical and Engineering Aspects* 526:76-81.
- Kim B, Park C-S, Murayama M, Hochella MF. 2010. Discovery and Characterization of Silver Sulfide Nanoparticles in Final Sewage Sludge Products. *Environmental Science & Technology* 44:7509-7514.
- Kittler S, Greulich C, Diendorf J, Köller M, Epple M. 2010. Toxicity of Silver Nanoparticles Increases during Storage Because of Slow Dissolution under Release of Silver Ions. *Chemistry of Materials* 22:4548-4554.
- Kloet SK, Walczak AP, Lousse J, van den Berg HHJ, Bouwmeester H, Tromp P, Fokkink RG, Rietjens IMCM. 2015. Translocation of positively and negatively charged polystyrene nanoparticles in an in vitro placental model. *Toxicology in Vitro* 29:1701-1710.
- Könen-Adıgüzel S, Ergene S. 2018. In vitro evaluation of the genotoxicity of CeO₂ nanoparticles in human peripheral blood lymphocytes using cytokinesis-block micronucleus test, comet assay, and gamma H2AX. *Toxicology and Industrial Health* 34:293-300.
- Kong F, Singh RP. 2010. A Human Gastric Simulator (HGS) to Study Food Digestion in Human Stomach. *Journal of Food Science* 75:E627-E635.

- Kroll A, Pillukat MH, Hahn D, Schnekenburger J. 2009. Current in vitro methods in nanoparticle risk assessment: Limitations and challenges. *European Journal of Pharmaceutics and Biopharmaceutics* 72:370-377.
- Kumar A, Pandey AK, Singh SS, Shanker R, Dhawan A. 2011. Cellular uptake and mutagenic potential of metal oxide nanoparticles in bacterial cells. *Chemosphere* 83:1124-1132.
- Kuo LJ, Yang L-X. 2008. γ -H2AX - A Novel Biomarker for DNA Double-strand Breaks. *In Vivo* 22:305-309.
- Landsiedel R, Kapp MD, Schulz M, Wiench K, Oesch F. 2009. Genotoxicity investigations on nanomaterials: Methods, preparation and characterization of test material, potential artifacts and limitations—Many questions, some answers. *Mutation Research/Reviews in Mutation Research* 681:241-258.
- Langevin D, Lozano O, Salvati A, Kestens V, Monopoli M, Raspaud E, Mariot S, Salonen A, Thomas S, Driessen M, Haase A, Nelissen I, Smisdom N, Pompa PP, Maiorano G, Puntès V, Puchowicz D, Stępnik M, Suárez G, Riediker M, Benetti F, Mičetić I, Venturini M, Kreyling WG, van der Zande M, Bouwmeester H, Milani S, Rädler JO, Mülhopt S, Lynch I, Dawson K. 2018. Inter-laboratory comparison of nanoparticle size measurements using dynamic light scattering and differential centrifugal sedimentation. *NanoImpact* 10:97-107.
- Lee J-Y, Kim JS, Cho H-J, Kim D-D. 2014. Poly(styrene)-b-poly(DL-lactide) copolymer-based nanoparticles for anticancer drug delivery. *International journal of nanomedicine* 9:2803-2813.
- Lefebvre DE, Venema K, Gombau L, Valerio LG, Raju J, Bondy GS, Bouwmeester H, Singh RP, Clippinger AJ, Collnot E-M, Mehta R, Stone V. 2015. Utility of models of the gastrointestinal tract for assessment of the digestion and absorption of engineered nanomaterials released from food matrices. *Nanotoxicology* 9:523-542.
- Lehman SE, Morris AS, Mueller PS, Salem AK, Grassian VH, Larsen SC. 2016. Silica nanoparticle-generated ROS as a predictor of cellular toxicity: mechanistic insights and safety by design. *Environmental Science: Nano* 3:56-66.
- Lesniak A, Campbell A, Monopoli MP, Lynch I, Salvati A, Dawson KA. 2010. Serum heat inactivation affects protein corona composition and nanoparticle uptake. *Biomaterials* 31:9511-9518.
- Lesniak A, Fenaroli F, Monopoli MP, Åberg C, Dawson KA, Salvati A. 2012. Effects of the Presence or Absence of a Protein Corona on Silica Nanoparticle Uptake and Impact on Cells. *ACS Nano* 6:5845-5857.
- Li Y, McClements DJ. 2010. New Mathematical Model for Interpreting pH-Stat Digestion Profiles: Impact of Lipid Droplet Characteristics on in Vitro Digestibility. *Journal of Agricultural and Food Chemistry* 58:8085-8092.
- Lichtenstein D, Ebmeyer J, Knappe P, Juling S, Böhmert L, Selve S, Niemann B, Braeuning A, Thünemann Andreas F, Lampen A. 2015. Impact of food components during in vitro digestion of silver nanoparticles on cellular uptake and cytotoxicity in intestinal cells. *Biological Chemistry*. 1255.
- Liu F, Soares MJ, Audus KL. 1997. Permeability properties of monolayers of the human trophoblast cell line BeWo. *American Journal of Physiology-Cell Physiology* 273:C1596-C1604.
- Liu L, Takenaka T, Zinchenko AA, Chen N, Inagaki S, Asada H, Kishida T, Mazda O, Murata S, Yoshikawa K. 2007. Cationic Silica Nanoparticles are Efficiently Transferred into Mammalian Cells. 2007 International Symposium on Micro-NanoMechatronics and Human Science. 281-285.

- Liu S, Liu Y, Pan B, He Y, Li B, Zhou D, Xiao Y, Qiu H, Vijver MG, Peijnenburg WJGM. 2020. The promoted dissolution of copper oxide nanoparticles by dissolved humic acid: Copper complexation over particle dispersion. *Chemosphere* 245:125612.
- López-Serrano A, Olivas RM, Landaluze JS, Cámara C. 2014. Nanoparticles: a global vision. Characterization, separation, and quantification methods. Potential environmental and health impact. *Analytical Methods* 6:38-56.
- Louisse J, Rijkers D, Stoopen G, Holleboom WJ, Delagrangé M, Molthof E, Mulder PPJ, Hoogenboom RLAP, Audebert M, Peijnenburg AACM. 2019. Determination of genotoxic potencies of pyrrolizidine alkaloids in HepaRG cells using the γ H2AX assay. *Food and Chemical Toxicology* 131:110532.
- Lynch I, Salvati A, Dawson KA. 2009. What does the cell see? *Nature Nanotechnology* 4:546.
- Mahler GJ, Shuler ML, Glahn RP. 2009. Characterization of Caco-2 and HT29-MTX cocultures in an in vitro digestion/cell culture model used to predict iron bioavailability. *The Journal of Nutritional Biochemistry* 20:494-502.
- Manley SW, Li H, Mortimer RH. 2005. The BeWo choriocarcinoma cell line as a model of iodide transport by placenta. *Placenta* 26:380-386.
- Mattarozzi M, Suman M, Cascio C, Calestani D, Weigel S, Undas A, Peters R. 2017. Analytical approaches for the characterization and quantification of nanoparticles in food and beverages. *Analytical and Bioanalytical Chemistry* 409:63-80.
- Maurer EI, Sharma M, Schlager JJ, Hussain SM. 2014. Systematic analysis of silver nanoparticle ionic dissolution by tangential flow filtration: toxicological implications. *Nanotoxicology* 8:718-727.
- McClements DJ, Xiao H. 2017. Is nano safe in foods? Establishing the factors impacting the gastrointestinal fate and toxicity of organic and inorganic food-grade nanoparticles. *npj Science of Food* 1:6.
- McTeer J, Dean AP, White KN, Pittman JK. 2014. Bioaccumulation of silver nanoparticles into *Daphnia magna* from a freshwater algal diet and the impact of phosphate availability. *Nanotoxicology* 8:305-316.
- Mirshafiee V, Kim R, Park S, Mahmoudi M, Kraft ML. 2016. Impact of protein pre-coating on the protein corona composition and nanoparticle cellular uptake. *Biomaterials* 75:295-304.
- Misra SK, Dybowska A, Berhanu D, Luoma SN, Valsami-Jones E. 2012. The complexity of nanoparticle dissolution and its importance in nanotoxicological studies. *Science of The Total Environment* 438:225-232.
- Monopoli MP, Åberg C, Salvati A, Dawson KA. 2012. Biomolecular coronas provide the biological identity of nanosized materials. *Nature Nanotechnology* 7:779.
- Mühlfeld C, Rothen-Rutishauser B, Vanhecke D, Blank F, Gehr P, Ochs M. 2007. Visualization and quantitative analysis of nanoparticles in the respiratory tract by transmission electron microscopy. *Particle and Fibre Toxicology* 4:11.
- Muraleetharan V, Mantaj J, Swedrowska M, Vllasaliu D. 2019. Nanoparticle modification in biological media: implications for oral nanomedicines. *RSC Advances* 9:40487-40497.

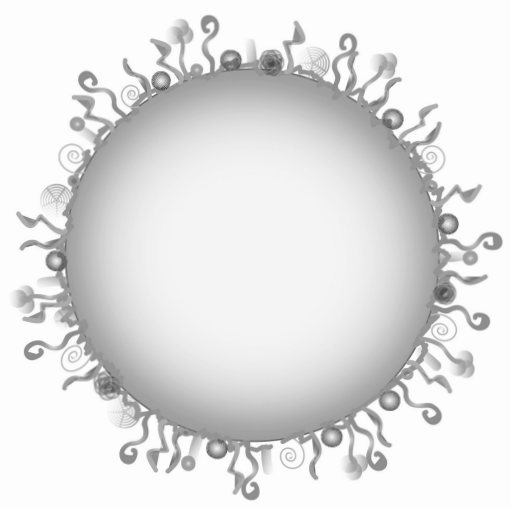
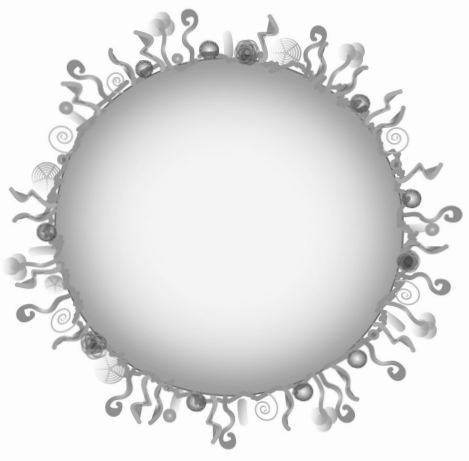
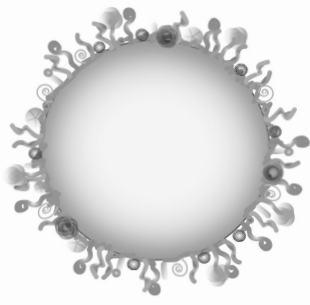
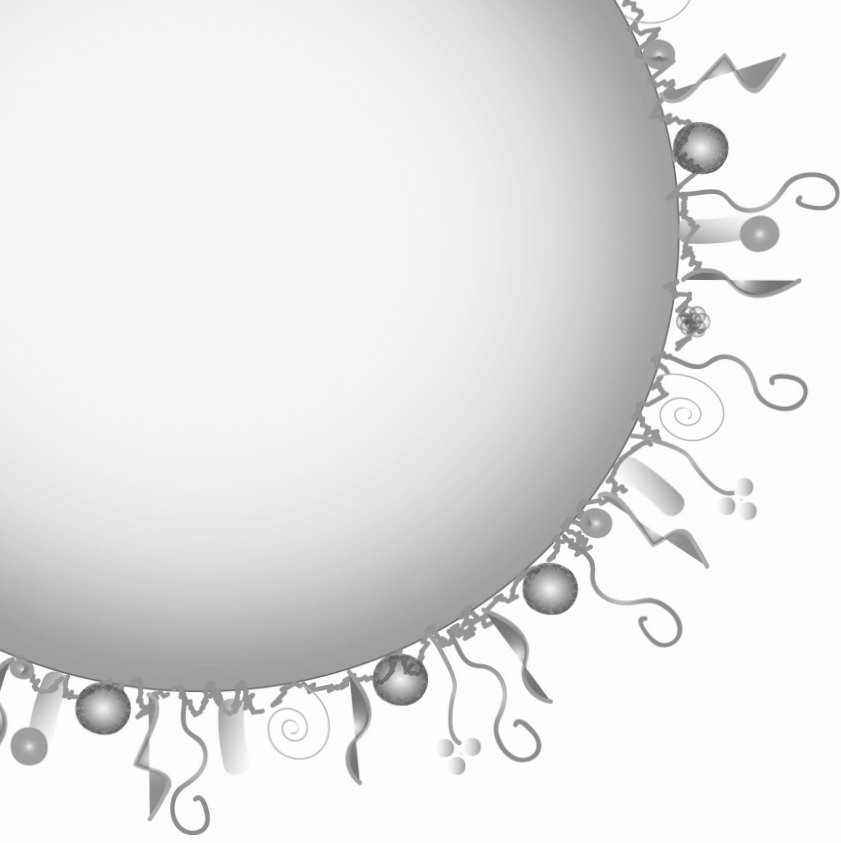
- Mwilu SK, El Badawy AM, Bradham K, Nelson C, Thomas D, Scheckel KG, Tolaymat T, Ma L, Rogers KR. 2013. Changes in silver nanoparticles exposed to human synthetic stomach fluid: Effects of particle size and surface chemistry. *Science of The Total Environment* 447:90-98.
- Myllynen PK, Loughran MJ, Howard CV, Sormunen R, Walsh AA, Vähäkangas KH. 2008. Kinetics of gold nanoparticles in the human placenta. *Reproductive Toxicology* 26:130-137.
- Nagy A, Zane A, Cole SL, Severance M, Dutta PK, Waldman WJ. 2011. Contrast of the Biological Activity of Negatively and Positively Charged Microwave Synthesized CdSe/ZnS Quantum Dots. *Chemical Research in Toxicology* 24:2176-2188.
- Nath Roy D, Goswami R, Pal A. 2017. Nanomaterial and toxicity: what can proteomics tell us about the nanotoxicology? *Xenobiotica* 47:632-643.
- Nowack B, Krug HF, Height M. 2011. 120 Years of Nanosilver History: Implications for Policy Makers. *Environmental Science & Technology* 45:1177-1183.
- Oberdörster G. 2010. Safety assessment for nanotechnology and nanomedicine: concepts of nanotoxicology. *Journal of Internal Medicine* 267:89-105.
- Oberdörster G, Maynard A, Donaldson K, Castranova V, Fitzpatrick J, Ausman K, Carter J, Karn B, Kreyling W, Lai D, Olin S, Monteiro-Riviere N, Warheit D, Yang H, Group ArftIRFRSINTSW. 2005. Principles for characterizing the potential human health effects from exposure to nanomaterials: elements of a screening strategy. *Particle and Fibre Toxicology* 2:8.
- OECD. 1997. Test No. 471: Bacterial Reverse Mutation Test.
- Oomen AG, Rempelberg CJM, Bruil MA, Dobbe CJG, Pereboom DPKH, Sips AJAM. 2003a. Development of an In Vitro Digestion Model for Estimating the Bioaccessibility of Soil Contaminants. *Archives of Environmental Contamination and Toxicology* 44:0281-0287.
- Oomen AG, Tolls J, Sips AJAM, Van den Hoop MAGT. 2003b. Lead Speciation in Artificial Human Digestive Fluid. *Archives of Environmental Contamination and Toxicology* 44:0107-0115.
- Osman IF, Baumgartner A, Cemeli E, Fletcher JN, Anderson D. 2010. Genotoxicity and cytotoxicity of zinc oxide and titanium dioxide in HEp-2 cells. *Nanomedicine* 5:1193-1203.
- Park MVDZ, Annema W, Salvati A, Lesniak A, Elsaesser A, Barnes C, McKerr G, Howard CV, Lynch I, Dawson KA, Piersma AH, de Jong WH. 2009. In vitro developmental toxicity test detects inhibition of stem cell differentiation by silica nanoparticles. *Toxicology and Applied Pharmacology* 240:108-116.
- Park MVDZ, Neigh AM, Vermeulen JP, de la Fonteyne LJJ, Verharen HW, Briedé JJ, van Loveren H, de Jong WH. 2011. The effect of particle size on the cytotoxicity, inflammation, developmental toxicity and genotoxicity of silver nanoparticles. *Biomaterials* 32:9810-9817.
- Pederzoli F, Tosi G, Vandelli MA, Belletti D, Forni F, Ruozi B. 2017. Protein corona and nanoparticles: how can we investigate on? *Wiley Interdisciplinary Reviews: Nanomedicine and Nanobiotechnology* 9:e1467.
- Peters R, Herrera-Rivera Z, Undas A, van der Lee M, Marvin H, Bouwmeester H, Weigel S. 2015. Single particle ICP-MS combined with a data evaluation tool as a routine technique for the analysis of nanoparticles in complex matrices. *Journal of Analytical Atomic Spectrometry* 30:1274-1285.

- Peters R, Kramer E, Oomen AG, Herrera Rivera ZE, Oegema G, Tromp PC, Fokkink R, Rietveld A, Marvin HJP, Weigel S, Peijnenburg AACM, Bouwmeester H. 2012. Presence of Nano-Sized Silica during In Vitro Digestion of Foods Containing Silica as a Food Additive. *ACS Nano* 6:2441-2451.
- Peters RJB, Oomen AG, van Bommel G, van Vliet L, Undas AK, Munniks S, Bleys RLAW, Tromp PC, Brand W, van der Lee M. 2020. Silicon dioxide and titanium dioxide particles found in human tissues. *Nanotoxicology*:1-13.
- Petersen EJ, Nelson BC. 2010. Mechanisms and measurements of nanomaterial-induced oxidative damage to DNA. *Analytical and Bioanalytical Chemistry* 398:613-650.
- Pindřáková L, Kašpárková V, Kejlová K, Dvořáková M, Krsek D, Jírová D, Kašparová L. 2017. Behaviour of silver nanoparticles in simulated saliva and gastrointestinal fluids. *International Journal of Pharmaceutics* 527:12-20.
- Pino Pd, Pelaz B, Zhang Q, Maffre P, Nienhaus GU, Parak WJ. 2014. Protein corona formation around nanoparticles – from the past to the future. *Materials Horizons* 1:301-313.
- Polak-Charcon S, Shoham J, Ben-Shaul Y. 1978. Junction formation in trypsinized cells of human adenocarcinoma cell line. *Experimental Cell Research* 116:1-13.
- Poulsen MS, Mose T, Maroun LL, Mathiesen L, Knudsen LE, Rytting E. 2015. Kinetics of silica nanoparticles in the human placenta. *Nanotoxicology* 9:79-86.
- Powers CM, Bale AS, Kraft AD, Makris SL, Trecki J, Cowden J, Hotchkiss A, Gillespie PA. 2013. Developmental Neurotoxicity of Engineered Nanomaterials: Identifying Research Needs to Support Human Health Risk Assessment. *Toxicological Sciences* 134:225-242.
- Prajitha N, Athira SS, Mohanan PV. 2019. Bio-interactions and risks of engineered nanoparticles. *Environmental Research* 172:98-108.
- Rahman Q, Lohani M, Dopp E, Pemsel H, Jonas L, Weiss DG, Schiffmann D. 2002. Evidence that ultrafine titanium dioxide induces micronuclei and apoptosis in Syrian hamster embryo fibroblasts. *Environmental Health Perspectives* 110:797-800.
- Ramos AP. 2017. 4 - Dynamic Light Scattering Applied to Nanoparticle Characterization. In: Da Róz AL, Ferreira M, de Lima Leite F, Oliveira ON, eds. *Nanocharacterization Techniques*. William Andrew Publishing, 99-110.
- Rasmussen K, Rauscher H, Kearns P, González M, Riego Sintes J. 2019. Developing OECD test guidelines for regulatory testing of nanomaterials to ensure mutual acceptance of test data. *Regulatory Toxicology and Pharmacology* 104:74-83.
- Riediker M, Zink D, Kreyling W, Oberdörster G, Elder A, Graham U, Lynch I, Duschl A, Ichihara G, Ichihara S, Kobayashi T, Hisanaga N, Umezawa M, Cheng T-J, Handy R, Gulumian M, Tinkle S, Cassee F. 2019. Particle toxicology and health - where are we? *Particle and Fibre Toxicology* 16:19.
- Ruby MV, Davis A, Schoof R, Eberle S, Sellstone CM. 1996. Estimation of Lead and Arsenic Bioavailability Using a Physiologically Based Extraction Test. *Environmental Science & Technology* 30:422-430.
- Sakho EHM, Allahyari E, Oluwafemi OS, Thomas S, Kalarikkal N. 2017. Chapter 2 - Dynamic Light Scattering (DLS). In: Thomas S, Thomas R, Zachariah AK, Mishra RK, eds. *Thermal and Rheological Measurement Techniques for Nanomaterials Characterization*. Elsevier, 37-49.

- Saunders M. 2009. Transplacental transport of nanomaterials. *Wiley Interdisciplinary Reviews: Nanomedicine and Nanobiotechnology* 1:671-684.
- Sedelnikova OA, Rogakou EP, Panyutin IG, Bonner WM. 2002. Quantitative Detection of ¹²⁵I-U-Induced DNA Double-Strand Breaks with γ -H2AX Antibody. *Radiation Research* 158:486-492, 7.
- Seiler AEM, Spielmann H. 2011. The validated embryonic stem cell test to predict embryotoxicity in vitro. *Nature Protocols* 6:961.
- Sieg H, Kästner C, Krause B, Meyer T, Burel A, Böhmert L, Lichtenstein D, Jungnickel H, Tentschert J, Laux P, Braeuning A, Estrela-Lopis I, Gauffre F, Fessard V, Meijer J, Luch A, Thünemann AF, Lampen A. 2017. Impact of an Artificial Digestion Procedure on Aluminum-Containing Nanomaterials. *Langmuir* 33:10726-10735.
- Singh N, Manshian B, Jenkins GJS, Griffiths SM, Williams PM, Maffei TGG, Wright CJ, Doak SH. 2009. NanoGenotoxicology: The DNA damaging potential of engineered nanomaterials. *Biomaterials* 30:3891-3914.
- Strugari AFG, Stan MS, Gharbia S, Hermenean A, Dinischiotu A. 2018. Characterization of Nanoparticle Intestinal Transport Using an In Vitro Co-Culture Model. *Nanomaterials (Basel)* 9:5.
- Studer AM, Limbach LK, Van Duc L, Krumeich F, Athanassiou EK, Gerber LC, Moch H, Stark WJ. 2010. Nanoparticle cytotoxicity depends on intracellular solubility: Comparison of stabilized copper metal and degradable copper oxide nanoparticles. *Toxicology Letters* 197:169-174.
- Su D. 2017. Advanced electron microscopy characterization of nanomaterials for catalysis. *Green Energy & Environment* 2:70-83.
- Sun X-Y, Gan Q-Z, Ouyang J-M. 2017. Size-dependent cellular uptake mechanism and cytotoxicity toward calcium oxalate on Vero cells. *Scientific Reports* 7:41949.
- Tedja R, Lim M, Amal R, Marquis C. 2012. Effects of Serum Adsorption on Cellular Uptake Profile and Consequent Impact of Titanium Dioxide Nanoparticles on Human Lung Cell Lines. *ACS Nano* 6:4083-4093.
- Thalmann B, Voegelin A, Sinnet B, Morgenroth E, Kaegi R. 2014. Sulfidation Kinetics of Silver Nanoparticles Reacted with Metal Sulfides. *Environmental Science & Technology* 48:4885-4892.
- Tina Buerki-Thurnherra UvM, Peter Wicki. 2012. Knocking at the door of the unborn child: engineered nanoparticles at the human placental barrier. *Swiss medical weekly* 142.
- Van de Wiele T, Van den Abbeele P, Ossieur W, Possemiers S, Marzorati M. 2015. The Simulator of the Human Intestinal Microbial Ecosystem (SHIME®). In: Verhoeckx K, Cotter P, López-Expósito I, Kleiveland C, Lea T, Mackie A, Requena T, Swiatecka D, Wichers H, eds. *The Impact of Food Bioactives on Health: in vitro and ex vivo models*. Cham: Springer International Publishing, 305-317.
- Van de Wiele TR, Oomen AG, Wragg J, Cave M, Minekus M, Hack A, Cornelis C, Rempelberg CJM, De Zwart LL, Klinck B, Van Wijnen J, Verstraete W, Sips AJAM. 2007. Comparison of five in vitro digestion models to in vivo experimental results: Lead bioaccessibility in the human gastrointestinal tract. *Journal of Environmental Science and Health, Part A* 42:1203-1211.

- van der Zande M, Undas AK, Kramer E, Monopoli MP, Peters RJ, Garry D, Antunes Fernandes EC, Hendriksen PJ, Marvin HJP, Peijnenburg AA, Bouwmeester H. 2016. Different responses of Caco-2 and MCF-7 cells to silver nanoparticles are based on highly similar mechanisms of action. *Nanotoxicology* 10:1431-1441.
- Vance ME, Kuiken T, Vejerano EP, McGinnis SP, Hochella MF, Jr., Rejeski D, Hull MS. 2015. Nanotechnology in the real world: Redeveloping the nanomaterial consumer products inventory. *Beilstein Journal of Nanotechnology* 6:1769-1780.
- Vandebriel RJ, De Jong WH. 2012. A review of mammalian toxicity of ZnO nanoparticles. *Nanotechnology, science and applications* 5:61-71.
- Vardakou M, Mercuri A, Barker SA, Craig DQM, Faulks RM, Wickham MSJ. 2011. Achieving antral grinding forces in biorelevant in vitro models: comparing the USP dissolution apparatus II and the dynamic gastric model with human in vivo data. *AAPS PharmSciTech* 12:620-626.
- Varela JA, Bexiga MG, Åberg C, Simpson JC, Dawson KA. 2012. Quantifying size-dependent interactions between fluorescently labeled polystyrene nanoparticles and mammalian cells. *Journal of Nanobiotechnology* 10:39.
- Versantvoort CHM, Oomen AG, Van de Kamp E, Rempelberg CJM, Sips AJAM. 2005. Applicability of an in vitro digestion model in assessing the bioaccessibility of mycotoxins from food. *Food and Chemical Toxicology* 43:31-40.
- Villanueva A, Cañete M, Roca AG, Calero M, Veintemillas-Verdaguer S, Serna CJ, del Puerto Morales M, Miranda R. 2009. The influence of surface functionalization on the enhanced internalization of magnetic nanoparticles in cancer cells. *Nanotechnology* 20:115103.
- Walczak AP, Fokkink R, Peters R, Tromp P, Herrera Rivera ZE, Rietjens IMCM, Hendriksen PJM, Bouwmeester H. 2012. Behaviour of silver nanoparticles and silver ions in an in vitro human gastrointestinal digestion model. *Nanotoxicology* 7:1198-1210.
- Walczak AP, Kramer E, Hendriksen PJM, Helsdingen R, van der Zande M, Rietjens IMCM, Bouwmeester H. 2015. In vitro gastrointestinal digestion increases the translocation of polystyrene nanoparticles in an in vitro intestinal co-culture model. *Nanotoxicology* 9:886-894.
- Wan R, Mo Y, Tong R, Gao M, Zhang Q. 2019. Determination of Phosphorylated Histone H2AX in Nanoparticle-Induced Genotoxic Studies. In: Zhang Q, ed. *Nanotoxicity: Methods and Protocols*. New York, NY: Springer New York, 145-159.
- Wan R, Mo Y, Zhang Z, Jiang M, Tang S, Zhang Q. 2017. Cobalt nanoparticles induce lung injury, DNA damage and mutations in mice. *Particle and Fibre Toxicology* 14:38.
- Wang S-H, Lee C-W, Chiou A, Wei P-K. 2010. Size-dependent endocytosis of gold nanoparticles studied by three-dimensional mapping of plasmonic scattering images. *Journal of Nanobiotechnology* 8:33.
- Watters GP, Smart DJ, Harvey JS, Austin CA. 2009. H2AX phosphorylation as a genotoxicity endpoint. *Mutation Research/Genetic Toxicology and Environmental Mutagenesis* 679:50-58.
- Weigel S, Peters R, Loeschner K, Grombe R, Linsinger TPJ. 2017. Results of an interlaboratory method performance study for the size determination and quantification of silver nanoparticles in chicken meat by single-particle inductively coupled plasma mass spectrometry (sp-ICP-MS). *Analytical and Bioanalytical Chemistry* 409:4839-4848.

- Wick P, Malek A, Manser P, Meili D, Maeder-Althaus X, Diener L, Diener P-A, Zisch A, Krug HF, Mandach Uv. 2010. Barrier Capacity of Human Placenta for Nanosized Materials. *Environmental Health Perspectives* 118:432-436.
- Wijnhoven SWP, Peijnenburg WJGM, Herberts CA, Hagens WI, Oomen AG, Heugens EHW. 2009. Nano-silver - a review of available data and knowledge gaps in human and environmental risk assessment. *Nanotoxicology* 3.
- Xie H, Mason Michael M, Wise John P. 2011. Genotoxicity of metal nanoparticles. *Reviews on Environmental Health*. 251.
- Yin Win K, Feng S-S. 2005. Effects of particle size and surface coating on cellular uptake of polymeric nanoparticles for oral delivery of anticancer drugs. *Biomaterials* 26:2713-2722.
- Zhang S, Li J, Lykotrafitis G, Bao G, Suresh S. 2009. Size-Dependent Endocytosis of Nanoparticles. *Advanced materials (Deerfield Beach, Fla.)* 21:419-424.
- Zhao X, Takabayashi F, Ibuki Y. 2016. Coexposure to silver nanoparticles and ultraviolet A synergistically enhances the phosphorylation of histone H2AX. *Journal of Photochemistry and Photobiology B: Biology* 162:213-222.
- Zhao Z, Ukidve A, Krishnan V, Mitragotri S. 2019. Effect of physicochemical and surface properties on in vivo fate of drug nanocarriers. *Advanced Drug Delivery Reviews* 143:3-21.



2

Impact of nanoparticle surface functionalization on the protein corona and cellular adhesion, uptake and transport

Ashraf Abdelkhalik, Meike van der Zande, Ans Punt, Richard Helsdingen, Sjef Boeren, Jacques J. M. Vervoort, Ivonne M. C. M. Rietjens and Hans Bouwmeester

Based on: Journal of Nanobiotechnology (2018) 16:70



ABSTRACT

Upon ingestion, nanoparticles can interact with the intestinal epithelial barrier potentially resulting in systemic uptake of nanoparticles (NPs). NPs properties have been described to influence the protein corona formation and subsequent cellular adhesion, uptake and transport. Here, we aimed to study the effects of NPs size and surface chemistry on the protein corona formation and subsequent cellular adhesion, uptake and transport. Caco-2 intestinal cells, were exposed to negatively charged polystyrene nanoparticles (PSNPs) (50 and 200 nm), functionalized with sulfone or carboxyl groups, at nine nominal concentrations (15-250 $\mu\text{g}/\text{mL}$) for 10 up to 120 minutes. The protein coronas were analysed by LC-MS/MS. Subtle differences in the protein composition of the two PSNPs with different surface chemistry were noted. High-content imaging analysis demonstrated that sulfone PSNPs were associated with the cells to a significantly higher extent than the other PSNPs. The apparent cellular adhesion and uptake of 200 nm PSNPs was not significantly increased compared to 50 nm PSNPs with the same surface charge and chemistry. Surface chemistry outweighs the impact of size on the observed PSNPs cellular associations. Also, transport of the sulfone PSNPs through the monolayer of cells was significantly higher than that of carboxyl PSNPs. The results suggest that the composition of the protein corona and the PSNPs surface chemistry influences cellular adhesion, uptake and monolayer transport, which might be predictive of the intestinal transport potency of NPs.

INTRODUCTION

Commercial, therapeutical and technological interests in engineered nanoparticles (NPs) are still increasing because of their unique physicochemical properties that make them promising materials for a wide range of new applications. NPs are currently being used in the agri-food sector in particular within domains like food processing, packaging and as nutraceutical delivery systems (Peters *et al.* 2016; Bouwmeester *et al.* 2014; Das *et al.* 2011). The unique size-related properties may also pose a risk to human health because of their interactions with biomolecules, cells and organs, potentially leading to adverse outcomes (Zhang *et al.* 2013; Hansen *et al.* 2008). The oral route of exposure is considered one of the main exposure routes, especially for NPs exploited in agri-food applications. To assess the likelihood of NPs to internalize and cross the intestinal epithelial barrier several *in vitro* intestinal epithelial models have been developed (Walczak *et al.* 2015; Yun *et al.* 2013; des Rieux *et al.* 2006; Shakweh *et al.* 2004). Rapid screening of the intestinal transport potential of NPs is important in a tiered risk assessment or grouping approach (Arts *et al.* 2015).

The cellular uptake/transport of NPs is highly dependent on both the intrinsic and extrinsic properties of NPs. It is well known that intrinsic NPs properties, such as size (des Rieux *et al.* 2006) and surface modifications affect cellular uptake (Bhattacharjee *et al.* 2013; He *et al.* 2010). Upon contact with biological matrices like gastrointestinal juices and body fluids NPs are immediately covered with proteins generating the so-called protein corona (Lynch *et al.* 2014). The composition of the protein corona formed on the NPs surfaces is highly influenced by the physicochemical properties of the NPs (Ritz *et al.* 2015; Hühn *et al.* 2013). Consequently, the NPs corona is considered as one of the major players affecting the biological interactions of the NPs, including their cytotoxicity, uptake and transport (Ritz *et al.* 2015; Kim *et al.* 2014; Walczyk *et al.* 2010). Additionally, the correlation between NPs properties and their cellular uptake/transport appears to be cell type dependent, indicating that different kinds of uptake/transport mechanisms could be in place (Fröhlich 2012; Yin Win and Feng 2005). Due to these complexities, no key descriptor has been identified so far for NPs uptake/transport.

Here we aimed to study the effects of the size and surface chemistry of NPs on the protein corona formation and their subsequent cellular adhesion, uptake and transport. Several

methods are available to study the cellular interactions of NPs at a single-cell level. High content (HC) imaging analysis has proven to be a highly successful and powerful tool in the field of drug discovery and toxicology, but it has rarely been used to study the behaviour and uptake of NPs (Anguissola 2014; Ramery and O'Brien 2014). Here, HC imaging was used to study the cellular associations of fluorescently labelled, negatively charged, polystyrene nanoparticles (PSNPs) on a single-cell level, using Caco-2 monolayers as an *in vitro* method that mimics the human intestinal epithelium. Also, the transport of these PSNPs was assessed to gain insights into the correlation between the cellular adhesion/uptake and transport of these PSNPs. Lastly, the composition of the protein corona was quantitatively determined using label-free liquid chromatography mass spectrometry (LC-MS/MS).

MATERIALS AND METHODS

Nanoparticles

Two 50 nm negatively charged, red fluorescently labelled PSNPs with different surface modifications were obtained from Magsphere[®] (Pasadena, USA). Namely, 2.5% (w/v) sulfonated particles and 2.5% (w/v) carboxylated PSNPs, further referred to as 50 nm (SM) and (CM) respectively. 50nm and 200nm negatively charged, 2.5% (w/v) yellow green fluorescently labelled carboxylated PSNPs (Fluoresbrite[®]) were obtained from Polysciences (Warrington, USA), further referred to as 50 nm (CP) and 200 nm (CP). All PSNPs suspensions were stored at 4°C and all experiments were performed using the same batch of PSNPs. Serial dilutions of the PSNPs were freshly prepared for every experiment in complete cell culture medium. Absence of detectable leakage of the fluorophores from the PSNPs used was confirmed by centrifugation of NPs after 24 hr incubations in cell culture medium at 37°C (Walczak *et al.* 2015).

Cell culture

Adherent human epithelial colorectal adenocarcinoma cells (Caco-2; ATCC[®] HTB-37[™]), were used at passage numbers 25-40. They were cultured and maintained in 75 cm² cell culture flasks (Corning[®]; New York, USA) at 37°C in a humidified 5% CO₂ atmosphere. Complete cell culture medium was prepared by supplementing Dulbecco's Modified Eagle Medium

(DMEM) culture medium (LONZA; Verviers, Belgium) with 10% (v/v) heat inactivated Foetal Bovine Serum (FBS) (Gibco®, Life technologies; New York, USA), 1% (v/v) of Penicillin-Streptomycin (Sigma-Aldrich; Steinheim, Germany) and 1% (v/v) of MEM Non-Essential Amino Acids (NEAA) (Gibco®, life technologies; New York, USA). The complete medium is further referred to as DMEM⁺.

Physicochemical characterization of PSNPs

Size and surface charge of PSNPs were characterized using dynamic light scattering (DLS) and zeta-potential measurements, respectively. Briefly, DLS measurements were performed on 10 µg/mL PSNPs suspended in water and/or DMEM⁺ using an ALV dynamic light scattering setup (ALV-Laser Vertriebsgesellschaft; Germany), consisting of a Thorn RFIB263KF photomultiplier detector, ALV-SP/86 goniometer, ALV 50/100/200/400/600 µm pinhole detection system, ALV7002 external correlator and a Cobolt Samba-300 DPSS laser. Each sample was measured 10 times for 30 seconds at an angle of 90°. The results are expressed as the hydrodynamic diameter that was calculated using AfterALV® software (AfterALV 1.0d, Dullware; USA). The zeta-potential was measured using a Malvern Zetasizer 2000 (Malvern Instruments; Malvern, UK) on 10 µg/mL PSNPs suspended in DMEM⁺. All samples were analysed in triplicate.

***In vitro* sedimentation, diffusion and dosimetry (ISDD) model for PSNPs**

The deposited fraction of the administered doses of the PSNPs (target cell dose) was calculated using the *In vitro* Sedimentation, Diffusion and Dosimetry (ISDD) model (Hinderliter *et al.* 2010). The following parameters were used as input in the ISDD model: the hydrodynamic diameters of the PSNPs in water and DMEM⁺ measured by DLS (Table 1), medium column height (10.9 mm), temperature (310°K), media density 1 g/mL and media viscosity 0.0009 N.s/m² (Elliott 2017; Fröhlich *et al.* 2013).

Cell viability

Cytotoxic effects of the PSNPs were determined using a Cell Proliferation Reagent WST-1 (Roche; Mannheim, Germany). Each well was seeded with 1×10⁵ cells/cm² in DMEM⁺ in 96-well flat bottom plates (Greiner bio-one; the Netherlands). Plates were incubated at 37°C, 5%

CO₂ for 24 hr. Attached cells were then exposed to 100 µL/well of freshly prepared serial dilutions of 50 nm- (SM), (CM), (CP) and 200 nm (CP) PSNPs (15, 25, 50, 75, 100, 200, 250, 500 and 750 µg/mL) for 3 and 24 hr. Afterwards the exposure medium was discarded and 10 µL of WST-1 solution was added with 90 µL of DMEM⁺ (without phenol red) to each well. The plates were incubated for 4 hr at 37°C, 5% CO₂ and absorbance was read at 490 nm and 630 nm on a plate reader (BioTek Synergy™ HT Multi-Mode Microplate reader; USA). Cell viability for each concentration of PSNPs was expressed as a percentage of the control. DMEM⁺ was used as a negative control and Triton-X100 (0.25%) (Sigma) was used as a positive control that decreased the viability to 29 ± 0.2 %.

PSNPs cellular adhesion and uptake studies and HC imaging

A cell suspension of 5×10⁴ cells/cm² was seeded in 96-well flat bottom black plates (Grenier bio-one; Frickenhausen, Germany) and incubated at 37°C, 5% CO₂ for 24 hr. Subsequently, the culture medium was aspirated and cells were exposed to 100 µL/well of 15, 25, 50, 75, 100, 200 and 250 µg/mL of each of the PSNPs (n=2) for 10, 20, 30, 60 and 120 minutes for the (SM) PSNPs and for 30, 60 and 120 minutes for the other PSNPs. Exposure medium was then aspirated and the cells were washed once with 100 µL/well PBS buffer at 37°C. As the PSNPs had different fluorescent labels, two different staining protocols were used. The cells exposed to the red 50 nm (SM) and (CM) PSNPs were incubated with a mixture (100 µL/well) of 4 µM Hoechst (Molecular Probes®, life technologies; USA) (blue; nucleus stain) and 1 µM Calcein AM cell permeant dye (Molecular Probes®, life technologies) (green; cytoplasm). The cells exposed to the yellow 50- and 200 nm (CP) PSNPs were incubated with a mixture (100 µL/well) of 4 µM Hoechst (blue; nucleus) and 1 µM deep red MitoTracker (Molecular Probes®, life technologies) (red; mitochondria). Cells were incubated in the dark at 37°C, 5% CO₂ for 30 minutes.

Cellular adhesion and uptake of PSNPs was analysed using a Cellavista™ HC imaging system (SynenTec Bio Services; Munster, Germany). This HC imaging system uses an automated, quantitative fluorescence microscope with image acquisition and software to analyse multiparameter fluorescent cellular signals to quantify the local fluorescence intensity (Franscini *et al.* 2011). The output data were further processed using Microsoft Excel® 2016 and Prism® (v.5.0; GraphPad®, USA). PSNPs adhesion and uptake was expressed as a

fluorescence intensity per cell and as a median fluorescence intensity of the entire cell population. Distribution profiles of PSNPs association and uptake in a cell population were made with Prism[®]. The number of cells correlating to each concentration bin was expressed as a percentage of the total number of exposed cells.

PSNPs cellular transport

Caco-2 cells were seeded at a density of 40,000 cells/cm² on transwell permeable PET inserts (0.4 µm pore size, 1.12 cm² surface area, Corning[®]; New York, USA). Cells were maintained for 21 days (37°C, 5% CO₂) and the apical and basolateral medium were changed every other day.

The integrity of the cell barrier was monitored by measuring the transepithelial electrical resistance (TEER) values with a chopstick electrode (STX01) connected to a Millicell ERS-2 Epithelial Volt- Ohm Meter (Millipore[®]; USA). Inserts with TEER values of 200 Ω.cm² and higher were used in the experiments. Additionally, the transport of lucifer yellow and 4- and 10 kDa- fluorescein isothiocyanate (FITC)-dextrans (Sigma-Aldrich; USA) was analysed by measuring the fluorescence intensity in the basolateral compartment after 1 hr exposure at 37°C at 485/530 nm using a BioTek Synergy™ HT Multi-Mode Microplate reader. Control samples received EGTA (Sigma-Aldrich) for 1 hr at 37°C to induce leakage of the cellular barrier (data not shown).

PSNPs exposure media were prepared at a concentration of 250 µg/mL in DMEM⁺, further diluted in DMEM⁺ when necessary and directly applied apically onto the cells (500 µl/insert) on day 21 of culture. After 24 hr of exposure, the basolateral medium was collected and fluorescence was measured at excitation/emission wavelengths of 530/590 nm and 485/530 nm, for red and yellow green PSNPs, respectively using a microplate reader. The results are expressed as a percentage of transported PSNPs from the total nominal dose of exposure. All experiments were conducted in triplicate.

Confocal microscopy

For confocal microscopy, 1.5×10⁴ cells/cm² were seeded into 8 well µ-Slides (Ibidi[®]; Martinsried, Germany) and incubated at 37°C, 5% CO₂ for 24 hr. Afterwards, medium was

discarded and cells were fixed with 200 μL /well of 4% paraformaldehyde for 15 minutes at room temperature. The fixation solution was discarded and cells were washed 3 times with 400 μL of PBS for 2 – 5 minutes, which was then replaced by 200 μL /well of permeabilization solution (FIX & PERM[®] Cell Fixation & Cell Permeabilization Kit, life Technologies). After 15 minutes incubation at room temperature the cells were washed 3 times with 400 μL PBS for 2-5 minutes and incubated for 30 minutes at room temperature with 400 μL /well blocking buffer (1% BSA in PBS). The blocking buffer was discarded and 100 μL of LAMP-1 mouse primary antibody (a lysosomal marker) was added to the cells and incubated for 60 minutes at room temperature. Cells were washed three times with 100 μL PBS and 100 μL /well of the secondary antibody (Alexa Fluor 488 for cells exposed to the red PSNPs or Alexa Fluor 594 for cells exposed to the yellow PSNPs) added and incubated with the cells for 30 minutes at room temperature in the dark. The samples were then washed 3 times with PBS before addition of 100 μL /well of DAPI (Molecular Probes[®], life technologies) which was incubated for 10 minutes at room temperature in the dark. Samples were washed three times with PBS and cells were stored in PBS 200 μL /well in the dark until analysis. The cells were analysed using a confocal laser scanning microscope (LSM 510-META, Zeiss, Germany) using 405, 488 and 543 nm lasers and the following filters for emission; BP420-480, BP505-530 and LP615.

Characterization/quantification of protein corona of NPs

PSNPs protein corona collection:

All 50 nm PSNPs at a concentration of 1 mg/mL and an equal total surface area of 200 nm PSNPs were incubated in DMEM⁺ for 10, 20, 30, 60 and 120 minutes at 37°C. Afterwards, the samples were centrifuged (Hettich; Tuttlingen, Germany) for 40 minutes at 18000 g/15°C. The pellets were three times re-suspended in 1 mL PBS and centrifuged for 25 minutes at 18000 g/4°C. Laemmli loading buffer (Biorad – USA) containing β -mercaptoethanol was used to re-suspend the final pellet before boiling for 5 minutes at 95°C followed by short centrifugation.

The total protein content in the samples was measured with a RC-DC Protein Assay (BIO-RAD) according to the manufacturer recommended protocol. All experiments were conducted in triplicate. DMEM⁺ was included as a control.

One dimensional sodium-dodecyl polyacrylamide gel-electrophoresis (1D - SDS-PAGE):

The required amount of protein (8 µg/well) was loaded onto pre-cast 12% SDS-PAGE gels of 1 mm thickness (BIO-RAD). 1D gel electrophoresis was then performed at 90 V for about 80 minutes. A protein ladder of 10-250 kDa was included in each gel. The gels were washed once with MQ water then with a water-based solution of 40% ethanol and 10% acetic acid for 15 minutes. Subsequently, the gels were stained overnight with Colloidal Coomassie Stain G-250 (BIO-RAD) on a rotating plate. After de-staining, the gels were scanned and the density of the bands was determined using an Odyssey scanner (Li-Cor ISO 9001, Odyssey Biosciences, Bad Homburg, Germany).

Proteomic analysis:

On-beads digestion - as described in (Wendrich *et al.* 2017) - and µColumn (C18) cleaning procedures were applied to the protein corona samples before measurement by reversed-phase nano LC-MS/MS. Briefly, 18 µL of the collected protein corona samples of all PSNPs incubated in DMEM⁺ for 10 and 30 minutes at 37°C were injected onto a Magic C18AQ 200A 5 µm beads (Bruker, USA) pre-concentration column (prepared in house) using a vacuum pump at a maximum pressure of 270 bar. Peptides were eluted and then injected into a 0.10 × 250 mm Magic C18AQ 200A 3 µm beads analytical column (prepared in-house) and eluted using an acetonitrile gradient at a flow of 0.5 µL/min with a Proxeon EASY nanoLC (Thermo Fisher Scientific, Waltham, MA, USA). The 1 hour gradient consisted of an increase from 8 to 33% acetonitril in water with 5mL/L acetic acid in 50 min, followed by a fast increase up to 80% acetonitril in water and 5mL/L acetic acid (in both the acetonitril and the water) in 3 minutes as a column cleaning step. Following, an electrospray potential of 3.5 kV was applied. Full scan positive mode fourier transform mass analysers (FTMS) spectra were measured between m/z 380 and 1400 on an LTQ-Orbitrap XL (Thermo electron, San Jose, CA, USA) at high resolution (60000). Tandem mass spectrometry (MS/MS) scans of the four most abundant 2 and 3⁺ charged peaks in the FTMS scan were recorded in a data dependent mode in the linear trap. LC-MS runs with all MS/MS spectra obtained were analysed with MaxQuant 1.5.2.8 (Cox *et al.* 2011; Cox and Mann 2008).

The concentrations of the identified proteins from the PSNPs coronas were determined using MassPREP tryptically digested standards (Water; Milford, USA). Standards contained a

mixture of yeast enolase (SwissProt P00924), phosphorylase b (SwissProt P00489), bovine haemoglobin (SwissProt HBA P01966, HBB P02081), yeast alcohol dehydrogenase (ADH, SwissProt P00330) and bovine serum albumin (BSA, SwissProt P02769) dissolved into a range of concentrations between 0.5 – 8 pmole in 1 mL/L formic acid. Before analysis on the LC-MS/MS, 5 μ L of each concentration of each standard was mixed with a sample of all PSNPs. This sample consisted of protein coronas isolated from equal amounts of all PSNPs used in this study after the digestion and cleaning up procedures - in a final volume of 50 μ L in 1mL/L formic acid.

Data processing and analysis:

To quantitatively identify the proteins in the PSNPs coronas a bovine database downloaded from Uniprot (released in July 2016) (<http://www.uniprot.org>, 20.343 entries) (Consortium 2017), as well as a small database containing the 4 internal standard proteins were used together with a contaminants database that contains sequences of common contaminants like Trypsins (P00760, bovine and P00761, porcine) and human keratins (Keratin K22E (P35908), Keratin K1C9 (P35527), Keratin K2C1 (P04264) and Keratin K1CI (P35527)) (Wendrich *et al.* 2017). The “label-free quantification” options were enabled and the MaxQuant protein Groups output file was filtered stringently by accepting only peptides and proteins with a false discovery rate (FDR) of less than 1% and proteins with at least 2 identified peptides of which at least one should be unique and at least one should be unmodified.

From the set of proteins standards, iBAQ intensities of phosphorylase b (SwissProt P00489) were selected for quantification of all proteins identified in the PSNPs corona and DMEM⁺ samples. Identified proteins were grouped based on their biological function using the aforementioned Uniprot database (Ritz *et al.* 2015). The mass of each group was expressed as a percentage of the total mass of proteins and as number of molecules per cm² (total copy number).

Statistical analysis

Each data point represents the average of three independent experiments (n = 3) and the results are shown as a mean \pm standard deviation after analysis by Prism[®]. A one-way analysis of variance (ANOVA) with a Bonferroni's post-test was used to test statistical

significance after testing the normality distribution of the data sets using Kolmogorov-Smirnov test. A *p-value* < 0.05 was considered significant.

RESULTS

Physicochemical characterization of the PSNPs

To characterize and assess the stability of the PSNPs suspensions, the hydrodynamic diameters (d_h) and zeta-potentials (ζ -potential) were measured in DMEM⁺ at the same incubation times used in the experiments. Compared to the samples in water among all PSNPs tested, only the 50 and 200 nm (CP) showed significant increases in size upon incubation in DMEM⁺, while the incubation time showed a significant influence only on the size of 200 nm (CP). The ζ -potentials of all the PSNPs suspended in DMEM⁺ were similar and stable during 24 hr incubation (Table 1).

Cell viability

Cytotoxicity experiments (WST-1 assay) were performed to derive non-toxic concentrations of PSNPs for the uptake studies. Results demonstrated that after 3 and 24 hr exposure the cellular viability of Caco-2 cells was not affected (viability was always higher than 85% and 80% after 3 and 24 hr, respectively compared to controls) in any of the concentrations tested (Figure 1 A and B).

Cellular adhesion and uptake of PSNPs

Cellular association of PSNPs was quantified using HC imaging analysis. The HC images are taken from above the cells, thereby merging the fluorescent signal of both internalized and membrane adhered PSNPs into one image. PSNPs internalization in Caco-2 cells was therefore confirmed using confocal microscopy (Figure 2). The PSNPs partially co-localized with lysosomes after 24 hr exposure indicating (partial) internalization of the PSNPs in the lysosomes.

Table 1: Physicochemical characteristics of PSNPs

PSNPs	Hydrodynamic diameter (d _h) (nm) of PSNPs in Water and DMEM ⁺		Simulated fraction of nominal dose deposited (ISDD modelling)		Zeta-potential (mV) of PSNPs in DMEM ⁺			
	Water (t = 0 min)	DMEM ⁺ (t = 0 min)	DMEM ⁺ (t = 30 min)	DMEM ⁺ (t = 24 hr)	DMEM ⁺ (t = 0 min)	DMEM ⁺ (t = 24 hr)		
50 nm (SM)	53 ± 0.2	78 ± 12	83 ± 14	56 ± 10	0.011	0.092	-13 ± 2	-12 ± 1
50 nm (CM)	44 ± 6	62 ± 12	58 ± 8	54 ± 20	0.013	0.093	-10 ± 1	-10 ± 1
50 nm (CP)	53 ± 9	112 ± 23*	96 ± 21*	94 ± 19*	0.010	0.071	-9 ± 2	-9 ± 1
200 nm (CP)	208 ± 7	267 ± 10*	238 ± 23	305 ± 9*#*	0.007	0.045	-11 ± 2	-10 ± 1

Hydrodynamic diameters (nm) of PSNPs in water and DMEM⁺ (n=3) and the zeta-potential (mV) in DMEM⁺ (n=3). Abbreviations: (SM); PSNPs functionalized with sulfone from Magsphere, (CM); PSNPs functionalized with carboxyl from Magsphere and (CP); PSNPs functionalized with carboxyl from Polysciences. (*) Significance difference versus water (0 minutes), (#) significance difference versus DMEM⁺ (0 minutes) and (*#) significance difference versus DMEM⁺ (30 minutes).

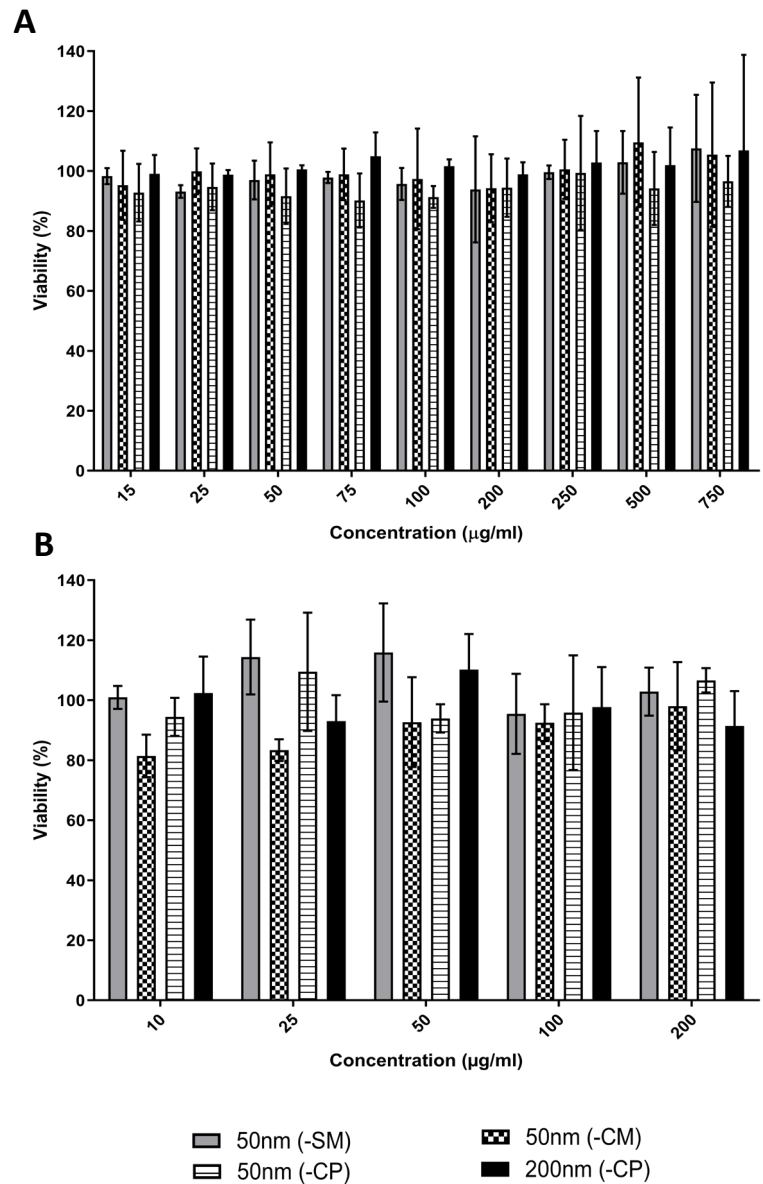


Figure 1: Caco-2 cell viability after exposure to a concentration series of 50 nm- (SM), (CM), (CP), and 200 nm (CP) PSNPs for **A)** 3 hr and **B)** 24 hr using the WST-1 viability assay. Viability is given as a percentage of the control (% ± SD; n=3).

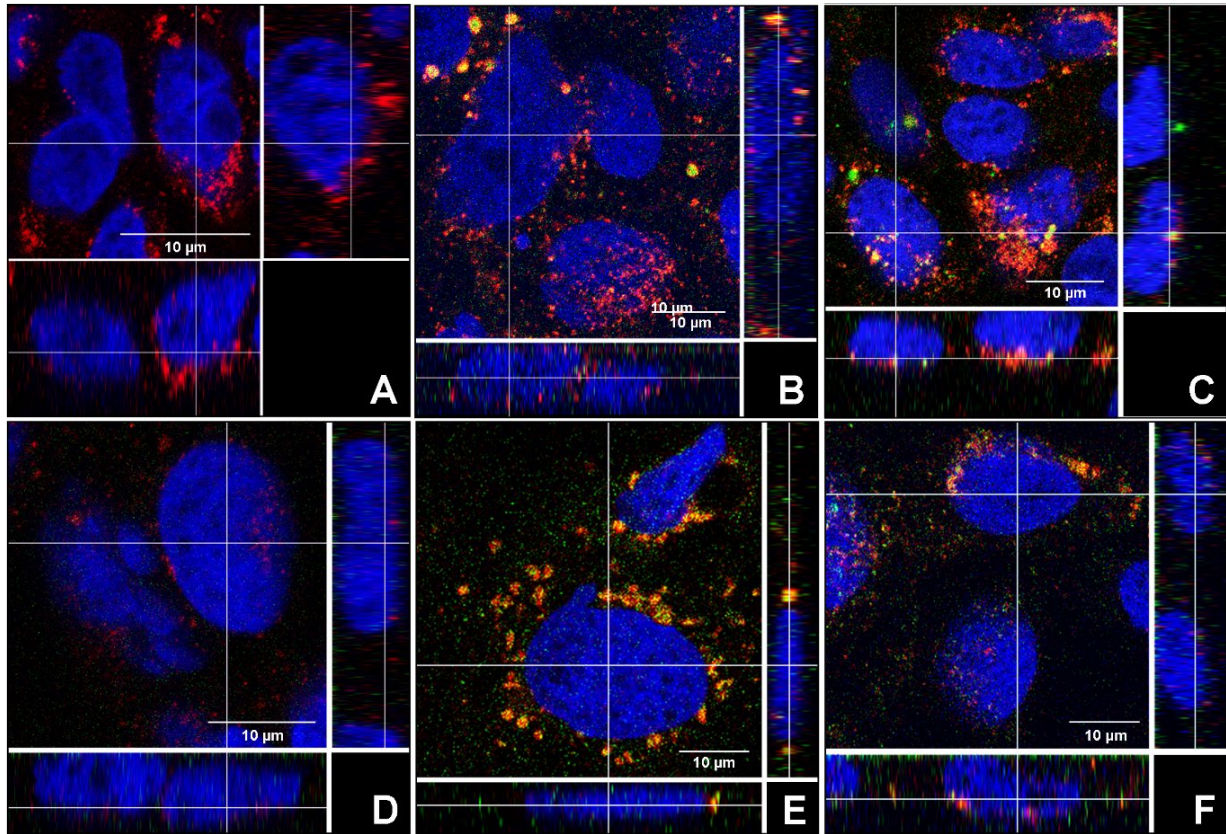


Figure 2: Confocal microscopy images of Caco-2 cells **A)** w/o exposure to PSNPs – as control for the (SM) and (CM) PSNPs. After exposure for 24 hr to a nominal concentration of 25 µg/mL **B)** 50 nm (SM) and **C)** 50 nm (CM). **D)** Caco-2 cells – w/o exposure to PSNPs – as control for the (CP) PSNPs. After exposure for 24 hr to **E)** 50 nm (CP) and **F)** 200 nm (CP). Nuclei were stained in blue, lysosomes in red and PSNPs in green.

Cellular adhesion and uptake of PSNPs were measured on a cell-per-cell basis using an HC imaging system during 10 to 120 minutes exposure to concentrations ranging between 15 and 250 µg/mL and expressed as median fluorescence intensity per cell. The cellular adhesion and uptake of the 50 nm (SM) PSNPs by Caco-2 cells were, at all time-points, significantly higher compared to the 50 nm (CM), (CP) and 200 nm (CP) PSNPs (Figure 3A). Cellular distribution profiles show that cellular association with the PSNPs increased upon increasing the PSNPs concentration, seen as a right shift of the median in the adhesion and uptake distribution curves (Figure 3B). The graph also shows that at concentrations of 75 µg/mL and higher, part of cell population has fluorescence signals that reached or exceeded the maximum detection limit of the HC imaging system. For all the PSNPs, cellular adhesion and

uptake increased with increasing concentration (Figure 3C). At the higher concentrations, the increase of cellular adhesion and uptake decline and stop, which is most likely due to the detection limit of the system. For the PSNPs that associated to the largest extent with the cells, namely the 50 nm (SM) PSNPs, the cellular adhesion and uptake distribution profile over the entire cell population was further analysed (Figure 3B) at the single cell level with HC imaging. The results obtained clearly point to an increased fluorescent signal associated with single cells with increasing dose levels.

Finally, the apparent cellular adhesion and uptake of the two PSNPs with different sizes (*i.e.* 50 and 200 nm) but with the same surface chemistry, were not significantly different at all concentrations and time points tested (Figure 3C). However, the ISDD model output (Table 1) indicates a 1.4-fold lower fraction deposited of the 200 nm (CP) PSNPs at 30 minutes compared with the 50 nm PSNPs with the same surface chemistry. The apparent cellular adhesion and uptake are comparable for both PSNPs. After correction of the lower deposition of the 200 nm (CP) PSNPs, the cellular adhesion and uptake of the 200 nm (CP) PSNPs at 30 minutes are 1.4-fold higher for the 200 nm (CP) compared with the 50 nm (CP) PSNPs with the same surface chemistry.

Transport of PSNPs across a monolayer of Caco-2 cells

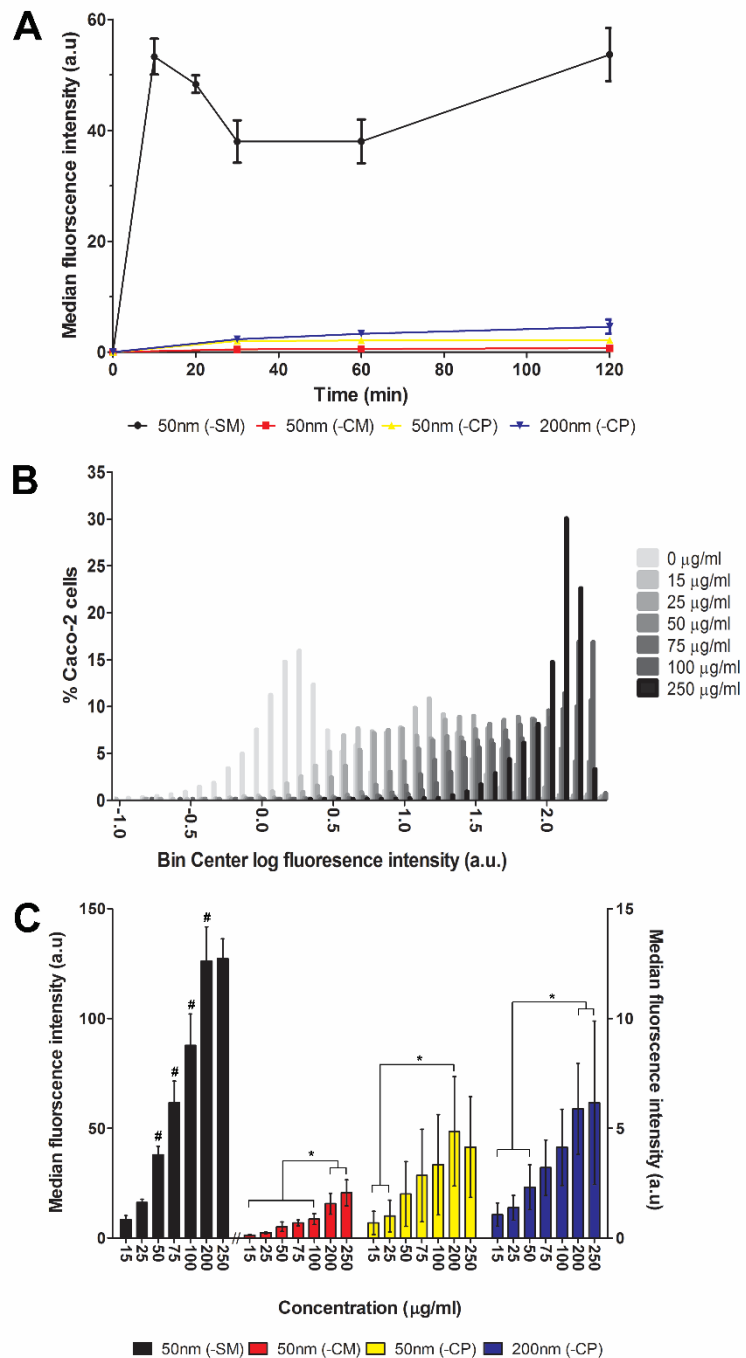
To assess if cellular adhesion and uptake of PSNPs are predictive for transport across a monolayer of Caco-2 cells, we performed additional experiments. A differentiated monolayer of Caco-2 cells was exposed to 250 µg/mL of each of the four PSNPs for 24 hours. The longer exposure of 24 hours was required to reach detectable concentration in the apical compartment of the transwell system. The transport markers used including lucifer yellow and dextrans showed very minimal transport through Caco-2 monolayers and upon the application of EGTA to open the tight junctions, the permeability of these monolayers increased significantly (data not shown), indicating the functionality of tight junction integrity of the monolayers used in the transport studies (Walczak *et al.* 2015; Bouwmeester *et al.* 2011).

Transport of the PSNPs was determined by PSNPs fluorescence measurement in the basolateral medium post exposure and expressed as a percentage of the amount of PSNPs fluorescence in the medium that was applied apically at the start of the experiment (Figure 4).

Figure 3: Cellular association of PSNPs with different surface chemistries by Caco-2 cells. Adhesion and uptake were determined by single-cell HC image analysis of PSNPs fluorescence. **A)** Time dependent adhesion and uptake of 4 types of PSNPs in Caco-2 cells exposed to a nominal concentration of 50 μg PSNPs/mL for 10 up to 120 minutes. **B)** Cellular association distribution profiles of 50 nm (SM) PSNPs in the entire cell population at exposure to nominal concentration ranging from 15 to 250 $\mu\text{g}/\text{mL}$ for 30 minutes. Note that the readings at the highest concentrations are hampered by saturation of the HC signal. **C)** Concentration dependent cellular association of 4 types of PSNPs after 30 minutes of exposure (the fluorescence intensities of 50 nm (SM) is plotted on the left y-axis while the rest of the PSNPs fluorescence intensities are plotted on the right y-axis).

#: significant difference versus all lower concentrations ($P < 0.05$).

***:** significant difference between indicated concentrations ($P < 0.05$).



The 50 nm (SM) PSNPs showed the highest transport among all PSNPs tested (13.9%; $p < 0.05$), followed by the 50 nm (CP) PSNPs (2.82%; $p < 0.05$). While the transport of the other carboxylated PSNPs – 50 nm (CM) and 200 nm (CP) – did not show significant transport to the basolateral compartment ($<1\%$). However, if the 1.6-fold lower deposited PSNPs fraction after 24 hr incubation of the PSNPs is taken into account (Table 1), the amount of the 200 nm (CP) PSNPs is comparable to the transported amount of the 50 nm PSNPs with the same surface chemistry. Here, we assume that the transport of the PSNPs increases with the concentration at the cell surface as shown for the cellular adhesion and uptake (Figure 3).

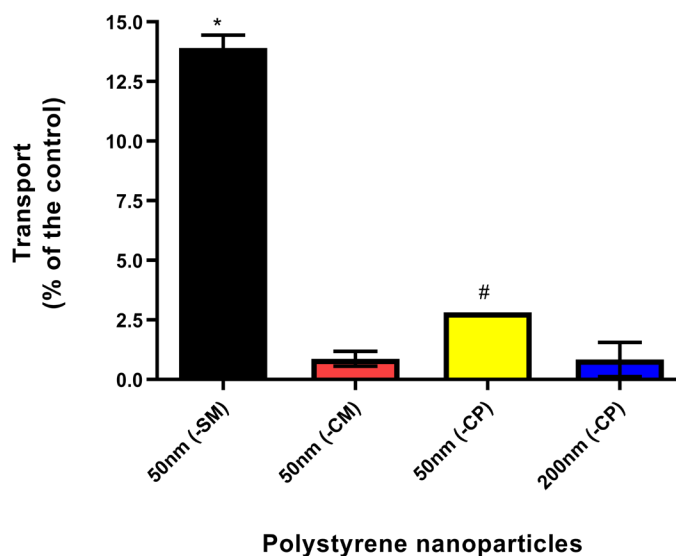


Figure 4: Transport of PSNPs with different surface chemistries by Caco-2 cells. Transport of 4 types of PSNPs in Caco-2 cells exposed to a nominal concentration of 250 μg PSNPs/mL for 24 hr. (*) Significant difference from all PSNPs. (#) Significant difference from 50 nm (CM) and 200 nm (CP) PSNPs ($p < 0.05$).

Characterization of PSNPs protein corona

All PSNPs were incubated in DMEM⁺ at 37°C for 10 and 30 minutes. The protein corona was then collected and analysed using SDS-PAGE. The gel was loaded with the same amount of protein for all tested PSNPs. The gels did not show large differences between the different PSNPs nor between the 10- and 30-minutes incubation time (Figure S1). Furthermore, the protein corona was quantified and characterized using label-free nano-LC/MS-MS, which resulted in approximately 172 different adsorbed proteins.

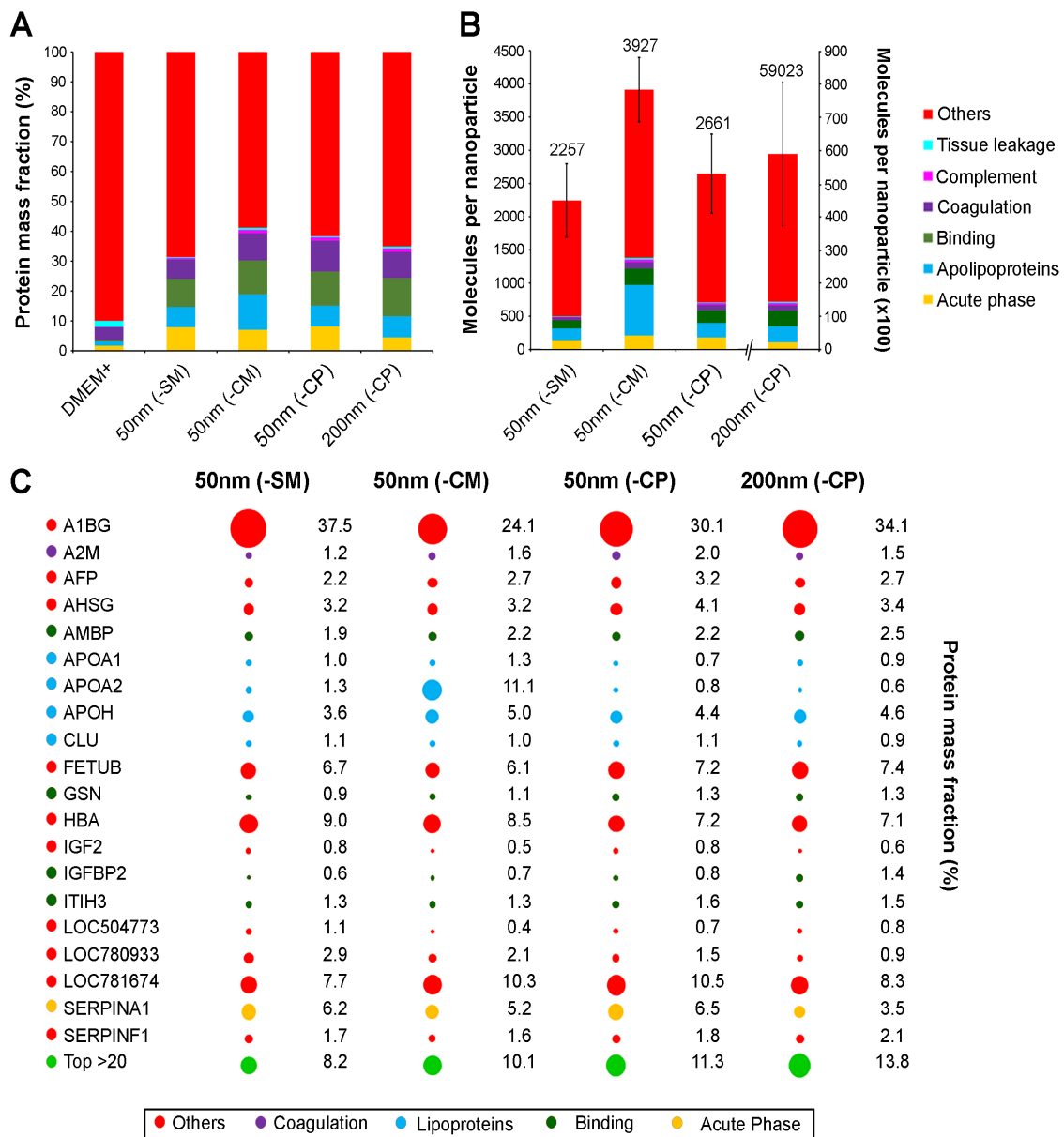


Figure 5: Composition of the protein corona on PSNPs with different surface chemistries determined with nano-LC-MS/MS. The proteins were classified into 7 groups according to their biological function using proteomics databases. **A)** Distribution of the protein groups in DMEM⁺ and in the protein coronas of the PSNPs, expressed as a percentage of the total protein mass. **B)** Number of protein molecules per particle clustered per protein group. **C)** Top 20 proteins with the highest protein adsorption on the respective PSNPs. Proteins are ordered alphabetically. The colour code indicates the protein group and the size of the spot represents the mass fraction (%), which is also given in numbers.

The complete list of identified proteins is provided in Table S1. Proteins were clustered into 6 classes according to their biological function (and 1 “other” group). Comparing the relative amount (*i.e.* abundance) of a protein class on each nanoparticle to the protein class distribution as present in the cell culture medium, we observed an enrichment of proteins involved in binding, apolipoproteins and acute phase proteins and a less pronounced enrichment of coagulation and complement factors (Figure 5a). Subsequently, the total number of protein molecules per particle was calculated.

On a single 50 nm PSNPs around 2,200 to 4,000 protein molecules were absorbed (with the number of proteins on the different types of 50 nm PSNPs not being significantly different), while on the 200 nm PSNPs about 59,000 proteins were absorbed (Figure 5b). The number of proteins per surface area is between 3×10^{13} and 5×10^{13} proteins per cm^2 for the 50 nm while it is about 6×10^{13} proteins per cm^2 for the 200 nm PSNPs. Comparable or slightly more proteins are absorbed per cm^2 on the 200 nm sized PSNPs compared to the 50 nm PSNPs, an observation that might be explained by less steric hindrance on the larger particles. Among the top 20 most abundant proteins in the coronas of the 4 PSNPs, the protein Alpha-1B-glycoprotein (A1BG) ranked highest (Figure 5c). More detailed statistical evaluation of the protein concentration on a single protein level in the coronas of the three different 50 nm PSNPs demonstrated differences in Alpha-2-macroglobulin (A2M), Alpha-fetoprotein (AFP), Apolipoprotein A-II (APOA2), Beta-2-glycoprotein 1 (APOH) and Haemoglobin foetal subunit beta (LOC781674 or HBB).

Corona concentrations of most of these proteins were lower in the coronas of the 50 nm (SM) PSNPs, this was reaching significance only compared to the (CM) PSNPs for the A2M, AFP and HBB, while compared to both (CM) and (CP) PSNPs, the concentrations of proteins APOA2 and APOH were lower in the coronas of (SM) PSNPs (Figure 6). For this evaluation only proteins with two or more copy numbers on at least one of the three different PSNPs were considered (~70 proteins in total).

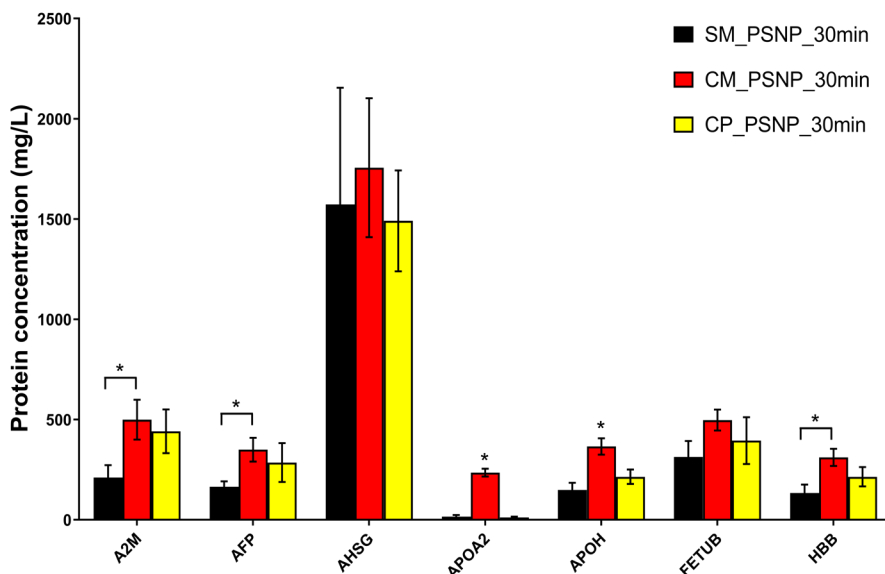


Figure 6: Comparison of differently adsorbed proteins to the surface of 50 nm PSNPs with a different surface chemistry. Only proteins with 2 or more copy numbers on at least 1 of the 3 different PSNPs were considered. Asterisks indicate significance difference ($p < 0.05$).

DISCUSSION

Here, the effects of size and surface chemistry of NPs on the protein corona formation and subsequent cellular association (*i.e.* adhesions and uptake) and transport across a monolayer of Caco-2 cells is reported. Fluorescently labelled PSNPs were selected as model particles owing to their dispersion stability in cell culture media and the commercial availability in different sizes and surface modifications.

Characterization of the PSNPs, by determining the hydrodynamic size and zeta-potential of the PSNPs in cell culture medium, showed that all 50 nm PSNPs suspensions were stable during the exposure times in the experiments. The DLS method as used here has been evaluated in an inter-laboratory testing project (Langevin *et al.* 2018) to characterize the size of the PSNPs in water or DMEM⁺ and it was found that the proteins present in the cell culture medium resulted in a signal indicating a hydrodynamic diameter of 27 ± 2 nm. The zeta-potential measurements of all PSNPs in cell culture medium were comparable and stable over time, irrespective of the PSNPs surface chemistry with a negative charge on the PSNPs' surface

resulting from the PSNPs, the proteins adsorbed on the surface of the PSNPs or from measuring protein aggregates of medium rather than PSNPs (Walczak *et al.* 2015).

The absence of cytotoxic effects of all PSNPs concentrations used in this study was in concordance with findings from previous studies using 50 nm PSNPs functionalized with carboxyl (CM and CP) and sulfone (SM) groups, using a variety of cell models (Anguissola 2014; Wang *et al.* 2013). Confocal microscopy imaging in different planes of the cells showed internalization of the PSNPs and partial co-localization of the PSNPs with lysosomes after 24 hr of exposure. Thereby, confirming previous studies indicating uptake of negatively charged 60 nm and 100 nm PSNPs (Åberg 2016) and 50 nm and 100 nm silica (SiO₂) NPs into the lysosomes (Shapero *et al.* 2011; Xia *et al.* 2008) and localization of NPs in the cytoplasm around the nucleus (for 50, 90 and 100 nm PSNPs) (Hemmerich and von Mikecz 2013; Bhattacharjee *et al.* 2012; Xia *et al.* 2008; Yacobi *et al.* 2008).

The cellular fluorescence as determined by HC resulting from sulfone (SM) functionalized PSNPs associated with Caco-2 cells was significantly higher compared to cells exposed to carboxylated (CP and CM) PSNPs of the same size. Cellular association of all functionalized PSNPs was dose dependent. Contrary to our expectations, no linear phase in the PSNPs uptake kinetics by Caco-2 cells was observed, or this happened before the first time point (10 minutes) assessed in this experiment. Accordingly, no uptake rates of these PSNPs could be derived. The PSNPs association kinetics as observed here could be due to two processes taking place in parallel: namely PSNPs cell membrane adhesion and cellular internalization. Lesniak *et al.* 2013, has reported very comparable time dependent changes in cellular fluorescence intensities in A549 (carcinoma human alveolar basal epithelial cells) exposed to 40 nm PSNPs over time. It was shown that during the first 10 minutes of exposure, cellular adhesion of PSNPs occurs rapidly, whereas after that the adsorption grows much slower (Lesniak *et al.* 2013; Salvati *et al.* 2011; Shapero *et al.* 2011). This confirms the fast increment in fluorescence at the cells as observed by us, in the first 10 minutes of exposure. Recent modelling of these processes (in A549 cells) confirmed these time lines, until 20 minutes after exposure, the PSNPs were mainly associated with the cell membranes, while after 2-3 hr exposure, the PSNPs were found close to the lysosomes located centrally in the cells (Åberg 2016). The subsequent increment in fluorescence between 60 and 120 minutes as we reported here, might suggest PSNPs uptake by the Caco-2 cells. In addition, earlier

studies using 100 nm polylactic polyglycolic acid (PLGA) NPs showed that their uptake by Caco-2 cells is taking place between 1 and 2 hr of exposure (Desai *et al.* 1997).

Earlier studies focused on potential optimal size for cellular uptake. By exposing Caco-2 cells to 25, 50, 100, 200 and 500 nm PSNPs, preferred uptake of 100 nm PSNPs was found using a microplate reader (Kulkarni and Feng 2013). Uptake of 50 nm mesoporous silica NPs by HeLa cells was higher compared to 100 nm NPs after 5 hr exposure (Lu *et al.* 2009). However, in EAhy926 cells, uptake of 200 nm PSNPs was higher than 20 nm PSNPs after 24 hr exposure (Fröhlich *et al.* 2012).

Comparing our observations and the data from literature point to cell type specific differences in uptake processes (Ritz *et al.* 2015; Daniela Baumann 2013). Here, we only compared studies using NPs with a comparable (effective) density. Comparing NP uptake data between studies needs to be performed with care as the reported cellular uptake is largely dependent on the particokinetics (*i.e.* diffusion and sedimentation) that is affected by the effective density of NPs (Hinderliter *et al.* 2010). Indeed when correcting the applied concentrations for the ISDD estimated deposited fraction (Hinderliter *et al.* 2010), the cellular association/uptake of 200 nm (CP) PSNPs becomes up to 1.4-fold higher compared to 50 nm PSNPs with the same surface chemistry, whereas without this correction the estimated uptake levels were found to be similar. Nonetheless, the surface chemistry was observed to outweigh the impact of size on the observed PSNPs cellular associations with the sulfone functionalized PNPSs being higher associated to the cells than the carbonyl functionalized nanoparticles. Reported differences in NP uptake thus not always reflect differences in biological processes, but merely the physiochemical interaction of NPs with the exposure media.

The type of surface functionalization on NPs was found earlier to be one of the major factors determining adhesions, uptake, transport and distribution of NPs, which appears to be mainly driven by the size of the protein corona (Walczak *et al.* 2015; Liu *et al.* 2012). Here, we extended our previous semi-quantitative protein corona analysis using SDS-PAGE (Figure S1) with a quantitative proteomic analysis using label-free LC-MS/MS, as described by (Ritz *et al.* 2015). As previously and commonly, done, the present study was performed in the presence of foetal bovine serum. It should be noted that different types of protein mixtures are being used for *in vitro* studies, which might affect the outcome and thus the comparability of studies (Daniela Baumann 2013). The proteomic analysis showed that the protein corona isolated

from the PSNPs was composed of 172 different proteins. We observed an enrichment of proteins involved in binding, apolipoproteins and acute phase proteins' groups and a less pronounced enrichment of complement factors proteins group. Among these proteins, the alpha-1B-glycoprotein (A1BG) protein was most abundantly present on all types of NPs, but the function of this protein is currently unknown. In other studies apolipoproteins have been identified as a dominant protein group in NPs protein coronas (Tenzer 2013; Lundqvist *et al.* 2008; Cedervall 2007). Comparing the protein corona composition among the PSNPs studied here, it was found that A2M, AFP, APOA2, APOH and HBB proteins were significantly less absorbed on the (SM) functionalized PSNPs. Strikingly, the cellular association and transport across a monolayer of Caco-2 cells of these (SM) functionalized PSNPs was also significantly different compared to the carboxylated PSNPs.

Two studies have successfully attempted to correlate the composition of the protein composition of the NPs protein corona with cellular interaction (Liu *et al.* 2015; Walkey *et al.* 2014). In these two correlative studies, different proteins were identified to correlate with cellular association of NPs. Some of the identified apolipoproteins and A2M were also found in our study to be differently enriched in the coronas of our PSNPs. It has however proven to be difficult to identify a set of specific proteins that is directly linked (mechanistically) with cellular membrane association and subsequent NPs uptake. Previously, using corona enrichment studies, it has been described that APOA2 and APOH interfere with the cellular uptake of NPs (Ritz *et al.* 2015). Here, we show that different surface chemistry of PSNPs to some extent specifically enriches some proteins, like lipoproteins, binding proteins and acute phase proteins in the corona. Some of these proteins have been associated with differential cellular interaction. And yet, the unresolved question is, what effects the presence of exogenous proteins from for instance food (allergy epitopes) proteins can have on the cellular interaction. As it was found that specific food related proteins in the NPs corona enhance the uptake of these NPs (Di Silvio *et al.* 2016).

Cellular association experiments using Caco-2 cells grown for 24 hr can be performed much faster compared to monolayer transport studies that require 21 days to differentiate Caco-2 cells. Therefore, cellular association profiles of the PSNPs studied here were compared with transported amounts of these PSNPs across a monolayer of Caco-2 cells. Both, the cellular association of the (SM) functionalized PSNPs and transported amount of these particles were

higher than for the other PSNPs. This supports the previous conclusion that the adhesion properties of NPs to the cell membrane are key determinants of NPs uptake (Lesniak *et al.* 2013) and thus likely also predictive for NPs transport. They could serve as a rapid screening of the intestinal transport potential of NPs in a tiered risk assessment or grouping approach (Arts *et al.* 2015).

CONCLUSIONS

The cellular uptake of NPs is highly dependent on both the intrinsic and extrinsic properties of NPs. Based on our findings, we conclude that NPs surface chemistry is a more important NPs property than NPs size, for the cellular association of PSNPs. The type and composition of the protein corona formed on the NPs surface is affected by the physicochemical properties of the NPs. The protein corona is consequently one of the major players affecting the NPs cellular interactions including their cytotoxicity, membrane adhesion, uptake and transport. Further studies are required to identify the set of corona proteins that affect the uptake and transport of NPs. Membrane adhesion and cellular uptake profiles correlate with the observed transport across a monolayer of Caco-2 cells, indicating membrane adhesion studies can potentially be used to predict the transport potential of NPs.

REFERENCES

- Åberg CV, Juan A. Fitzpatrick, Laurence W. Dawson, Kenneth A. 2016. Spatial and structural metrics for living cells inspired by statistical mechanics. *Scientific Reports* 6.
- Anguissola SG, David Salvati, Anna O'Brien, Peter J. Dawson, Kenneth A. 2014. High content analysis provides mechanistic insights on the pathways of toxicity induced by amine-modified polystyrene nanoparticles. *PLoS ONE* 9.
- Arts JHE, Hadi M, Irfan M-A, Keene AM, Kreiling R, Lyon D, Maier M, Michel K, Petry T, Sauer UG, Warheit D, Wiench K, Wohlleben W, Landsiedel R. 2015. A decision-making framework for the grouping and testing of nanomaterials (DF4nanoGrouping). *Regulatory Toxicology and Pharmacology* 71:S1-S27.
- Bhattacharjee S, Ershov D, Fytianos K, van der Gucht J, Alink GM, Rietjens IMCM, Marcelis ATM, Zuilhof H. 2012. Cytotoxicity and cellular uptake of tri-block copolymer nanoparticles with different size and surface characteristics. *Particle and Fibre Toxicology* 9:1-19.
- Bhattacharjee S, Ershov D, Gucht Jvd, Alink GM, Rietjens IMCM, Zuilhof H, Marcelis ATM. 2013. Surface charge-specific cytotoxicity and cellular uptake of tri-block copolymer nanoparticles. *Nanotoxicology* 7:71-84.
- Bouwmeester H, Brandhoff P, Marvin HJP, Weigel S, Peters RJB. 2014. State of the safety assessment and current use of nanomaterials in food and food production. *Trends in Food Science & Technology* 40:200-210.
- Bouwmeester H, Poortman J, Peters RJ, Wijma E, Kramer E, Makama S, Puspitaninganindita K, Marvin HJP, Peijnenburg AACM, Hendriksen PJM. 2011. Characterization of translocation of silver nanoparticles and effects on whole-genome gene expression using an in vitro intestinal epithelium coculture model. *ACS Nano* 5:4091-4103.
- Cedervall T, Lynch, Iseult, Lindman, Stina, Berggård, Tord, Thulin, Eva, Nilsson, Hanna, Dawson, Kenneth A. and Linse, Sara. 2007. Understanding the nanoparticle–protein corona using methods to quantify exchange rates and affinities of proteins for nanoparticles. *Proceedings of the National Academy of Sciences* 104:2050-2055.
- Consortium TU. 2017. UniProt: the universal protein knowledgebase. *Nucleic Acids Research* 45:D158-D169.
- Cox J, Mann M. 2008. MaxQuant enables high peptide identification rates, individualized p.p.b.-range mass accuracies and proteome-wide protein quantification. *Nat Biotech* 26:1367-1372.
- Cox J, Neuhauser N, Michalski A, Scheltema RA, Olsen JV, Mann M. 2011. Andromeda: a peptide search engine integrated into the MaxQuant environment. *Journal of Proteome Research* 10:1794-1805.
- Daniela Baumann DH, Sven Nullmeier, Patricia Panther, Claudia Dietze, Anna Musyanovych, Sandra Ritz, Katharina Landfester and Volker Mailänder. 2013. Complex encounters: nanoparticles in whole blood and their uptake into different types of white blood cells. *Nanomedicine* 8:699-713.
- Das M, Ansari KM, Tripathi A, Dwivedi PD. 2011. Need for safety of nanoparticles used in food industry. *Journal of Biomedical Nanotechnology* 7:13-14.

- des Rieux A, Fievez V, Garinot M, Schneider Y-J, Pr at V. 2006. Nanoparticles as potential oral delivery systems of proteins and vaccines: a mechanistic approach. *Journal of Controlled Release* 116:1-27.
- Desai MP, Labhassetwar V, Walter E, Levy RJ, Amidon GL. 1997. The mechanism of uptake of biodegradable microparticles in caco-2 cells is size dependent. *Pharmaceutical Research* 14:1568-1573.
- Di Silvio D, Rigby N, Bajka B, Mackie A, Baldelli Bombelli F. 2016. Effect of protein corona magnetite nanoparticles derived from bread in vitro digestion on Caco-2 cells morphology and uptake. *The International Journal of Biochemistry & Cell Biology* 75:212-222.
- Elliott J, R osslein, M., Song, N., Toman, B., Kinsner- Ovaskainen, A., Maniratanachote, R., Salit, M., Petersen, E., Sequeira, F., Romsos, E., Kim, S., Lee, J., von Moos, N., Rossi, F., Hirsch, C., Krug, H., Suchaoin, W. and Wick, P. . 2017. Toward achieving harmonization in a nanocytotoxicity assay measurement through an interlaboratory comparison study. *ALTEX - Alternatives to animal experimentation* 34:201-218.
- Francini N, Wuertz K, Patocchi-Tenzer I, Durner R, Boos N, Graf-Hausner U. 2011. Development of a Novel Automated Cell Isolation, Expansion, and Characterization Platform. *JALA: Journal of the Association for Laboratory Automation* 16:204-213.
- Fr ohlich E. 2012. The role of surface charge in cellular uptake and cytotoxicity of medical nanoparticles. *International Journal of Nanomedicine* 7:5577–5591.
- Fr ohlich E, Bonstingl G, H ofler A, Meindl C, Leitinger G, Pieber TR, Roblegg E. 2013. Comparison of two in vitro systems to assess cellular effects of nanoparticles-containing aerosols. *Toxicology in Vitro* 27-360:409-417.
- Fr ohlich E, Meindl C, Roblegg E, Ebner B, Absenger M, Pieber TR. 2012. Action of polystyrene nanoparticles of different sizes on lysosomal function and integrity. *Particle and Fibre Toxicology* 9:26-26.
- Hansen S, Michelson E, Kamper A, Borling P, Stuer-Lauridsen F, Baun A. 2008. Categorization framework to aid exposure assessment of nanomaterials in consumer products. *Ecotoxicology* 17:438-447.
- He C, Hu Y, Yin L, Tang C, Yin C. 2010. Effects of particle size and surface charge on cellular uptake and biodistribution of polymeric nanoparticles. *Biomaterials* 31:3657-3666.
- Hemmerich PH, von Mikecz AH. 2013. Defining the subcellular interface of nanoparticles by live-cell imaging. *PLoS ONE* 8.
- Hinderliter PM, Minard KR, Orr G, Chrisler WB, Thrall BD, Pounds JG, Teeguarden JG. 2010. ISDD: A computational model of particle sedimentation, diffusion and target cell dosimetry for in vitro toxicity studies. *Particle and Fibre Toxicology* 7:36.
- H uhn D, Kantner K, Geidel C, Brandholt S, De Cock I, Soenen SJH, Rivera_Gil P, Montenegro J-M, Braeckmans K, M ullen K, Nienhaus GU, Klapper M, Parak WJ. 2013. Polymer-coated nanoparticles interacting with proteins and cells: focusing on the sign of the net charge. *ACS Nano* 7:3253-3263.
- Kim JA, Salvati A, Aberg C, Dawson KA. 2014. Suppression of nanoparticle cytotoxicity approaching in vivo serum concentrations: limitations of in vitro testing for nanosafety. *Nanoscale* 6:14180-14184.

- Kulkarni SA, Feng S-S. 2013. Effects of Particle Size and Surface Modification on Cellular Uptake and Biodistribution of Polymeric Nanoparticles for Drug Delivery. *Pharmaceutical Research* 30:2512-2522.
- Langevin D, Lozano O, Salvati A, Kestens V, Monopoli M, Raspaud E, Mariot S, Salonen A, Thomas S, Driessen M, Haase A, Nelissen I, Smisdom N, Pompa PP, Maiorano G, Puntès V, Puchowicz D, Stępnik M, Suárez G, Riediker M, Benetti F, Mičetić I, Venturini M, Kreyling WG, van der Zande M, Bouwmeester H, Milani S, Rädler JO, Mülhopt S, Lynch I, Dawson K. 2018. Inter-laboratory comparison of nanoparticle size measurements using dynamic light scattering and differential centrifugal sedimentation. *NanoImpact* 10:97-107.
- Lesniak A, Salvati A, Santos-Martinez MJ, Radomski MW, Dawson KA, Åberg C. 2013. Nanoparticle Adhesion to the Cell Membrane and Its Effect on Nanoparticle Uptake Efficiency. *Journal of the American Chemical Society* 135:1438-1444.
- Liu J, Legros S, Ma G, Veinot JGC, von der Kammer F, Hofmann T. 2012. Influence of surface functionalization and particle size on the aggregation kinetics of engineered nanoparticles. *Chemosphere* 87:918-924.
- Liu R, Jiang W, Walkey CD, Chan WCW, Cohen Y. 2015. Prediction of nanoparticles-cell association based on corona proteins and physicochemical properties. *Nanoscale* 7:9664-9675.
- Lu F, Wu S-H, Hung Y, Mou C-Y. 2009. Size effect on cell uptake in well-suspended, uniform mesoporous silica nanoparticles. *Small* 5:1408-1413.
- Lundqvist M, Stigler J, Elia G, Lynch I, Cedervall T, Dawson KA. 2008. Nanoparticle size and surface properties determine the protein corona with possible implications for biological impacts. *Proc Natl Acad Sci USA* 105:14265-14270.
- Lynch I, Weiss C, Valsami-Jones E. 2014. A strategy for grouping of nanomaterials based on key physico-chemical descriptors as a basis for safer-by-design NMs. *Nano Today* 9:266-270.
- Peters RJB, Bouwmeester H, Gottardo S, Amenta V, Arena M, Brandhoff P, Marvin HJP, Mech A, Moniz FB, Pesudo LQ, Rauscher H, Schoonjans R, Undas AK, Vettori MV, Weigel S, Aschberger K. 2016. Nanomaterials for products and application in agriculture, feed and food. *Trends in Food Science & Technology* 54:155-164.
- Ramery E, O'Brien PJ. 2014. Evaluation of the cytotoxicity of organic dust components on THP1 monocytes-derived macrophages using high content analysis. *Environmental Toxicology* 29:310-319.
- Ritz S, Schöttler S, Kotman N, Baier G, Musyanovych A, Kuharev J, Landfester K, Schild H, Jahn O, Tenzer S, Mailänder V. 2015. Protein corona of nanoparticles: distinct proteins regulate the cellular uptake. *Biomacromolecules* 16:1311-1321.
- Salvati A, Åberg C, dos Santos T, Varela J, Pinto P, Lynch I, Dawson KA. 2011. Experimental and theoretical comparison of intracellular import of polymeric nanoparticles and small molecules: toward models of uptake kinetics. *Nanomedicine* 7:818-826.
- Shakweh M, Ponchel G, Fattal E. 2004. Particle uptake by peyer's patches: a pathway for drug and vaccine delivery. *Expert Opinion on Drug Delivery* 1:141-163.
- Shapero K, Fenaroli F, Lynch I, Cottell DC, Salvati A, Dawson KA. 2011. Time and space resolved uptake study of silica nanoparticles by human cells. *Molecular BioSystems* 7:371-378.

- Tenzer S, Docter, Dominic, Kuharev, Jörg, Musyanovych, Anna, Fetz, Verena, Hecht, Rouven, Schlenk, Florian, Fischer, Dagmar, Kiouptsi, Klytaimnitra, Reinhardt, Christoph, Landfester, Katharina, Schild, Hansjörg, Maskos, Michael, Knauer, Shirley K. and Stauber, Roland H. 2013. Rapid formation of plasma protein corona critically affects nanoparticle pathophysiology. *Nature Nanotechnology* 8:772 - 781.
- Walczak AP, Kramer E, Hendriksen PJM, Tromp P, Helsper JPF, van der Zande M, Rietjens IMCM, Bouwmeester H. 2015. Translocation of differently sized and charged polystyrene nanoparticles in in vitro intestinal cell models of increasing complexity. *Nanotoxicology* 9:453-461.
- Walczyk D, Bombelli FB, Monopoli MP, Lynch I, Dawson KA. 2010. What the cell "sees" in bionanoscience. *J Am Chem Soc* 132.
- Walkey CD, Olsen JB, Song F, Liu R, Guo H, Olsen DWH, Cohen Y, Emili A, Chan WCW. 2014. Protein Corona Fingerprinting Predicts the Cellular Interaction of Gold and Silver Nanoparticles. *ACS Nano* 8:2439-2455.
- Wang F, Yu L, Monopoli MP, Sandin P, Mahon E, Salvati A, Dawson KA. 2013. The biomolecular corona is retained during nanoparticle uptake and protects the cells from the damage induced by cationic nanoparticles until degraded in the lysosomes. *Nanomedicine: Nanotechnology, Biology and Medicine* 9:1159-1168.
- Wendrich JR, Boeren S, Möller BK, Weijers D, De Rybel B. 2017. *In vivo* identification of plant protein complexes using IP-MS/MS. In: Kleine-Vehn J, Sauer M, eds. *Plant Hormones: Methods and Protocols*. New York, NY: Springer New York, 147-158.
- Xia T, Kovochich M, Liong M, Zink JI, Nel AE. 2008. Cationic polystyrene nanosphere toxicity depends on cell-specific endocytic and mitochondrial injury pathways. *ACS Nano* 2:85-96.
- Yacobi NR, DeMaio L, Xie J, Hamm-Alvarez SF, Borok Z, Kim K-J, Crandall ED. 2008. Polystyrene nanoparticle trafficking across alveolar epithelium. *Nanomedicine: Nanotechnology, Biology and Medicine* 4:139-145.
- Yin Win K, Feng S-S. 2005. Effects of particle size and surface coating on cellular uptake of polymeric nanoparticles for oral delivery of anticancer drugs. *Biomaterials* 26:2713-2722.
- Yun Y, Cho YW, Park K. 2013. Nanoparticles for oral delivery: targeted nanoparticles with peptidic ligands for oral protein delivery. *Advanced Drug Delivery Reviews* 65:822-832.
- Zhang J, Cai X, Zhang Y, Li X, Li W, Tian Y, Li A, Yu X, Fan C, Huang Q. 2013. Imaging cellular uptake and intracellular distribution of TiO₂ nanoparticles. *Analytical Methods* 5:6611-6616.

SUPPLEMENTARY MATERIAL

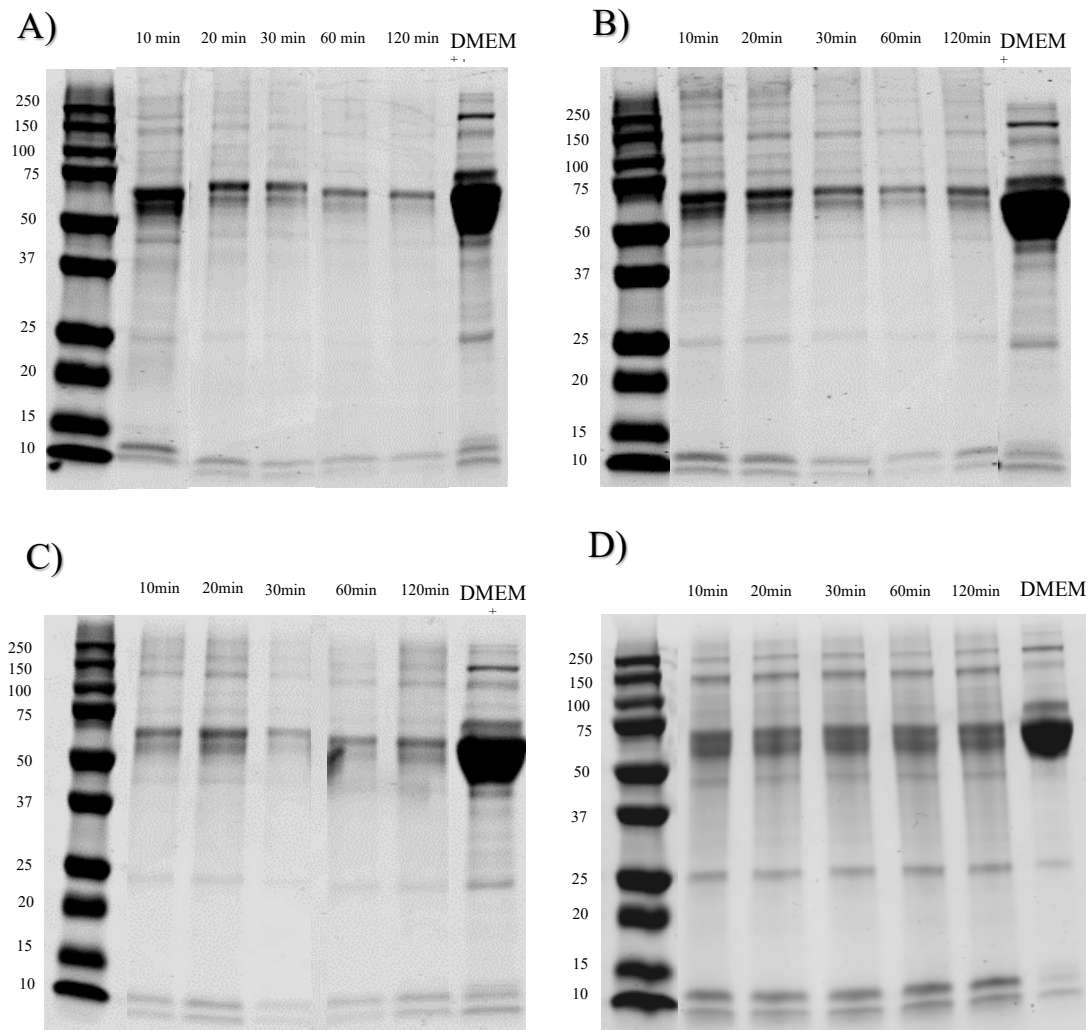
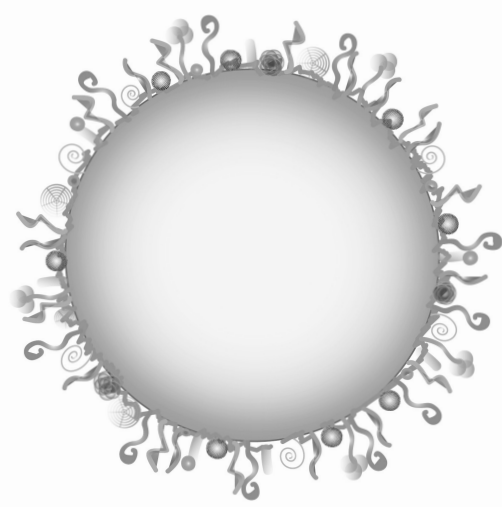
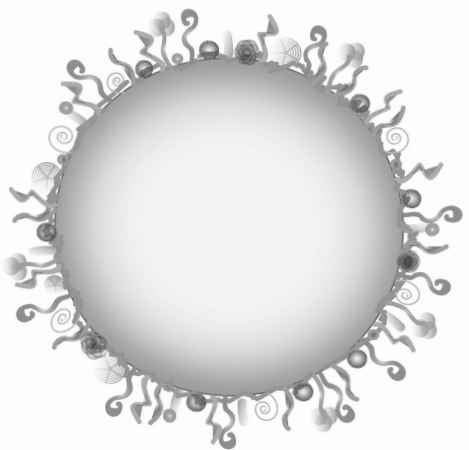
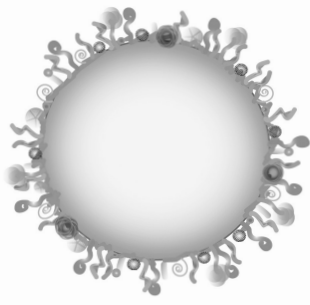
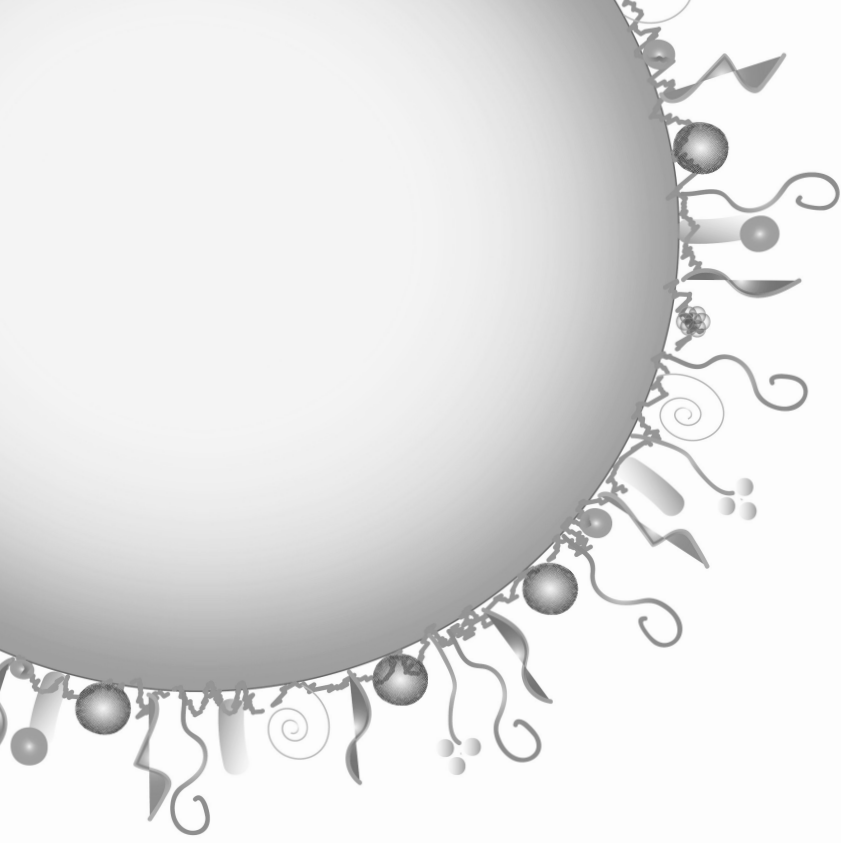


Figure S 1: SDS-PAGE showing the protein corona of PSNPs after 10, 20, 30, 60 and 120 minutes incubation in DMEM⁺. **A)** 50 nm (SM), **B)** 50 nm (CM), **C)** 50 nm (CP), and **D)** 200 nm (CP). The amount of proteins at all-time points for each PSNPs was adjusted to load the same amount. The molecular weights of the proteins in the standard ladder are given on the left side of each gel. DMEM⁺ is the medium control.

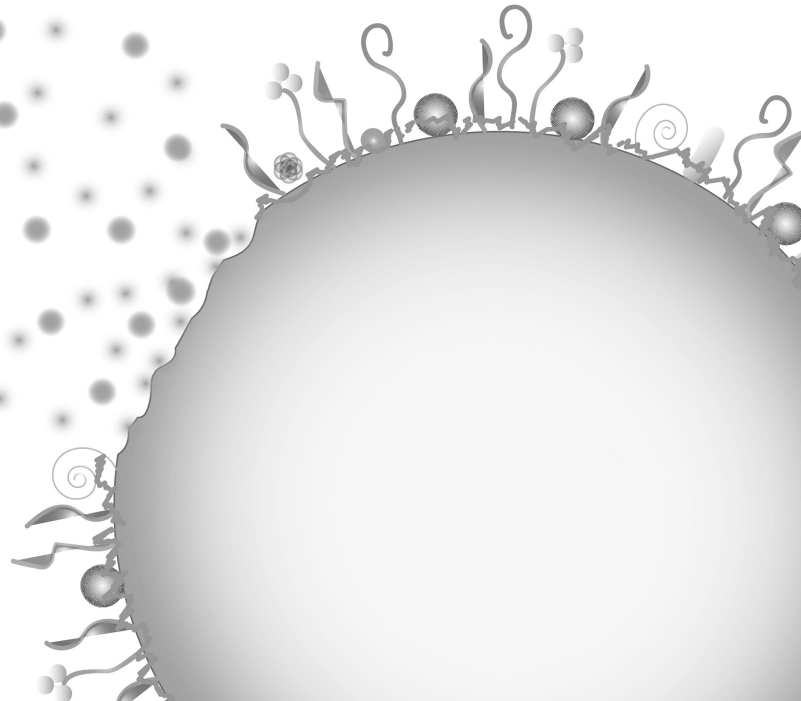


3

Impact of *in vitro* digestion on gastrointestinal fate and uptake of silver nanoparticles with different surface modifications

Ashraf Abdelkhalig, Meike van der Zande, Anna K. Undas, Ruud J. B. Peters and
Hans Bouwmeester

Based on: Nanotoxicology (2020) 14:1, 111 - 126



ABSTRACT

Nanomaterials especially silver nanoparticles (AgNPs) are used in a broad range of products owing to their antimicrobial potential. Oral ingestion is considered as a main exposure route to AgNPs. This study aimed to investigate the impact of the biochemical conditions within the human digestive tract on the intestinal fate of AgNPs across an intestinal *in vitro* model of differentiated Caco-2/HT29-MTX cells. The co-culture model was exposed to different concentrations (250 – 2500 µg/L) of pristine and *in vitro* digested (IVD) AgNPs and silver nitrate for 24 hr. ICP-MS and spICP-MS measurements were performed for quantification of total Ag and AgNPs. The AgNPs size distribution, dissolution and particle concentration (mass- and number-based) were characterized in the cell fraction and in the apical and basolateral compartments of the monolayer cultures. A significant fraction of the AgNPs dissolved (86 - 92% for the (LA) AgNPs and 48 – 70% for the (Cit) AgNPs) during the digestion. Cellular exposure to increasing concentrations of pristine or IVD AgNPs resulted in a concentration dependent increase of total Ag and AgNPs content in the cellular fractions. The cellular concentrations were significantly lower following exposure to IVD AgNPs compared to the pristine AgNPs. Transport of silver as either total Ag or AgNPs was limited (< 0.1%) following exposure to pristine and IVD AgNPs. We conclude that the surface chemistry of AgNPs and their digestion influence their dissolution properties, uptake/association with the Caco-2/HT29-MTX monolayer. This highlights the need to take *in vitro* digestion into account when studying nanoparticle toxicokinetics and toxicodynamics in cellular *in vitro* model systems.

INTRODUCTION

Nanomaterials are used in a broad range of products and applications such as textiles, medical devices, water disinfection, personal hygiene and food products (Abdelkhalik *et al.* 2018; Imai 2017; Lichtenstein *et al.* 2015; Chaudhry *et al.* 2008). Because of the antimicrobial potential of silver nanoparticles (AgNPs), they are amongst the most frequently used nanoparticles (NPs) in food associated products (*e.g.* packaging and kitchen utensils) (Choi *et al.* 2018; Lichtenstein *et al.* 2015). Therefore, oral ingestion is considered as a main exposure route for humans to AgNPs. From a risk assessment perspective, understanding the fate, cellular interactions (*i.e.* cellular uptake) and bioavailability of AgNPs upon digestion is of key importance to assess their impact on health (Lichtenstein *et al.* 2017; Hsiao *et al.* 2016; Lichtenstein *et al.* 2015; Bouwmeester *et al.* 2011)

Upon oral ingestion of AgNPs, these particles pass through several compartments of the gastrointestinal tract (mouth, stomach and intestine), each with a specific pH and biochemical composition. These varying conditions can affect the AgNPs physicochemical properties (*e.g.* agglomeration and dissolution) and accordingly affect their bioavailability and toxicological properties (Lichtenstein *et al.* 2017; Sieg *et al.* 2017; Böhmert *et al.* 2014; Murdock *et al.* 2008). Upon reaching the intestine, the biological interactions (*e.g.* uptake and transport) of the AgNPs with the intestinal epithelial cells determine their bioavailability and possible subsequent systemic effects upon oral ingestion (McCracken *et al.* 2015). AgNPs size and surface chemistry play an important role in their stability, cellular internalization and transport (Lichtenstein *et al.* 2017; Mwilu *et al.* 2013). Several *in vitro* models have been developed to represent the intestinal epithelial barrier (Lefebvre *et al.* 2015) which are exposed to NPs to simulate real-life human exposure conditions to NPs (Sieg *et al.* 2017; Nel *et al.* 2006). Among these model, the co-cultures of monolayers of Caco-2 intestinal cells and HT29-MTX mucus secreting cells are widely used as an *in vitro* intestinal epithelium model (Georgantzopoulou *et al.* 2016; Lefebvre *et al.* 2015; Stone *et al.* 2009; Bailey *et al.* 1996). These models however do not consider possible effects of digestion on toxicokinetics and toxicodynamics of NPs.

Detection, characterization and quantification of (metal) nanoparticles is of importance in studying the fate of NPs. For this, several analytical methods have been developed (López-Serrano *et al.* 2014). Single particle-inductively coupled plasma mass spectrometry (spICP-MS)

has shown high efficacy and sensitivity to detect metal NPs at low concentrations in addition to its ability to distinguish between metal ions and NPs (Abdolahpur Monikh *et al.* 2019; Ding *et al.* 2018; Weigel *et al.* 2017; van der Zande *et al.* 2016). In addition, spICP-MS provides information on the size, size distribution and mass- and number-based NPs concentration (Hsiao *et al.* 2016; Peters *et al.* 2015; Laborda *et al.* 2011). To study the cellular uptake and internalization of AgNPs, however, additional techniques need to be used. For this we used confocal fluorescence microscopy exploiting the light scattering properties of AgNPs in combination with immunohistochemistry (van der Zande *et al.* 2016; Kittler *et al.* 2010).

Here, we aimed to investigate the impact of *in vitro* digestion (IVD) on two 50 nm AgNPs with different surface chemistries, while silver nitrate (AgNO₃) was used as an ionic control. An *in vitro* human digestion model was used to mimic the oral, gastric and small intestinal conditions (Lichtenstein *et al.* 2015; Walczak *et al.* 2012; Versantvoort *et al.* 2005). The size, size distribution, dissolution and particle concentration (mass- and number-based) of the AgNPs after *in vitro* digestion using spICP-MS and ICP-MS were measured and quantified. Also, we investigated the impact of *in vitro* digestion on the uptake/association and transport of the AgNPs in or through the intestinal barrier using an *in vitro* Caco-2 and HT29-MTX co-culture transwell model.

MATERIALS AND METHODS

Nanoparticles and chemicals

Two 50 nm negatively charged AgNPs with different surface modifications were purchased from Nanocomposix Inc. (USA); lipoic acid BioPure™ (pH=6.1) in milli-Q water and citrate BioPure™ (pH = 7.4) in 2 mM citrate buffer, further referred to as (LA) and (Cit) AgNPs, respectively. The silver mass concentration in the stock suspensions of both AgNPs was 1 mg/mL. All the AgNPs suspensions were stored at 4°C in the dark. Dilutions of the AgNPs were freshly prepared for every experiment in complete cell culture medium (DMEM⁺), prepared by supplementing Dulbecco's Modified Eagle Medium (DMEM) culture medium (LONZA; Switzerland) with 10% (v/v) heat inactivated Foetal Bovine Serum (FBS) (Gibco®, Life technologies; USA), 1% (v/v) of Penicillin-Streptomycin 10,000 units penicillin and 10 mg streptomycin/mL (Sigma-Aldrich; USA) and 1% (v/v) of MEM Non-Essential Amino Acids

(NEAA) (Gibco[®], life technologies; USA). Silver nitrate (AgNO₃) (Sigma; USA) was used as a control (source of Ag⁺ ions) in all the experiments. Dilutions of AgNO₃ were freshly prepared for every experiment in DMEM⁺.

Physicochemical characterization of AgNPs

Hydrodynamic diameters of AgNPs were determined using dynamic light scattering (DLS). Measurements were performed on samples containing 10 mg/L AgNPs suspended in nano-pure water using an ALV dynamic light scattering setup (ALV-Laser Vertriebsgesellschaft; Germany), consisting of a Thorn RFIB263KF photomultiplier detector, an ALV-SP/86 goniometer, an ALV 50/100/200/400/600 µm pinhole detection system, an ALV7002 external correlator and a Cobolt Samba-300 DPSS laser. Measurements were performed at t = 0 hr and at t = 24 hr at room temperature, samples were incubated at 37°C. For each condition, samples were analysed in triplicate; each measurement consisted of 10 technical replicates measurements of 30 seconds each, at an angle of 90°. The results are expressed as the average hydrodynamic diameter (nm) ± standard deviation (SD) that was calculated using AfterALV[®] software (AfterALV 1.0d, Dullware; USA).

The AgNPs surface charges were determined by measuring the zeta-potential of 10 µg/mL AgNPs suspensions in nano-pure water using a Malvern Nanosizer (Malvern Instruments; UK). All samples were analysed in triplicate.

The total silver content of pristine AgNPs suspensions and AgNO₃ solution was analysed using a NexION 350D (PerkinElmer; USA) ICP-MS. Before analysis, samples were digested using an aqua-regia (1: 3 (v/v), 70% HNO₃: 37% HCl) acid digestion for 30 minutes at 60°C and diluted with nano-pure water. Silver was measured using the selected element-monitoring mode with *m/z* values of 107 and 109. A matrix-matched calibration curve of an ionic Ag standard (AgNO₃) (Merck; Germany) ranging from 0.1 to 50 µg/L was included. Rhodium (Merck; Germany) was used as an internal standard. The limit of detection (LOD_{conc}) and limit of quantification (LOQ_{conc}) were 4 and 13.5 ng/L respectively and they were calculated by the measurement of blank samples as mass concentration in the blank + 3 × SD and 10 × SD, respectively. All samples were analysed in triplicate.

The particle size, size distribution, mass- and number-based particle concentration of pristine AgNPs suspensions and AgNO₃ solution were quantified using spICP-MS. The method for the spICP-MS measurements was described previously (Peters *et al.* 2015). Briefly, the sample flow rate to the nebulizer was determined before the start of each series of measurements. The dwell time was set at 3 milliseconds and the total acquisition time was set at 60 seconds. A diluted suspension of 60 nm gold NPs (Nanocomposix; USA) with a mass concentration of 50 ng/L was used before each analysis to verify the performance of the ICP-MS and to determine the transport efficiency. A calibration curve of ionic silver (AgNO₃) with a concentration range of 0.1 – 20 µg/L was used. The time scan data of the spICP-MS measurements were exported as CSV files and the calculation of the particle size, size distribution and mass- and number-based concentrations from the spICP-MS data were performed using a dedicated spreadsheet. Details about the spreadsheet have been described previously (Peters *et al.* 2015). The LOD_{conc} and LOQ_{conc} were estimated to be 22 and 75 ng/L respectively and they were calculated by the measurement of blank samples as mass concentration in the blank + 3 × SD and 10 × SD, respectively. The NP size was calculated based on the particle mass, assuming spherical particles. The size detection limit (LOD_{size}) was 20 nm and accordingly any silver particles with sizes below this limit were included in the ionic silver fraction.

***In vitro* digestion of AgNPs and AgNO₃**

The two AgNPs suspensions and the AgNO₃ solution were digested using an *in vitro* human gastrointestinal digestion model with a pH gradient ranging from 7 (mouth), to 5 (stomach), to 7 (intestine). The pH of 5 in the stomach is meant to resemble the conditions upon food consumption which leads to a decrease of stomach acidity, opposed to a pH of ~2 under fasted conditions (Minekus *et al.* 2014). Briefly, all digestive juices were freshly prepared and warmed to 37°C before use as described in Table 1 (Walczak *et al.* 2012; Versantvoort *et al.* 2005).

A volume of 1 mL, with a concentration of 500 mg/L of AgNPs suspensions or 95 mg/L AgNO₃ solution, was mixed with 3 mL of saliva (pH = 6.8 ± 0.1) and incubated (head-over-heals at 55 rpm) for 5 minutes at 37°C to simulate the digestion in the mouth. Subsequently, 6 mL of gastric juice (pH = 1.3 ± 0.1) was added to the mixture and the pH was checked and adjusted

to 5 ± 0.5 with NaOH (5 M) to simulate the digestion in the stomach. The samples were further incubated while rotating at head-over-heads at 37°C for 2 hr. Lastly, 6 mL of duodenal juice (pH=8.1) and 3 mL of bile (pH = 8.2) were added to the mixture and the pH was checked and adjusted to 6.5 ± 0.5 with NaOH (1M) or HCl (37%) to simulate the digestion in the small intestine. Again, the samples were incubated while rotating head-over-heads at 37°C for 2 hr. The complete mixture of all the digestive juices is further referred to as chyme.

The total silver content of the IVD AgNPs suspensions and AgNO₃ solution was analysed using ICP-MS as described earlier. spICP-MS measurements were used to quantify the particle size, size distribution and mass- and number-based concentrations of the IVD AgNPs suspensions and AgNO₃ solution as described earlier. The silver ions calibration curves were prepared in a similar matrix as the samples of interest.

Table 1: Composition of the artificial digestion fluids of the *in vitro* digestion model (per 1000 mL) *

Saliva (pH = 6.8 ± 0.1)	Gastric fluid (pH = 1.3 ± 0.1)	Duodenal fluid (pH = 8.1 ± 0.1)	Bile fluid (pH = 8.2 ± 0.1)
<ul style="list-style-type: none"> • 896 mg KCl • 200 mg KSCN • 1,021 mg NaH₂PO₄.H₂O • 570 mg Na₂SO₄ • 298 mg NaCl • 1,694 mg NaHCO₃ • 200 mg urea • 290 mg amylase • 15 mg uric acid • 25 mg mucin • nano-pure water 	<ul style="list-style-type: none"> • 2,752 mg NaCl • 306 mg NaH₂PO₄.H₂O • 824 mg KCl • 302 mg CaCl₂ • 306 mg NH₄Cl • 6.5 mL 37% HCl • 650 mg glucose • 20 mg glucuronic acid • 85 mg urea • 330 mg glucosamine-hydrochloride • 1 g BSA • 2.5 g pepsin • 3 g mucin • nano-pure water 	<ul style="list-style-type: none"> • 7,012 mg NaCl • 3,388 mg NaHCO₃ • 80 mg KH₂PO₄ • 564 mg KCl • 50 mg MgCl₂.6H₂O • 180 mL HCl (37%) • 100 mg urea • 151 mg CaCl₂ • 1 g BSA • 9 g pancreatin • 1.5 g lipase • nano-pure water 	<ul style="list-style-type: none"> • 5,259 mg NaCl • 5,785 mg NaHCO₃ • 376 mg KCl • 150 mL HCl (37%) • 250 mg urea • 167.5 mg CaCl₂ • 1.8 g BSA • 30 g bile • nano-pure water Sodium carbonate solution • 84.7 g NaHCO₃ • nano-pure water

* (Walczak *et al.* 2012; Versantvoort *et al.* 2005)

Cell culture

A co-culture of adherent human epithelial colorectal adenocarcinoma cells (Caco-2; ATCC® HTB-37™; USA) and human colon adenocarcinoma mucus secreting cells (HT29-MTX; ECACC; Ireland) was prepared of cells at passage numbers of 25 - 40 and 8 - 40, respectively. Both cell lines were cultured and separately maintained in 75 cm² cell culture flasks (Corning®; USA) at 37°C in a humidified 5% CO₂ atmosphere in DMEM⁺.

Cell viability

Cytotoxic effects of the pristine and IVD AgNPs and AgNO₃ were determined using the WST-1 cell viability assay (Roche; Germany). Each well was seeded with 100 µL of a 1×10⁵ cells/mL suspension with a 3: 1 ratio Caco-2: HT29-MTX in DMEM⁺ in 96-well flat bottom plates (Grenier bio-one; the Netherlands). Plates were incubated at 37°C, 5% CO₂ for 24 hr. The attached cells were then exposed to 100 µL/well of freshly prepared dilutions (100 – 100,000 µg/L) of pristine and (500 – 2500 µg/L) IVD AgNPs suspensions and/or (125 – 500 µg/L) AgNO₃ solution. All the IVD AgNPs and AgNO₃ dilutions had a 9: 1 DMEM⁺: chyme ratio, to prevent toxicity of the chyme. After 24 hr of exposure, the exposure medium was discarded and the cells were washed once with 100 µL/well HBSS buffer before addition of 10 µL of WST-1 solution with 90 µL of DMEM⁺ (without phenol red) to each well. The plates were incubated for 4 hr at 37°C, 5% CO₂ and absorbance was read at 490 and 630 nm on a plate reader (BioTek Synergy™ HT Multi-Mode Microplate reader; USA). The cell viability was expressed as % of control. DMEM⁺ was used as a negative control and Triton-X100 (0.25%) (Sigma) was used as a positive control.

In vitro intestinal monolayer barrier integrity assessment

The Caco-2 and HT29-MTX cells were grown in a ratio of 3: 1 (Kleiveland 2015; Walczak *et al.* 2015a) at a density of 4 x 10⁴ cells/cm² on the upper side of transwell polyester inserts (0.4 µm pore size, 1.12 cm² surface area) (Corning; USA) for 21 days. The integrity of the monolayer was assessed before AgNPs exposure by measuring the transepithelial electrical resistance (TEER) values using a Millicell ERS-2 Epithelial Volt- Ohm Meter (Millipore; USA). On day 21, only inserts with TEER values above 200 Ω.cm² before exposure were used. In addition, a maximum of 20% reduction in TEER values was accepted after exposure.

Additionally, the transport efficacy of each of three different integrity markers namely; lucifer yellow (LY) (Sigma; USA) and low (4 kDa) and high (10 kDa) molecular weights fluorescein isothiocyanate dextrans (FITC-D) (Sigma; USA) was evaluated in the presence and absence of EGTA (a tight-junction disruptor) (Sigma, USA) to assess the cell monolayer integrity. In the absence of EGTA, 500 μL /insert of 1 mg/mL in DMEM⁺ of the integrity markers were added apically. After 1 hr incubation at 37°C, the basolateral medium was collected and the transport of the markers was determined by measuring the fluorescence at 485/530 nm using the fluorescence plate reader. For samples evaluated in the presence of EGTA, 500 μL of a solution of 2.5 mM EGTA/DMEM⁺ was added apically and basolaterally followed by incubation of the monolayers for 1 hr at 37°C. The wells were then refreshed with 2.5 mM EGTA/DMEM⁺ solution in the basolateral compartment while apically the integrity markers in DMEM⁺ were added at a concentration of 1 mg/mL. The cells were incubated for 1 hr at 37°C and the basolateral medium was collected and analysed for the presence of the markers as described above.

Cellular uptake/association and transport of AgNPs and AgNO₃

The cellular monolayer was exposed apically to 500 μL /insert of 250, 500 and 2500 $\mu\text{g}/\text{L}$ of pristine or IVD AgNPs suspensions and to 250 $\mu\text{g}/\text{L}$ of pristine or IVD AgNO₃ solutions for 24 hr at 37°C, 5% CO₂. Then, the media from the apical and basolateral compartments were collected and the cells were collected by trypsinization and sonication (40 kHz for 15-20 minutes) to lyse the cells. The total silver content of all the samples was analysed using ICP-MS as described earlier. spICP-MS was used to quantify the particle size, size distribution and mass- and number-based concentrations of all samples as described above.

Confocal microscopy

For confocal imaging, Caco-2/HT29-MTX co-cultures were cultured in transwells and exposed to both pristine and IVD AgNPs suspensions and AgNO₃ solution using similar conditions as used in the uptake/association and transport experiments. After exposure, the exposure medium was discarded and the cells were fixed with 4% paraformaldehyde (Sigma; USA) for 15 minutes. The cells were washed 3 times with PBS for 5 minutes after discarding the fixation solution. The cells were permeabilized with 0.25% Triton X-100/PBS for 15

minutes. The cells were then washed again 3 times with PBS for 5 minutes before incubating them with the blocking buffer (1% BSA in PBS) for 30 minutes. After discarding the blocking buffer, Phalloidin - Alexa 488 (6 units) (Dyomics; Germany) was added to stain cellular actin and the cells were incubated for 30 minutes. Cells were washed three times with PBS before incubating the cells for 10 minutes with RedDot-2 (1: 200) (Biotium; USA) to stain the nuclei. Finally, the cells were washed with PBS and stored in the dark until analysis. The cells were analysed using a confocal laser scanning microscope (SP5X-SMD; Leica Microsystems, Germany). Samples were excited with 665 and 495 nm lasers and backscattered light was used to detect AgNPs using a 543 nm laser. All preparations steps have been done at room temperature.

Transmission electron microscopy energy-dispersive spectroscopy (TEM-EDS) analysis

Following the 24 hr exposure of the Caco-2/HT29-MTX co-culture to pristine or IVD AgNPs or AgNO₃, samples from the basolateral compartments were withdrawn. The samples were deposited on a holey carbon coated Cu TEM grid (Agar Scientific; UK) and dried at room temperature before examination using a TEM-EDS system. The grid examination was performed on a JEM-2100 equipped with EDS system of OI Aztec 80 mm X-max detector.

Statistical analysis

Each data point of all the experiments performed represents the average from three replicates ($n = 3$) and the results are shown as mean \pm standard deviation after analysis by Prism[®] (v.8.0.1; GraphPad[®], USA) software. Bonferroni's post-test was used to test statistical significance upon performing a one-way analysis of variance (ANOVA). A *p-value* < 0.05 was considered significant.

RESULTS

Physicochemical characterization of the pristine AgNPs suspensions and AgNO₃ solution

Two differently coated AgNPs were used in this study: lipoic acid-coated (LA) AgNPs and citrate-coated (Cit) AgNPs. The nominal sizes provided by the supplier of the (LA) and (Cit) AgNPs measured by transmission electron microscopy (TEM) were 51 ± 5 and 52 ± 6 nm, respectively. The hydrodynamic sizes and the ζ - potential of both AgNPs, measured in nano-pure water after 0 and 24 hr incubation at 37°C, are listed in Table 2. There were no significant differences in the hydrodynamic diameters or the charges of both AgNPs over time.

Table 2. Physicochemical characteristics of AgNPs

Medium	Incubation time (hr)	Hydrodynamic diameter (nm) \pm SD		ζ - potential (mV) \pm SD	
		(LA) AgNPs	(Cit) AgNPs	(LA) AgNPs	(Cit) AgNPs
Nano-pure water	0	56 ± 8	51 ± 1	-56 ± 10	-37 ± 7
	24	49 ± 2	48 ± 4	-36 ± 10	-29 ± 12

The suspensions of both AgNPs and AgNO₃ were analysed as pristine suspensions and after *in vitro* digestion (IVD suspensions) to quantify the total silver content and silver in particulate form (AgNPs) using ICP-MS and spICP-MS, respectively (Figure 1).

The AgNPs content in the pristine suspensions of both types of AgNPs was equal to the total Ag content and corresponded to the theoretical (nominal) concentration. The pristine solution of AgNO₃ did not contain detectable levels of AgNPs.

Upon IVD, the total Ag content of both AgNPs suspensions and the AgNO₃ solution remained unchanged (compared to the pristine suspension) except the highest concentration of AgNPs (Figure 1A). The AgNPs content of both types of AgNPs was significantly reduced upon digestion at all concentrations tested.

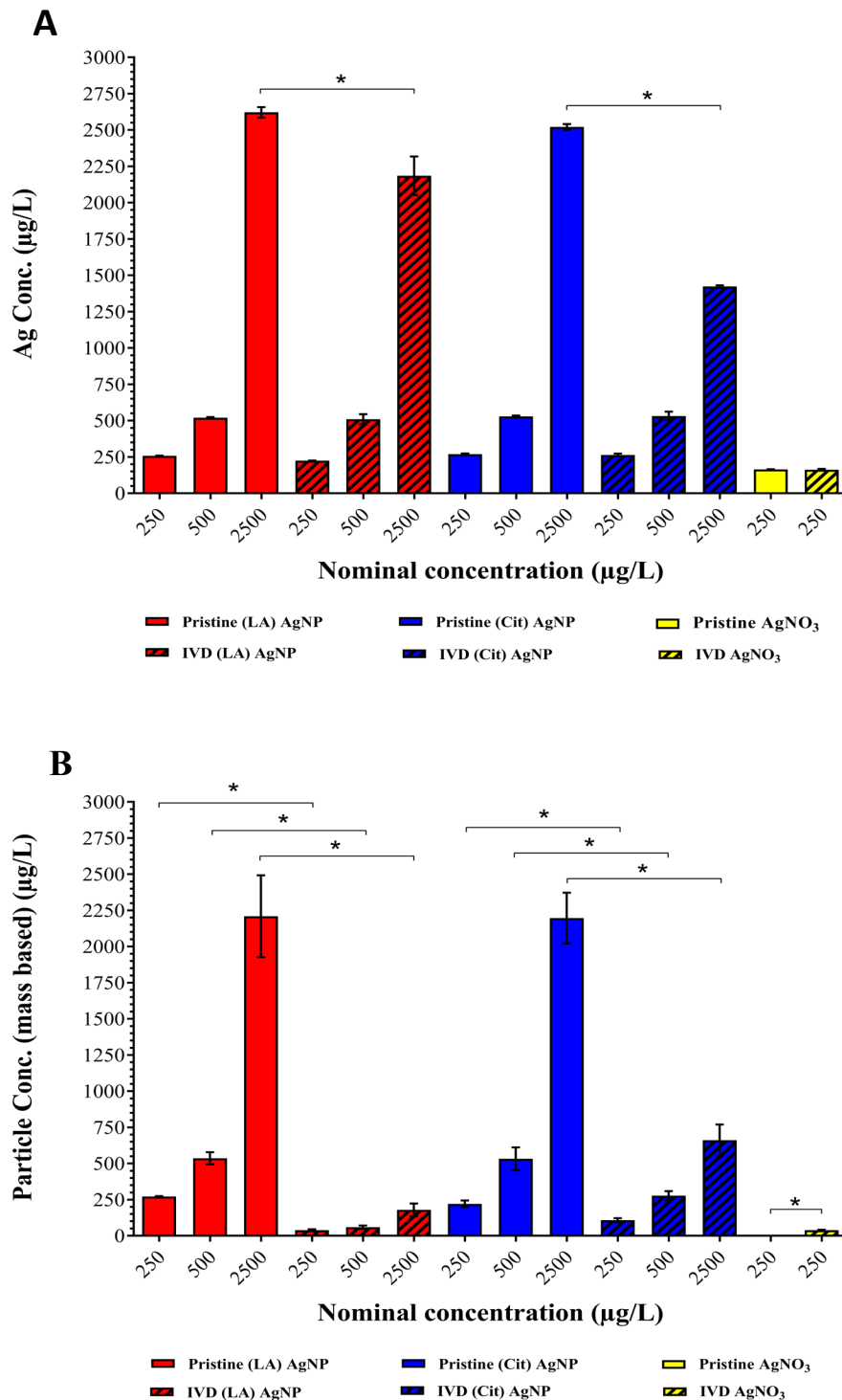


Figure 1: Silver content in pristine and in vitro digested (IVD) AgNPs suspensions and AgNO_3 solution. **A)** Silver content measured as total Ag using ICP-MS. **B)** Silver content measured as AgNPs using spICP-MS. Concentrations are given as the mean \pm SD ($n=3$). * Significant difference between the pristine and IVD suspension of the same AgNPs ($p < 0.05$).

The IVD (LA) AgNPs suspension showed a reduction in particulate silver (mass-based) between 86 – 92% while the IVD (Cit) AgNPs suspension showed a reduction between 48 – 70% in particulate silver (mass-based), compared to the pristine suspensions. Interestingly, a low but significantly elevated concentration of newly formed silver particulates (*de novo*) was observed in the AgNO₃ solution upon digestion (Figure 1B).

Assessment of AgNPs and AgNO₃ cytotoxicity

The viability of the Caco-2/HT29 co-culture was assessed using the WST-1 assay (cellular mitochondrial activity determination) upon 24 hr exposure to increasing concentrations of pristine or IVD AgNPs suspensions and AgNO₃ solution (Figure 2). The pristine AgNO₃ induced concentration dependent cytotoxicity. The cell viability of all the concentrations used in the subsequent experiments of pristine or IVD AgNPs suspensions (up to 2500 µg/L) and AgNO₃ solution (up to 500 µg/L) was higher than 85%.

Cellular barrier integrity assessment

For the transport studies, monolayers of Caco-2/HT29-MTX coculture were grown for 21 days in transwells to allow cells to form a tight junction and differentiated monolayer. Only monolayers that had TEER values > 200 Ω.cm² were used for subsequent cellular uptake/association and transport studies. The monolayer integrity was also confirmed by assessing the transport of lucifer yellow (LY) and 4 kDa and 10 kDa FITC-dextran in the presence or absence of a tight junction disruptor (EGTA). The transport of the three markers was very limited (< 0.5%) in the absence of the EGTA, while upon addition of EGTA the transport increased significantly (up to 20 - 140-fold) (Figure S 1).

Cellular uptake/association of AgNPs and AgNO₃ by monolayers of intestinal epithelial cells

Monolayers of 21 days old Caco-2/HT29-MTX coculture were exposed for 24 hr to increasing concentrations of either pristine or IVD AgNPs suspensions or AgNO₃ solution. The resulting cellular uptake/association of Ag was quantified and expressed as total Ag and AgNPs (Figure 3).

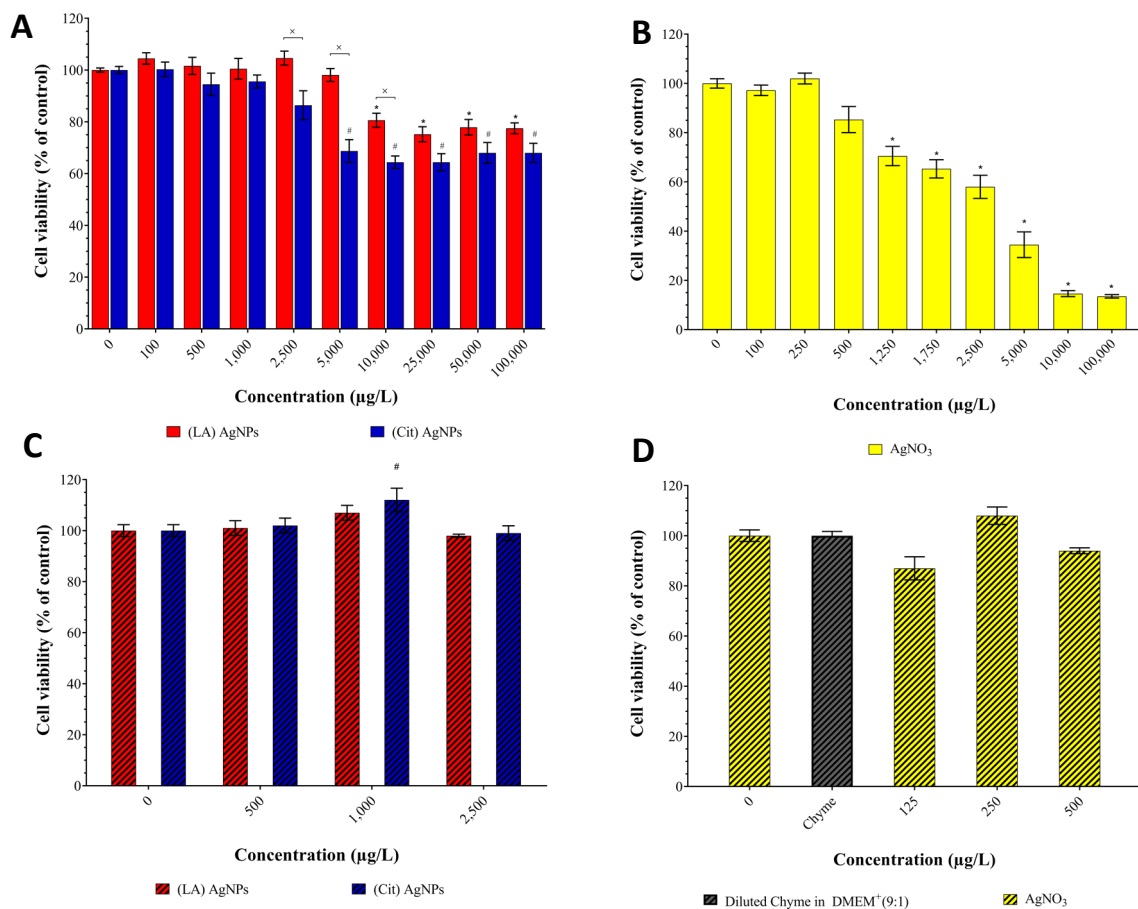


Figure 2: Cell viability of a Caco-2/HT29-MTX co-culture after 24 hr exposure to a concentration range of pristine; **A)** (LA) and (Cit) AgNPs and **B)** AgNO₃, and IVD; **C)** (LA) and (Cit) AgNPs and **D)** AgNO₃ using the WST-1 viability assay. Viability is given as a percentage of the control (mean \pm SD; n=3). * Significant difference between AgNPs at the same concentration ($p < 0.05$). *# Significant difference between any concentration and the control within the same treatment ($p < 0.05$).

The total Ag and AgNPs content in the cell fraction increased in a concentration - dependent manner for both AgNPs irrespective of their treatment (pristine or IVD) (Figure 3). Upon the pristine AgNPs exposure, the total Ag contents in the cellular fraction of (LA) AgNPs samples were significantly higher than that in the (Cit) AgNPs samples (Figure 3A). While the cellular fraction content of AgNPs exposed to (LA) AgNPs was significantly higher at the highest concentration compared to (Cit) AgNPs samples (Figure 3B). After IVD, comparable levels of Ag and AgNPs were detected in the (LA) and (Cit) AgNPs samples except for the highest

concentration where the (Cit) AgNPs samples had a significant higher Ag and AgNPs concentrations than the (LA) AgNPs samples (Figure 3C and D). In the cell fraction samples upon exposure to both pristine and IVD AgNO₃, mainly total Ag was detected, but after IVD a limited number of AgNPs was detected.

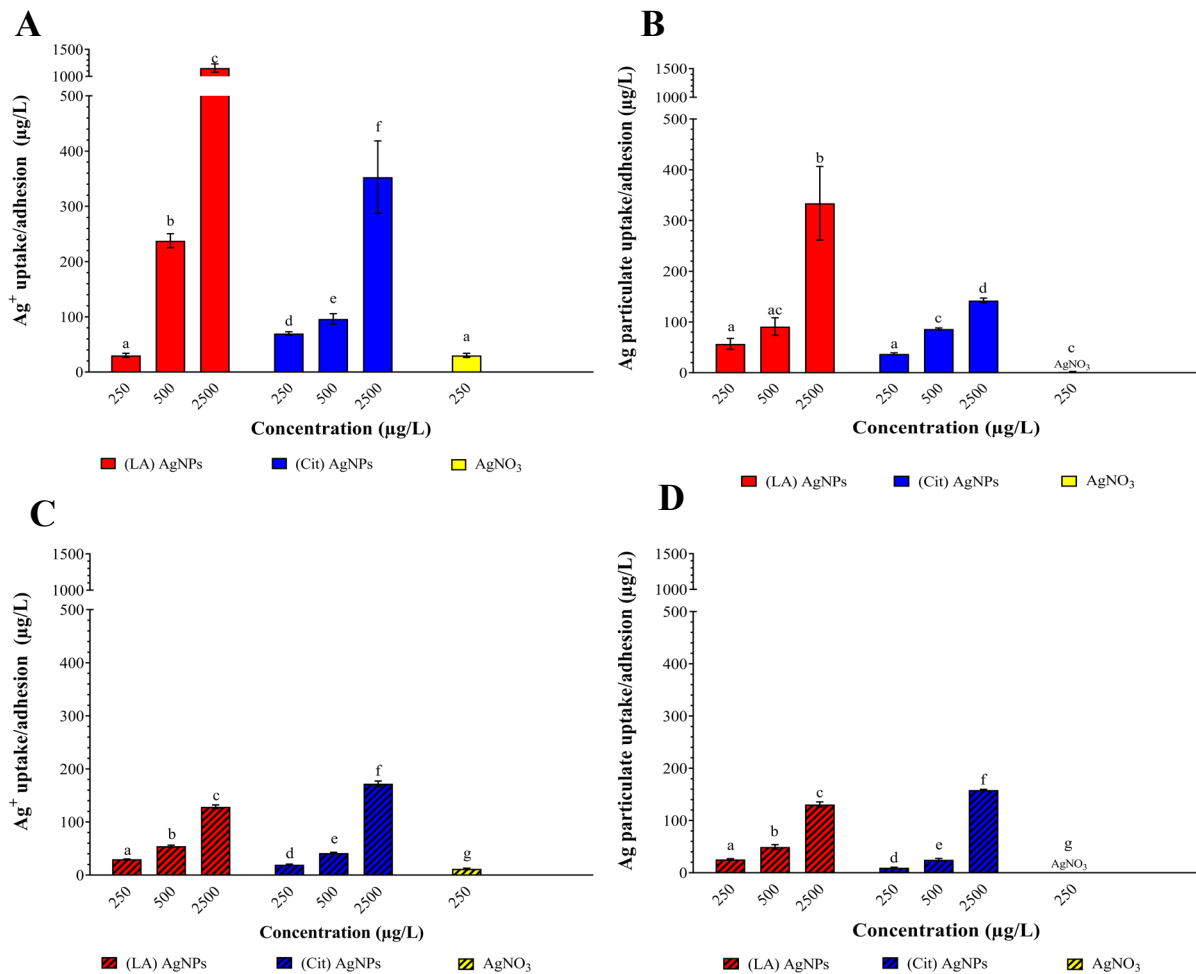


Figure 3: Silver uptake/adhesion of (LA) and (Cit) AgNPs and AgNO₃ in differentiated Caco-2/HT29-MTX cells after 24 hr exposure, measured and expressed as total Ag after; **A)** exposure to pristine AgNPs and AgNO₃. **C)** exposure to in vitro digested AgNPs and AgNO₃. Also expressed as AgNPs after; **B)** exposure to pristine AgNPs and AgNO₃. **D)** exposure to in vitro digested AgNPs and AgNO₃. Concentrations are given as the mean ± SD (n=3). Values with different letters are significantly different at the same concentration (p < 0.05).

In general, the cellular silver contents as total Ag or AgNPs upon exposure to IVD AgNPs was significantly lower compared to exposure to pristine AgNPs. Confocal microscopy was applied to evaluate cellular internalization of both AgNPs (pristine or IVD). Various planes through the cells were assessed showing that clusters of silver or AgNPs were mainly localized in the cytoplasm and to some extent in the nucleus (Figure 4).

Transport of AgNPs and AgNO₃ across monolayers of intestinal epithelial cells

The transport of either pristine or IVD AgNPs and AgNO₃ through the Caco-2/HT29-MTX monolayers was minimal (< 0.1%) either as total Ag or AgNPs. Also, using TEM-EDS, no AgNPs could be detected in samples from the basolateral compartments in any of the exposure groups. Only in small areas of the examined grids, an increased number of silver counts were found, but they were not visible in a particulate form (data not shown).

spICP-MS size distribution in pristine and IVD suspensions

The spICP-MS measurements were transformed into size distribution plots depicting the number of particles corresponding to each AgNPs diameter cluster (5 nm) on y- and x- axis, respectively (Figure 5). The number of particles measured in the AgNPs suspensions and AgNO₃ solution are presented in Table S1. There was no apparent difference in the size distributions of the pristine suspensions of both AgNPs, with a median size of 50 nm (Figure 5 A and B). No AgNPs could be detected in the pristine solution of AgNO₃ (Figure 5 C).

In vitro digestion affected the size and size distribution of (LA) AgNPs, as the mass - concentration were reduced (~90% lower) compared to the pristine samples (Figure 5D; also reflected in Figure 1). In addition, the size distribution curves of the IVD suspensions showed broadened distributions, indicating the presence of both smaller and larger particles. The size distribution of the (Cit) AgNPs was less affected by *in vitro* digestion, where the majority of both the pristine and IVD (Cit) AgNPs had a median size of 50 nm (Figure 5 B and E). The total number of particles was reduced (~38% lower) compared to the pristine particles. Upon *in vitro* digestion, newly formed silver particulates (*de novo*) were found in the AgNO₃ solution with a median size of 25 nm (Figure 5 F). All the size distributions of the three concentrations of AgNPs were following similar trend, accordingly all the size distributions reported in Figure 5 are only for of 500 µg/L of AgNPs and 250 µg/L AgNO₃ for simplicity and clarity purposes.

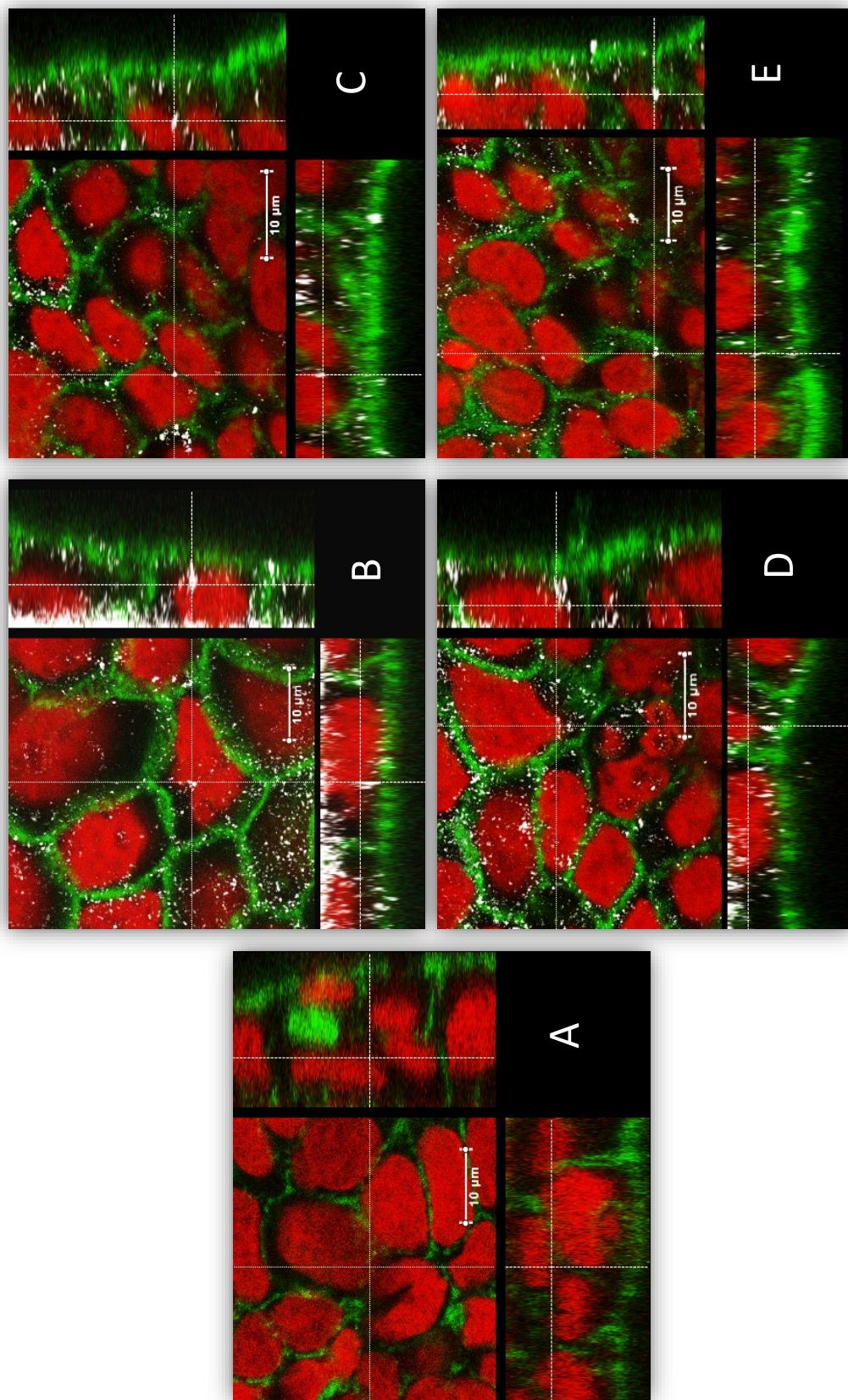


Figure 4: Uptake/adhesion of AgNPs after 24 hr exposure. Confocal microscopy images of 21-day old Caco-2/HT29-MTX cells. **A)** without exposure to AgNPs (negative control), after exposure to 2500 $\mu\text{g/L}$ **B)** pristine (LA) AgNPs, **C)** pristine (Cit) AgNPs, **D)** IVD (LA) AgNPs, and **E)** IVD (Cit) AgNPs. Nuclei were stained in red (RedDot-2). Actin was stained in green (Alexa -488 Phalloidin) and AgNPs are shown in white (back scatter).

spICP-MS size distribution in cellular fraction

The size distributions (Figure 6) and number of particles (Table S1) of both AgNPs measured in the cellular fraction were different depending on the surface chemistry of the AgNPs and on whether they were pristine or IVD. Following exposure to pristine (LA) AgNPs, a broad size distribution was observed without a clear peak (Figure 6 A). This distribution was highly different from the size distribution in the pristine suspension (Figure 5 A). For the pristine (Cit) AgNPs, the cellular fraction has AgNPs with a median size of 35 nm and the size distribution (Figure 6 B) was comparable to that of the pristine (Cit) AgNPs suspension (Figure 5 B). Among pristine AgNPs, the number of NPs in the cell fraction exposed to (LA) AgNPs ($3.1 \times 10^5 \pm 4.6 \times 10^4$) was significantly lower than the number of particles detected in the cells exposed to (Cit) AgNPs ($2.6 \times 10^6 \pm 1.7 \times 10^5$). The size distribution of IVD (LA) AgNPs in the cell fraction - compared to the IVD suspension distribution of these AgNPs (Figure 5 D) - was right skewed with a median size of 45 nm (Figure 6 D).

The broadening of the size distribution and longer tail showed the appearance of bigger particles (aggregates) up to 200 nm. The size distribution of IVD (Cit) AgNPs in the cell fraction (Figure 6 E) also showed a longer tail compared to the IVD (Cit) AgNPs suspension (Figure 5 E), showing bigger particles (aggregates) up to 200 nm with a median size of 50 nm. Among IVD AgNPs, the number of NPs in the cell fraction exposed to (LA) AgNPs ($4.2 \times 10^5 \pm 3.6 \times 10^4$) was comparable to the number of particles detected in the cells exposed to (Cit) AgNPs ($4.4 \times 10^5 \pm 6 \times 10^4$).

The cellular fraction exposed to pristine AgNO₃ contained particulate Ag with a median size of 30 nm (Figure 6 C), while the pristine AgNO₃ solution did not contain particles (Figure 5 C). Upon exposure to IVD AgNO₃ solution, the cellular fraction contained silver particulates with a median size of 50 nm (Figure 5 F and Figure 6 F). The number of particles measured in the cellular fraction upon exposure to AgNPs and AgNO₃ are presented in Table S1. All the size distributions of the three concentrations of AgNPs were following similar trend, accordingly all the size distributions reported in Figure 6 are only for of 500 µg/L of AgNPs and 250 µg/L AgNO₃ for simplicity and clarity purposes.

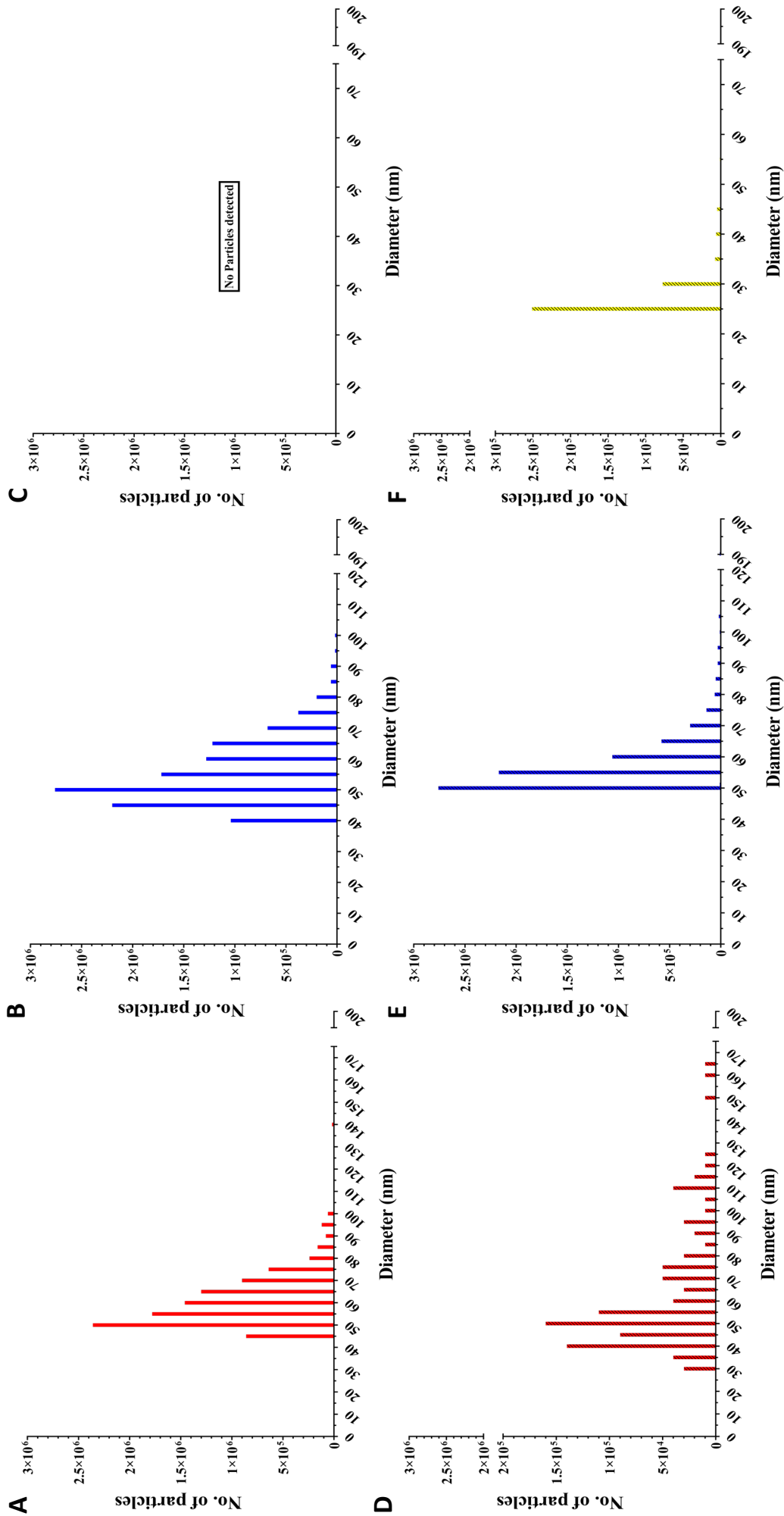


Figure 5: Number-weighted size distributions generated by spICP-MS measurement of suspension: **A)** 500 µg/L pristine (LA) AgNPs, **B)** 500 µg/L pristine (Cit) AgNPs, **C)** 250 µg/L pristine AgNO₃, **D)** (LA) 500 µg/L IVD AgNPs, **E)** 500 µg/L IVD (Cit) AgNPs and **F)** 250 µg/L IVD AgNO₃

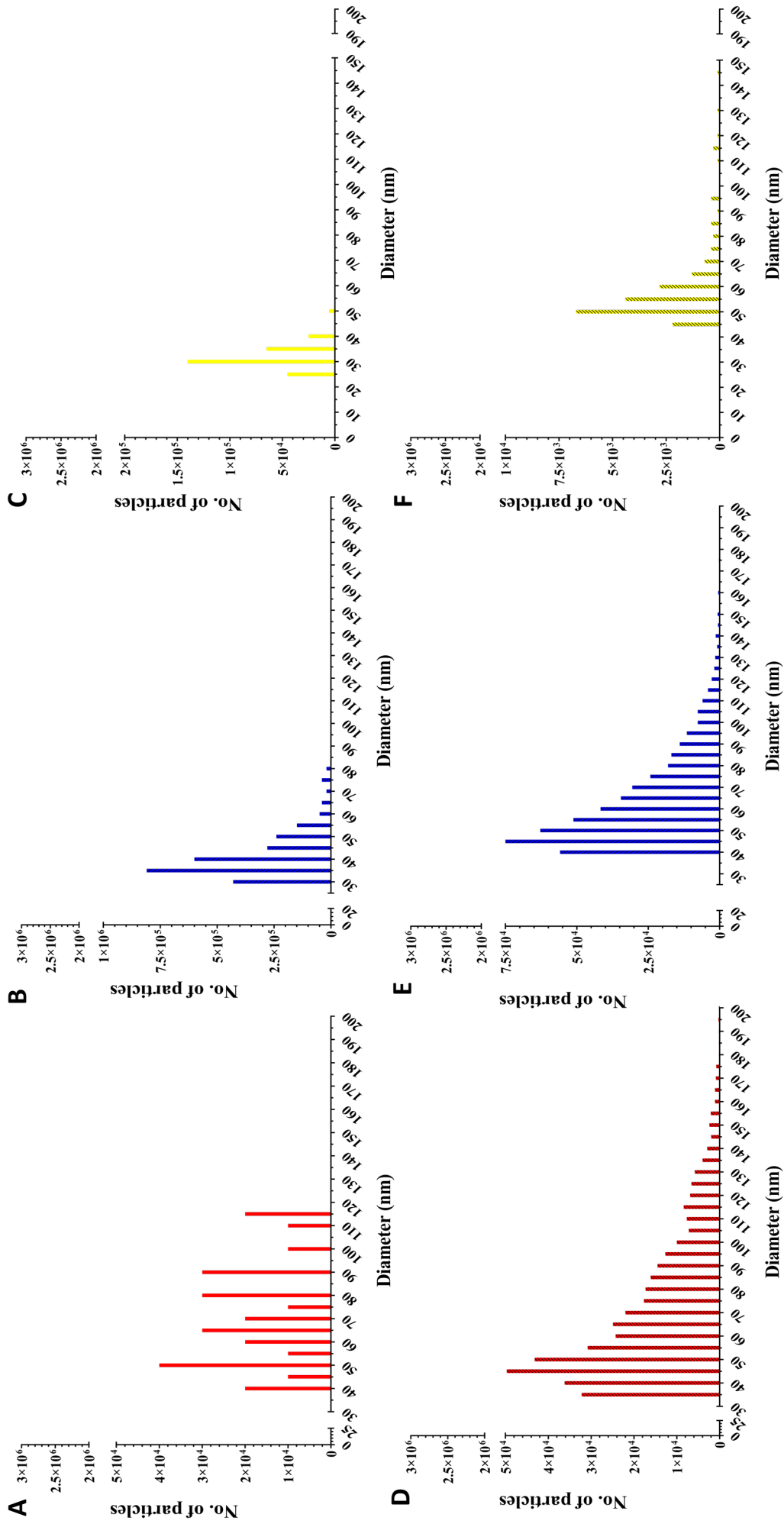


Figure 6: Number-weighted size distributions generated by spICP-MS measurement of Caco-2/HT29-MTX cellular silver content after 24 hr exposure to: **A)** 500 µg/L pristine

(LA) AgNPs, **B)** 500 µg/L pristine 50 nm (Cit) AgNPs, **C)** 250 µg/L IVD (LA) AgNPs, **D)** 500 µg/L IVD (LA) AgNPs, **E)** 500 µg/L IVD (Cit) AgNPs, and **F)** 250 µg/L IVD AgNO₃.

DISCUSSION

This study aimed to investigate the impact of the different biochemical conditions within the human digestive tract - mimicked in *in vitro* incubations - on the intestinal fate and subsequent cellular uptake/association and passage across a monolayer of differentiated Caco-2/HT29-MTX intestinal cells. We observed that a significant fraction of the AgNPs dissolved after the *in vitro* digestion. Exposure of the monolayers of intestinal cells to increasing concentrations of pristine AgNPs resulted in a concentration dependent increase of total Ag and AgNPs contents in the cellular fractions. These concentrations were significantly lower following the exposure to the IVD AgNPs. Finally, passage of silver as total Ag or AgNPs was not detectable following the exposure to either pristine or IVD AgNPs.

The *in vitro* digestion model used here was adopted from the model described by Versantvoort (Walczak *et al.* 2012; Versantvoort *et al.* 2005). The pH in the gastric digestion phase was set at 5 ± 0.5 to simulate the gastric environment upon ingestion of a meal (Minekus *et al.* 2014; Gardner *et al.* 2002; Richardson and Feldman 1986). While this is the most realistic exposure scenario, it might underestimate the dissolution of AgNPs if consumed in fasted (empty stomach) conditions, where the stomach pH is lower (pH 2) (Liu *et al.* 2012). Before *in vitro* digestion (*i.e.* the pristine suspensions), both AgNPs suspensions contained similar masses of total Ag and AgNPs, indicating that before *in vitro* digestion, the silver was present mainly in particulate form. In addition, the spICP-MS derived size distributions of both AgNPs suspensions were highly comparable.

Upon completion of all three digestion phases (oral, gastric and intestinal), the total Ag content in both of the IVD AgNPs suspensions and the AgNO₃ solution was similar to that of the corresponding pristine suspensions and solution, except for the highest concentration of both AgNPs, with the total Ag content being ~10% and ~40% lower for (LA) and (Cit) AgNPs, respectively. The reduction in total Ag content of samples taken from the highest concentrations could be due to a lower (analytical) recovery due to adsorption of AgNPs to the digestion matrix and tubing and/or to the short centrifugation step applied to the AgNPs samples after digestion to spin down large protein precipitates before ICP-MS measurement (Versantvoort *et al.* 2005) to which the AgNPs could potentially adsorb (Noireaux *et al.* 2019). This centrifugation set is required to avoid the presence of large proteins that

destabilize the plasma of the ICP-MS (Noireaux *et al.* 2019). On the other hand, a significant reduction in the mass- and number-based AgNPs content was observed for both AgNPs upon completion of all digestion phases, demonstrating that the *in vitro* digestion could induce dissolution, aggregation, or protein binding of the AgNPs (Böhmert *et al.* 2014). Significantly more of the (Cit) AgNPs endured the digestion conditions than the (LA) AgNPs, which is most likely due to the differences in surface chemistry of the AgNPs which is influencing the adsorption and agglomeration characteristics of the AgNPs. For example, the dissolution of (Cit) AgNPs in fresh river water was reported by Li and Lenhart to be much slower than that of tween coated AgNPs, where (Cit) AgNPs needed an incubation of 15 days to dissolve to the same extent as the tween coated AgNPs within 6 hr (Li and Lenhart 2012). Besides, in cell culture medium, (Cit) AgNPs have been shown to dissolve much slower compared to 5-kDa PEG-thiol-coated AgNPs (Zook *et al.* 2011). Dissolution of (LA) coated AgNPs, reported in the present study, has not been studied before.

Interestingly, a significant number of silver particles was detected in the AgNO₃ solution after *in vitro* digestion, whereas in its pristine solution no particles were detected. The digestive juices have a high ionic strength including a high concentration of chloride, which is known to form particulate complexes with silver ions or the *de novo* formed AgNPs (Huynh and Chen 2011; Zook *et al.* 2011). This could explain the higher amount detected of cellular *de novo* formed AgNPs upon exposure to pristine AgNO₃ than exposure to IVD AgNO₃. Formation of *de novo* complexes of silver ions with chloride, sulphur or thiocyanate has been described before both *in vitro* (Kästner *et al.* 2018; Wildt *et al.* 2016; Walczak *et al.* 2012) and *in vivo* (Levard *et al.* 2011; Loeschner *et al.* 2011).

In the present study, we used monolayers of differentiated Caco-2/HT29-MTX cells. The presence of mucus producing cells increases the physiological relevance of the model compared to using Caco-2 cells alone (Georgantzopoulou *et al.* 2016; Yuan *et al.* 2013; Mahler *et al.* 2009; Hilgendorf *et al.* 2000). Non-cytotoxic concentrations of AgNPs (and ionic controls) were used in our study. As chyme from the *in vitro* digestion model results in cytotoxic responses, the chyme was diluted in a 1: 9 ratio with cell culture medium as described previously to avoid any cytotoxic effects (Lichtenstein *et al.* 2015; Walczak *et al.* 2015a; Böhmert *et al.* 2014).

After 24 hr of exposure to suspension of three concentrations of either pristine or IVD AgNPs, the total Ag and AgNPs contents of the cellular fraction increased in a concentration dependent manner. Both the total Ag and AgNPs contents in the cellular fractions were significantly lower following exposure to IVD AgNPs compared to the exposure to similar concentrations of pristine suspensions of AgNPs. Similar observations were reported for a differentiated Caco-2 cell model exposed to pristine and IVD AgNPs, although in that study only the total Ag content was measured (Lichtenstein *et al.* 2015). Furthermore, cellular uptake of total and particulate silver or titanium was also shown to be concentration dependent after 24 hours exposure in Neuro-2a cells (Hsiao *et al.* 2016).

The total Ag concentration found in the cellular fraction was in general higher than the AgNPs concentration, whereas upon digestion, the total Ag and AgNPs levels in the cellular fractions were highly comparable. As AgNPs tends to dissolve intracellularly (Singh and Ramarao 2012) and form protein corona upon IVD (Walczak *et al.* 2015a), it is likely that the *in vitro* digestion is protecting the AgNPs from dissolving inside the cells. In general, the AgNPs content in the cellular fraction appeared to be higher in the (LA) AgNPs samples than in the (Cit) AgNPs samples, following exposure to pristine AgNPs. The difference in the cellular total Ag content between (LA) and (Cit) AgNPs could be explained by possible formation of different types of protein coronas on the AgNPs due to their differences in surface chemistry, as previously described for AgNPs and other NPs (Abdelkhalik *et al.* 2018; Monteiro-Riviere *et al.* 2013; Tenzer *et al.* 2013; Lesniak *et al.* 2012). Another factor influencing the interaction of AgNPs with cells could be the stability of the coating which might be affected by the ionic strength, protein content, or pH of the medium (Sharma *et al.* 2014).

Although spICP-MS is a very sensitive technique to quantify total Ag and AgNPs concentrations, it does not provide insights in the (sub)cellular localization of the Ag. Here, the confocal imaging showed that a fraction of the AgNPs was internalized in the cells.

Following exposure of the monolayers to AgNO₃ (pristine and IVD), AgNPs were detected in the cell fraction which suggests the *de novo* formation of AgNPs. However, the sizes of these AgNPs differed with a peak shift from 30 nm in the pristine samples to 50 nm in the digested samples. The *de novo* AgNPs are most likely to be firstly formed as silver salt complexes following the *in vitro* digestion and upon cellular exposure and internalization, these

complexes may further interact with other cellular molecules rich in sulphur (*i.e.* cysteine and glutathione) and grow forming *de novo* nanoparticles *in situ* (Wildt *et al.* 2016; Maurer *et al.* 2014; Loeschner *et al.* 2011).

Lastly, we assessed the passage of total Ag and AgNPs across the monolayers of Caco-2/HT29-MTX cells. We performed all our experiments in transwells and sampled the basolateral compartment following an exposure to both pristine and IVD AgNPs suspensions; the transport of silver as either total Ag or AgNPs was < 0.1%. From an analytical perspective, the sensitivity and power of the methods used for detection and quantification of Ag and AgNPs (ICP-MS and spICP-MS respectively) were high compared to other methods that have been used before. That explains, why we could use low exposure concentrations (*i.e.* 250 µg/L) and still were able to detect total Ag and AgNPs in the cellular fractions. Other studies reported that the silver content in the cellular fractions after a higher exposure concentration (*i.e.* 1000 µg/L) of either pristine or IVD AgNO₃ solutions for the same exposure time was lower than the LOQ (20 µg/cm²) (Lichtenstein *et al.* 2015).

In addition, the basolateral samples were screened for AgNPs using TEM-EDS, but again no particles were detected. Previously, we have shown minimal passage (less than 1%) of smaller (20 nm) AgNPs across a monolayer of Caco-2/M-cells exposed for 4 hr (Bouwmeester *et al.* 2011). For larger AgNPs it can be expected that the passage/transport is lower, in addition, we currently used membranes with a smaller pore size that might hinder the transport of the AgNPs (Cartwright *et al.* 2012). However, *in vivo* studies indicate that silver can reach the systemic circulation, as oral feeding studies with rodents have reported low oral bioavailability of silver after exposure to AgNPs of different sizes (van der Zande *et al.* 2012; Loeschner *et al.* 2011).

The Caco-2/HT29-MTX intestinal model shows potential for screening AgNPs. Addition of M-cells to the model is not of added value in the current case, as it was reported before to reduce the transport of NPs to a similar level of transport through Caco-2 monolayer where no mucus is present (Walczak *et al.* 2015b). In another study, AgNPs transport via a Caco-2/M-cell intestinal model could be detected (Bouwmeester *et al.* 2011) but the AgNPs used were of smaller size and in pristine status which might facilitate the possibility of detection. Applying longer exposure periods or higher non-toxic concentrations of AgNPs might increase the

chance of detecting and quantifying transported AgNPs, owing to the limitation of the AgNPs stock concentration and the necessity to high dilution upon the digestion to avoid chyme toxicity. The broad spectrum of AgNPs with diverse physicochemical characteristics might exhibit different behaviours upon *in vitro* digestion and intestinal uptake and transport which highlight the importance of detailed characterization of AgNPs studied and the difficulty to group the AgNPs.

CONCLUSIONS

The surface chemistry of AgNPs had a significant influence on their dissolution and on their biological interactions with the Caco-2/HT29-MTX intestinal model. The (LA) AgNPs dissolved to a significantly higher extent during the digestion process compared to (Cit) AgNPs. Cellular uptake/association was in general higher for the (LA) AgNPs, although this difference disappeared after digestion. Upon *in vitro* digestion, the cellular uptake/association of both AgNPs decreased compared to the cellular uptake/association of pristine AgNPs. Transport of AgNPs across the monolayers of intestinal cells was < 0.1%. *De novo* formation of AgNPs was shown in the suspensions and in the cellular fractions upon digestion and cellular exposure of cells to AgNPs and AgNO₃.

The combination of *in vitro* digestion and intestinal barrier models used here confirms the interference and the influence of the digestion process on the biological interaction of the AgNPs upon oral ingestion. This highlights the need to take *in vitro* digestion into account when studying nanoparticle toxicokinetics and toxicodynamics in cellular *in vitro* model systems. Additionally, this combination is of added value to the safer-by-design NPs development by identifying the physicochemical property (here the surface chemistry) that affects the uptake/association and cellular internalization.

ACKNOWLEDGMENTS

The authors would like to thank Kerstin Jurkschat (Oxford University, UK) for TEM-EDS analysis.

REFERENCES

- Abdelkhalik A, van der Zande M, Punt A, Helsdingen R, Boeren S, Vervoort JJM, Rietjens IMCM, Bouwmeester H. 2018. Impact of nanoparticle surface functionalization on the protein corona and cellular adhesion, uptake and transport. *Journal of Nanobiotechnology* 16:70.
- Abdolahpur Monikh F, Chupani L, Zusková E, Peters R, Vancová M, Vijver MG, Porcal P, Peijnenburg WJGM. 2019. Method for Extraction and Quantification of Metal-Based Nanoparticles in Biological Media: Number-Based Biodistribution and Bioconcentration. *Environmental Science & Technology* 53:946-953.
- Bailey CA, Bryla P, Malick AW. 1996. The use of the intestinal epithelial cell culture model, Caco-2, in pharmaceutical development. *Adv Drug Deliv Rev* 22.
- Böhmert L, Girod M, Hansen U, Maul R, Knappe P, Niemann B, Weidner SM, Thünemann AF, Lampen A. 2014. Analytically monitored digestion of silver nanoparticles and their toxicity on human intestinal cells. *Nanotoxicology* 8:631-642.
- Bouwmeester H, Poortman J, Peters RJ, Wijma E, Kramer E, Makama S, Puspitaninganindita K, Marvin HJP, Peijnenburg AACM, Hendriksen PJM. 2011. Characterization of translocation of silver nanoparticles and effects on whole-genome gene expression using an in vitro intestinal epithelium coculture model. *ACS Nano* 5.
- Cartwright L, Poulsen MS, Nielsen HM, Pojana G, Knudsen LE, Saunders M, Rytting E. 2012. In vitro placental model optimization for nanoparticle transport studies. *Int J Nanomedicine* 7:497-510.
- Chaudhry Q, Scotter M, Blackburn J, Ross B, Boxall A, Castle L, Aitken R, Watkins R. 2008. Applications and implications of nanotechnologies for the food sector. *Food Additives & Contaminants: Part A* 25:241-258.
- Choi JI, Chae SJ, Kim JM, Choi JC, Park SJ, Choi HJ, Bae H, Park HJ. 2018. Potential silver nanoparticles migration from commercially available polymeric baby products into food simulants. *Food Additives & Contaminants: Part A* 35:996-1005.
- Ding R, Yang P, Yang Y, Yang Z, Luo L, Li H, Wang Q. 2018. Characterisation of silver release from nanoparticle-treated baby products. *Food Additives & Contaminants: Part A* 35:2052-2061.
- Gardner JD, Ciociola AA, Robinson M. 2002. Measurement of meal-stimulated gastric acid secretion by in vivo gastric autotitration. *Journal of Applied Physiology* 92:427-434.
- Georgantzopoulou A, Serchi T, Cambier S, Leclercq CC, Renaut J, Shao J, Kruszewski M, Lentzen E, Grysan P, Eswara S, Audinot J-N, Contal S, Ziebel J, Guignard C, Hoffmann L, Murk AJ, Gutleb AC. 2016. Effects of silver nanoparticles and ions on a co-culture model for the gastrointestinal epithelium. *Particle and Fibre Toxicology* 13:9.
- Hilgendorf C, Spahn-Langguth H, Regårdh CG, Lipka E, Amidon GL, Langguth P. 2000. Caco-2 versus Caco-2/HT29-MTX co-cultured cell lines: permeabilities via diffusion, inside- and outside-directed carrier-mediated transport. *J Pharm Sci* 89.
- Hsiao I-L, Bierkandt FS, Reichardt P, Luch A, Huang Y-J, Jakubowski N, Tentschert J, Haase A. 2016. Quantification and visualization of cellular uptake of TiO₂ and Ag nanoparticles: comparison of different ICP-MS techniques. *Journal of Nanobiotechnology* 14:50.

- Huynh KA, Chen KL. 2011. Aggregation Kinetics of Citrate and Polyvinylpyrrolidone Coated Silver Nanoparticles in Monovalent and Divalent Electrolyte Solutions. *Environmental Science & Technology* 45:5564-5571.
- Imai S, Morishita, Yuki Hata, Tomoyuki Kondoh, Masuo Yagi, Kiyohito Gao, Jian-Qing Nagano, Kazuya Higashisaka, Kazuma Yoshioka, Yasuo Tsutsumi, Yasuo. 2017. Cellular internalization, transcellular transport, and cellular effects of silver nanoparticles in polarized Caco-2 cells following apical or basolateral exposure. *Biochemical and Biophysical Research Communications* 484:543-549.
- Kästner C, Lampen A, Thünemann AF. 2018. What happens to the silver ions? – Silver thiocyanate nanoparticle formation in an artificial digestion. *Nanoscale* 10:3650-3653.
- Kittler S, Greulich C, Diendorf J, Köller M, Epple M. 2010. Toxicity of Silver Nanoparticles Increases during Storage Because of Slow Dissolution under Release of Silver Ions. *Chemistry of Materials* 22:4548-4554.
- Kleiveland CR. 2015. Co-cultivation of Caco-2 and HT-29MTX. In: Verhoeckx K, Cotter P, López-Expósito I, Kleiveland C, Lea T, Mackie A, Requena T, Swiatecka D, Wichers H, eds. *The Impact of Food Bioactives on Health: in vitro and ex vivo models*. Cham: Springer International Publishing, 135-140.
- Laborda F, Jimenez-Lamana J, Bolea E, Castillo JR. 2011. Selective identification, characterization and determination of dissolved silver(i) and silver nanoparticles based on single particle detection by inductively coupled plasma mass spectrometry. *Journal of Analytical Atomic Spectrometry* 26:1362-1371.
- Lefebvre DE, Venema K, Gombau L, Valerio LG, Raju J, Bondy GS, Bouwmeester H, Singh RP, Clippinger AJ, Collnot E-M, Mehta R, Stone V. 2015. Utility of models of the gastrointestinal tract for assessment of the digestion and absorption of engineered nanomaterials released from food matrices. *Nanotoxicology* 9:523-542.
- Lesniak A, Fenaroli F, Monopoli MP, Åberg C, Dawson KA, Salvati A. 2012. Effects of the Presence or Absence of a Protein Corona on Silica Nanoparticle Uptake and Impact on Cells. *ACS Nano* 6:5845-5857.
- Levard C, Reinsch BC, Michel FM, Oumahi C, Lowry GV, Brown GE. 2011. Sulfidation Processes of PVP-Coated Silver Nanoparticles in Aqueous Solution: Impact on Dissolution Rate. *Environmental Science & Technology* 45:5260-5266.
- Li X, Lenhart JJ. 2012. Aggregation and Dissolution of Silver Nanoparticles in Natural Surface Water. *Environmental Science & Technology* 46:5378-5386.
- Lichtenstein D, Ebmeyer J, Knappe P, Juling S, Böhmert L, Selve S, Niemann B, Braeuning A, Thünemann Andreas F, Lampen A. 2015. Impact of food components during *in vitro* digestion of silver nanoparticles on cellular uptake and cytotoxicity in intestinal cells. *Biological Chemistry*. 1255.
- Lichtenstein D, Ebmeyer J, Meyer T, Behr A-C, Kästner C, Böhmert L, Juling S, Niemann B, Fahrenson C, Selve S, Thünemann AF, Meijer J, Estrela-Lopis I, Braeuning A, Lampen A. 2017. It takes more than a coating to get nanoparticles through the intestinal barrier *in vitro*. *European Journal of Pharmaceutics and Biopharmaceutics* 118:21-29.
- Liu J, Wang Z, Liu FD, Kane AB, Hurt RH. 2012. Chemical transformations of nanosilver in biological environments. *ACS nano* 6:9887-9899.

- Loeschner K, Hadrup N, Qvortrup K, Larsen A, Gao X, Vogel U, Mortensen A, Lam HR, Larsen EH. 2011. Distribution of silver in rats following 28 days of repeated oral exposure to silver nanoparticles or silver acetate. *Particle and Fibre Toxicology* 8:18.
- López-Serrano A, Olivas RM, Landaluze JS, Cámara C. 2014. Nanoparticles: a global vision. Characterization, separation, and quantification methods. Potential environmental and health impact. *Analytical Methods* 6:38-56.
- Mahler GJ, Shuler ML, Glahn RP. 2009. Characterization of Caco-2 and HT29-MTX cocultures in an in vitro digestion/cell culture model used to predict iron bioavailability. *J Nutr Biochem* 20.
- Maurer EI, Sharma M, Schlager JJ, Hussain SM. 2014. Systematic analysis of silver nanoparticle ionic dissolution by tangential flow filtration: toxicological implications. *Nanotoxicology* 8:718-727.
- McCracken C, Zane A, Knight DA, Hommel E, Dutta PK, Waldman WJ. 2015. Oxidative stress-mediated inhibition of intestinal epithelial cell proliferation by silver nanoparticles. *Toxicology in Vitro* 29:1793-1808.
- Minekus M, Alminger M, Alvito P, Ballance S, Bohn T, Bourlieu C, Carrière F, Boutrou R, Corredig M, Dupont D, Dufour C, Egger L, Golding M, Karakaya S, Kirkhus B, Le Feunteun S, Lesmes U, Macierzanka A, Mackie A, Marze S, McClements DJ, Ménard O, Recio I, Santos CN, Singh RP, Vegarud GE, Wickham MSJ, Weitschies W, Brodkorb A. 2014. A standardised static in vitro digestion method suitable for food – an international consensus. *Food & Function* 5:1113-1124.
- Monteiro-Riviere NA, Samberg ME, Oldenburg SJ, Riviere JE. 2013. Protein binding modulates the cellular uptake of silver nanoparticles into human cells: implications for in vitro to in vivo extrapolations? *Toxicology letters* 220:286-293.
- Murdock RC, Braydich-Stolle L, Schrand AM, Schlager JJ, Hussain SM. 2008. Characterization of Nanomaterial Dispersion in Solution Prior to In Vitro Exposure Using Dynamic Light Scattering Technique. *Toxicological Sciences* 101:239-253.
- Mwilu SK, El Badawy AM, Bradham K, Nelson C, Thomas D, Scheckel KG, Tolaymat T, Ma L, Rogers KR. 2013. Changes in silver nanoparticles exposed to human synthetic stomach fluid: Effects of particle size and surface chemistry. *Science of The Total Environment* 447:90-98.
- Nel A, Xia T, Mädler L, Li N. 2006. Toxic Potential of Materials at the Nanolevel. *Science* 311:622-627.
- Noireaux J, Grall R, Hullo M, Chevillard S, Oster C, Brun E, Sicard-Roselli C, Loeschner K, Fiscaro P. 2019. Gold Nanoparticle Uptake in Tumor Cells: Quantification and Size Distribution by sp-ICPMS. *Separations* 6:3.
- Peters R, Herrera-Rivera Z, Undas A, van der Lee M, Marvin H, Bouwmeester H, Weigel S. 2015. Single particle ICP-MS combined with a data evaluation tool as a routine technique for the analysis of nanoparticles in complex matrices. *Journal of Analytical Atomic Spectrometry* 30:1274-1285.
- Richardson CT, Feldman M. 1986. Salivary response to food in humans and its effect on gastric acid secretion. *American Journal of Physiology-Gastrointestinal and Liver Physiology* 250:G85-G91.
- Sharma VK, Siskova KM, Zboril R, Gardea-Torresdey JL. 2014. Organic-coated silver nanoparticles in biological and environmental conditions: Fate, stability and toxicity. *Advances in Colloid and Interface Science* 204:15-34.

- Sieg H, Kästner C, Krause B, Meyer T, Burel A, Böhmert L, Lichtenstein D, Jungnickel H, Tentschert J, Laux P, Braeuning A, Estrela-Lopis I, Gauffre F, Fessard V, Meijer J, Luch A, Thünemann AF, Lampen A. 2017. Impact of an Artificial Digestion Procedure on Aluminum-Containing Nanomaterials. *Langmuir* 33:10726-10735.
- Singh RP, Ramarao P. 2012. Cellular uptake, intracellular trafficking and cytotoxicity of silver nanoparticles. *Toxicology Letters* 213:249-259.
- Stone V, Johnston H, Schins RPF. 2009. Development of *in vitro* systems for nanotoxicology: methodological considerations. *Critical Reviews in Toxicology* 39:613-626.
- Tenzer S, Docter D, Kuharev J, Musyanovych A, Fetz V, Hecht R, Schlenk F, Fischer D, Kiouptsi K, Reinhardt C, Landfester K, Schild H, Maskos M, Knauer SK, Stauber RH. 2013. Rapid formation of plasma protein corona critically affects nanoparticle pathophysiology. *Nat Nanotechnol* 8.
- van der Zande M, Undas AK, Kramer E, Monopoli MP, Peters RJ, Garry D, Antunes Fernandes EC, Hendriksen PJ, Marvin HJP, Peijnenburg AA, Bouwmeester H. 2016. Different responses of Caco-2 and MCF-7 cells to silver nanoparticles are based on highly similar mechanisms of action. *Nanotoxicology* 10:1431-1441.
- van der Zande M, Vandebriel RJ, Van Doren E, Kramer E, Herrera Rivera Z, Serrano-Rojero CS, Gremmer ER, Mast J, Peters RJB, Hollman PCH, Hendriksen PJM, Marvin HJP, Peijnenburg AACM, Bouwmeester H. 2012. Distribution, Elimination, and Toxicity of Silver Nanoparticles and Silver Ions in Rats after 28-Day Oral Exposure. *ACS Nano* 6:7427-7442.
- Versantvoort CHM, Oomen AG, Van de Kamp E, Rempelberg CJM, Sips AJAM. 2005. Applicability of an *in vitro* digestion model in assessing the bioaccessibility of mycotoxins from food. *Food and Chemical Toxicology* 43:31-40.
- Walczak AP, Fokkink R, Peters R, Tromp P, Herrera Rivera ZE, Rietjens IMCM, Hendriksen PJM, Bouwmeester H. 2012. Behaviour of silver nanoparticles and silver ions in an *in vitro* human gastrointestinal digestion model. *Nanotoxicology* 7:1198-1210.
- Walczak AP, Kramer E, Hendriksen PJM, Helsdingen R, van der Zande M, Rietjens IMCM, Bouwmeester H. 2015a. *In vitro* gastrointestinal digestion increases the translocation of polystyrene nanoparticles in an *in vitro* intestinal co-culture model. *Nanotoxicology* 9:886-894.
- Walczak AP, Kramer E, Hendriksen PJM, Tromp P, Helsper JPDFG, van der Zande M, Rietjens IMCM, Bouwmeester H. 2015b. Translocation of differently sized and charged polystyrene nanoparticles in *in vitro* intestinal cell models of increasing complexity. *Nanotoxicology* 9:453-461.
- Weigel S, Peters R, Loeschner K, Grombe R, Linsinger TPJ. 2017. Results of an interlaboratory method performance study for the size determination and quantification of silver nanoparticles in chicken meat by single-particle inductively coupled plasma mass spectrometry (sp-ICP-MS). *Analytical and bioanalytical chemistry* 409:4839-4848.
- Wildt BE, Celedon A, Maurer EI, Casey BJ, Nagy AM, Hussain SM, Goering PL. 2016. Intracellular accumulation and dissolution of silver nanoparticles in L-929 fibroblast cells using live cell time-lapse microscopy. *Nanotoxicology* 10:710-719.
- Yuan H, Chen C, Chai G, Du Y, Hu F. 2013. Improved transport and absorption through gastrointestinal tract by PEGylated solid lipid nanoparticles. *Mol Pharm* 10.

Zook JM, Long SE, Cleveland D, Geronimo CLA, MacCuspie RI. 2011. Measuring silver nanoparticle dissolution in complex biological and environmental matrices using UV–visible absorbance. *Analytical and Bioanalytical Chemistry* 401:1993.

SUPPLEMENTARY MATERIAL

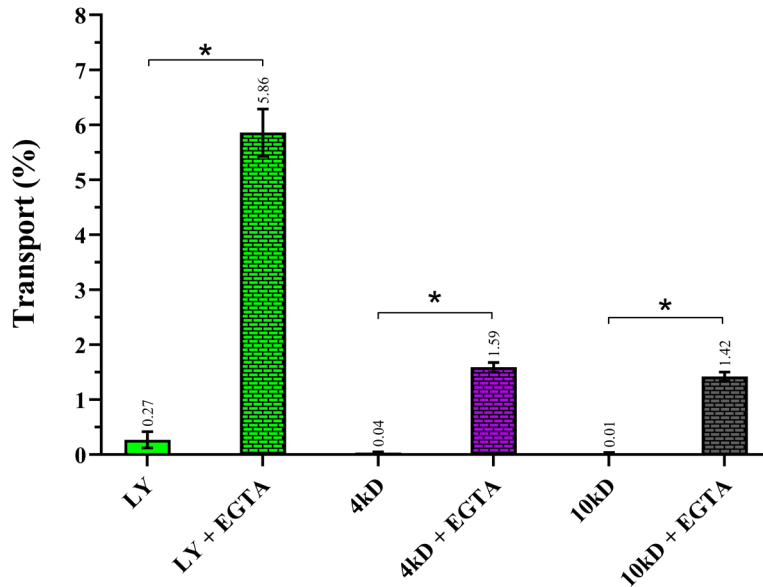
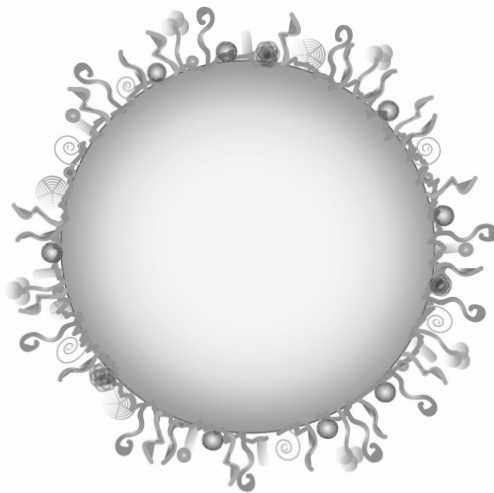
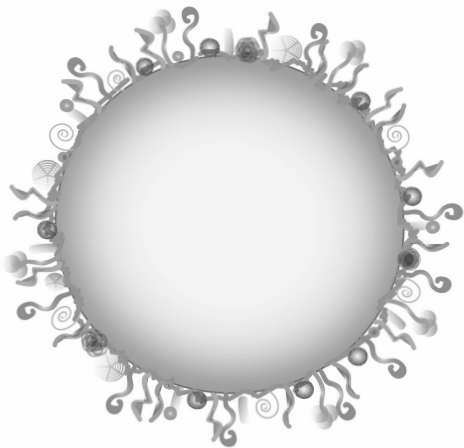
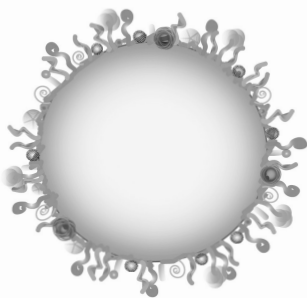
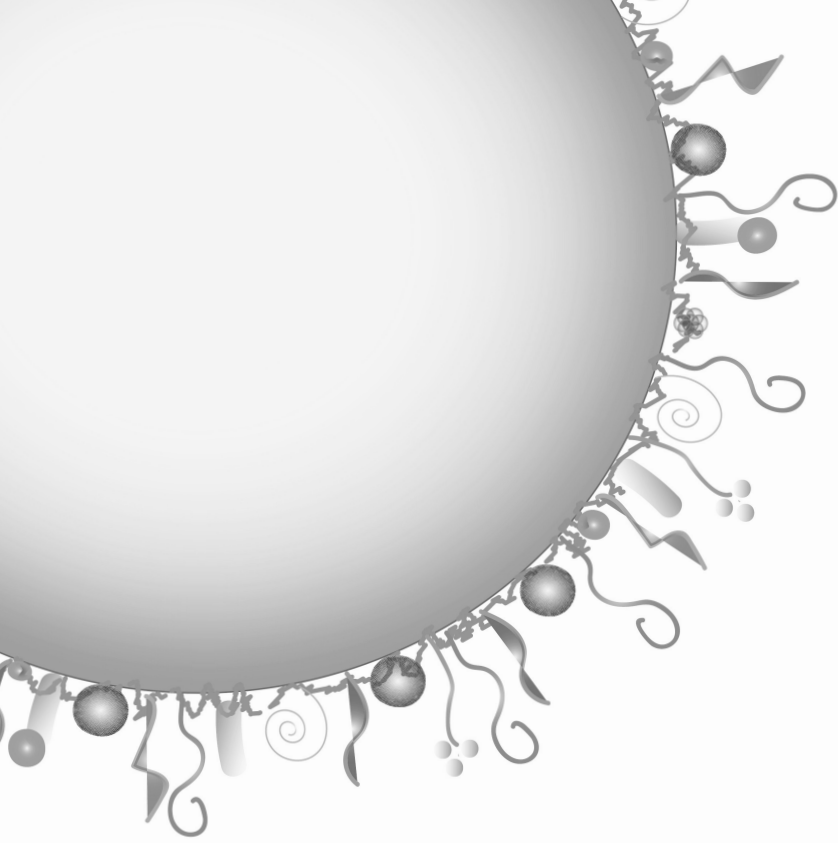


Figure S1: Cell barrier integrity of a Caco-2/HT29-MTX co-culture transwell model expressed as the % transport (mean \pm SD) of lucifer yellow (LY), and 4 kDa and 10 kDa FITC-dextrans in presence and absence of EGTA (tight junction disruptor). * Significant difference in transport between presence and absence of EGTA ($p < 0.05$).

Table S1: The number of particles in pristine and IVD AgNPs suspensions and in the cell fraction

Status	AgNPs	Sample	Concentration ($\mu\text{g/L}$)	Number of particles \pm SD
Pristine	(LA) AgNPs	Suspension	250	$5.9 \times 10^6 \pm 1.4 \times 10^6$
			500	$9.8 \times 10^6 \pm 2.3 \times 10^5$
			2500	$2.7 \times 10^7 \pm 1.9 \times 10^6$
		Cell fraction	250	$1.8 \times 10^5 \pm 4.9 \times 10^4$
			500	$3.1 \times 10^5 \pm 4.6 \times 10^4$
			2500	$1.3 \times 10^6 \pm 5.1 \times 10^5$
	(Cit) AgNPs	Suspension	250	$8.1 \times 10^6 \pm 1.3 \times 10^6$
			500	$1.4 \times 10^7 \pm 2.8 \times 10^6$
			2500	$3.5 \times 10^7 \pm 5.0 \times 10^6$
		Cell fraction	250	$1.3 \times 10^6 \pm 1.6 \times 10^5$
			500	$2.6 \times 10^6 \pm 1.7 \times 10^5$
			2500	$4.5 \times 10^6 \pm 2.3 \times 10^5$
IVD	(LA) AgNPs	Suspension	250	$3.2 \times 10^5 \pm 4.7 \times 10^4$
			500	$7.1 \times 10^5 \pm 2.2 \times 10^5$
			2500	$1.9 \times 10^6 \pm 4.5 \times 10^5$
		Cell fraction	250	$2.4 \times 10^5 \pm 2.8 \times 10^4$
			500	$4.2 \times 10^5 \pm 3.6 \times 10^4$
			2500	$1.3 \times 10^6 \pm 1.7 \times 10^5$
	(Cit) AgNPs	Suspension	250	$3.0 \times 10^6 \pm 7.8 \times 10^5$
			500	$7.4 \times 10^6 \pm 2.8 \times 10^5$
			2500	$2.0 \times 10^7 \pm 5.8 \times 10^6$
		Cell fraction	250	$2.1 \times 10^5 \pm 2.6 \times 10^4$
			500	$4.4 \times 10^5 \pm 6.0 \times 10^4$
			2500	$1.9 \times 10^6 \pm 1.8 \times 10^5$

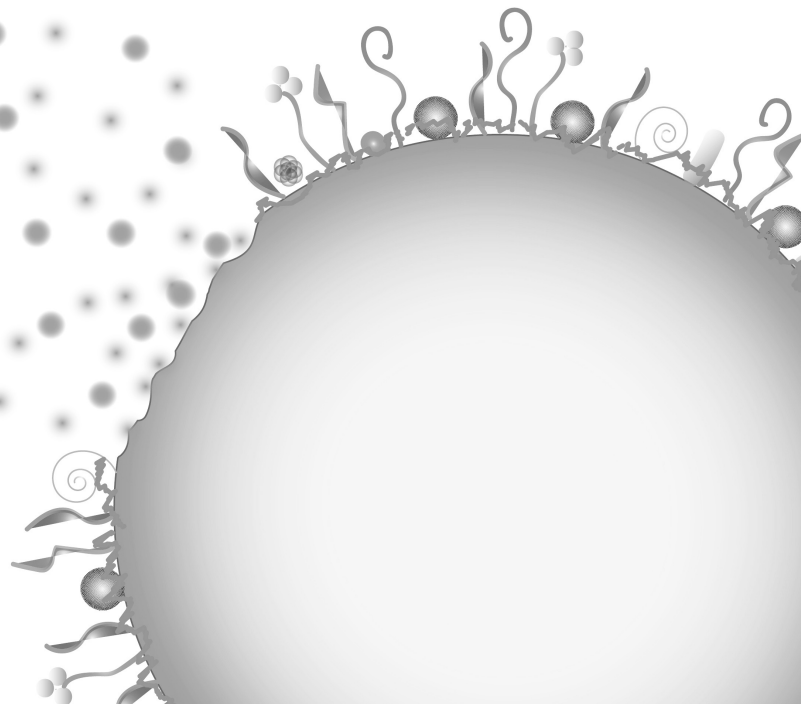


4

Combination of the BeWo b30 placental transport model and the embryonic stem cell test to assess the potential developmental toxicity of silver nanoparticles

Ashraf Abdelkhalig, Meike van der Zande, Ruud J. B. Peters and Hans
Bouwmeester

Based on: Particle and Fibre Toxicology (2020) 17:11



ABSTRACT

Silver nanoparticles (AgNPs) are used extensively in various consumer products because of their antimicrobial potential. This requires insight in their potential hazards and risks including adverse effects during pregnancy on the developing foetus. Using a combination of the BeWo b30 placental transport model and the mouse embryonic stem cell test (EST), we investigated the capability of pristine AgNPs with different surface chemistries and aged AgNPs (silver sulphide (Ag₂S) NPs) to cross the placental barrier and induce developmental toxicity. The uptake/association and transport of AgNPs through the BeWo b30 was characterized using ICP-MS and single particle (sp)ICP-MS after different exposure time points. The developmental toxicity of the AgNPs was investigated by characterizing their potential to inhibit the differentiation of mouse embryonic stem cells (mESCs) into beating cardiomyocytes. The AgNPs are able to cross the BeWo b30 cell layer to a level that was limited and dependent on their surface chemistry. In the EST, no *in vitro* developmental toxicity was observed as the effects on differentiation of the mESCs were only detected at cytotoxic concentrations. The aged AgNPs were significantly less cytotoxic, less bioavailable and did not induce developmental toxicity. Pristine AgNPs are capable to cross the placental barrier to an extent that is influenced by their surface chemistry and this transport is likely low but not negligible. Next to that, the tested AgNPs have low intrinsic potencies for developmental toxicity. The combination of the BeWo b30 model with the EST is of added value in screening and prioritization the developmental toxicity of AgNPs.

INTRODUCTION

Engineered nanoparticles (NPs) have gained much attention in the last decades due to their unique properties compared to the corresponding bulk material, resulting in applications in a wide diversity of products (Nam and Luong 2019; Prajitha *et al.* 2019; Missaoui *et al.* 2018). Silver nanoparticles (AgNPs) are used in very diverse consumer related products such as textile, toys and food containers, where they are generally applied because of their antimicrobial properties (Thomas 2014; Samberg *et al.* 2012). This widespread use has increased the potential for human exposure to AgNPs (Meghan E. Samberg and Monteiro-Riviere 2014).

Humans can be exposed to various forms and types of AgNPs resulting from their release during a product's life cycle (Dekkers *et al.* 2016). AgNPs with different chemical surface modifications are currently being explored to find the optimum between maximal functionality for the application balanced against minimal toxicological hazards, which is known as the Safe-by-Design approach (Arts *et al.* 2015; Lynch *et al.* 2014). Upon release of AgNPs into the environment, they are susceptible to sulfidation processes resulting in silver sulphide nanoparticles (Ag₂S NPs), which are considered the main form of particulate silver in the environment (Liu *et al.* 2018). In addition, *in vivo* systemically available AgNPs or ionic silver have also been shown to transform into Ag₂S NPs (Loeschner *et al.* 2011). Direct use of Ag₂S NPs has also been described in engineering and biomedical applications (Liu *et al.* 2018; Li *et al.* 2017). Ag₂S NPs have been shown to be stable in soils resulting in a potential uptake and accumulation of Ag₂S NPs in plants and the human food chain (Wang *et al.* 2017). In our studies, we therefore not only included AgNPs with different chemical surface modifications, but also Ag₂S NPs.

Previously, we studied the potential transport of AgNPs with different surface modifications across monolayers of intestinal epithelial cells *in vitro* (Abdelkhalik *et al.* 2020). We showed that *in vitro* simulated human digestion had a drastic effect on the dissolution of AgNPs, an effect that was surface coating dependent. A concentration dependent cellular uptake and/or association, albeit low, was observed. Also available sub-chronic data from rodent studies indicate systemic uptake and retention of Ag in tissues (van der Zande *et al.*

2012; Loeschner *et al.* 2011). Therefore, in the current work we assessed whether AgNPs would also be able to pass the placental barrier and if so, to what extent. In addition, to obtain further insight in possible hazards for the developing foetus, the *in vitro* developmental toxicity of the AgNPs was investigated using the mouse embryonic stem cell test (EST).

The placental barrier has received special consideration in the field of toxicology as foetal exposure to NPs might be associated with reduced foetal growth and embryotoxicity (Aengenheister *et al.* 2018b; Cartwright *et al.* 2012; Saunders 2009; Tran *et al.* 2007). NPs uptake and transport across the placental barrier has been reported to be dependent on the surface chemistry, size and the chemical composition of the NPs (Aengenheister *et al.* 2018a; Muoth *et al.* 2016). To date, several alternative *in vitro* and *ex vivo* models have been developed and used to study the transport of NPs across the human placental barrier, *i.e.* *ex vivo* placental perfusion and *in vitro* models using primary cells and cell lines (Aengenheister *et al.* 2018b; Levkovitz *et al.* 2013; Wick *et al.* 2010). BeWo b30 placental cell layer has been used as a model to study the barrier for maternal-foetal exchange (Poulsen *et al.* 2015; Omata *et al.* 2013). This model is considered an easy and robust screening method to predict the placental transfer of xenobiotics, nutrients, compounds and NPs (Correia Carreira *et al.* 2015; Rytting 2015; Bode *et al.* 2006). The BeWo b30 cells form a polarized cell layer and express placental differentiation markers (Li *et al.* 2013; Parry and Zhang 2007; Bode *et al.* 2006; Vardhana and Illsley 2002). Additionally, the BeWo b30 cell layer model has been optimized for NPs transport studies using fluorescent polystyrene (PS) NPs (Cartwright *et al.* 2012). The human silver concentration in blood is usually below 1 µg/L, but can reach levels of up to 194 µg/L in individuals with a compromised skin treated with silver containing creams (Hadrup *et al.* 2018; Chaby *et al.* 2005; Bader 1966). In our *in vitro* study we exposed layers of BeWo b30 cells to AgNPs concentration of 1 mg/L.

Combining the BeWo cell layer model with the EST has proven to be a way to predict relative *in vivo* developmental toxicity (Dimopoulou *et al.* 2018; Li *et al.* 2016; Li *et al.* 2015). The EST has been validated by the European Centre for the Validation of Alternative Methods (ECVAM) (Lee *et al.* 2012a; Seiler and Spielmann 2011), where the differentiation of the mouse embryonic stem cells (mESCs) into beating cardiomyocytes is representing the early stages of

embryonic development (Gao *et al.* 2017; Tandon and Jyoti 2012). Only few studies used the EST to examine the developmental toxicity of AgNPs (Gao *et al.* 2017).

This study aims to determine the potential prenatal developmental toxicity of pristine AgNPs with different surface chemistries compared to the 'aged' AgNPs and AgNO₃. For this, a combination of the BeWo b30 placental transfer model and the EST was used. Uptake/association and transport of ionic silver and AgNPs across the placental cell layer were determined using inductively coupled plasma mass spectrometry (ICP-MS) and single particle (sp) ICP-MS, respectively. Confocal imaging was used to assess cellular penetration of AgNPs into the differentiated cardiomyocytes.

MATERIALS AND METHODS

Nanoparticles and chemicals

Negatively charged 20 nm 'aged' silver sulphide nanoparticles (Ag₂S NPs) suspensions in milli-Q water were obtained from Applied Nanoparticles (Barcelona, Spain) with a mass concentration of 4.7 g/L. Three types of 50 nm AgNPs with different surface modifications were purchased from Nanocomposix Inc. (San Diego, CA, USA); negatively charged lipoic acid BioPure (LA) AgNPs (pH = 6.1) suspended in milli-Q water, negatively charged citrate BioPure (Cit) AgNPs (pH = 7.4) suspended in 2 mM citrate buffer and positively charged branched polyethylenimine (BPEI) BioPure AgNPs (pH = 7.0) suspended in milli-Q water. The silver mass concentration in the stock suspensions of the three AgNPs was 1 g/L. All AgNPs suspensions were stored at 4°C in the dark. Silver nitrate (AgNO₃) (Sigma Aldrich; St. Louis, MO, USA) was used as a control (source of Ag⁺) in all experiments. Dilutions of the AgNPs or AgNO₃ were freshly prepared for every exposure experiment in complete cell culture media (depending on the cell line used in the experiment). 5-Fluorouracil (5-FU) was purchased from Sigma-Aldrich.

Physicochemical characterization of AgNPs

Hydrodynamic diameters of the AgNPs were determined using dynamic light scattering (DLS). Measurements were performed on samples containing 10 mg/L AgNPs suspended in nano-pure water using an ALV dynamic light scattering setup (ALV-Laser Vertriebsgesellschaft;

Germany), consisting of a Thorn RFB263KF photomultiplier detector, an ALV-SP/86 goniometer, an ALV 50/100/200/400/600 μm pinhole detection system, an ALV7002 external correlator and a Cobolt Samba-300 DPSS laser. The measurements were performed immediately after preparation at room temperature. For each condition, samples were analysed in triplicate; each measurement consisted of 10 technical replicate-measurements of 30 seconds each, at an angle of 90° . The results are expressed as the average hydrodynamic diameter (nm) \pm standard deviation (SD) that was calculated using AfterALV software (AfterALV 1.0d, Dullware; USA).

The total silver content of the AgNPs suspensions and AgNO_3 solution was analysed using a NexION 350D inductively coupled plasma mass spectrometer (ICP-MS) (PerkinElmer, Waltham, MA, USA). Before analysis, samples were digested using an aqua-regia (1:3, 70% HNO_3 : 37% HCl) acid digestion for 30 minutes at 60°C and diluted with nano-pure water. Silver was measured using the selected element-monitoring mode with m/z values of 107 and 109. A calibration curve of an ionic Ag standard (NIST-AgNO_3) (Merck; Darmstadt, Germany) ranging from 0.1 to 50 $\mu\text{g/L}$ was included. Rhodium (Merck) was used as an internal standard. The limit of detection (LOD_{conc}) and limit of quantification (LOQ_{conc}) were estimated to be 2 and 6 ng/L , respectively. The cell culture media (vehicle controls) did not contain detectable levels of Ag. All samples were analysed in triplicate.

The particle sizes, size distributions, particle mass- and number-based concentrations of the AgNPs in the AgNPs suspensions and AgNO_3 solution were quantified using single particle (sp) ICP-MS. The method for the spICP-MS measurements was described previously (Peters *et al.* 2015). Briefly, the sample flow rate to the nebulizer was determined before the start of each series of measurements. The dwell time was set at 3 milliseconds and the total acquisition time was set at 60 seconds. A diluted suspension of 60 nm gold (Au) NPs (Nanocomposix) with a mass concentration of 50 ng/L was used before each analysis to verify the performance of the ICP-MS and to determine the transport efficiency. A calibration curve of ionic silver (NIST-AgNO_3) with a concentration range of 0.1 – 20 $\mu\text{g/L}$ was used for particle mass and size determination. The time scan data of the spICP-MS measurements were exported as .csv files and the particle size, size distribution and mass- and number-based concentrations were calculated from the spICP-MS data, using a dedicated spreadsheet.

Details about the spreadsheet have been described previously (Peters *et al.* 2015). The LOD_{conc} and LOQ_{conc} were estimated to be 20 and 67 ng/L, respectively. The NP size was calculated based on the particle mass, assuming spherical particles. The size detection limit (LOD_{size}) was 20 nm and accordingly silver particles with sizes below this limit were included in the ionic silver fraction.

Cell culture

ES-D3 adherent mouse embryonic multipotent stem cells (mESCs; ATCC; Wesel, Germany) were used at passage numbers between 4 and 12. The cells were cultured and maintained in 25 cm² cell culture flasks (Corning; Oneonta, NY, USA) coated with 0.1% gelatine at 37° C in a humidified 5% CO₂ atmosphere in complete cell culture medium (DMEM⁺). DMEM⁺ was prepared by supplementing HyClone AdvanceSTEM Low Osmo Dulbecco's modified Eagle's medium (DMEM) culture medium (GE Healthcare Life Sciences; USA) with 20% (v/v) heat inactivated Foetal Bovine Serum (FBS) (ATCC; Manassas, VA, USA), 1% (v/v) Penicillin-Streptomycin-Glutamine 10,000 units penicillin, 10 mg streptomycin/mL and 29.2 mg/mL L-glutamine (Gibco, Life Technologies; Paisley, UK). The cells were sub-cultured every 2 - 3 days using non-enzymatic cell dissociation solution (Sigma Aldrich) to detach the cells. The cells were maintained in an undifferentiated state by adding mouse leukaemia inhibitory factor (mLIF; Sigma-Aldrich).

The adherent placental choriocarcinoma clone b30 (BeWo b30) was kindly provided by the Institute of Public Health of the Faculty of Health Sciences (University of Copenhagen, Denmark) with permission from Dr. Alan Schwartz (Washington University, St. Louis, MO) and confirmed to be mycoplasma free. The cells were used at passage numbers between 14 and 22. The cells were cultured and maintained in 75 cm² cell culture flasks (Corning) at 37°C in a humidified 5% CO₂ atmosphere in complete cell culture medium (DMEM⁺). The DMEM⁺ was prepared by supplementing DMEM culture medium-GlutaMAX supplement-pyruvate (Gibco, Life Technologies) with 10% (v/v) heat inactivated FBS (Gibco, Life Technologies), 1% (v/v) Penicillin-Streptomycin 10,000 units penicillin and 10 mg streptomycin/mL (Gibco, Life Technologies). The cells were sub-cultured every 3 - 4 days using trypsin-EDTA (Sigma Aldrich) to detach the cells.

Cell viability

Cytotoxic effects of the AgNPs and AgNO₃ were evaluated using the ATPlite luminescence assay system (PerkinElmer; Waltham MA, USA). In 96-well black flat bottom plates (Greiner bio-one; Frickenhausen Germany) each well was seeded with 100 μL of 1×10⁵ cells/mL BeWo b30 cell suspension in DMEM⁺. Plates were incubated at 37° C and 5% CO₂ for 24 hr. The attached cells were then washed with 100 μL/well pre-warmed HBSS buffer w/o phenol red and exposed to 100 μL/well of freshly prepared dilutions (0.1 – 100 mg/L) of AgNPs or AgNO₃. After 24 hr exposure, the exposure medium was aspirated and 50 μL/well of mammalian cell lysis solution were added and the plates were shaken (700 rpm) for 5 minutes at room temperature using an orbital shaker (Heidolph-Trimax 1000; Schwabach, Germany). Next, 50 μL/well of substrate solution were added and the plates were shaken (700 rpm) for 5 minutes at room temperature and then incubated for 10 minutes in the dark at room temperature. The luminescence was then measured using a plate reader (BioTek Synergy™ HT Multi-Mode Microplate reader; Winooski VT, USA). The cell viability was expressed as percentage of the control. DMEM⁺ was used as a negative control and Triton-X100 (0.25%) (Sigma-Aldrich) was used as a positive control.

BeWo b30 placental cell layer barrier integrity assessment

BeWo b30 cells were grown at a density of 1 × 10⁴ cells/cm² on the upper side of transwell polycarbonate inserts (3 μm pore size, 1.12 cm² surface area) (Corning) for 6 days (based on (Cartwright *et al.* 2012)). The integrity of the cell layer was assessed before exposure by measuring the transepithelial electrical resistance (TEER) using a Millicell ERS-2 Epithelial Volt- Ohm Meter (Millipore; Darmstadt, Germany). On day 6 post-seeding, only inserts with TEER values between 80 – 100 Ω.cm² were used for further experiments. The TEER was also measured after exposure to confirm the barrier integrity and comparability of the TEER values before and after exposure.

Additionally, the cell layer integrity was evaluated before exposure to AgNPs suspensions and AgNO₃ solution by measuring the transport efficacy of three different markers namely; lucifer yellow (LY) (Sigma-Aldrich) and low (4 kDa) and high (10 kDa) molecular weight fluorescein isothiocyanate dextrans (FITC-D) (Sigma-Aldrich). To the apical

compartment, 500 μL /insert of 1 mg/mL of each of the integrity markers in DMEM⁺ were added separately. After 1 hr incubation at 37° C, the basolateral medium was collected and the transport of the markers was determined by measuring the fluorescence at 485/530 nm using a fluorescence plate reader (BioTek Synergy™ HT Multi-Mode Microplate reader) and expressed as a percentage of the exposure concentration.

BeWo b30 cellular uptake/association and transport of AgNPs and AgNO₃

Six-day old BeWo b30 cell layer were exposed apically to 500 μL /insert of 1 mg/L of the AgNPs suspensions or the AgNO₃ solution for 4, 6, 18 and 24 hr at 37°C and 5% CO₂. Then, the media from the apical and basolateral compartments were collected. The cells were collected by trypsinization (500 μL) and sonication (40 kHz for 15-20 minutes) to form cell lysate. The total silver content in all samples (apical, basolateral and cell lysate) was analysed using ICP-MS. The particle size, size distribution and mass- and number-based concentration in all samples (apical, basolateral and cell lysate) after 24 hr exposure using spICP-MS. The total Ag mass balance in the placental transport model upon exposure to AgNPs and AgNO₃ was > 90%.

***In vitro* developmental toxicity assessment of AgNPs and AgNO₃**

For the assessment of cell viability of mESCs used in the EST, the potential cytotoxicity of AgNPs and AgNO₃ was evaluated after 24 and 120 hr exposure, reflecting the shortest and longest exposure time during the EST. Each well was seeded with 100 μL of a 2×10^4 (for the 24 hr exposure) or 1×10^3 cells/mL (for the 120 hr exposure) cell suspension in DMEM⁺ without mLIF in 96-well black flat bottom plates (Greiner bio-one). The viability was assessed as mentioned above.

The potential of the AgNPs and AgNO₃ to inhibit mESCs differentiation into beating cardiomyocytes was evaluated using the EST. The cells were exposed from day 3 to 10 of the 10-day mESCs differentiation. The wells of the 96-well plate (Corning) were filled with 200 μL /well PBS. To start the assay hanging droplets (20 μL) of a 3.75×10^4 cells/mL mESCs suspension were placed on the inner side of a lid of a 96-well plate. Sterile lids of Eppendorf tubes were placed on each corner of the 96-well plate lid to avoid contact of the droplets with the plate. Then the plate was sealed with Micropore tape (3M; Germany) to prevent

4

evaporation of the hanging drops. The plates were incubated for three days at 37°C and 5% CO₂ in a humidified atmosphere to allow the formation of embryoid bodies (EBs). On day 3, the formed EBs were transferred to 6 cm non-treated tissue culture petri dishes (Greiner bio-one) with 5 mL of DMEM⁺ containing AgNPs or AgNO₃ and incubated at 37°C and 5% CO₂ in a humidified atmosphere for 2 days to allow growth of the EBs. A concentration range between 0.1 – 25 mg/L was used for each type of AgNPs, while for AgNO₃ a concentration range between 0.05 – 5 mg/L was used. DMEM⁺ was used as a negative control and 1 μM 5-FU was used as a positive control. On day 5, the EBs were transferred to a 24-well plate (Corning) where each well contained one EB in 1 mL of the same concentration of AgNPs or AgNO₃. On day 10, using a light microscope, the wells were visually inspected for contracting cardiomyocytes. The number of wells/plate containing contracting cardiomyocytes were recorded where the experiment was considered valid if at least 21 of the 24 wells of the negative control sample contained contracting cardiomyocytes. For each concentration of each treatment, the fraction of successfully differentiated EBs into contracting cardiomyocytes was calculated and expressed as percentages of the number of wells with beating cardiomyocytes from the number of wells initially seeded with EBs for each concentration.

Characterization of AgNPs dissolution in DMEM⁺

The stability and dissolution properties of the four AgNPs were evaluated in 1 mg/L AgNPs suspensions in DMEM⁺ upon incubation in the dark at 37°C. At 0 and 120 hr, aliquots from each AgNPs suspension were extracted for analysis. spICP-MS was used to quantify the total Ag content, particle size, size distribution and mass- and number-based concentration in all samples as described earlier.

Confocal microscopy of differentiated cardiomyocytes

For confocal imaging, the EBs formed in the EST were transferred into 8-well μ-slides (Ibidi; Gräfelfing, Germany) for exposure and differentiation into cardiomyocytes. The EBs were exposed to the AgNPs suspensions or AgNO₃ solution using similar conditions as used in the EST. After 5 days exposure, the exposure medium was discarded and the cells were fixed with 4% paraformaldehyde (Sigma-Aldrich) for 15 minutes at room temperature. The cells

were washed 3 times with PBS for 5 minutes after discarding the fixation solution. The cells were permeabilized with 0.25% Triton X-100/PBS for 15 minutes at room temperature. The cells were then washed again 3 times with PBS for 5 minutes before incubating them with the blocking buffer (1%BSA in PBS) for 30 minutes at room temperature. After discarding the blocking buffer, Phalloidin - Alexa 488 (6 units) (Dyomics; Jena, Germany) was added to stain cellular actin and the cells were incubated for 30 minutes at room temperature. Cells were washed three times with PBS before incubating the cells for 10 minutes at room temperature with RedDot-2 (1: 200) (Biotium; Fremont, CA, USA) to stain the nuclei. Finally, the cells were washed with PBS and stored in the dark until analysis. The cells were analysed using a confocal laser scanning microscope (SP5X-SMD; Leica Microsystems, Wetzlar, Germany). Samples were excited with 665 and 495 nm lasers and backscattered light was used to detect AgNPs using a 543 nm laser.

Statistical analysis

Each data point represents the average of three replicates ($n = 3$) and the results are shown as mean \pm standard deviation. Prism (v.8.0.1; GraphPad, USA) software was used for statistical analysis using a one-way analysis of variance (ANOVA) with a Bonferroni's post-test. A p-value <0.05 was considered significant.

RESULTS

Physicochemical characterization of the AgNPs suspensions and AgNO₃ solution

Four AgNPs were used in this study: lipoic acid-coated (LA), citrate-coated (Cit), branched polyethylenimine-coated (BPEI) AgNPs and silver sulphide nanoparticles (Ag₂S) NPs that are regarded as aged AgNPs (Liu *et al.* 2018). The hydrodynamic sizes of all the AgNPs were measured in nano-pure water at room temperature using DLS (Table 1). Only the (BPEI) AgNPs were positively charged, while the other AgNPs were negatively charged. All the AgNPs suspensions and the AgNO₃ solution, prepared in DMEM⁺, were analysed immediately after preparation to quantify the total silver content and the fraction of silver in particulate form using ICP-MS and spICP-MS, respectively (Figure S1). In addition, sp-ICP-MS was used to

characterize the suspensions of AgNPs, the results are presented in Figure 4 and explained along with the results of the transport study across the layer of BeWo cells. The sp-ICP-MS characterization of AgNPs in the cell culture medium used for the EST can be found in the supplementary information (Figure S2).

Upon preparing the (1 mg/L) AgNPs suspensions and AgNO₃ solution (t = 0), the percentages of dissolution of (LA), (Cit) and (BPEI) AgNPs in the DMEM⁺ were between 15 – 25%, while in the Ag₂S NPs suspension it was 31%. The AgNO₃ solution did not contain detectable levels of AgNPs. The dissolution of the AgNPs in DMEM⁺ was measured following a maximal incubation of 120 hr which represents the total exposure time in the mESCs differentiation assay (Table 1). For the (LA) and (BPEI) AgNPs suspensions, the percentage of dissolution of AgNPs increased over these 120 hr by ~2 fold, while for (Cit) AgNPs and Ag₂S NPs no significant difference in the percentage of dissolved AgNPs between the two time points was detected (Table 1).

Table 1. Physicochemical characteristics of AgNPs

	Size (TEM)	Hydrodynamic size	ζ- potential	Dissolution (%) ± SD**	
	nm ± SD**	(DLS) nm ± SD*	(mV) ± SD**	0 hr	120 hr
(LA) AgNPs	51 ± 5	70 ± 8	-54 ± 3	15 ± 4	32 ± 2 [#]
(Cit) AgNPs	48 ± 5	61 ± 5	-46 ± 1	25 ± 3	31 ± 1
(BPEI) AgNPs	47 ± 5	62 ± 1	+73 ± 1	17 ± 1	29 ± 2 [#]
Ag ₂ S NPs	28 ± 20	201 ± 28	-22 ± 1	31 ± 1	25 ± 6
AgNO ₃	-	-	-	-	-

* Measured in nano-pure water

** Measured in complete cell culture medium (DMEM⁺).

^x Provided by Nanocomposix Inc.

[#] Significant difference between 0 and 120 hr incubation within the same AgNPs (p-value <0.05).

Cytotoxicity assessment of AgNPs and AgNO₃ in BeWo b30 cells

The viability of BeWo b30 placental cells was assessed upon 24 hr exposure to a concentration series of AgNPs suspensions or AgNO₃ solutions (Figure 1). Exposure to AgNO₃ showed the highest cytotoxicity with an IC₅₀ of 2 mg/L, while exposure to Ag₂S NPs resulted in substantially less cytotoxicity with an IC₅₀ > 100 mg/L (Table 2). For the subsequent BeWo b30

cell layer exposure studies, a non-toxic concentration of the AgNPs was used (1 mg/L). Following the 24 hr exposure to 1 mg/L for AgNO₃, the cell viability was decreased to 67%.

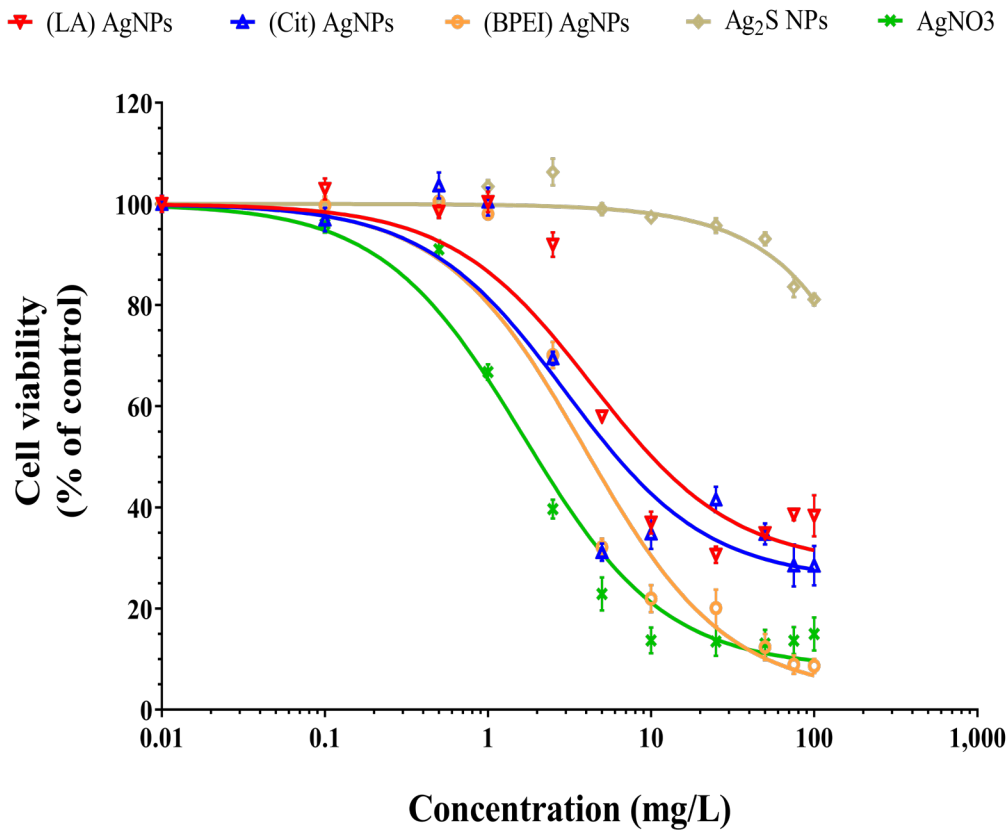


Figure 1: Concentration dependent effect of (LA)-, (Cit)-, (BPEI) AgNPs, Ag₂S NPs, and AgNO₃ on the viability of BeWo b30 cells after 24 hr exposure quantified using the ATPlite viability assay. Viability is given as a percentage of the control (mean ± SD; n=3).

Table 2: The IC₅₀ values of AgNPs and AgNO₃ in BeWo b30 placental cells after 24 hr exposure

Treatment	IC ₅₀ (mg/L)
(LA) AgNPs	11
(Cit) AgNPs	6.2
(BPEI) AgNPs	4.3
Ag ₂ S NPs	>100
AgNO ₃	2

IC₅₀: the concentration where 50% of BeWo b30 cells are viable

Cellular uptake/association and transport of AgNPs and AgNO₃ through the BeWo b30 placental barrier

For the uptake/association and transport studies cell layer of BeWo b30 placental cells were used after 6 days of differentiation. Good integrity was confirmed by TEER values ranging between 80 - 100 $\Omega \cdot \text{cm}^2$ (as defined by others (Li *et al.* 2013)) and low transport values of three paracellular transport marker compounds (*i.e.* 8, 6, 7% for LY and 4kDa and 10kDa FITC-dextran, respectively). The BeWo b30 cell layer were exposed for 4, 6, 18 and 24 hr to 1 mg/L of the different AgNPs suspensions, or the AgNO₃ solution. The silver content in the media from the apical, cellular and basolateral compartments was quantified using ICP-MS measurements at all exposure times and expressed as total Ag (*i.e.* ionic silver and particulate silver; Figure 2). In addition, the silver fraction as AgNPs was quantified using sp-ICP-MS measurements, but only after 24 hr exposure (Figure 3). The TEER measurements performed after the exposure to the AgNPs and AgNO₃ indicated that the BeWo b30 barrier integrity was not affected.

The total Ag content (as determined by the ICP-MS measurements) in the apical compartment declined significantly in a time-dependent manner in the (LA), (Cit), (BPEI) AgNPs and AgNO₃ exposure groups (Figure 2A). In the Ag₂S NPs exposure group, the total Ag content of the apical compartment declined rapidly at early time points but remained stable from 4 hr exposure onwards. This early decline was significantly larger compared to the decline observed for the other AgNPs. The fractions of total Ag present as AgNPs in the apical compartments upon 24 hr exposure to (LA), (Cit), (BPEI) AgNPs and Ag₂S NPs were comparable (Figure 3A; Table 3). The fraction of AgNPs was lower for the AgNO₃ group.

For the cellular compartment of the BeWo b30 cell model, the total Ag content increased significantly in a time-dependent manner for the (LA), (Cit) and (BPEI) AgNPs, except for the 6 hr time point where the increase versus the 4 hr time point was not statistically significant (Figure 2B). While the time-dependent increase in the total Ag content was less pronounced upon exposure to Ag₂S NPs or AgNO₃, the total Ag concentration in the cellular compartment increased significantly after 24 hr exposure compared to that observed after 4 and 6 hr exposure.

In the cellular compartment, the concentration of AgNPs upon 24 hr exposure to (BPEI) AgNPs was higher compared to what was observed following exposure to the other AgNPs and AgNO₃ (Fig 3B). However, upon expressing the AgNPs concentrations in the cellular compartment after 24 hr exposure as percentages of the total Ag present in the cellular compartments, these percentages between (LA), (Cit) and (BPEI) AgNPs were comparable.

Upon exposure to Ag₂S NPs, the cellular compartment contained a lower percentage of AgNPs (Figure 3B, Table 3). The cellular compartment exposed to AgNO₃ contained only 4% of AgNPs of the total Ag content in this compartment (Figure 3B, Table 3).

In spite of the time-dependent decrease in the amount of total Ag in the apical compartment and an increase in the amount of total Ag in the cellular compartment (Figure 2A and B), no time-dependent transport of total Ag across the cell layer to the basolateral compartment was observed upon exposure to all the AgNPs, apart from incidental significant differences for the (Cit) AgNPs (Figure 2 C). Upon AgNO₃ exposure, the total Ag content in the basolateral compartment showed a time-dependent increase. Additionally, AgNPs were detected in the basolateral compartment. The highest percentage of AgNPs from the total Ag content was detected in the basolateral compartments exposed to the (LA) AgNPs followed by (Cit) and (BPEI) AgNPs and Ag₂S NPs (Figure 3C and Table 3). Following exposure to AgNO₃ only 2% of the compartment's total Ag content was present as AgNPs.

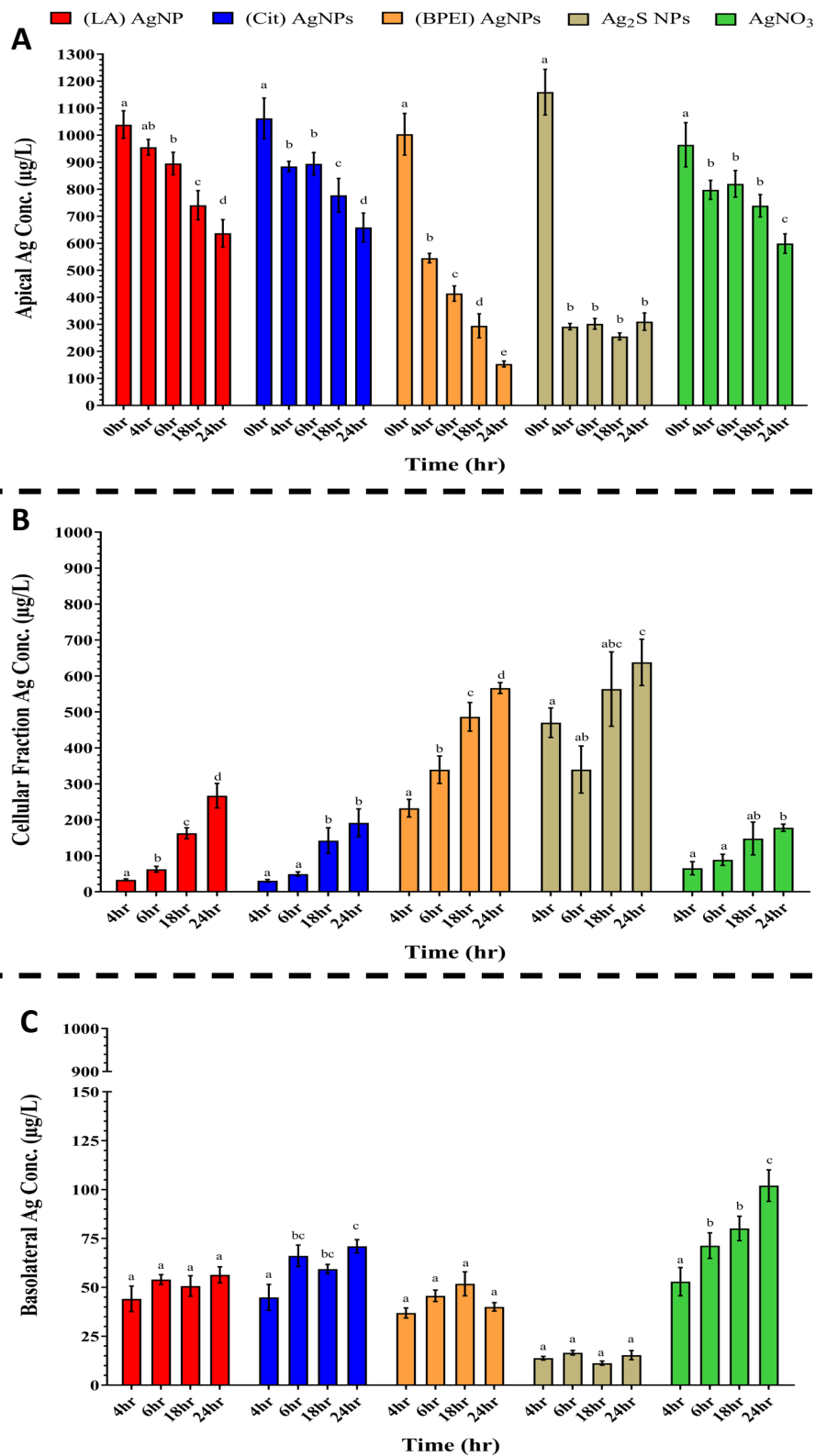


Figure 2: Total silver content in the **A)** apical, **B)** cell lysate, and **C)** basolateral compartments of the BeWo b30 placental transfer model after 4, 6, 18 and 24 hr exposure to 1 mg/L of (LA), (Cit), (BPEI) AgNPs, Ag₂S NPs, or AgNO₃, measured using ICP-MS. Concentrations are given as the mean \pm SD ($n=3$). Values with different letters are significantly different within the same treatment ($p \leq 0.05$).

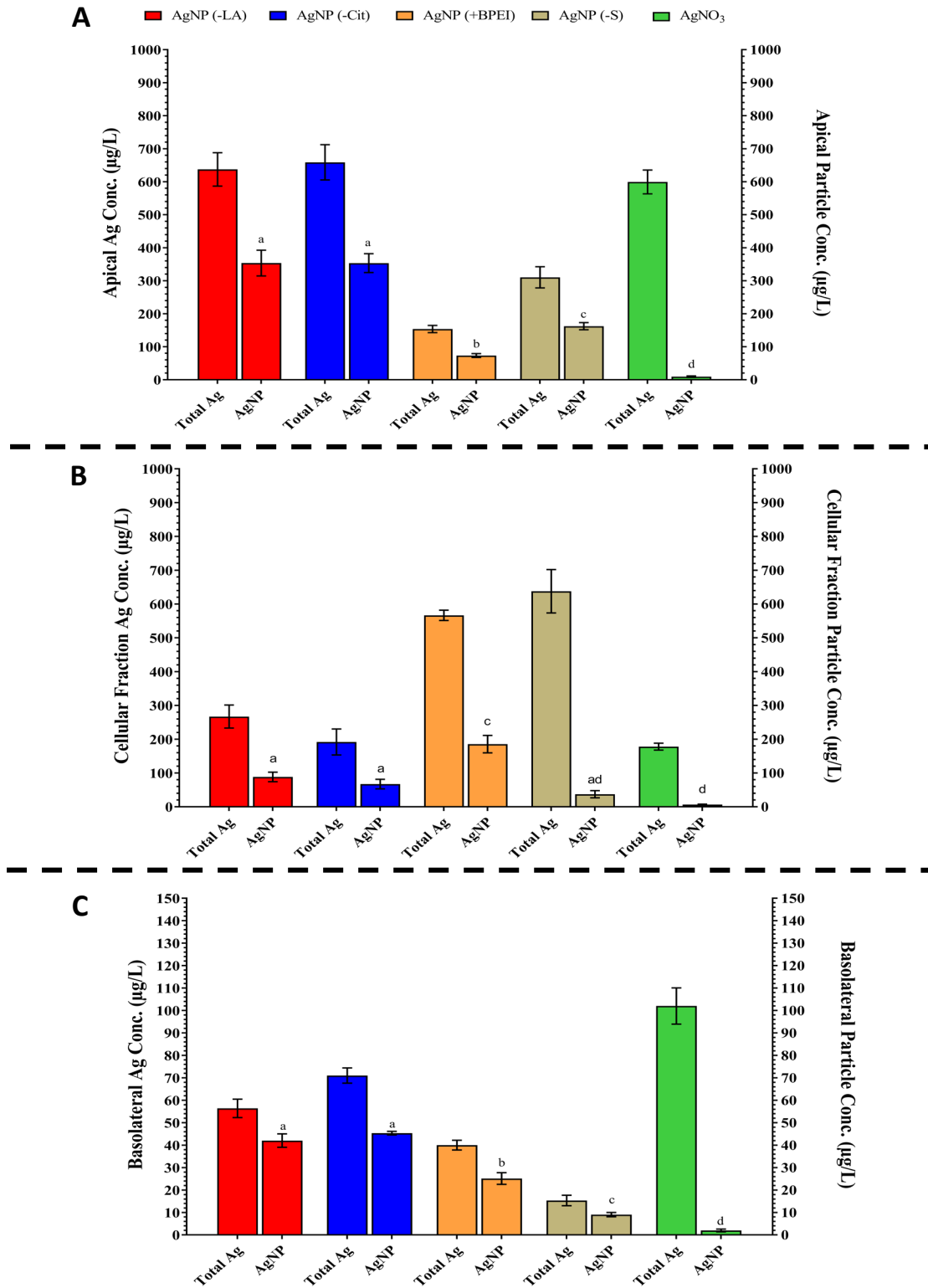


Figure 3: Total silver content (on the left axis) versus the AgNPs content (mass-based on the right axis) in the **A)** apical, **B)** cell lysate, and **C)** basolateral compartments of the BeWo b30 placental transfer model after 24 hr exposure to 1 mg/L of (LA), (Cit), (BPEI) AgNPs, Ag₂S NPs, or AgNO₃, measured using spICP-MS. Concentrations are given as the mean ± SD (n=3). Values with different letters are significantly different within the same treatment (p ≤ 0.05).

Table 3: The fraction of AgNPs as % of total Ag content in the apical, cellular and basolateral compartments of the BeWo b30 placental cell model after 24 hr exposure as calculated from the data presented in figure 3.

Treatment	Compartment		
	Apical	Cellular	Basolateral
(LA) AgNPs	55%	33% *	77% * #
(Cit) AgNPs	54%	35% *	64% #
(BPEI) AgNPs	52%	32% *	63% #
Ag ₂ S NPs	48%	6% *	59% #
AgNO ₃	2%	4% *	2%

* Significant difference compared to the apical compartment of the same exposure group (p-value <0.05).

Significant difference between cell and basolateral compartments of the same exposure group (p-value <0.05).

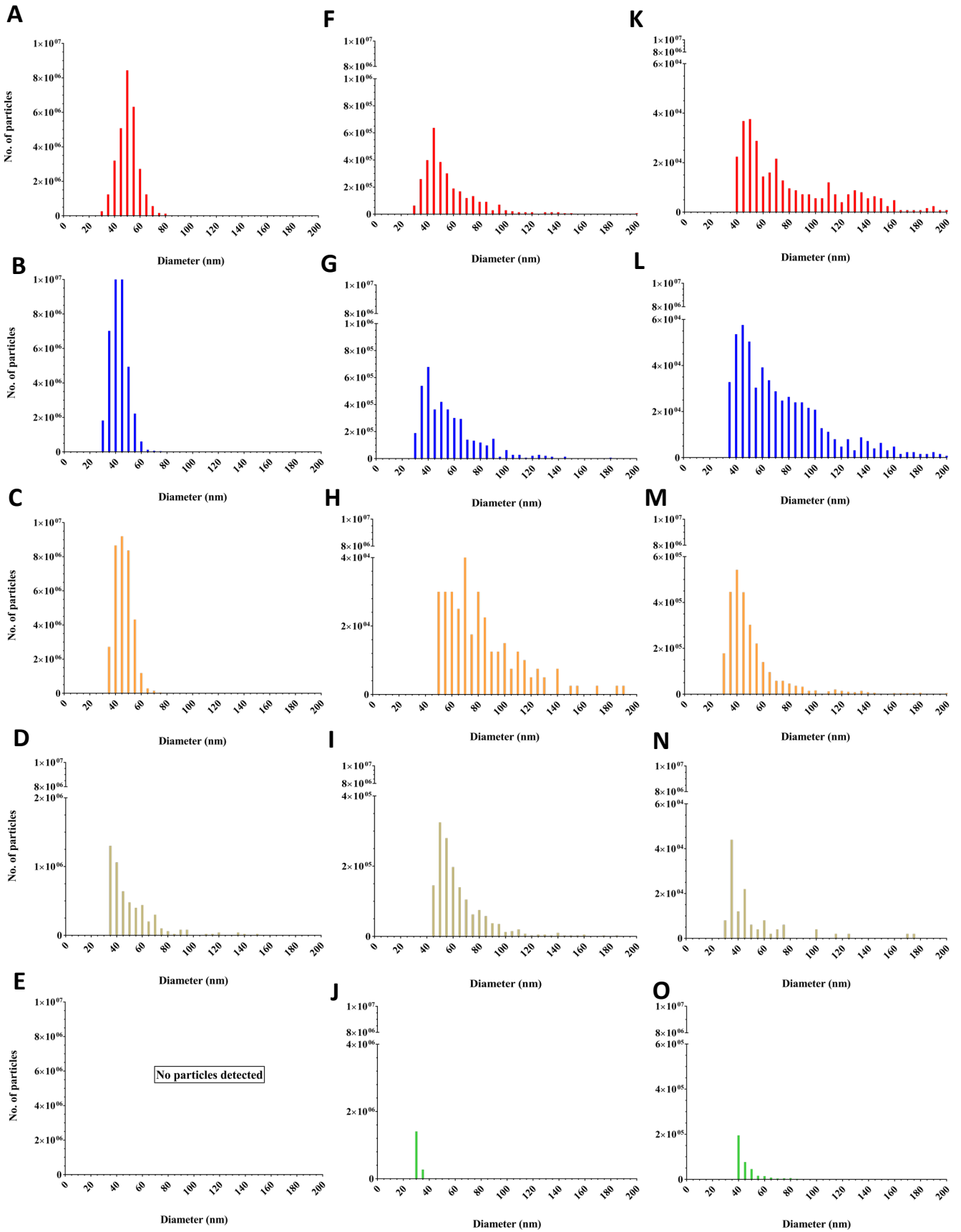
Size distribution of AgNPs before and after BeWo b30 exposure

The size distributions of the AgNPs were assessed in the different compartments (apical, cellular and basolateral) of the BeWo b30 model. The sp-ICP-MS data were transformed into size distribution plots depicting the number of particles corresponding to the size, clustered in 5 nm diameter clusters (Figure 4). The size distributions of the (LA), (Cit) and (BPEI) AgNPs exposure suspensions were comparable, with median particle sizes of 50, 45 and 45 nm, respectively (Figure 4 A, B and C). The size distribution of Ag₂S NPs suspension demonstrated a right-skewed size distribution with a median particle size of 35 nm (Figure 4 D). No AgNPs were detected in the AgNO₃ solution (Figure 4 E).

After 24 hr exposure, the total number of AgNPs that was detected in the apical compartments decreased for all four AgNPs (Figure 4 F-I) where the (BPEI) AgNPs (Figure 4 H) showed the largest decrease. The size distributions of all the AgNPs in the apical compartment were right skewed. The size distributions of (LA) and (Cit) AgNPs were the least affected with a median size of 45 and 40 nm, respectively (Figure 4 F and G). The size distribution of both the (BPEI) AgNPs and Ag₂S NPs indicated an increased median size of 70 nm and 50 nm, respectively, indicating agglomeration of the particles. (Figure 4 H and I). Some AgNPs were detected in the AgNO₃ sample with a median size of 30 nm (Figure 4 J).

The size distributions of all AgNPs in the cellular compartments were also right skewed. For the (LA) and (Cit) AgNPs (Figure 4 K and L), this was more pronounced than in the apical compartments, with median sizes of 50 and 45 nm, respectively. It was less pronounced for the (BPEI) AgNPs and Ag₂S NPs (Figure 4 M and N), with median sizes of 40 nm and 35 nm, respectively. The AgNPs that were detected in the cellular compartment upon exposure to AgNO₃ had a median size of 40 nm (Figure 4 O).

The size distributions of all AgNPs in the basolateral compartments were right skewed and were very similar in shape but different in number of particles. The (LA) and (Cit) AgNPs were less right skewed (Figure 4 P and Q) than in the cellular compartments and had median sizes of 50 and 40 nm, respectively. The size distribution curve of (BPEI) AgNPs was very wide, with a median size of 45 nm (Figure 4 R). The Ag₂S NPs had a median size of 45 nm and featured a size distribution pattern very similar to that in the starting suspension (Figure 4 S and D). For AgNO₃, AgNPs with median size of 35 nm were detected (Figure 4 T).



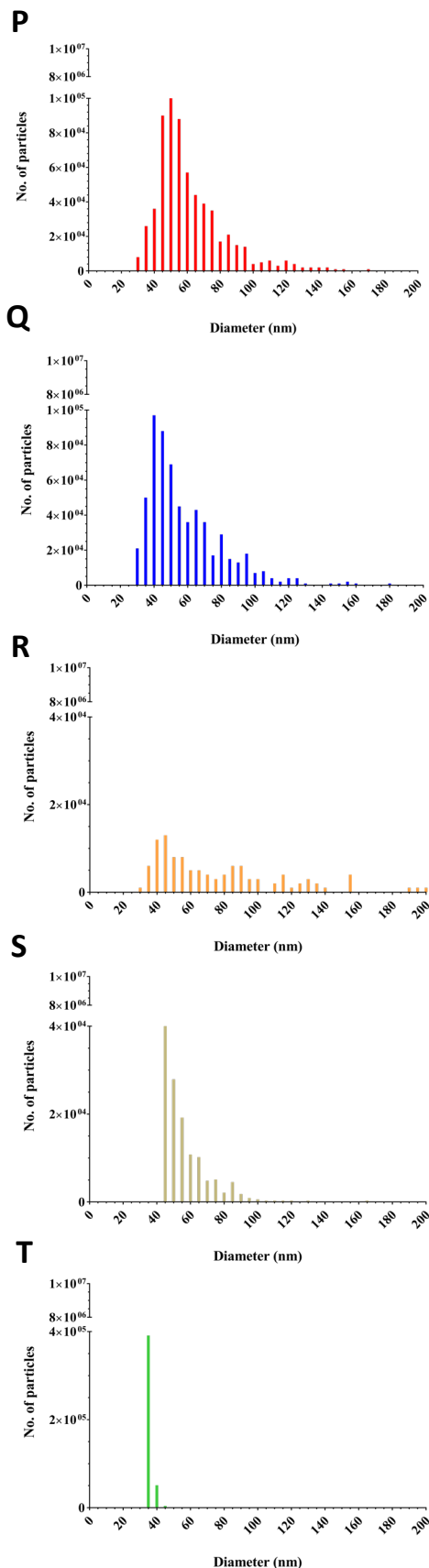


Figure 4: Number-weighted size distributions of AgNPs generated by spICP-MS measurements of the suspensions (1 mg/L) of **A)** (LA) AgNPs, **B)** (Cit) AgNPs, **C)** (BPEI) AgNPs, **D)** Ag₂S NPs, and **E)** AgNO₃. Number-weighted size distributions of AgNPs in the apical compartments of the BeWo b30 monolayer model upon 24 hr exposure to 1 mg/L of: **F)** (LA) AgNPs, **G)** (Cit) AgNPs, **H)** (BPEI) AgNPs, **I)** Ag₂S NPs, and **J)** AgNO₃. Number-weighted size distributions of AgNPs in the cellular compartments of the BeWo b30 monolayer model upon 24 hr exposure to 1 mg/L of: **K)** (LA) AgNPs, **L)** (Cit) AgNPs, **M)** (BPEI) AgNPs, **N)** Ag₂S NPs, and **O)** AgNO₃. Number-weighted size distributions of AgNPs in the basolateral compartments of the BeWo b30 monolayer model upon 24 hr to 1 mg/L of: **P)** (LA) AgNPs, **Q)** (Cit) AgNPs, **R)** (BPEI) AgNPs, **S)** Ag₂S NPs, and **T)** AgNO₃.

***In vitro* developmental toxicity assessment of AgNPs and AgNO₃**

To assess the potential *in vitro* developmental toxicity of AgNPs and AgNO₃, the EST was employed. First, the viability of the mESCs was assessed upon 24 and 120 hr exposure to a concentration series of AgNPs and AgNO₃ using the ATPlite assay (Figure 5). The Ag₂S NPs showed lowest toxicity after 24 and 120 hr exposure with an IC₅₀ of > 100 and 29 mg/L, respectively, while AgNO₃ showed the highest toxicity after 24 and 120 hr exposure with an IC₅₀ of 25 and 0.33 mg/L, respectively (Table 4).

All tested AgNPs and AgNO₃ induced a concentration-dependent reduction in viability of the mESCs with higher cytotoxicity after 120 hr compared with 24 hr exposure. Subsequently, the potential inhibitory effects of AgNPs and AgNO₃ on the differentiation of mESCs into contracting cardiomyocytes was studied. Except for the Ag₂S NPs, all tested AgNPs and AgNO₃ induced a concentration-dependent inhibition of the differentiation of the mESCs into contracting cardiomyocytes (Figure 5). The (BPEI) AgNPs were the most potent to inhibit the differentiation of mESCs with an ID₅₀ of 8 mg/L. The AgNO₃, (LA) and (Cit) AgNPs had ID₅₀ of 9.5, 13 and 16 mg/L, respectively, while the ID₅₀ of Ag₂S NPs was >100 mg/L (Table 3). For all AgNPs and AgNO₃, the inhibitory effects on the mESCs differentiation were observed at higher concentrations than those associated with the decrease in mESCs viability after 120 hr exposure, as indicated by a higher ID₅₀ than IC₅₀. This indicates that effects on mESCs differentiation are likely due to cytotoxicity.

In order to estimate the influence of Ag ions released from dissolving AgNPs on the mESCs differentiation, we interpolated the concentration of Ag ions present at the ID₅₀ for each AgNPs (Table 3). The concentration of Ag ions present at the ID₅₀ was estimated to account for 16, 23 and 31% of the observed inhibition of the mESCs differentiation upon exposure to (BPEI), (LA) and (Cit) AgNPs at their ID₅₀, respectively. In case of Ag₂S NPs, no inhibition of the mESCs was found up to the highest concentration tested of the Ag₂S NPs. Confocal imaging demonstrated that AgNPs were internalized into the differentiated cardiomyocytes. AgNPs were mainly localized in the cytoplasm and to some extent in the nucleus (Figure 6).

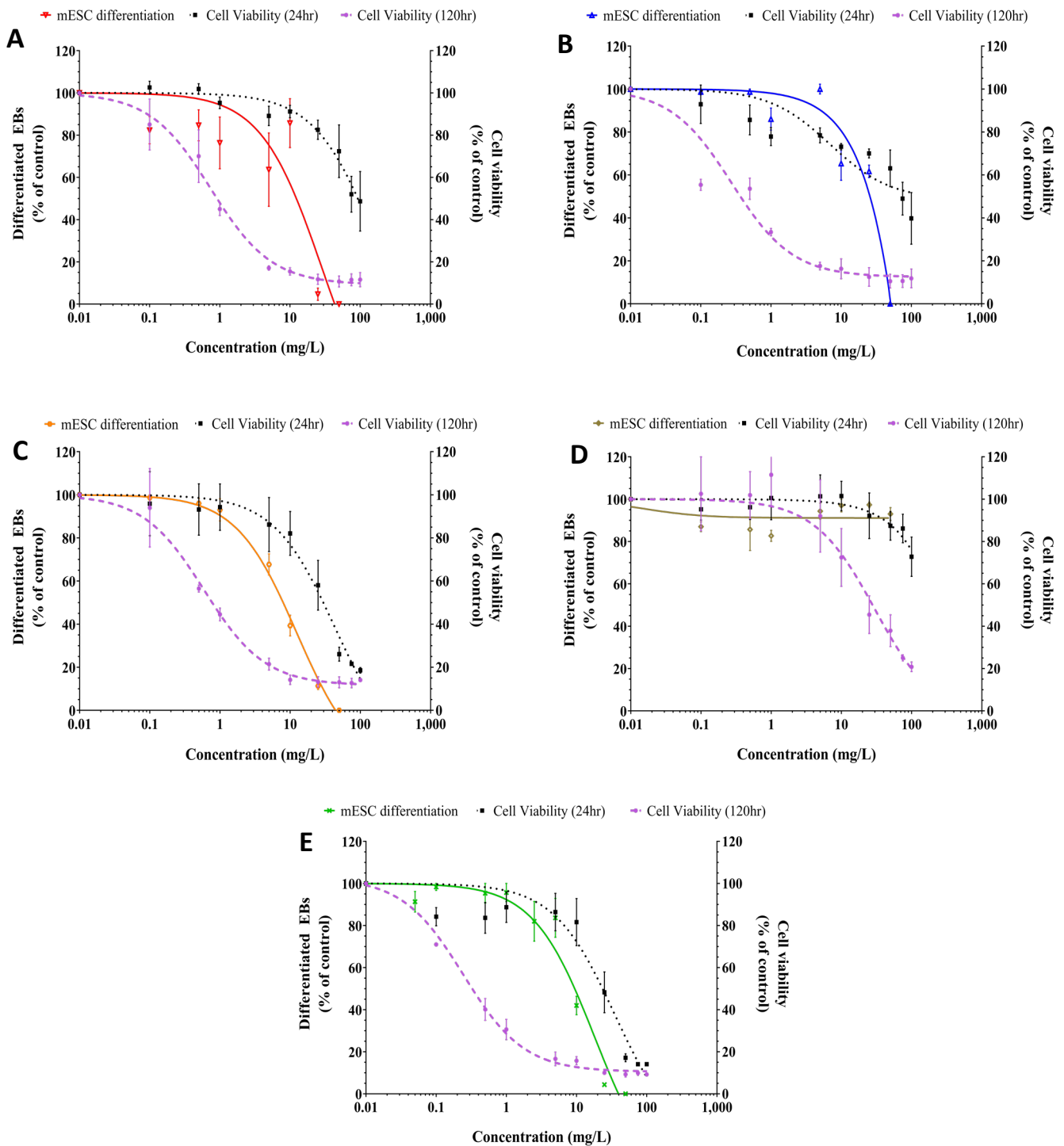


Figure 5: Concentration–response curves for cytotoxicity towards mESCs and for the effect on differentiation into contracting cardiomyocytes of: **A)** (LA) AgNPs, **B)** (Cit) AgNPs, **C)** (BEPI) AgNPs, **D)** (Ag₂S) NPs, and **E)** AgNO₃. The viability of mESCs (right y-axis) was assessed using the ATPlite assay after 24 hr (■) and 120 hr (●) exposure. The differentiation of mESCs into contracting cardiomyocytes (left y-axis) was scored after microscopical evaluation. Values are given as a percentage of the control (mean ± SD; n=3).

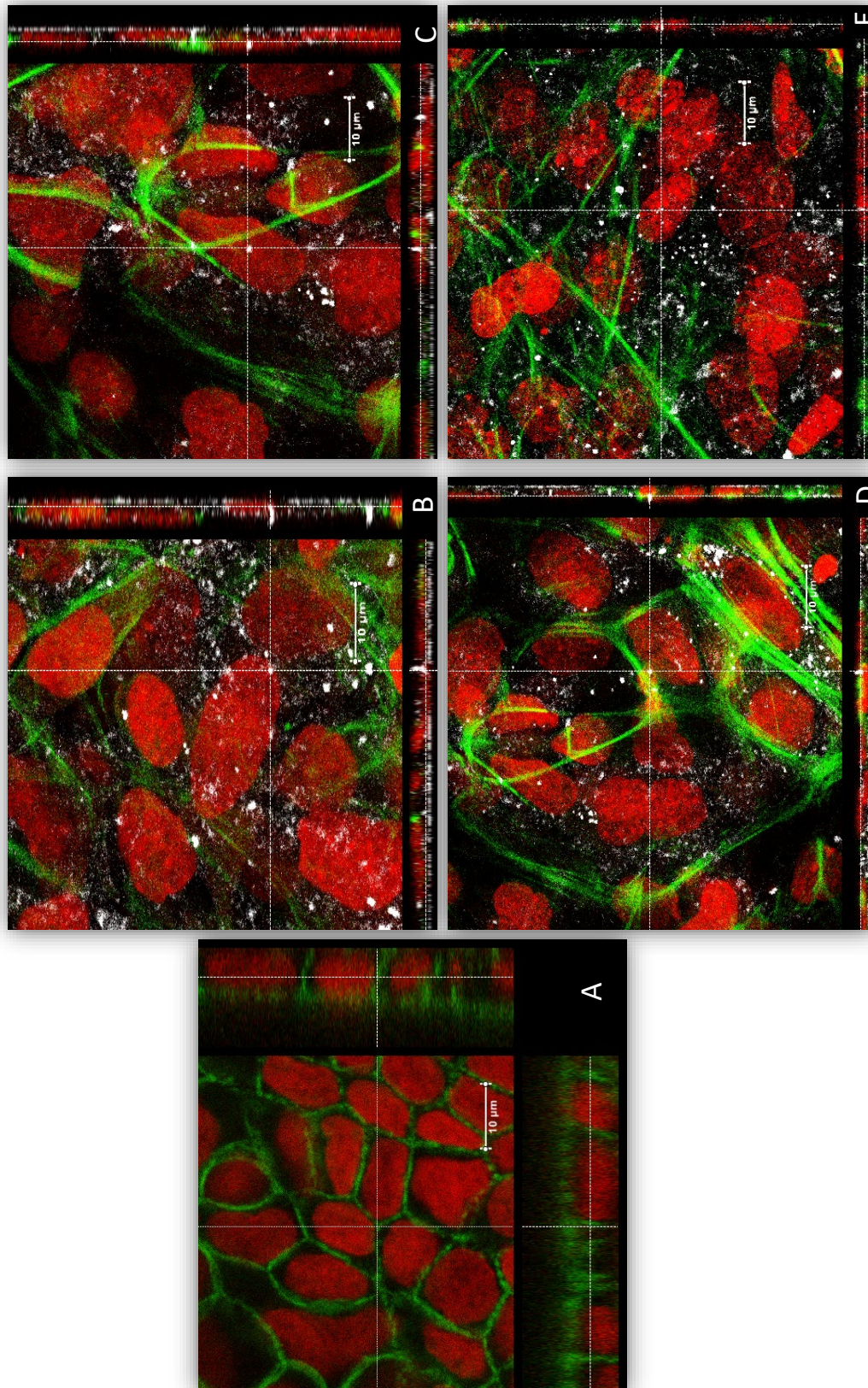


Figure 6: Confocal microscopic images of differentiated cardiomyocytes after 10 days of differentiation. **A)** Negative control, **B)** cells exposed to 1 mg/L (LA) AgNPs, **C)** (Cit) AgNPs, **D)** (BEPI) AgNPs and **E)** Ag₂S NPs. Nuclei were stained in red (RedDot-2), actin was stained in green (Alexa -488 Phalloidin), and AgNPs are shown in white (back scatter).

DISCUSSION

This study aimed to investigate the potential prenatal developmental toxicity of pristine AgNPs with different surface chemistries and of aged Ag₂S NPs. For this, we combined the BeWo b30 placental transport model with the EST. This enabled us to evaluate the potential foetal exposure to AgNPs and to study the likelihood of AgNPs to induce *in vitro* developmental toxicity.

The interaction of Ag and AgNPs with BeWo b30 placental cells

Exposure to the (LA), (Cit) and (BPEI) AgNPs and AgNO₃ showed a concentration-dependent decrease in BeWo b30 cell viability. The positively charged (BPEI) coated AgNPs were more toxic, especially at concentrations higher than 1 mg/L, compared to the negatively charged (LA) and (Cit) coated AgNPs. In line with this observation, higher cytotoxicity for positively charged versus negatively charged NPs in BeWo b30 cells has been reported previously for polystyrene NPs (Kloet *et al.* 2015). Additionally, it has been reported that oleate coated ferric oxide NPs were more toxic to BeWo b30 cells than uncoated ones (Correia Carreira *et al.* 2015), indicating that both the surface charge and surface chemistry can cause differences in toxicity.

Exposure of the placental BeWo cell layer to 1 mg/L of (LA), (Cit), (BPEI) AgNPs and AgNO₃ for different durations resulted in a time-dependent increase of total Ag in the cellular compartments. The transport of silver across the placental cell layer was favourable as ionic silver rather than particulate, which was similarly reported using the *ex vivo* human placental perfusion model where the transport of ionic silver was ~10-fold higher than that of particulates (Vidmar *et al.* 2018).

The spICP-MS measurements after 24 hr exposure to the different AgNPs showed the presence of AgNPs in the cellular and basolateral compartments. The surface chemistry of the AgNPs significantly affected the detected concentration of AgNPs in the cellular compartment where the highest concentrations of AgNPs were observed following exposure to (BPEI) AgNPs followed by (LA) AgNPs, (Cit) AgNPs and Ag₂S NPs. A comparable effect of the surface chemistry of NPs on the cellular uptake/association was also reported for ferric oxide NPs where oleate coated NPs were significantly lower associated with the BeWo cell layer than

uncoated NPs (Correia Carreira *et al.* 2015). Besides, the cellular compartment contained a lower AgNPs percentage (of the total Ag content) compared to the AgNPs percentage in the exposure concentration in the apical compartment. This suggests a preference towards cellular uptake/association of ionic silver over AgNPs or possible dissolution of the AgNPs cellularly following their uptake (Graf *et al.* 2018; van der Zande *et al.* 2016; Behra *et al.* 2013).

In the basolateral compartments of all the exposure groups, AgNPs were detected. In general, the AgNPs percentage (of the total Ag content) in the basolateral compartment was higher than the AgNPs percentage (of the total Ag content) in the cellular compartment. This could suggest a preference towards cellular excretion of AgNPs over ionic silver. Also, the AgNPs measured could result from *de novo* formation of AgNPs from ionic silver that might reflect a tendency of the ionic silver to form these new particles in the cell culture medium more than the cellular environment. This later scenario is likely to happen taking into consideration the presence of AgNPs in all compartments upon exposure to AgNO₃.

Contribution of AgNPs surface chemistry in AgNPs transport across BeWo b30 cell layer

The surface chemistry of the AgNPs significantly affected the detected concentration of AgNPs also in the basolateral compartment where the highest concentrations of AgNPs were observed following exposure to (LA) AgNPs and (Cit) AgNPs followed by (BPEI) AgNPs and Ag₂S NPs. The surface chemistry of NPs was reported to play a role in the transport of ferric oxide NPs where the placental transport was significantly higher for oleate coated NPs than uncoated NPs (Correia Carreira *et al.* 2015). Also, the placental transport of pegylated AuNPs was reported to be higher than that of sodium carboxylated AuNPs of the same size (Aengenheister *et al.* 2018a).

Next to the surface chemistry of NPs, their size (Muoth *et al.* 2016; Wick *et al.* 2010) and composition (Poulsen *et al.* 2015) are also suggested to influence their transport through the placental barrier model. The transport of PSNPs was described to be size dependent, where transport of 50 nm PSNPs was six times higher than that of 100 nm PSNPs (Cartwright *et al.* 2012). The placental transport of AuNPs also showed a size-dependency, where 10 to 30 nm AuNPs did not cross the placental barrier (Myllynen *et al.* 2008) and the smaller 3 and 4 nm AuNP crossed the placental barrier (Aengenheister *et al.* 2018a). Upon the exposure of either

the BeWo b30 (up to 24 hr) or the perfused human placenta (up to 6 hr) to 25 and 50 nm silica NPs, no placental transport could be detected (Poulsen *et al.* 2015). Following exposure of perfused human placenta to AgNPs with different surface chemistries (polyethylene glycol and sodium carboxylate and a primary size of 7-15 nm) very low transport has been observed. In the foetal circulation 0.02 to 0.2% of the administered dose was detected as total silver in the foetal circulation. Only a small mass fraction of this silver was detected in particulate form (>25 nm). Interestingly, the authors pointed out that AgNPs in the foetal circulation could originate from *de novo* formation following ionic Ag transport (Vidmar *et al.* 2018). From the limited number of *in vivo* studies of placental transport of NPs where pregnant animals were used, AgNPs were found to be able to cross the placental barrier of rats and reach the foetus (Fennell *et al.* 2017; Wu *et al.* 2015; Lee *et al.* 2012b; Menezes *et al.* 2011; Lyon *et al.* 2002). The study of Fennell *et al.* reported that after 24 hr of intravenous administration of pregnant rats with AgNPs, about 3 - 4%, measured as total Ag, of the administered dose was found in the foetus (Fennell *et al.* 2017). The transported levels that we observed ranged between 1 and 8% as total Ag and between 1 and 5% as AgNPs and are thus in between the observations in rodents and the human placenta perfusion studies.

Potential foetal toxicity following exposure to AgNPs and AgNO₃

Following the capability of the AgNPs and AgNO₃ to cross the BeWo b30 cell layer *in vitro* either as ionic or as particulate silver, induction of adverse outcomes upon reaching the embryo cannot be excluded. Therefore, we assessed the potential developmental toxicity of the AgNPs using the EST. The EST represents a good tool to measure the developmental toxicity *in vitro* as it has been validated by ECVAM and it showed a good level of concordance in the *in vitro* to *in vivo* comparisons (Corradi *et al.* 2015; Vecchione *et al.* 2013). Combining the EST with the BeWo placental transport model even resulted in an increased predictability of *in vivo* developmental toxicity of chemicals (Li *et al.* 2015).

Our data from the EST did not point towards potential developmental toxicity because the effects of the AgNPs and AgNO₃ on differentiation of mESCs into contracting cardiomyocytes were only observed at cytotoxic concentrations (Seiler and Spielmann 2011). These results are in line with the observations of Park *et al.* and Corradi *et al.* where 7, 20, 80 and 113 nm AgNPs induced dose-dependent cytotoxicity and inhibition of mESCs

differentiation only at concentrations higher than the ones associated with cytotoxicity (Corradi *et al.* 2015; Park *et al.* 2011). Besides, the IC₅₀ values for cytotoxicity of the AgNPs in the mESCs were higher than what would be considered realistic *in vivo* concentrations as our results from the BeWo b30 transport experiments indicated low transport of AgNPs into the foetal compartment. Additionally, considering the oral route as one of the main exposure routes of the AgNPs, it is important to take into account also their very low transport across the intestinal barrier *in vitro* (Abdelkhalik *et al.* 2020; Bouwmeester *et al.* 2011) and *in vivo* (van der Zande *et al.* 2012) which will consequently lower the concentrations of the AgNPs that might reach the foetus.

Effects following exposure to aged AgNPs

4 It is of interest to note that the aged silver sulphide NPs showed a different behaviour compared to the pristine AgNPs. Although the dissolution and charge of the Ag₂S NPs were comparable to those of the (LA) and (Cit) pristine AgNPs, their effects on the cellular viability of the BeWo cells and their transport across the BeWo cell layer were significantly lower. Upon placental exposure to Ag₂S NPs, a relatively high concentration of total Ag in the cellular compartment was detected after 4 hr exposure which remained unchanged upon longer exposure up to 24 hr. This was in contrast with the time dependent behaviour of the pristine AgNPs. Also, the lowest amount of total Ag, in comparison with the pristine AgNPs, was transported through the placental cell layer, even though the total Ag concentration in the cellular fraction was relatively higher in comparison with the pristine AgNPs. Additionally, the aged particles did not induce any inhibition of the mESCs differentiation in the EST. The lower bioavailability of the Ag₂S NPs could be explained by the sulfidation processes that these aged particles go through during their formation. The sulfidation of the AgNPs is likely to change the colloidal dynamics of these particles which increases the probability of these particles to aggregate and settle compared to the pristine NPs (Liu *et al.* 2018; Yin *et al.* 2015; Reinsch *et al.* 2012). Possibly these aggregates bind strongly to the outer cell membrane, leading to high total Ag concentrations in the cellular fractions, but low transport through the cells. Taking these results into account, these aged AgNPs are imposing a very low risk for developmental toxicity. It is important to highlight that this study is one of the first studies that considered the potential hazards of aged AgNPs on the developing human foetus.

CONCLUSION

To conclude, the AgNPs tested here were able to transport across BeWo b30 cell layer where the surface chemistry of these AgNPs influenced the amounts of AgNPs transported. The particles detected in the basolateral compartment, could result from transport of the original AgNPs or partly from *de novo* AgNPs formed from ionic silver that was transported. The observed inhibitory effects of the AgNPs on differentiation of mESCs were most likely the result of cytotoxicity rather than specific effects related to developmental toxicity. The aged AgNPs were significantly less cytotoxic and bioavailable and did also not induce *in vitro* inhibition of differentiation of mESCs. The combination of the BeWo placental transport model with the mESCs differentiation assay (EST) is considered a valuable alternative *in vitro* methodology for prenatal developmental toxicity screening and prioritization of silver nanoparticles.

REFERENCES

- Abdelkhalik A, Van der Zande M, Undas AK, Peters RJB, Bouwmeester H. 2020. Impact of in vitro digestion on gastrointestinal fate and uptake of silver nanoparticles with different surface modifications. *Nanotoxicology*:14:1, 111-126.
- Aengenheister L, Dietrich D, Sadeghpour A, Manser P, Diener L, Wichser A, Karst U, Wick P, Buerki-Thurnherr T. 2018a. Gold nanoparticle distribution in advanced in vitro and ex vivo human placental barrier models. *J Nanobiotechnology* 16:79.
- Aengenheister L, Keevend K, Muoth C, Schonenberger R, Diener L, Wick P, Buerki-Thurnherr T. 2018b. An advanced human in vitro co-culture model for translocation studies across the placental barrier. *Sci Rep* 8:5388.
- Arts Jh, Hadi M, Irfan Ma, Keene Am, Kreiling R, Lyon D, Maier M, Michel K, Petry T, Sauer Ug, Warheit D, Wiench K, Wohlleben W, Landsiedel R. 2015. A decision-making framework for the grouping and testing of nanomaterials (Df4nanogrouping). *Regul Toxicol Pharmacol* 71:S1-27.
- Bader Kf. 1966. Organ deposition of silver following silver nitrate therapy of burns. *Plast Reconstr Surg* 37:550-1.
- Behra R, Sigg L, Clift Mj, Herzog F, Minghetti M, Johnston B, Petri-Fink A, Rothen-Rutishauser B. 2013. Bioavailability of silver nanoparticles and ions: from a chemical and biochemical perspective. *J R Soc Interface* 10:20130396.
- Bode Cj, Jin H, Rytting E, Silverstein Ps, Young Am, Audus Kl. 2006. In vitro models for studying trophoblast transcellular transport. *Methods Mol Med* 122:225-39.
- Bouwmeester H, Poortman J, Peters Rj, Wijma E, Kramer E, Makama S, Puspitaninganindita K, Marvin Hjp, Peijnenburg Aacm, Hendriksen Pjm. 2011. Characterization of translocation of silver nanoparticles and effects on whole-genome gene expression using an in vitro intestinal epithelium coculture model. *Acs Nano* 5:4091-4103.
- Cartwright L, Poulsen Ms, Nielsen Hm, Pojana G, Knudsen Le, Saunders M, Rytting E. 2012. In vitro placental model optimization for nanoparticle transport studies. *Int J Nanomedicine* 7:497-510.
- Chaby G, Viseux V, Poulain Jf, De Cagny B, Denoeux Jp, Lok C. 2005. Topical silver sulfadiazine-induced acute renal failure. *Ann Dermatol Venereol* 132:891-3.
- Corradi S, Dakou E, Yadav A, Thomassen Lc, Kirsch-Volders M, Leyns L. 2015. Morphological observation of embryoid bodies completes the in vitro evaluation of nanomaterial embryotoxicity in the embryonic stem cell test (EST). *Toxicol In Vitro* 29:1587-96.
- Correia Carreira S, Walker L, Paul K, Saunders M. 2015. The toxicity, transport and uptake of nanoparticles in the in vitro bewo b30 placental cell barrier model used within nanotest. *Nanotoxicology* 9 Suppl 1:66-78.
- Dekkers S, Oomen Ag, Bleeker Ea, Vandebriel Rj, Micheletti C, Cabellos J, Janer G, Fuentes N, Vazquez-Campos S, Borges T, Silva Mj, Prina-Mello A, Movia D, Nessler F, Ribeiro Ar, Leite Pe, Groenewold M, Cassee Fr, Sips Aj, Dijkzeul A, Van Teunenbroek T, Wijnhoven Sw. 2016. Towards a nanospecific approach for risk assessment. *Regul Toxicol Pharmacol* 80:46-59.

- Dimopoulou M, Verhoef A, Gomes Ca, Van Dongen Cw, Rietjens I, Piersma Ah, Van Ravenzwaay B. 2018. A comparison of the embryonic stem cell test and whole embryo culture assay combined with the bewo placental passage model for predicting the embryotoxicity of azoles. *Toxicol Lett* 286:10-21.
- Fennell Tr, Mortensen Np, Black Sr, Snyder Rw, Levine Ke, Poitras E, Harrington Jm, Wingard Cj, Holland Na, Pathmasiri W, Sumner Sc. 2017. Disposition of intravenously or orally administered silver nanoparticles in pregnant rats and the effect on the biochemical profile in urine. *J Appl Toxicol* 37:530-544.
- Gao X, Topping Vd, Keltner Z, Sprando Rl, Yourick Jj. 2017. Toxicity of nano- and ionic silver to embryonic stem cells: a comparative toxicogenomic study. *J Nanobiotechnology* 15:31.
- Graf C, Nordmeyer D, Sengstock C, Ahlberg S, Diendorf J, Raabe J, Epple M, Koller M, Lademann J, Vogt A, Rancan F, Ruhl E. 2018. Shape-dependent dissolution and cellular uptake of silver nanoparticles. *Langmuir* 34:1506-1519.
- Hadrup N, Sharma Ak, Loeschner K. 2018. Toxicity of silver ions, metallic silver, and silver nanoparticle materials after in vivo dermal and mucosal surface exposure: a review. *Regul Toxicol Pharmacol* 98:257-267.
- Kloet Sk, Walczak Ap, Louise J, Van Den Berg Hh, Bouwmeester H, Tromp P, Fokkink Rg, Rietjens Im. 2015. Translocation of positively and negatively charged polystyrene nanoparticles in an in vitro placental model. *Toxicol In Vitro* 29:1701-10.
- Lee Hy, Inselman Al, Kanungo J, Hansen Dk. 2012a. Alternative models in developmental toxicology. *Syst Biol Reprod Med* 58:10-22.
- Lee Y, Choi J, Kim P, Choi K, Kim S, Shon W, Park K. 2012b. A transfer of silver nanoparticles from pregnant rat to offspring. *Toxicol Res* 28:139-41.
- Levkovitz R, Zaretsky U, Gordon Z, Jaffa Aj, Elad D. 2013. In vitro simulation of placental transport: part i. Biological model of the placental barrier. *Placenta* 34:699-707.
- Li H, Flick B, Rietjens Im, Louise J, Schneider S, Van Ravenzwaay B. 2016. Extended evaluation on the es-d3 cell differentiation assay combined with the bewo transport model, to predict relative developmental toxicity of triazole compounds. *Arch Toxicol* 90:1225-37.
- Li H, Rietjens Im, Louise J, Blok M, Wang X, Sniijders L, Van Ravenzwaay B. 2015. Use of the ES-D3 cell differentiation assay, combined with the bewo transport model, to predict relative in vivo developmental toxicity of antifungal compounds. *Toxicol In Vitro* 29:320-8.
- Li H, Van Ravenzwaay B, Rietjens Im, Louise J. 2013. Assessment of an in vitro transport model using bewo b30 cells to predict placental transfer of compounds. *Arch Toxicol* 87:1661-9.
- Li L, Xu Z, Wimmer A, Tian Q, Wang X. 2017. New insights into the stability of silver sulfide nanoparticles in surface water: dissolution through hypochlorite oxidation. *Environ Sci Technol* 51:7920-7927.
- Liu Sq, Wang C, Hou J, Wang Pf, Miao Lz, Li Tf. 2018. Effects of silver sulfide nanoparticles on the microbial community structure and biological activity of freshwater biofilms. *Environmental Science-Nano* 5:2899-2908.

- Loeschner K, Hadrup N, Qvortrup K, Larsen A, Gao X, Vogel U, Mortensen A, Lam Hr, Larsen Eh. 2011. Distribution of silver in rats following 28 days of repeated oral exposure to silver nanoparticles or silver acetate. *Part Fibre Toxicol* 8:18.
- Lynch I, Weiss C, Valsami-Jones E. 2014. A strategy for grouping of nanomaterials based on key physico-chemical descriptors as a basis for safer-by-design nms. *Nano Today* 9:266-270.
- Lyon Td, Patriarca M, Howatson G, Fleming Pj, Blair Ps, Fell Gs. 2002. Age dependence of potentially toxic elements (Sb, Cd, Pb, Ag) in human liver tissue from paediatric subjects. *J Environ Monit* 4:1034-9.
- Meghan E. Samberg, Monteiro-Riviere Na. 2014. Silver nanoparticles in biomedical applications. In: Nancy A. Monteiro-Riviere, Tran Cl, Eds. *Nanotoxicology : progress toward nanomedicine*. 2nd Edition. Boca Raton: Crc Press, 405-421.
- Menezes V, Malek A, Keelan Ja. 2011. Nanoparticulate drug delivery in pregnancy: placental passage and fetal exposure. *Curr Pharm Biotechnol* 12:731-42.
- Missaoui Wn, Arnold Rd, Cummings Bs. 2018. Toxicological status of nanoparticles: what we know and what we don't know. *Chem Biol Interact* 295:1-12.
- Muoth C, Aengenheister L, Kucki M, Wick P, Buerki-Thurnherr T. 2016. Nanoparticle transport across the placental barrier: pushing the field forward! *Nanomedicine (Lond)* 11:941-57.
- Myllynen Pk, Loughran Mj, Howard Cv, Sormunen R, Walsh Aa, Vahakangas Kh. 2008. Kinetics of gold nanoparticles in the human placenta. *Reprod Toxicol* 26:130-7.
- Nam Nh, Luong Nh. 2019. Nanoparticles: synthesis and applications. In: Grumezescu V, Grumezescu Am, Eds. *Materials for biomedical engineering*. Elsevier, 211-240.
- Omata W, Ackerman Wet, Vandre Dd, Robinson Jm. 2013. Trophoblast cell fusion and differentiation are mediated by both the protein kinase c and a pathways. *Plos One* 8:E81003.
- Park Mv, Neigh Am, Vermeulen Jp, De La Fonteyne Lj, Verharen Hw, Briede Jj, Van Loveren H, De Jong Wh. 2011. The effect of particle size on the cytotoxicity, inflammation, developmental toxicity and genotoxicity of silver nanoparticles. *Biomaterials* 32:9810-7.
- Parry S, Zhang J. 2007. Multidrug resistance proteins affect drug transmission across the placenta. *Am J Obstet Gynecol* 196:476 E1-6.
- Peters R, Herrera-Rivera Z, Undas A, Van Der Lee M, Marvin H, Bouwmeester H, Weigel S. 2015. Single particle ICP-MS combined with a data evaluation tool as a routine technique for the analysis of nanoparticles in complex matrices. *J Anal Atom Spectrom* 30:1274-1285.
- Poulsen Ms, Mose T, Maroun Ll, Mathiesen L, Knudsen Le, Rytting E. 2015. Kinetics of silica nanoparticles in the human placenta. *Nanotoxicology* 9 Suppl 1:79-86.
- Prajitha N, Athira Ss, Mohanan Pv. 2019. Bio-interactions and risks of engineered nanoparticles. *Environ Res* 172:98-108.
- Reinsch Bc, Levard C, Li Z, Ma R, Wise A, Gregory Kb, Brown Ge, Jr., Lowry Gv. 2012. Sulfidation of silver nanoparticles decreases escherichia coli growth inhibition. *Environ Sci Technol* 46:6992-7000.
- Rytting E. 2015. Exploring the interactions of nanoparticles with multiple models of the maternal--fetal interface. *Nanotoxicology* 9 Suppl 1:137-8.

- Samberg Me, Lobo Eg, Oldenburg Sj, Monteiro-Riviere Na. 2012. Silver nanoparticles do not influence stem cell differentiation but cause minimal toxicity. *Nanomedicine (Lond)* 7:1197-209.
- Saunders M. 2009. Transplacental transport of nanomaterials. *Wiley Interdisciplinary Reviews: Nanomedicine And Nanobiotechnology* 1:671-684.
- Seiler Ae, Spielmann H. 2011. The validated embryonic stem cell test to predict embryotoxicity in vitro. *Nat Protoc* 6:961-78.
- Tandon S, Jyoti S. 2012. Embryonic stem cells: an alternative approach to developmental toxicity testing. *J Pharm Bioallied Sci* 4:96-100.
- Thomas Ta. 2014. Nanotechnology in consumer products : addressing potential health and safety implications for consumers. In: Nancy A. Monteiro-Riviere, Tran Cl, Eds. *Nanotoxicology : progress toward nanomedicine*. 2nd Edition. Boca Raton: Crc Press, 97-112.
- Tran Dn, Ota Lc, Jacobson Jd, Patton Wc, Chan Pj. 2007. Influence of nanoparticles on morphological differentiation of mouse embryonic stem cells. *Fertil Steril* 87:965-70.
- Van Der Zande M, Undas Ak, Kramer E, Monopoli Mp, Peters Rj, Garry D, Antunes Fernandes Ec, Hendriksen Pj, Marvin Hj, Peijnenburg Aa, Bouwmeester H. 2016. Different responses of caco-2 and mcf-7 cells to silver nanoparticles are based on highly similar mechanisms of action. *Nanotoxicology* 10:1431-1441.
- Van Der Zande M, Vandebriel Rj, Van Doren E, Kramer E, Herrera Rivera Z, Serrano-Rojero Cs, Gremmer Er, Mast J, Peters Rj, Hollman Pc, Hendriksen Pj, Marvin Hj, Peijnenburg Aa, Bouwmeester H. 2012. Distribution, elimination, and toxicity of silver nanoparticles and silver ions in rats after 28-day oral exposure. *Acs Nano* 6:7427-42.
- Vardhana Pa, Illsley Np. 2002. Transepithelial glucose transport and metabolism in bewo choriocarcinoma cells. *Placenta* 23:653-60.
- Vecchione L, Massimiani M, Camaioni A, Sifrani L, Magrini A, Pietroiusti A, Campagnolo L. 2013. A comparative study of metal oxide nanoparticles embryotoxicity using the embryonic stem cell test. *Bionanomaterials*. 61.
- Vidmar J, Loeschner K, Correia M, Larsen Eh, Manser P, Wichser A, Boodhia K, Al-Ahmady Zs, Ruiz J, Astruc D, Buerki-Thurnherr T. 2018. Translocation of silver nanoparticles in the ex vivo human placenta perfusion model characterized by single particle ICP-MS. *Nanoscale* 10:11980-11991.
- Wang P, Lombi E, Sun Sk, Scheckel Kg, Malysheva A, Mckenna Ba, Menzies Nw, Zhao Fj, Kopittke Pm. 2017. Characterizing the uptake, accumulation and toxicity of silver sulfide nanoparticles in plants. *Environmental Science-Nano* 4:448-460.
- Wick P, Malek A, Manser P, Meili D, Maeder-Althaus X, Diener L, Diener Pa, Zisch A, Krug Hf, Von Mandach U. 2010. Barrier capacity of human placenta for nanosized materials. *Environ Health Perspect* 118:432-6.
- Wu J, Yu C, Tan Y, Hou Z, Li M, Shao F, Lu X. 2015. Effects of prenatal exposure to silver nanoparticles on spatial cognition and hippocampal neurodevelopment in rats. *Environ Res* 138:67-73.

Yin Y, Yu S, Shen M, Liu J, Jiang G. 2015. Fate and transport of silver nanoparticles in the environment. In: Liu J, Jiang G, Eds. Silver nanoparticles in the environment. Berlin, Heidelberg: Springer Berlin Heidelberg, 73-108.

SUPPLEMENTARY MATERIAL

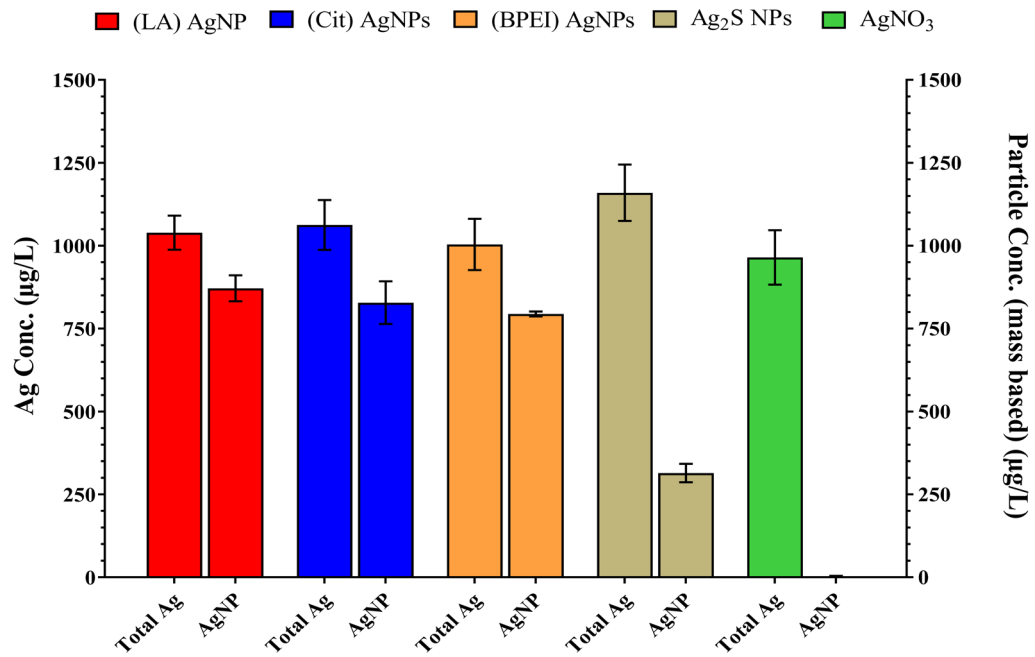


Figure S 1: Silver content in 1 mg/L AgNPs suspension and AgNO₃ solution expressed as total Ag and as AgNPs measured using ICP-MS spICP-MS, respectively. Concentrations are given as the mean \pm SD (n=3). No AgNPs were detected in the AgNO₃ solution (< LOD).

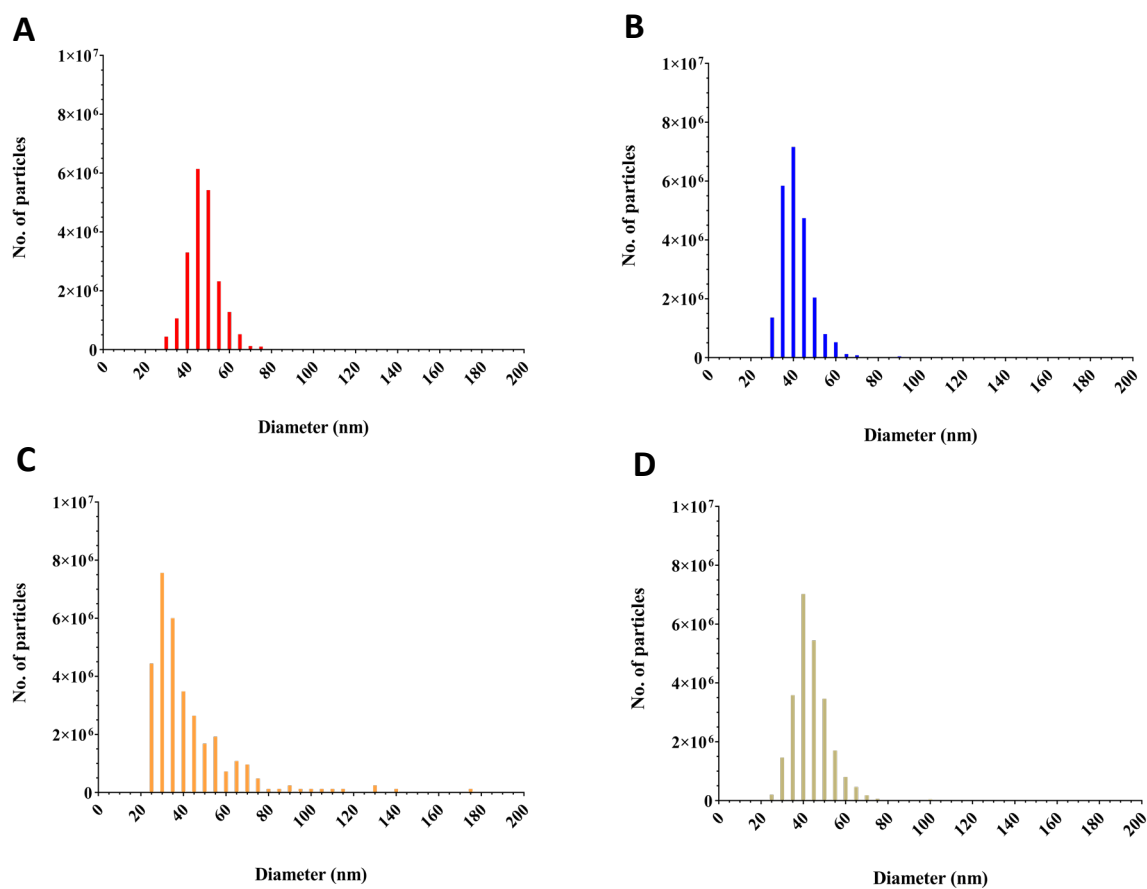
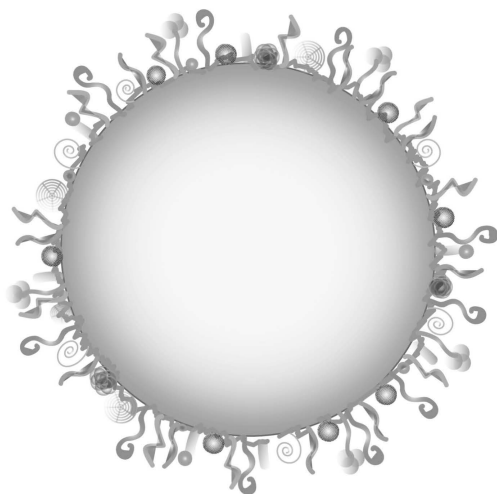
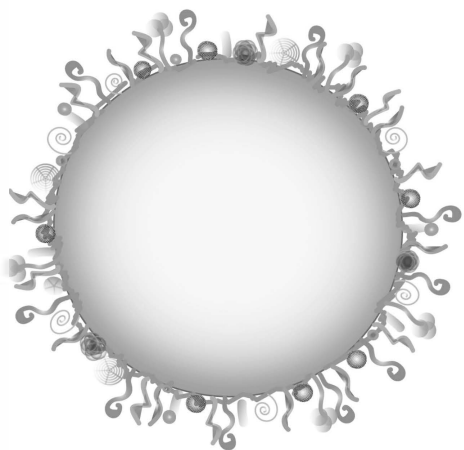
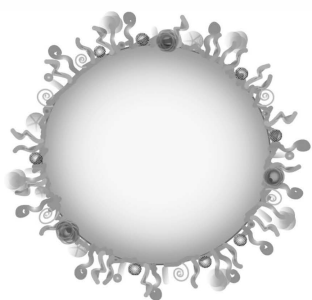
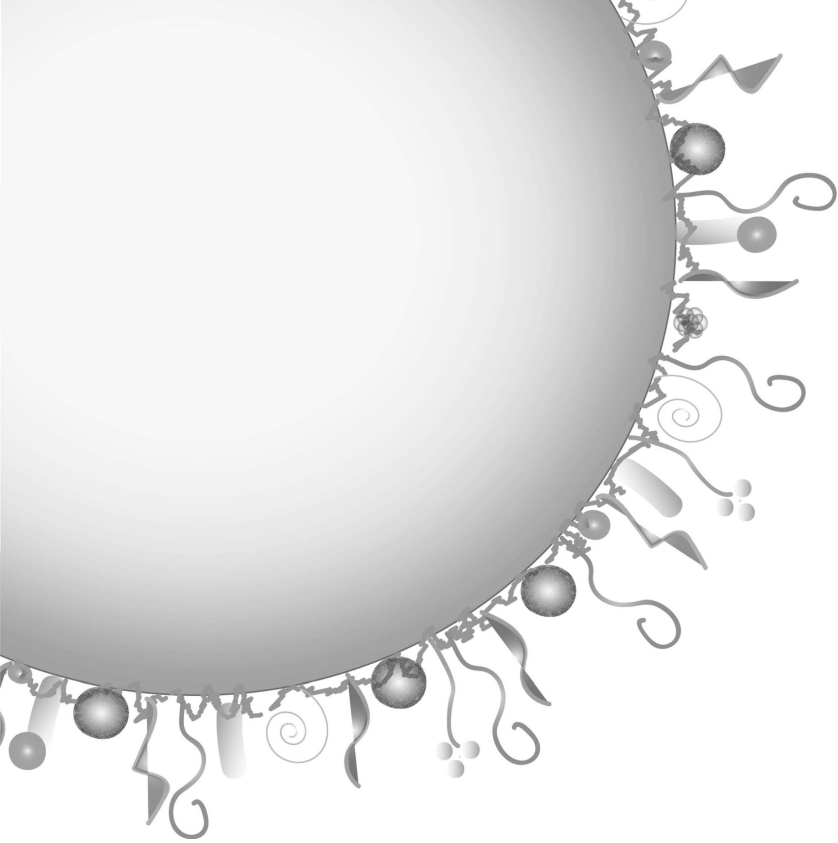


Figure S2: Number-weighted size distributions of AgNPs generated by spICP-MS measurements of DMEM⁺ suspensions of **A)** (LA) AgNPs, **B)** (Cit) AgNPs, **C)** (BPEI) AgNPs and **D)** Ag₂S NPs.



5

Induction of γ -H₂AX lesions and cytotoxicity in HepG2 cells by silver nanoparticles

Ashraf Abdelkhalig, Meike van der Zande and Hans Bouwmeester

In preparation



ABSTRACT

The increased usage and incorporation of silver nanoparticles (AgNPs) in different consumer associated products require more knowledge on how to assure the safety of these materials. Previous *in vitro* and *in vivo* studies have indicated that systemic exposure, following oral exposure, to AgNPs is likely. Some studies have suggested that AgNPs can accumulate in the liver. The aim of this study was to assess the potential of the In Cell-Western (ICW)- γ -H₂AX assay as an alternative *in vitro* assay to assess the potential of aged (silver sulphide NPs) and pristine AgNPs with different surface chemistries to induce phosphorylation of H₂AX in HepG2 liver cells following induction of DNA double-strand breaks. In addition, we explored whether these AgNPs induce oxidative stress as a possible underlying mechanism for DNA damage. Results showed no increase in ROS levels upon exposure to the AgNPs for 4 or 24 h, while an increase in ROS levels was detected upon AgNO₃ exposure. Using the ICW- γ -H₂AX assay, induction of γ -H₂AX was detected, which was higher after 24 hr exposure compared to 4 hr and was accompanied by a significant cytotoxicity in the HepG2 cells. Silver sulphide NPs did not show significant cytotoxicity nor induction of γ -H₂AX. The decrease in the cellular viability that accompanied the γ -H₂AX induction points toward a positive signal in the ICW- γ -H₂AX assay that is ascribed to initiation of DNA damage resulting from apoptosis in affected cells. Altogether the present results do not point at a positive response for genotoxicity of the different AgNPs in the ICW- γ -H₂AX assay. To further exclude the genotoxicity of these AgNPs further genotoxicity testing is required.

INTRODUCTION

Over the last decades, potential applications of engineered nanoparticles (NPs) have been studied intensively because of their unique physicochemical properties. These properties led the NPs to be incorporated in a great diversity of applications and products (Prajitha *et al.* 2019; Savage *et al.* 2019; Contado 2015). Among all NPs, silver nanoparticles (AgNPs) are frequently used in consumer products *e.g.* textile, toys and food packaging materials (Zare *et al.* 2019; Zhao *et al.* 2016; Avalos *et al.* 2014; Thomas 2014) likely because of their claimed antimicrobial properties (Flores-López *et al.* 2019; Perde-Schrepler *et al.* 2019; Juarez-Moreno *et al.* 2017). AgNPs are produced in a diverse range of sizes, shapes and surface chemistries, which offers a wide range of possibilities to modify their functionality in products and their biological interactions (Borowik *et al.* 2019; Syafiuddin *et al.* 2017; Zhang *et al.* 2016; Arts *et al.* 2015; Lynch *et al.* 2014).

Irrespective of their original size, shape or surface chemistry, once released in the environment or in organisms following systemic uptake, the AgNPs are prone to sulfidation processes, which result in formation of silver sulphide nanoparticles (Ag₂S NPs) or so called 'aged' AgNPs (He *et al.* 2019; Liu *et al.* 2018; Loeschner *et al.* 2011). Ag₂S NPs can also be directly released into the environment given their use in biomedical applications (Liu *et al.* 2018; Mitra *et al.* 2017). These aged Ag₂S NPs are the main form of particulate silver in the environment (Liu *et al.* 2018). The high stability of the Ag₂S NPs in soils resulted in their uptake and accumulation in plants by which they enter the (human) food chain (Wang *et al.* 2017). This adds to the potential human exposure to AgNPs and the potential accompanying hazards and risks (Sharma *et al.* 2019; Zhao *et al.* 2016; Meghan E. Samberg and Monteiro-Riviere 2014).

Several *in vivo* studies have shown that AgNPs (with different surface chemistries) are systemically available upon ingestion (Walker and Parsons 2014; Larese *et al.* 2009), subsequently reaching several organs including the liver (van der Zande *et al.* 2012; Loeschner *et al.* 2011). The liver has been considered one of the most affected organs following AgNPs exposure (Wen *et al.* 2017; Hendrickson *et al.* 2016; Kim *et al.* 2008; Sung *et al.* 2008), resulting in various forms of toxicity, including genotoxicity (Kim *et al.* 2019).

Several *in vitro* studies indicated that AgNPs were capable to induce cytotoxicity, irreversible DNA damage and genotoxicity (Juarez-Moreno *et al.* 2017; de Lima *et al.* 2012; Mukherjee *et al.* 2012). Furthermore, upon exposure to AgNPs, an increase was detected in two markers of DNA double strand breaks (DSBs), the expression of Rad51 protein and in the phosphorylation of histone H₂AX at serine 139 (γ -H₂AX) (Kim and Ryu 2013; Ahamed *et al.* 2008). However, it is not clear if the potential genotoxicity of AgNPs originates from a direct interaction of the AgNPs with the DNA or via indirect processes (Li *et al.* 2017; Foldbjerg *et al.* 2011). In addition, it has been suggested that not the AgNPs themselves but the silver ions released from the AgNPs damage the DNA by generating reactive oxygen species (ROS) *in vitro* (Kim and Ryu 2013; Foldbjerg *et al.* 2011).

Several methods are available to detect the DNA-DSBs, *e.g.* the TUNEL assay and the neutral comet assay, which both are laborious and insensitive in detecting low levels of DNA-DSBs. The γ -H₂AX assay has proven to be a sensitive and powerful alternative method to detect DNA-DSBs with a low false-positive rate (Heylmann and Kaina 2016; Nikolova *et al.* 2014; Khoury *et al.* 2013). The high sensitivity of the γ -H₂AX assay is assumed to be due to detecting the phosphorylation of H₂AX as a readout, which occurs at early stages of DNA-DSBs formation in mammalian cells and is thus considered an early marker for DNA-DSBs (Heylmann and Kaina 2016; Khoury *et al.* 2013; Sedelnikova *et al.* 2010; Rogakou *et al.* 1998). The In Cell Western (ICW)- γ -H₂AX assay has been used in HepG2 liver cells as a high-throughput genotoxicity assay (Khoury *et al.* 2013).

The present study aimed to explore the possibility to employ the ICW- γ -H₂AX assay to assess the potential of aged AgNPs and pristine AgNPs with different surface chemistries to induce phosphorylation of H₂AX in HepG2 human hepatoblastoma cells. In addition, the capability of AgNPs to produce ROS, as a potential underlying mechanism of inducing DNA-DSBs, was assessed, both under cell-free conditions and in HepG2 cells.

MATERIALS AND METHODS

Nanoparticles and chemicals

Negatively charged 20 nm silver sulphide nanoparticles (Ag₂S NPs) in milli-Q water were obtained from Applied Nanoparticles (Barcelona, Spain) with a Ag mass concentration of 4.7 g/L. Three 50 nm silver nanoparticles with different surface chemistries were purchased from Nanocompositix Inc. (San Diego, CA, USA); negatively charged lipoic acid BioPure (LA) AgNPs (pH = 6.1) in milli-Q water, negatively charged citrate BioPure (Cit) AgNPs (pH = 7.4) in 2 mM citrate buffer and positively charged branched polyethylenimine (BPEI) BioPure AgNPs (pH = 7.0) in milli-Q water. The silver mass concentration in the stock suspensions of the three AgNPs was 1 g/L. Positively charged 50 nm BioPure copper oxide nanoparticles (CuO NPs) in polyvinylpyrrolidone (PVP) solution were obtained from Nanocompositix Inc. with a copper mass concentration of 1 g/L. All NPs suspensions were stored at 4°C in the dark. Silver nitrate (AgNO₃), purchased from Sigma-Aldrich (St. Louis, MO, USA), was used as a control (source of silver ions) in all experiments. Dilutions of the AgNPs, CuO NPs or AgNO₃ were freshly prepared for every exposure experiment in complete cell culture media (MEM⁺). MEM⁺ was prepared by supplementing Minimum Essential Medium (MEM) (Gibco, Life Technologies; Paisley, UK) with 10% (v/v) heat inactivated Foetal Bovine Serum (FBS) (Gibco, Life Technologies), 1% (v/v) of MEM Non-Essential Amino Acids (NEAA) (Gibco, life technologies), 1% (v/v) of Glutamax (Gibco, life technologies), 1% (v/v) of 100 mM sodium pyruvate (Gibco, life technologies) and 1% (v/v) of penicillin-streptomycin 10,000 units penicillin and 10 mg streptomycin/mL (Gibco, life technologies). Hydrogen peroxide 30% Suprapur was purchased from Merck (Darmstadt, Germany). Ammonium chloride (NH₄Cl), Triton X-100, phosphatase inhibitor (PhosStop™; Roche, Mannheim, Germany), bovine ribonuclease A (RNase), benzo(a)pyrene (BaP) and etoposide were purchased from (Sigma-Aldrich). Anti-Phospho Histone H₂AX primary antibody (ser139) Rabbit was purchased from Cell Signaling (Leiden, The Netherlands). Goat anti Rabbit IgG secondary antibody and RedDot-2 were purchased from Biotium (Fremont, CA, USA).

Physicochemical characterization of nanoparticles

Hydrodynamic diameters of the NPs in suspension were determined using dynamic light scattering (DLS). Measurements were performed on samples containing 10 mg/L NPs suspended in nano-pure water using an ALV dynamic light scattering setup (ALV-Laser Vertriebsgesellschaft; Germany), consisting of a Thorn RFB263KF photomultiplier detector, an ALV-SP/86 goniometer, an ALV 50/100/200/400/600 μ m pinhole detection system, an

ALV7002 external correlator and a Cobolt Samba-300 DPSS laser. Measurements were performed at room temperature immediately after preparation. For each condition, samples were analysed in triplicate; each measurement consisted of 10 technical replicate-measurements of 30 seconds each, at an angle of 90°. The results are expressed as the average hydrodynamic diameter (nm) \pm standard deviation (SD) that was calculated using AfterALV software (AfterALV 1.0d, Dullware; USA).

Cell culture

HepG2 human hepatoblastoma cells (ATCC; Wesel, Germany) were used at passage numbers 12 - 16. The cells were cultured and maintained in 75 cm² cell culture flasks (Corning; Oneonta, NY, USA) at 37° C in a humidified 5% CO₂ atmosphere in MEM⁺. The cells were sub-cultured every 3 - 4 days using trypsin-EDTA (Sigma-Aldrich) to detach the cells.

Cell viability

Cytotoxic effects of the AgNPs, CuO NPs and AgNO₃ were evaluated using the ATPlite luminescence assay system (PerkinElmer; Waltham MA, USA). Each well of 96-well black flat bottom plates (Greiner bio-one; Frickenhausen Germany) was seeded with 100 μ L/well of 2×10^4 cells/mL of a HepG2 cell suspension in MEM⁺. Plates were incubated at 37° C in a humidified 5% CO₂ atmosphere for 24 hr. The attached cells were then washed with 100 μ L/well pre-warmed phosphate buffered saline (PBS) (Gibco, Life Technologies) and exposed to 100 μ L/well of freshly prepared dilutions (0.1 – 100 mg/L) of AgNPs, CuO NPs and AgNO₃ in MEM⁺ for 4 and 24 hr. Then, the exposure medium was aspirated and 50 μ L/well of mammalian cell lysis solution were added and the plates were shaken (700 rpm) for 5 minutes at room temperature in an orbital shaker (Heidolph-Trimax 1000; Schwabach, Germany). Next, 50 μ L/well of substrate solution were added and the plates were shaken (700 rpm) for 5 minutes at room temperature and then incubated for 10 minutes in the dark at room temperature before measuring the luminescence on a plate reader (BioTek Synergy™ HT Multi-Mode Microplate reader; Winooski VT, USA). The MEM⁺ was used as a negative control and Triton-X100 (0.25%) was used as a positive control. The cell viability was expressed as a percentage of the response observed for the negative control. For each condition, all samples were analysed in triplicate.

Cytotoxic effects of the BaP were evaluated using a cell proliferation reagent WST-1 (Roche; Mannheim, Germany). Each well of 96-well flat bottom plates (Greiner bio-one) was seeded with 100 μ L of 2×10^4 cells/mL of a HepG2 cell suspension in MEM⁺. Plates were incubated at 37° C in a humidified 5% CO₂ atmosphere for 24 hr. Attached cells were then exposed to 100 μ L/well of freshly prepared serial dilutions of BaP (0.3 – 30 μ M) for 24 hr. Afterwards, the exposure medium was discarded and 10 μ L of WST-1 solution was added with 90 μ L of MEM⁺ (without phenol red) to each well. The plates were incubated for 4 hr at 37°C in a humidified 5% CO₂ atmosphere and absorbance was read at 490 nm and 630 nm on a plate reader (BioTek Synergy™ HT Multi-Mode Microplate reader). Cell viability for each concentration of BaP was expressed as a percentage of the control. MEM⁺ was used as a negative control and Triton-X100 (0.25%) (Sigma) was used as a positive control.

Reactive oxygen species (ROS) measurement

Cellular and cell-free ROS production by the AgNPs and AgNO₃ were determined using 2',7'-dichlorodihydrofluorescein diacetate (DCFDA) (Sigma-Aldrich) which is hydrolysed chemically or by the cellular esterase to non-fluorescent dichlorofluorescein (DCFH), which is then oxidized by ROS to highly fluorescent dichlorofluorescein (DCF) (Avalos *et al.* 2014). For cell-free ROS production measurement, the DCFDA was chemically hydrolysed to DCFH by incubating the DCFDA with 0.01 M sodium hydroxide in the dark for 30 minutes (Shi *et al.* 2012). Then 50 μ L/well of DCFH were incubated with 50 μ L/well of freshly prepared dilutions of AgNPs and AgNO₃ (with final concentrations of 0.1 – 100 mg/L) in 96-well black flat bottom plates for 4 and 24 hr. The fluorescence intensity was then measured after 4 and 24 hr at excitation and emission wavelengths of 485 and 535 nm, respectively, using a fluorescence plate reader (BioTek Synergy™ HT Multi-Mode Microplate reader). MEM⁺ was used as a negative control and H₂O₂ (0.03%) was used as a positive control. The ROS production was expressed as a percentage of the negative control.

For measurement of cellular ROS production, 100 μ L/well of 2.5×10^4 cells/mL of HepG2 cell suspension in MEM⁺ were seeded in 96-well black flat bottom plates (Greiner bio-one). Plates were incubated at 37° C in a humidified 5% CO₂ atmosphere for 24 hr. The attached cells were then washed with 100 μ L/well pre-warmed PBS followed by addition of 100 μ L/well 25 μ M DCFDA and incubation at 37° C in a humidified 5% CO₂ atmosphere for 45 minutes. The

DCFDA solution was then removed and the cells were washed once with 100 μL /well pre-warmed PBS buffer before they were exposed to 100 μL /well of freshly prepared dilutions (0.1 – 100 mg/L) of AgNPs and AgNO₃ in MEM⁺ for 4 and 24 hr. The fluorescence measurement and expression of results were performed in a similar way to the cell-free ROS measurement. For each condition, all samples were analysed in triplicate.

ICW- γ -H₂AX assay

The potential genotoxic effects of AgNPs and AgNO₃ were assessed using the ICW- γ -H₂AX- assay performed as described previously (Kopp *et al.* 2019; Khoury *et al.* 2013; Audebert *et al.* 2010). Briefly, each well of 96-well black flat bottom plates was seeded with 100 μL of 3.2×10^5 cells/mL of HepG2 cell suspension in MEM⁺. Plates were incubated at 37° C, in a humidified 5% CO₂ atmosphere for 24 hr. The attached cells were then washed with 100 μL /well PBS and exposed to 100 μL /well of freshly prepared dilutions (0.1 – 100 mg/L) of AgNPs and AgNO₃ in MEM⁺ for 4 and 24 hr. The exposure media were then removed and cells were washed with PBS. Then the cells were fixed with 4% paraformaldehyde (Merck) in PBS. Subsequently, the cells were washed with PBS and incubated for 2 minutes with a 50 μL 50 mM NH₄Cl solution to neutralize the paraformaldehyde. The cells were then washed with PBS and permeabilized using 50 μL 0.2% Triton X-100 in PBS, followed by a washing step using 100 μL 0.2% TritonX-100 and 2% FBS in PBS (PST solution). Subsequently, the cells were incubated for 1 hr with a saturation solution (MAXblock™ Blocking Medium (Active Motif; La Hulpe, Belgium) supplemented with PhosStop™ and RNase). The cells were then incubated for 2 hr at room temperature with the 200 X diluted primary antibody (Phospho-Histone H₂AX (Ser139) Rabbit) in PST solution. The cells were then washed three times with the PST solution and incubated for 1 hr with the secondary antibody (goat anti rabbit IgG antibody conjugated to an infrared fluorescent dye of 700 nm absorption wavelength (Biotium) and RedDot-2 (of 800 nm absorption wavelength for DNA staining; Biotium) in PST solution. Afterwards, the cells were washed three times with the PST solution before being scanned using an Odyssey Imaging System (Li-Cor ISO 9001, Odyssey Biosciences; Bad Homburg, Germany). The γ -H₂AX/DNA fluorescence ratio of each treatment was determined and the fold change in γ -H₂AX/DNA fluorescence ratio of each treatment, compared to the negative control was determined. For (LA), (Cit) and (BPEI) AgNPs, the highest concentration for which data are reported were 25, 25 and 10 mg/L, respectively as the higher concentrations tested up to 100

mg/L induced interference with the RedDot-2 signal and they were discarded accordingly. In each experiment, negative controls (MEM⁺ and 0.1% DMSO) and positive controls (5 μ M BaP, 5 μ M etoposide and 40 mg/L CuO NPs (Karlsson *et al.* 2008)) were included. For each condition, all samples were analysed in triplicate.

Statistical analysis

Each data point represents the average of three replicates ($n = 3$) and the results are shown as mean \pm standard deviation. Prism (v.8.0.1; GraphPad, USA) software was used for statistical analysis using a one-way analysis of variance (ANOVA) with a Bonferroni's post-test. A p -value < 0.05 was considered significant.

RESULTS

Physicochemical characterization of the AgNPs suspensions and AgNO₃ solution

Four types of AgNPs were used in this study: lipoic acid, citrate, branched polyethylenimine coated AgNPs and Ag₂S NPs. CuO NPs were used in this study as a positive control in the ICW- γ -H₂AX assay as CuO NPs have been shown to induce genotoxicity using the comet assay (Chelomin *et al.* 2017; Alarifi *et al.* 2013; Midander *et al.* 2009; Karlsson *et al.* 2008) and micronucleus assay (Perreault *et al.* 2012). The hydrodynamic sizes of all the NPs were measured in nano-pure water at room temperature using DLS (Table 1). The (BPEI) AgNPs and CuO NPs were positively charged, while the rest of the AgNPs were negatively charged.

ROS measurement

Following incubation for 4 and 24 hr of different concentrations of AgNPs and AgNO₃ in cell-free or HepG2 cellular systems, the levels of ROS generation were measured using the DCFDA assay. The levels of cell-free ROS generation in the suspensions of all the AgNPs were low and comparable following both 4 and 24 hr incubation (Figure 1). Only at higher concentrations (~50 mg/L and higher) of (LA), (Cit) and (BPEI) AgNPs suspensions, ROS generation was significantly lower compared with the control (Figure 1 A, B and C). Following incubation with Ag₂S NPs, no significant changes in ROS generation were observed (Figure 1

D), while a concentration dependent increase in the levels of ROS generation was observed for AgNO₃ solutions (Figure 1 E). For all the tested samples, generally no differences in cell-free ROS generation were noticed between 4 and 24 hr incubation.

Table 1. Physicochemical characteristics of NPs *

	Size (TEM) nm ± SD *	Hydrodynamic size (DLS) nm ± SD	ζ- potential (mV) ± SD *
(LA) AgNPs	51 ± 5	75 ± 3	-54 ± 3
(Cit) AgNPs	48 ± 5	67 ± 5	-46 ± 1
(BPEI) AgNPs	47 ± 5	61 ± 1	+73 ± 1
Ag ₂ S NPs	28 ± 20	220 ± 25	-22 ± 1
CuO NPs	48 ± 7	244 ± 14	+6 ± 1

* Measured in nano-pure water at t = 0 hr

× Provided by the manufacturer.

Upon 4 hr exposure of HepG2 cells to AgNPs, only at higher exposure concentrations (50 mg/L and higher) of (LA), (Cit) and (BPEI) AgNPs, the levels of cellular ROS generation decreased significantly compared with the control (Figure 2 A, B and C). The Ag₂S NPs did not induce changes in ROS generation in HepG2 cells (Figure 2 D), while the ROS generation increased significantly at concentrations of 50 mg/L and higher upon exposure to AgNO₃ (Figure 2 E).

Following 24 hr exposure of HepG2 cells to AgNPs, at concentrations ≥ 5 mg/L of the (LA) AgNPs, concentrations ≥ 25 mg/L of the (Cit) and (BPEI) AgNPs and concentrations ≥ 1 mg/L of Ag₂S NPs, the cellular levels of ROS generation were lower compared with the control (Figure 2 A, B, C and D). ROS generation upon exposure to AgNO₃ for 24 hr however did not change significantly compared to the control (Figure 2 E). Comparing 4 and 24 hr exposure, the levels of ROS generation in HepG2 cells were lower after 24 hr exposure to concentrations ≥ 25 mg/L (LA), (Cit) and (BPEI) AgNPs and concentrations ≥ 100 mg/L of Ag₂S NPs. ROS generation was higher after 24 hr exposure to concentrations ≥ 5 mg/L AgNO₃.

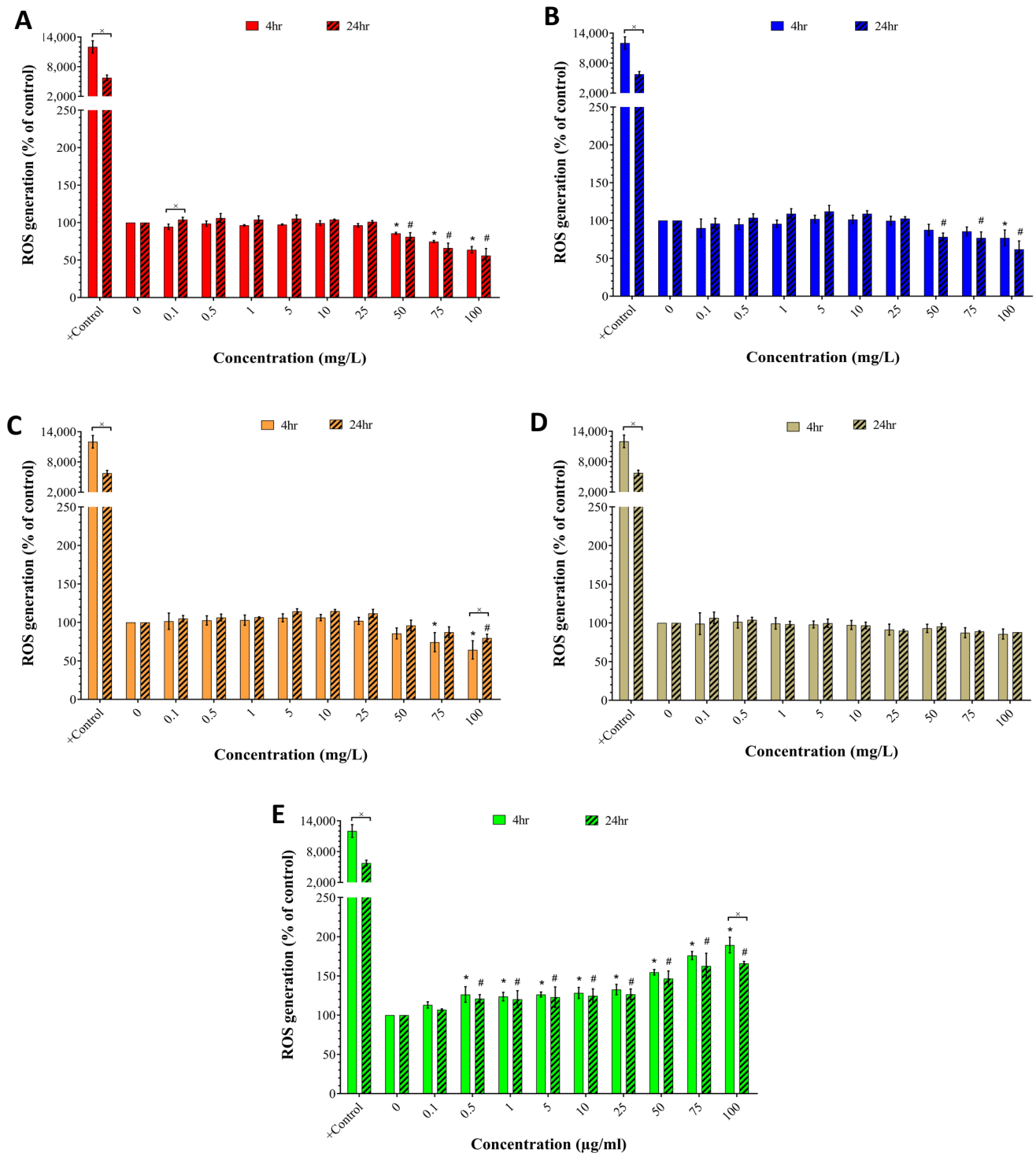


Figure 1: Concentration–response of reactive oxygen species (ROS) generation under cell-free conditions upon 4 and 24 hr incubation with: **A)** (LA) AgNPs, **B)** (Cit) AgNPs, **C)** (BPEI) AgNPs, **D)** (Ag₂S) NPs, and **E)** AgNO₃, measured using DCFDA assay. H₂O₂ (0.03%) was used as a positive control. Values are given as a percentage of the control (mean ± SD; n=3). Significant difference (p ≤ 0.05) from blank after 4 hr (*), from blank after 24 hr (#), between 4 and 24 hr for the same concentration (X).

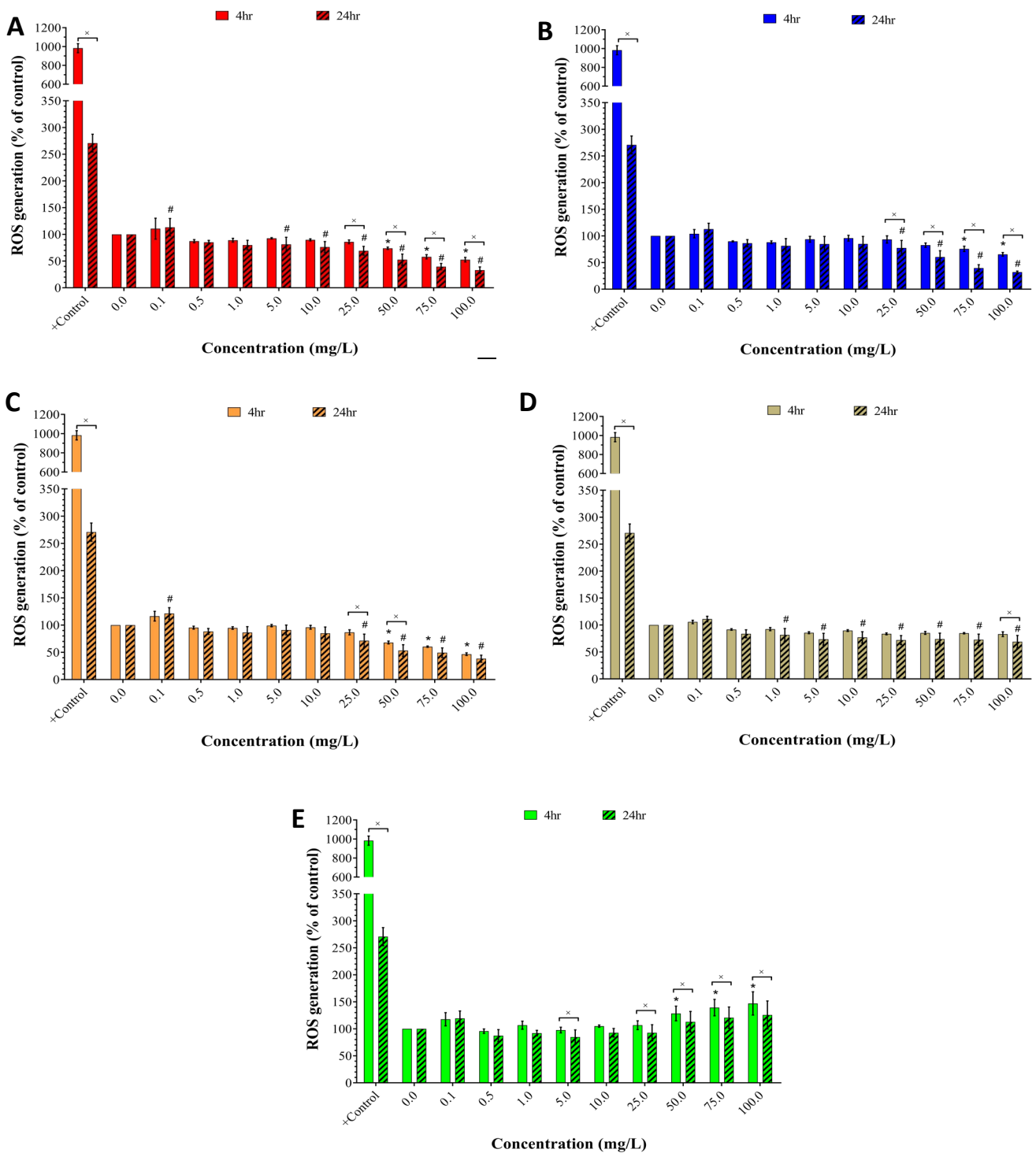


Figure 2: Concentration–response of reactive oxygen species (ROS) generation upon 4 and 24 hr exposure of HepG2 cells to: **A)** (LA) AgNPs, **B)** (Cit) AgNPs, **C)** (BPEI) AgNPs, **D)** (Ag₂S) NPs, and **E)** AgNO₃, measured using DCFDA assay. Hydrogen peroxide (0.03%) was used as a positive control. Values are given as a percentage of the negative control (mean ± SD; n=3). Significant difference ($p \leq 0.05$) from blank after 4 hr (*), from blank after 24 hr (#), between 4 and 24 hr for the same concentration (x).

Considering the trend of the materials to alter ROS generation levels in cell-free versus HepG2 cellular conditions, no clear difference was found after 4 or 24 hr incubation of (LA), (Cit), (BPEI) AgNPs. In case of Ag₂S NPs, a decrease in the levels of generated ROS was detected upon 24 hr exposure under cellular conditions. For AgNO₃, there was an increase in the levels of generated ROS upon 4 and 24 hr exposure under both cell-free and HepG2 conditions, the increase in the levels of generated ROS started at lower concentrations under cell-free conditions.

Cytotoxicity assessment

Cytotoxic effects of increasing concentrations of the AgNPs, CuO NPs and AgNO₃ to HepG2 liver cells were assessed upon 4 and 24 hr exposure using the ATPlite assay (Figures 3 and 4). The (LA), (Cit) and (BPEI) AgNPs and Ag₂S NPs did not reduce the viability of the HepG2 cells after 4 hr exposure (Figure 3A, B, C and D). The AgNO₃ induced a concentration-dependent reduction in viability (Figure E). After 24 hr exposure, the (LA), (Cit) and (BPEI) AgNPs and AgNO₃ induced a reduction in the viability of the HepG2 cells (Figure 4 A, B, C and E), whereas the Ag₂S NPs did not reduce the viability (Figure 4 D). The cytotoxicity curves reached a plateau phase upon exposure to concentrations \geq 5 mg/L for (LA), (Cit) and (BPEI) AgNPs (Figures 4 A, B, C). The AgNO₃ showed a concentration-dependent cytotoxicity upon 4 and 24 hr exposure and imposed a higher potency of toxicity than all the NPs tested (Figure 3 E and 4 E). The resulting IC₅₀ values for all the exposure groups at 4 and 24 hr exposure are summarized in Table 2. The CuO NPs, showed a dose-dependent cytotoxicity upon 4 and 24 hr exposure (Figure S1), while the BaP did not induce any cytotoxicity following exposure of the HepG2 cells for 24 hr (Figure S2).

ICW- γ -H₂AX- assay

The potential of AgNPs to induce phosphorylation of histone H₂AX (γ -H₂AX) was assessed using the γ -H₂AX assay. The fold induction of γ -H₂AX levels, compared with the negative control, was calculated for each treatment. Upon 4 hr exposure, induction of γ -H₂AX was significantly higher than the negative control following exposure to 1 – 25 mg/L (LA) AgNPs, 5 – 25 mg/L (Cit) AgNPs, 10 mg/L (BPEI) AgNPs, 5, 75 – 100 mg/L Ag₂S NPs and 0.25 - 0.5 mg/L AgNO₃.

Table 2: The IC₅₀ values (mg/L) of AgNPs, CuO NPs and AgNO₃ in HepG2 liver cells after 4 and 24 hr exposure

Treatment	IC ₅₀ (mg/L) (4hr)	IC ₅₀ (mg/L) (24hr)
(LA) AgNPs	>100	>100
(Cit) AgNPs	>100	>100
(BPEI) AgNPs	>100	4.7
Ag ₂ S NPs	>100	>100
AgNO ₃	4.5	2.1
CuO NPs	100	52

IC₅₀: the concentration where 50% of the HepG2 cells are viable

After 24 hr exposure, a higher induction of γ -H₂AX formation compared to 4 hr exposure was observed for 5 – 25 mg/L of (LA) and (Cit) AgNPs, 5 – 10 mg/L of (BPEI) AgNPs and for 0.25 – 2.5 mg/L of AgNO₃ (Figure 4). The Ag₂S NPs did not induce γ -H₂AX formation after 24 hr. Exposure of the HepG2 cells to the positive controls resulted in a clear induction of the γ -H₂AX levels upon 4 hr exposure to Etoposide and CuO NPs and upon 24 hr exposure to BaP, Etoposide and CuO NPs.

Upon 24 hr exposure to (LA), (Cit) and (BPEI) AgNPs, the induction of γ -H₂AX levels was always accompanied with a substantial decrease in the cell viability approaching 50% (Figure 4 A, B and C). For the Ag₂S NPs, no effects on viability were observed following 4 and 24 hr exposure, but after 4 hr exposure minor but significant increases in γ -H₂AX levels were detected (Figures 3 D and 4 D). In case of 4 hr exposure to AgNO₃, significant increases in γ -H₂AX levels were detected without viability decrease, although the cell viability reduced rapidly at higher concentrations. After 24 hr exposure to AgNO₃, increases in γ -H₂AX levels were accompanied with strong reductions in cell viability approaching 50% or more (Figures 3E and 4 E).

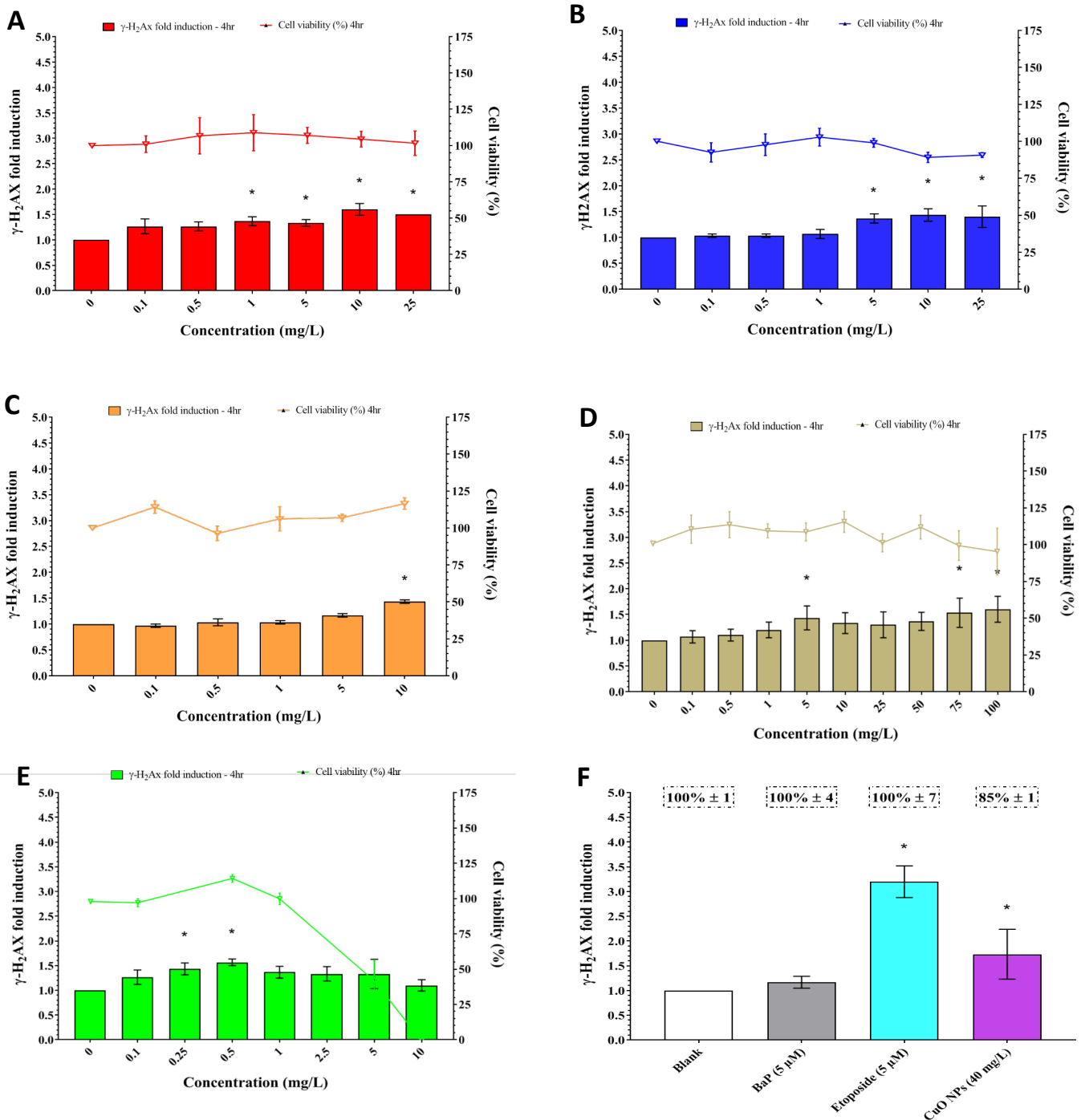


Figure 3: Concentration–response of cytotoxicity (lines, right y-axis) and γ -H₂AX induction (bars, left y-axis) in HepG2 cells upon 4 hr exposure to: **A**) (LA) AgNPs, **B**) (Cit) AgNPs, **C**) (BPEI) AgNPs, **D**) (Ag₂S) NPs, **E**) AgNO₃, and **F**) positive controls: 5 μ M B(a)P, 5 μ M etoposide and 40 mg/L CuO NPs. The cell viability of the positive controls is reported in the dotted box, values are given as a percentage of the negative control (mean \pm SD; n=3).

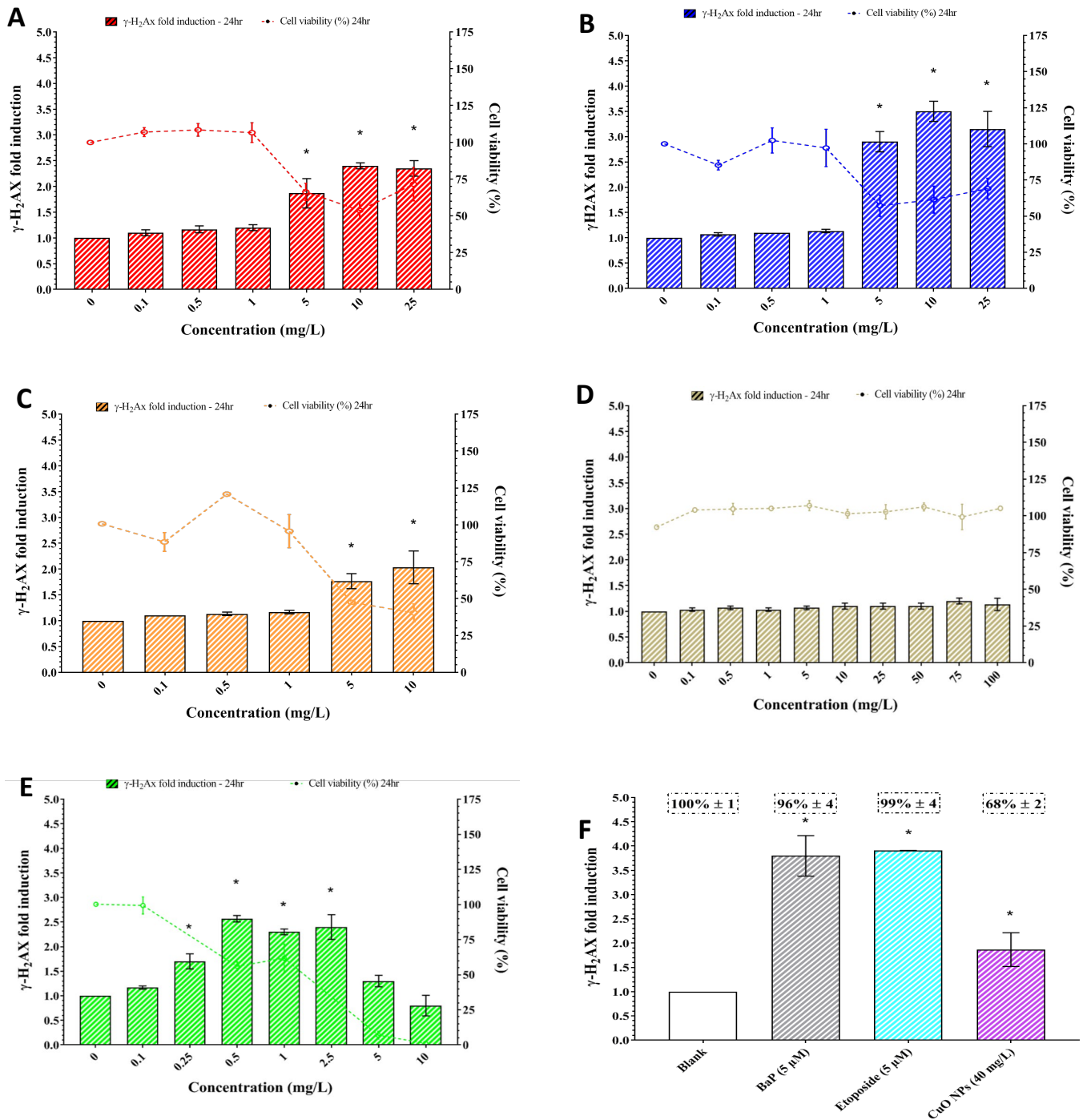


Figure 4: Concentration–response of cytotoxicity (lines, right y-axis) and γ -H₂AX induction (bars, left y-axis) of HepG2 cells upon 24 hr exposure to: **A**) (LA) AgNPs, **B**) (Cit) AgNPs, **C**) (BPEI) AgNPs, **D**) (Ag₂S) NPs, **E**) AgNO₃ and **F**) positive controls: 5 μ M B(a)P, 5 μ M etoposide and 40 mg/L CuO NPs. The cell viability of the positive controls is reported in the dotted box, values are given as a percentage of the negative control (mean \pm SD; n=3).

Exposure of the HepG2 cells to CuO NPs induced the γ -H₂AX levels but did not result in cytotoxicity after 4 hr exposure. However, after 24 hr exposure the viability was reduced to 68% (Figures 3 F and 4 F).

Upon 24 hr exposure to (LA), (Cit) and (BPEI) AgNPs, the induction of γ -H₂AX levels was always accompanied with a substantial decrease in the cell viability approaching 50% (Figure 4 A, B and C). For the Ag₂S NPs, no effects on viability were observed following 4 and 24 hr exposure, but after 4 hr exposure minor but significant increases in γ -H₂AX levels were detected (Figures 3 D and 4 D). In case of 4 hr exposure to AgNO₃, significant increases in γ -H₂AX levels were detected without viability decrease, although the cell viability reduced rapidly at higher concentrations. After 24 hr exposure to AgNO₃, increases in γ -H₂AX levels were accompanied with strong reductions in cell viability approaching 50% or more (Figures 3E and 4 E). Exposure of the HepG2 cells to CuO NPs induced the γ -H₂AX levels but did not result in cytotoxicity after 4 hr exposure. However, after 24 hr exposure the viability was reduced to 68% (Figures 3 F and 4 F).

DISCUSSION

In this study, we aimed to investigate the possibility to use the ICW- γ -H₂AX assay to study the potential of aged AgNPs and pristine AgNPs with different surface chemistries to induce phosphorylation of H₂AX in HepG2 cells as an indication of genotoxicity. Our results show that in most cases where AgNPs induced phosphorylation of γ -H₂AX in HepG2 cells, cytotoxic responses were associated. While no cellular ROS generation was detected at these levels of γ -H₂AX induction.

Although both ionic and nano forms of silver induced cytotoxic responses of HepG2 cells, these responses were more potent upon exposure to AgNO₃ compared to AgNPs. This confirms other studies that reported higher cytotoxic potency of AgNO₃ compared to AgNPs with different sizes and surface chemistries (Sahu *et al.* 2016a; Sahu *et al.* 2016b; Veronesi *et al.* 2016; Vrček *et al.* 2016; Xue *et al.* 2016; Sahu *et al.* 2014a).

Oxidative stress is considered a common mechanism underlying cytotoxicity and DNA damage following exposure to NPs (Xue *et al.* 2016; Li *et al.* 2014; Gaiser *et al.* 2012). In our experiments, we did not observe an increase in intracellular ROS levels upon exposure to

different AgNPs for 4 and 24 hr. However, increases in ROS generation were detected following exposure to AgNO₃. In the literature, highly variable reports on the capability of AgNPs to induce ROS generation can be found. Several studies described the capability of AgNPs to induce ROS generation (Flores-López *et al.* 2019; Sharma *et al.* 2019; Zhu *et al.* 2016; Avalos *et al.* 2014). While others reported the absence of ROS generation by AgNPs, *e.g.* after exposure of HepG2 cells to 20 nm (Cit) AgNPs (Vrček *et al.* 2016; Sahu *et al.* 2014b) and 6 nm (PVA) AgNPs (Vrček *et al.* 2016), or after exposure of C3A hepatocytes to 17 nm NM300 AgNPs (Gaiser *et al.* 2012). This variability in ROS induction has been suggested to be related to the type of AgNPs used or the amount of Ag ions released from the AgNPs. As Ag ions generally induce ROS generation, AgNPs with a high Ag ions release are also more likely to induce ROS generation (Völker *et al.* 2015; Gaiser *et al.* 2012).

Induction of γ -H₂AX is an indication of formation of DNA-DSBs. This induction can be triggered by ROS, but even in the absence of ROS, 20 nm (Cit) coated AgNPs have been described to induce DNA-DSBs in HepG2 cells (Guo *et al.* 2016; Sahu *et al.* 2014a; Sahu *et al.* 2014b). We observed upon 24 hr exposure of HepG2 cells to (LA), (Cit) and (BPEI) AgNPs and AgNO₃ that induction of γ -H₂AX was accompanied by a substantial reduction in cellular viability. This warrants a very careful interpretation of the results. A distinct correlation between cytotoxicity, more specifically apoptosis and DNA-DSBs has been proven and has been discussed to be one of the main causes of false-positive results in *in vitro* genotoxicity assays (Roos and Kaina 2013; Lips and Kaina 2001; Müller and Sofuni 2000) including the γ -H₂AX assay. In a study by Nikolova *et al.*, the induction of γ -H₂AX was studied using a microscope-based approach. Ten selected cytotoxic (non-genotoxic) compounds showed a clear cytotoxic effect without inducing γ -H₂AX formation, suggesting that cytotoxicity not always results in γ -H₂AX formation (Nikolova *et al.* 2014). However, the read-out of the γ -H₂AX assay in the study of Nikolova *et al.*, was different than our study as the number of foci per cell was microscopically counted, allowing exclusion of apoptotic cells from the results. In the ICW approach of the γ -H₂AX assay that was used in the current study, the fluorescence signal per well is measured. Accordingly, the induction of γ -H₂AX caused by apoptotic cells cannot be excluded, possibly resulting in a false-positive outcome. Therefore, we have to conclude that further, in depth, studies focusing on apoptotic responses have to be incorporated in the

ICW- γ -H₂AX assay to render this assay suitable for a definitive conclusion on the potential genotoxicity of NPs.

The aged Ag₂S NPs showed different behaviour compared with the pristine AgNPs. The aged Ag₂S NPs go through sulfidation processes during their formation, which likely change their colloidal dynamics making them prone to aggregation and sedimentation (Liu *et al.* 2018; Yin *et al.* 2015; Reinsch *et al.* 2012). In our previous studies, we found that, although the dissolution and charge of the Ag₂S NPs are comparable to those of the (LA) and (Cit) pristine AgNPs, they were not cytotoxic and their transport through the BeWo b30 cell layer were significantly lower (Abdelkhalik *et al.* 2020). In the present study, using the same Ag₂S NPs, we noticed a similar absence of cytotoxicity in HepG2 cells. Furthermore, the Ag₂S NPs did not induce ROS generation while γ -H₂AX induction was very limited. So far, no single genotoxicity assay can be used alone to estimate, compare and rank the potential of different NPs to induce DNA damage (Nelson *et al.* 2017). While a panel of *in vitro* and *in vivo* genotoxicity tests are established for conventional chemicals, the situation is more complex for the assessment of potential genotoxicity of NPs (Doak *et al.* 2012; Garcia-Canton *et al.* 2012). For instance, the routinely used Ames test (*in vitro* bacterial reverse gene mutation test; OECD 1997) cannot be used in combination with NPs (Nelson *et al.* 2017), as a lack of or insufficient uptake of the NPs by the bacterial cells has been reported (Doak *et al.* 2012). Other approaches like the *in vitro* comet assay can be used but owing to the lack of standardization, the time consuming nature of the assay and the fact that most positive responses were not associated with realistic human exposure to NPs, this assay was not recommended to screen for genotoxicity of NPs (Elespuru *et al.* 2018).

CONCLUSION

In conclusion, we found that the surface chemistry of AgNPs has a significant influence on their cytotoxic effects and possibly on the induction of γ -H₂AX levels in HepG2 cells. The aged Ag₂S NPs were biologically less active as cytotoxicity and induction of γ -H₂AX were absent in the dose range tested here. The absence of cellular ROS generation upon exposure to all AgNPs indicates that the observed effects were not ROS-mediated. The induction of γ -H₂AX levels following exposure to AgNPs was accompanied by cytotoxic responses in HepG2 cells,

suggesting false-positive confounders limiting the use of the ICW- γ -H₂AX assay in its current form for evaluation of cytotoxic NPs. Therefore, additional tests, to rule out apoptotic mediated false-positive signals, need to be incorporated into the ICW- γ -H₂AX assay, to render this interesting assay into a robust screening method for the potential genotoxicity of NPs. Alternatively, further genotoxicity testing is required to investigate and exclude the genotoxicity of these AgNPs.

REFERENCES

- Abdelkhalig A, van der Zande M, Peters R, Rietjens IMCM, Bouwmeester H. 2020. Combination of the BeWo b30 placental transport model and the embryonic stem cell test to assess the potential developmental toxicity of silver nanoparticles. *Part Fibre Toxicol.* 2020;17(1):11.
- Ahamed M, Karns M, Goodson M, Rowe J, Hussain SM, Schlager JJ, Hong Y. 2008. DNA damage response to different surface chemistry of silver nanoparticles in mammalian cells. *Toxicology and Applied Pharmacology* 233:404-410.
- Alarifi S, Ali D, Verma A, Alakhtani S, Ali BA. 2013. Cytotoxicity and Genotoxicity of Copper Oxide Nanoparticles in Human Skin Keratinocytes Cells. *International Journal of Toxicology* 32:296-307.
- Arts JHE, Hadi M, Irfan M-A, Keene AM, Kreiling R, Lyon D, Maier M, Michel K, Petry T, Sauer UG, Warheit D, Wiench K, Wohlleben W, Landsiedel R. 2015. A decision-making framework for the grouping and testing of nanomaterials (DF4nanoGrouping). *Regulatory Toxicology and Pharmacology* 71:S1-S27.
- Audebert M, Riu A, Jacques C, Hillenweck A, Jamin EL, Zalko D, Cravedi JP. 2010. Use of the γ H2AX assay for assessing the genotoxicity of polycyclic aromatic hydrocarbons in human cell lines. *Toxicology Letters* 199:182-192.
- Avalos A, Haza AI, Mateo D, Morales P. 2014. Cytotoxicity and ROS production of manufactured silver nanoparticles of different sizes in hepatoma and leukemia cells. *Journal of Applied Toxicology* 34:413-423.
- Borowik A, Butowska K, Konkel K, Banasiuk R, Derewonko N, Wyrzykowski D, Davydenko M, Cherepanov V, Styopkin V, Prylutsky Y, Pohl P, Krolicka A, Piosik J. 2019. The Impact of Surface Functionalization on the Biophysical Properties of Silver Nanoparticles. *Nanomaterials* 9:973.
- Chelomin VP, Slobodskova VV, Zakhartsev M, Kukla S. 2017. Genotoxic potential of copper oxide nanoparticles in the bivalve mollusk *Mytilus trossulus*. *Journal of Ocean University of China* 16:339-345.
- Contado C. 2015. Nanomaterials in consumer products: a challenging analytical problem. *Frontiers in Chemistry* 3.
- de Lima R, Seabra AB, Durán N. 2012. Silver nanoparticles: a brief review of cytotoxicity and genotoxicity of chemically and biogenically synthesized nanoparticles. *Journal of Applied Toxicology* 32:867-879.
- Doak SH, Manshian B, Jenkins GJS, Singh N. 2012. In vitro genotoxicity testing strategy for nanomaterials and the adaptation of current OECD guidelines. *Mutation Research/Genetic Toxicology and Environmental Mutagenesis* 745:104-111.
- Elespuru R, Pfuhler S, Aardema MJ, Chen T, Doak SH, Doherty A, Farabaugh CS, Kenny J, Manjanatha M, Mahadevan B, Moore MM, Ouédraogo G, Stankowski LF, Jr, Tanir JY. 2018. Genotoxicity Assessment of Nanomaterials: Recommendations on Best Practices, Assays, and Methods. *Toxicological Sciences* 164:391-416.
- Flores-López LZ, Espinoza-Gómez H, Somanathan R. 2019. Silver nanoparticles: Electron transfer, reactive oxygen species, oxidative stress, beneficial and toxicological effects. Mini review. *Journal of Applied Toxicology* 39:16-26.

- Foldbjerg R, Dang DA, Autrup H. 2011. Cytotoxicity and genotoxicity of silver nanoparticles in the human lung cancer cell line, A549. *Archives of Toxicology* 85:743-750.
- Gaiser BK, Hirn S, Kermanizadeh A, Kanase N, Fytianos K, Wenk A, Haberl N, Brunelli A, Kreyling WG, Stone V. 2012. Effects of Silver Nanoparticles on the Liver and Hepatocytes In Vitro. *Toxicological Sciences* 131:537-547.
- Garcia-Canton C, Anadón A, Meredith C. 2012. γ H2AX as a novel endpoint to detect DNA damage: Applications for the assessment of the in vitro genotoxicity of cigarette smoke. *Toxicology in Vitro* 26:1075-1086.
- Guo X, Li Y, Yan J, Ingle T, Jones MY, Mei N, Boudreau MD, Cunningham CK, Abbas M, Paredes AM, Zhou T, Moore MM, Howard PC, Chen T. 2016. Size- and coating-dependent cytotoxicity and genotoxicity of silver nanoparticles evaluated using in vitro standard assays. *Nanotoxicology* 10:1373-1384.
- He D, Garg S, Wang Z, Li L, Rong H, Ma X, Li G, An T, Waite TD. 2019. Silver sulfide nanoparticles in aqueous environments: formation, transformation and toxicity. *Environmental Science: Nano* 6:1674-1687.
- Hendrickson OD, Klochkov SG, Novikova OV, Bravova IM, Shevtsova EF, Safenkova IV, Zherdev AV, Bachurin SO, Dzantiev BB. 2016. Toxicity of nanosilver in intragastric studies: Biodistribution and metabolic effects. *Toxicology Letters* 241:184-192.
- Heylmann D, Kaina B. 2016. The γ H2AX DNA damage assay from a drop of blood. *Scientific Reports* 6:22682.
- Juarez-Moreno K, Gonzalez E, Girón-Vazquez N, Chávez-Santoscoy R, Mota-Morales J, Perez-Mozqueda L, Garcia-Garcia M, Pestryakov A, Bogdanchikova N. 2017. Comparison of cytotoxicity and genotoxicity effects of silver nanoparticles on human cervix and breast cancer cell lines. *Human & Experimental Toxicology* 36:931-948.
- Karlsson HL, Cronholm P, Gustafsson J, Möller L. 2008. Copper Oxide Nanoparticles Are Highly Toxic: A Comparison between Metal Oxide Nanoparticles and Carbon Nanotubes. *Chemical Research in Toxicology* 21:1726-1732.
- Khoury L, Zalko D, Audebert M. 2013. Validation of high-throughput genotoxicity assay screening using γ H2AX in-cell western assay on HepG2 cells. *Environmental and Molecular Mutagenesis* 54:737-746.
- Kim S, Ryu D-Y. 2013. Silver nanoparticle-induced oxidative stress, genotoxicity and apoptosis in cultured cells and animal tissues. *Journal of Applied Toxicology* 33:78-89.
- Kim YJ, Rahman MM, Lee SM, Kim JM, Park K, Kang J-H, Seo YR. 2019. Assessment of in vivo genotoxicity of citrated-coated silver nanoparticles via transcriptomic analysis of rabbit liver tissue. *International journal of nanomedicine* 14:393-405.
- Kim YS, Kim JS, Cho HS, Rha DS, Kim JM, Park JD, Choi BS, Lim R, Chang HK, Chung YH, Kwon IH, Jeong J, Han BS, Yu IJ. 2008. Twenty-Eight-Day Oral Toxicity, Genotoxicity, and Gender-Related Tissue Distribution of Silver Nanoparticles in Sprague-Dawley Rats. *Inhalation Toxicology* 20:575-583.
- Kopp B, Khoury L, Audebert M. 2019. Validation of the γ H2AX biomarker for genotoxicity assessment: a review. *Archives of Toxicology*.

- Larese FF, D'Agostin F, Crosera M, Adami G, Renzi N, Bovenzi M, Maina G. 2009. Human skin penetration of silver nanoparticles through intact and damaged skin. *Toxicology* 255:33-37.
- Li Y, Bhalli JA, Ding W, Yan J, Pearce MG, Sadiq R, Cunningham CK, Jones MY, Monroe WA, Howard PC, Zhou T, Chen T. 2014. Cytotoxicity and genotoxicity assessment of silver nanoparticles in mouse. *Nanotoxicology* 8:36-45.
- Li Y, Qin T, Ingle T, Yan J, He W, Yin J-J, Chen T. 2017. Differential genotoxicity mechanisms of silver nanoparticles and silver ions. *Archives of Toxicology* 91:509-519.
- Lips J, Kaina B. 2001. DNA double-strand breaks trigger apoptosis in p53-deficient fibroblasts. *Carcinogenesis* 22:579-585.
- Liu S, Wang C, Hou J, Wang P, Miao L, Li T. 2018. Effects of silver sulfide nanoparticles on the microbial community structure and biological activity of freshwater biofilms. *Environmental Science: Nano* 5:2899-2908.
- Loeschner K, Hadrup N, Qvortrup K, Larsen A, Gao X, Vogel U, Mortensen A, Lam HR, Larsen EH. 2011. Distribution of silver in rats following 28 days of repeated oral exposure to silver nanoparticles or silver acetate. *Particle and fibre toxicology* 8:18-18.
- Lynch I, Weiss C, Valsami-Jones E. 2014. A strategy for grouping of nanomaterials based on key physico-chemical descriptors as a basis for safer-by-design NMs. *Nano Today* 9:266-270.
- Meghan E. Samberg, Monteiro-Riviere NA. 2014. Silver Nanoparticles in Biomedical Applications. In: Nancy A. Monteiro-Riviere, Tran CL, eds. *Nanotoxicology : Progress toward Nanomedicine*. 2nd edition. Boca Raton: CRC Press, 405-421.
- Midander K, Cronholm P, Karlsson HL, Elihn K, Möller L, Leygraf C, Wallinder IO. 2009. Surface Characteristics, Copper Release, and Toxicity of Nano- and Micrometer-Sized Copper and Copper(II) Oxide Particles: A Cross-Disciplinary Study. *Small* 5:389-399.
- Mitra C, Gummadidala PM, Afshinnia K, Merrifield RC, Baalousha M, Lead JR, Chanda A. 2017. Citrate-Coated Silver Nanoparticles Growth-Independently Inhibit Aflatoxin Synthesis in *Aspergillus parasiticus*. *Environmental Science & Technology* 51:8085-8093.
- Mukherjee SG, O'Clonadh N, Casey A, Chambers G. 2012. Comparative in vitro cytotoxicity study of silver nanoparticle on two mammalian cell lines. *Toxicology in Vitro* 26:238-251.
- Müller L, Sofuni T. 2000. Appropriate levels of cytotoxicity for genotoxicity tests using mammalian cells in vitro. *Environmental and Molecular Mutagenesis* 35:202-205.
- Nelson BC, Wright CW, Ibuki Y, Moreno-Villanueva M, Karlsson HL, Hendriks G, Sims CM, Singh N, Doak SH. 2017. Emerging metrology for high-throughput nanomaterial genotoxicology. *Mutagenesis* 32:215-232.
- Nikolova T, Dvorak M, Jung F, Adam I, Krämer E, Gerhold-Ay A, Kaina B. 2014. The γ H₂AX Assay for Genotoxic and Nongenotoxic Agents: Comparison of H₂AX Phosphorylation with Cell Death Response. *Toxicological Sciences* 140:103-117.
- OECD. 1997. Test No. 471: Bacterial Reverse Mutation Test.
- Perde-Schrepler M, Florea A, Brie I, Virag P, Fischer-Fodor E, Ican A, Gurz, u E, Lisencu C, Maniu A. 2019. Size-Dependent Cytotoxicity and Genotoxicity of Silver Nanoparticles in Cochlear Cells In Vitro. *Journal of Nanomaterials* 2019:12.

- Perreault F, Melegari SP, da Costa CH, de Oliveira Franco Rossetto AL, Popovic R, Matias WG. 2012. Genotoxic effects of copper oxide nanoparticles in Neuro 2A cell cultures. *Science of The Total Environment* 441:117-124.
- Prajitha N, Athira SS, Mohanan PV. 2019. Bio-interactions and risks of engineered nanoparticles. *Environmental Research* 172:98-108.
- Reinsch BC, Levard C, Li Z, Ma R, Wise A, Gregory KB, Brown GE, Lowry GV. 2012. Sulfidation of Silver Nanoparticles Decreases *Escherichia coli* Growth Inhibition. *Environmental Science & Technology* 46:6992-7000.
- Rogakou EP, Pilch DR, Orr AH, Ivanova VS, Bonner WM. 1998. DNA Double-stranded Breaks Induce Histone H2AX Phosphorylation on Serine 139. *Journal of Biological Chemistry* 273:5858-5868.
- Roos WP, Kaina B. 2013. DNA damage-induced cell death: From specific DNA lesions to the DNA damage response and apoptosis. *Cancer Letters* 332:237-248.
- Sahu SC, Njoroge J, Bryce SM, Yourick JJ, Sprando RL. 2014a. Comparative genotoxicity of nanosilver in human liver HepG2 and colon Caco2 cells evaluated by a flow cytometric in vitro micronucleus assay. *Journal of Applied Toxicology* 34:1226-1234.
- Sahu SC, Njoroge J, Bryce SM, Zheng J, Ihrle JCJATR. 2016a. Flow cytometric evaluation of the contribution of ionic silver to genotoxic potential of nanosilver in human liver HepG2 and colon Caco2 cells. *Journal of Applied Toxicology* 36:521-531.
- Sahu SC, Roy S, Zheng J, Ihrle JCJATR. 2016b. Contribution of ionic silver to genotoxic potential of nanosilver in human liver HepG2 and colon Caco2 cells evaluated by the cytokinesis-block micronucleus assay. *Journal of Applied Toxicology* 36:532-542.
- Sahu SC, Zheng J, Graham L, Chen L, Ihrle J, Yourick JJ, Sprando RL. 2014b. Comparative cytotoxicity of nanosilver in human liver HepG2 and colon Caco2 cells in culture. *Journal of Applied Toxicology* 34:1155-1166.
- Savage DT, Hilt JZ, Dziubla TD. 2019. In Vitro Methods for Assessing Nanoparticle Toxicity. In: Zhang Q, ed. *Nanotoxicity: Methods and Protocols*. New York, NY: Springer New York, 1-29.
- Sedelnikova OA, Redon CE, Dickey JS, Nakamura AJ, Georgakilas AG, Bonner WM. 2010. Role of oxidatively induced DNA lesions in human pathogenesis. *Mutation research* 704:152-159.
- Sharma A, Gorey B, Casey A. 2019. In vitro comparative cytotoxicity study of aminated polystyrene, zinc oxide and silver nanoparticles on a cervical cancer cell line. *Drug and Chemical Toxicology* 42:9-23.
- Shi M, Kwon HS, Peng Z, Elder A, Yang H. 2012. Effects of Surface Chemistry on the Generation of Reactive Oxygen Species by Copper Nanoparticles. *ACS Nano* 6:2157-2164.
- Sung JH, Ji JH, Park JD, Yoon JU, Kim DS, Jeon KS, Song MY, Jeong J, Han BS, Han JH, Chung YH, Chang HK, Lee JH, Cho MH, Kelman BJ, Yu IJ. 2008. Subchronic Inhalation Toxicity of Silver Nanoparticles. *Toxicological Sciences* 108:452-461.
- Syafiuddin A, Salmiati, Salim MR, Beng Hong Kueh A, Hadibarata T, Nur H. 2017. A Review of Silver Nanoparticles: Research Trends, Global Consumption, Synthesis, Properties, and Future Challenges. *Journal of the Chinese Chemical Society* 64:732-756.

- Thomas TA. 2014. Nanotechnology in Consumer Products : Addressing Potential Health and Safety Implications for Consumers. In: Nancy A. Monteiro-Riviere, Tran CL, eds. *Nanotoxicology : Progress toward Nanomedicine*. 2nd edition. Boca Raton: CRC Press, 97-112.
- van der Zande M, Vandebriel RJ, Van Doren E, Kramer E, Herrera Rivera Z, Serrano-Rojero CS, Gremmer ER, Mast J, Peters RJB, Hollman PCH, Hendriksen PJM, Marvin HJP, Peijnenburg AACM, Bouwmeester H. 2012. Distribution, Elimination, and Toxicity of Silver Nanoparticles and Silver Ions in Rats after 28-Day Oral Exposure. *ACS Nano* 6:7427-7442.
- Veronesi G, Deniaud A, Gallon T, Jouneau PH, Villanova J, Delange P, Carrière M, Kieffer I, Charbonnier P, Mintz E, Michaud-Soret I. 2016. Visualization, quantification and coordination of Ag⁺ ions released from silver nanoparticles in hepatocytes. *Nanoscale* 8:17012-17021.
- Völker C, Kämpken I, Boedicker C, Oehlmann J, Oetken M. 2015. Toxicity of silver nanoparticles and ionic silver: Comparison of adverse effects and potential toxicity mechanisms in the freshwater clam *Sphaerium corneum*. *Nanotoxicology* 9:677-685.
- Vrček IV, Žuntar I, Petlevski R, Pavičić I, Dutour Sikirić M, Ćurlin M, Goessler W. 2016. Comparison of in vitro toxicity of silver ions and silver nanoparticles on human hepatoma cells. *Environmental Toxicology* 31:679-692.
- Walker M, Parsons D. 2014. The biological fate of silver ions following the use of silver-containing wound care products – a review. *International Wound Journal* 11:496-504.
- Wang P, Lombi E, Sun S, Scheckel KG, Malysheva A, McKenna BA, Menzies NW, Zhao F-J, Kopittke PM. 2017. Characterizing the uptake, accumulation and toxicity of silver sulfide nanoparticles in plants. *Environmental Science: Nano* 4:448-460.
- Wen H, Dan M, Yang Y, Lyu J, Shao A, Cheng X, Chen L, Xu L. 2017. Acute toxicity and genotoxicity of silver nanoparticle in rats. *PloS one* 12:e0185554-e0185554.
- Xue Y, Zhang T, Zhang B, Gong F, Huang Y, Tang M. 2016. Cytotoxicity and apoptosis induced by silver nanoparticles in human liver HepG2 cells in different dispersion media. *Journal of Applied Toxicology* 36:352-360.
- Yin Y, Yu S, Shen M, Liu J, Jiang G. 2015. Fate and Transport of Silver Nanoparticles in the Environment. In: Liu J, Jiang G, eds. *Silver Nanoparticles in the Environment*. Berlin, Heidelberg: Springer Berlin Heidelberg, 73-108.
- Zare T, Fardid R, Naderi S. 2019. Synergetic Effect of Silver Nanoparticles and UVC Irradiation on H2AX Gene Expression in TK6 Cells. *Cell journal* 21:204-209.
- Zhang X-F, Liu Z-G, Shen W, Gurunathan S. 2016. Silver Nanoparticles: Synthesis, Characterization, Properties, Applications, and Therapeutic Approaches. *International journal of molecular sciences* 17:1534.
- Zhao X, Takabayashi F, Ibuki Y. 2016. Coexposure to silver nanoparticles and ultraviolet A synergistically enhances the phosphorylation of histone H2AX. *Journal of Photochemistry and Photobiology B: Biology* 162:213-222.
- Zhu B, Li Y, Lin Z, Zhao M, Xu T, Wang C, Deng N. 2016. Silver Nanoparticles Induce HePG-2 Cells Apoptosis Through ROS-Mediated Signaling Pathways. *Nanoscale Research Letters* 11:198.

SUPPLEMENTARY MATERIAL

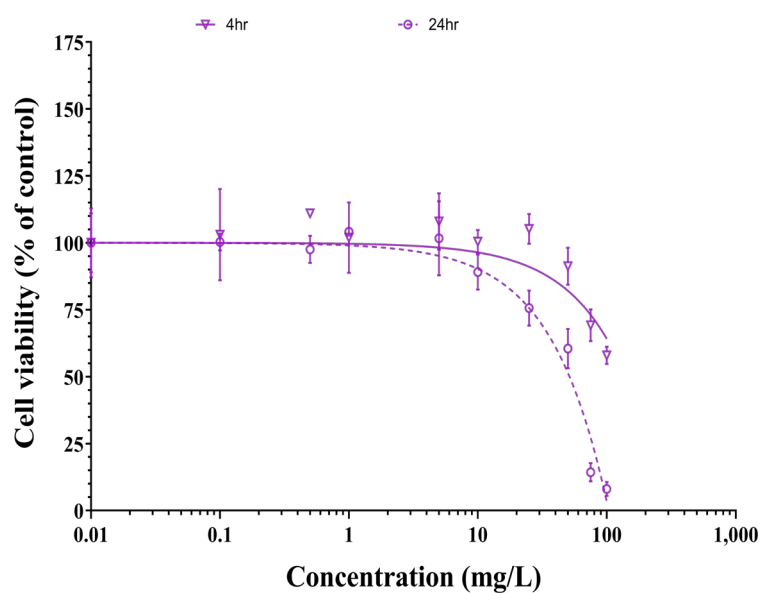


Figure S1: Cell viability of HepG2 cells after 4 and 24 hr exposure to a concentration range of (PVP) CuO NPs, measured using an ATPlite viability assay. Viability is given as a percentage of the control (mean \pm SD; n=3).

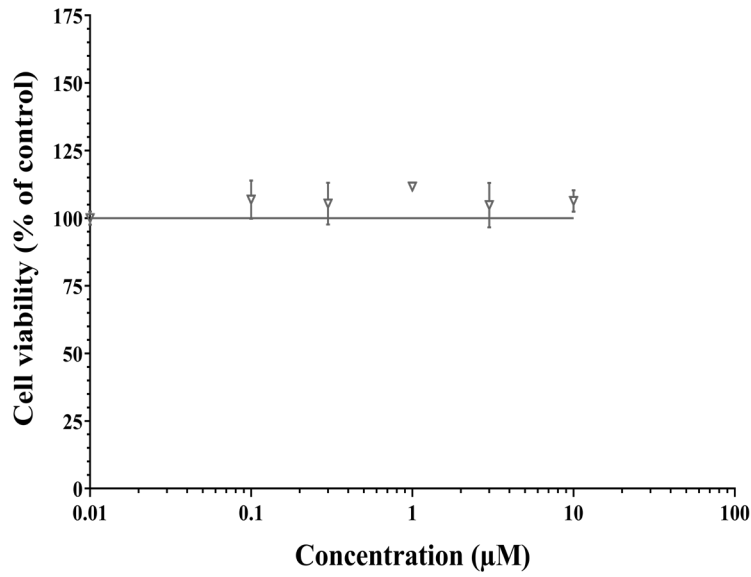
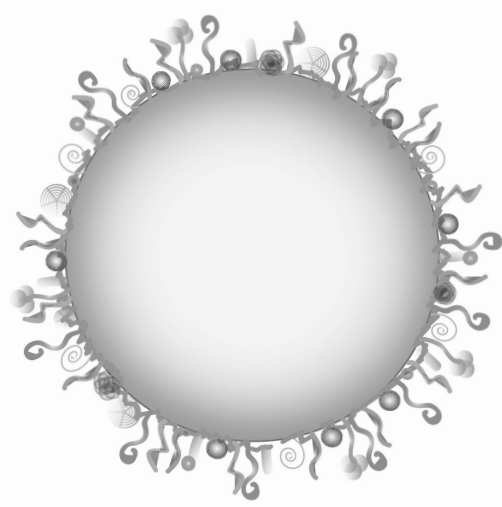
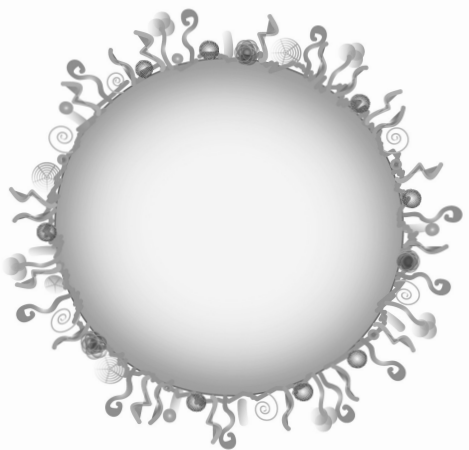
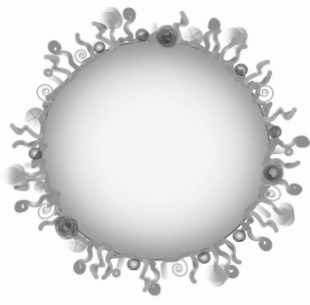
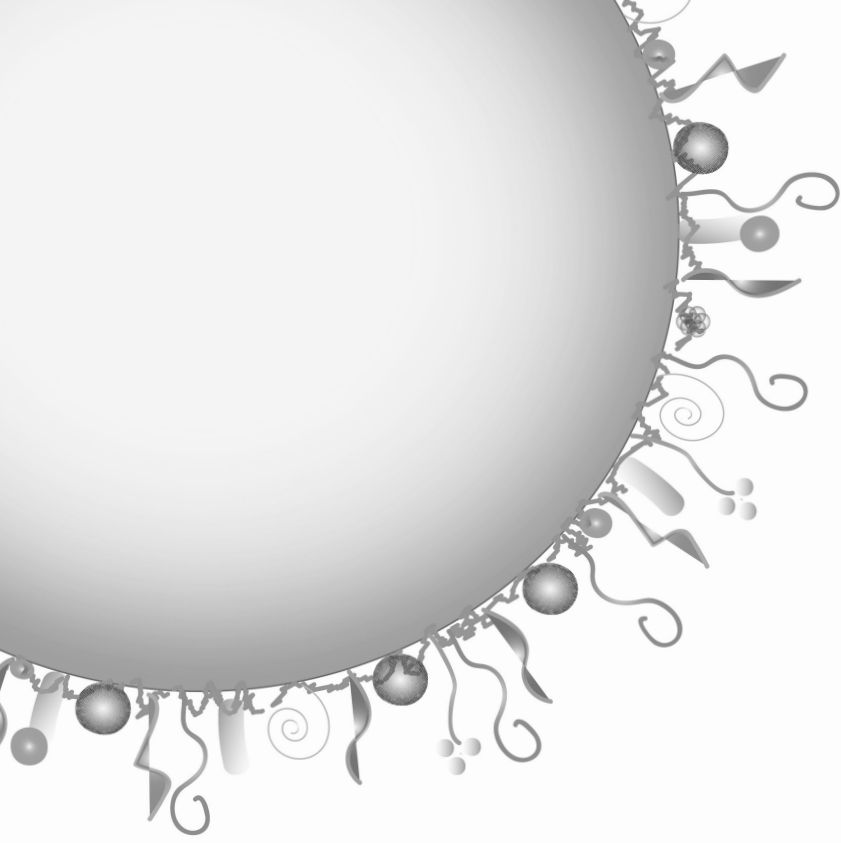
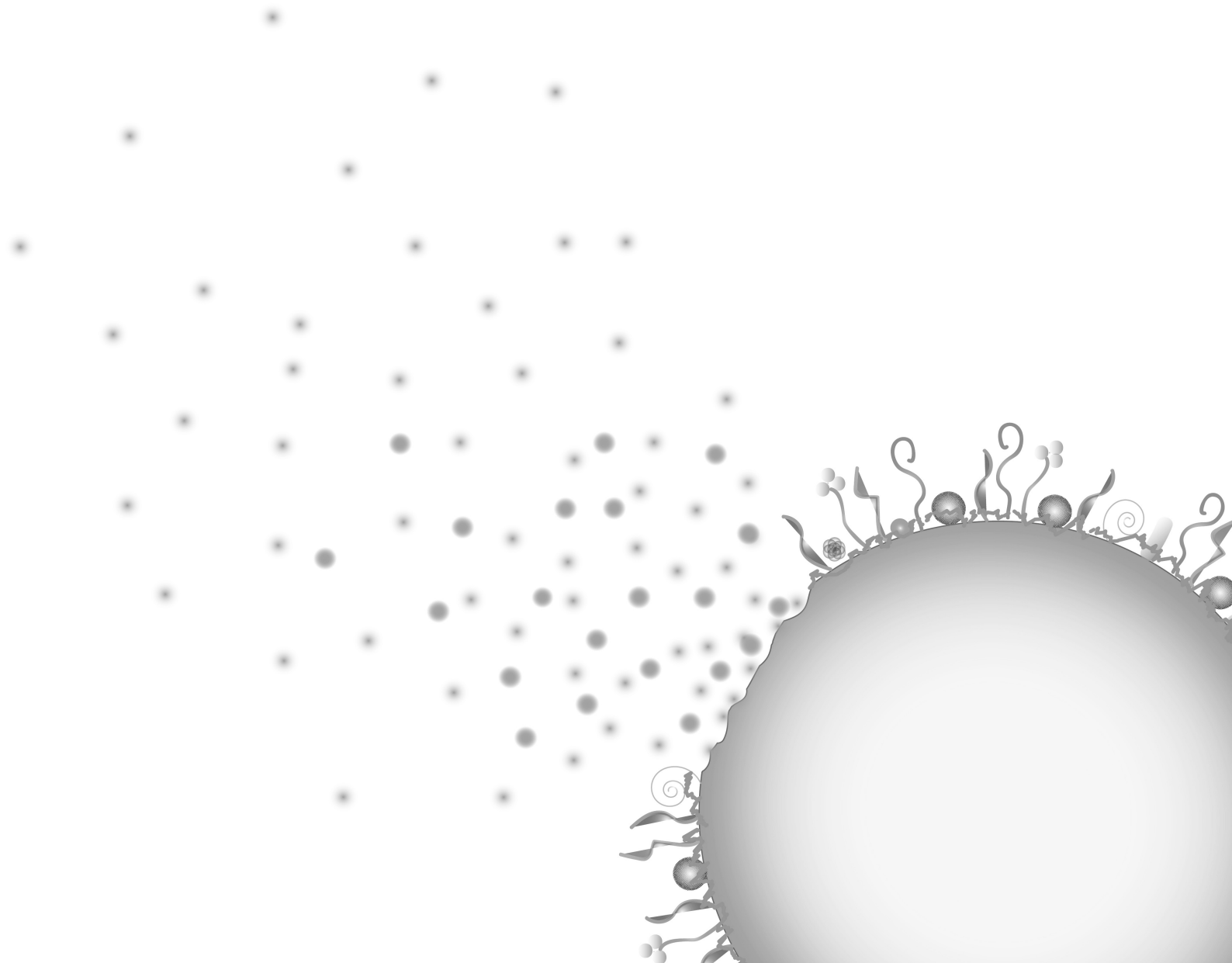


Figure S2: Cell viability of HepG2 cells after 24 hr exposure to a concentration range of BaP, measured using a WST-1 viability assay. Viability is given as a percentage of the control (mean \pm SD; n=3).



6

General discussion, future perspectives and overall conclusions





GENERAL DISCUSSION

The increasing use of nanoparticles (NPs) in a wide range of applications results in an increased likelihood of human exposure to NPs (Sierra *et al.* 2016). For more than a decade, concerns have been raised about their hazards and their potential to induce adverse health effects in humans (Riediker *et al.* 2019; Hussain *et al.* 2015; Oberdörster *et al.* 2005a). This has led to the emerging of the field of nanotoxicology as a sub-discipline at the interface of toxicology and nanomaterial science (Shvedova *et al.* 2016; Krug and Wick 2011; Oberdörster *et al.* 2005b). Humans can be exposed to NPs via different exposure routes including dermal, inhalation or oral routes (Fröhlich and Roblegg 2016; Warheit and Sayes 2015; Schleh *et al.* 2012) where the latter represents the exposure route that was considered in the present thesis.

At the present state-of-the-art, the safety assessment of NPs relies heavily on animal *in vivo* studies (Hardy *et al.* 2018). Considering the great diversity in the types of NPs in terms of their intrinsic properties and how these can be modified by external factors, the number of laboratory animals required to evaluate the potential toxicity of all these types of NPs would be unacceptably large (Burden *et al.* 2017; Kroll *et al.* 2009). Therefore, alternative testing strategies that are scientifically solid, but also cost-, time- and animal friendly, need to be developed and optimised. The present thesis aimed to investigate the potential of different *in vitro* methods combined with advanced analytical techniques as a screening strategy to study the toxicokinetics and toxicodynamics of NPs.

Effect of matrix conditions on NPs properties

Upon ingestion, NPs come in contact with biological matrices like gastrointestinal (GI) fluids that change substantially upon passing through the GI tract. These dynamic luminal conditions may affect the physicochemical properties of the NPs (Lynch *et al.* 2014). How and to which extent the biological matrices affect the NPs characteristics depends on the physicochemical properties of NPs themselves. The stability of the NPs and the composition of the protein corona that is formed on the surface of the NPs are affected by the composition of the biological matrix in which the NPs are suspended (Sutton *et al.* 2017; Ritz *et al.* 2015; Warheit and Sayes 2015; Arts *et al.* 2014; Hühn *et al.* 2013; Fröhlich and Roblegg 2012). The

corona influences the cellular interactions of the NPs (with, for instance, the intestinal epithelium) affecting their potential cytotoxicity and cellular uptake and transport (Ritz *et al.* 2015; Kim *et al.* 2014; Walczyk *et al.* 2010a; Lynch *et al.* 2009).

Therefore, in **chapter 2** of this thesis, the effects of NPs size and surface chemistry on the protein corona formation were investigated. In addition, the cellular interactions (association, uptake and transport) of these NPs-corona complexes were characterised. Four fluorescently labelled and negatively charged PSNPs were used with different surface chemistries: 50 nm sulfone and carboxyl coated PSNPs and 200 nm carboxyl coated PSNPs. High-content (HC) imaging was used to study the Caco-2 cellular uptake/associations of the PSNPs on a single-cell level while the transport of these PSNPs was measured via measuring their fluorescence intensity.

The results demonstrated that the cellular uptake/association and transport of sulfone functionalized PSNPs were significantly higher compared to that of the carboxyl functionalized PSNPs. No significant impact of the size nor the charge of the NPs on the cellular uptake/association was noticed, indicating that the sulfone surface coating affects these characteristics via other intrinsic properties. The composition of the protein corona of all the PSNPs was quantitatively determined using label-free liquid chromatography mass spectrometry (LC-MS/MS) after incubation in cell culture medium for periods equivalent to the cellular exposure. Subtle differences in the protein composition were detected between the sulfone and carboxyl coated PSNPs. Next to measuring a pronounced enrichment of apolipoproteins, binding proteins and acute phase proteins, a less pronounced enrichment of complement factors was detected in the sulfone coated NPs as compared to the carboxyl coated NPs. Among the proteins detected in the NPs coronas, the alpha-1B-glycoprotein (A1BG) protein was the most abundant protein present on all types of NPs, as also shown by others (Tenzer *et al.* 2013; Lundqvist *et al.* 2008; Cedervall *et al.* 2007). Yet, the function of this protein is currently unknown.

Comparing the protein corona compositions among the PSNPs studied here, it was found that alpha-2-macroglobulin (A2M) proteins were significantly less absorbed on the sulfone coated PSNPs than on the carboxyl coated PSNPs of the same size. Also, the AFP, APOH and FETUB and LOC781674 protein levels tended to be lower on the sulfone coated PSNPs

than on the carboxyl coated NPs. Previously, it has been described that APOA2 and APOH interfere with the cellular uptake of NPs (Ritz *et al.* 2015). These results suggest that the cellular uptake/association of NPs is highly dependent on the surface chemistry of NPs, that governs the composition of the protein corona. The results also indicate that the combination of surface chemistry and protein corona appears to be more important for the biological effect of the NPs than their size.

Combining *in vitro* models to emulate human physiological processes

Upon oral ingestion, NPs pass through mouth, stomach and intestinal compartments of the GI tract, each with a specific pH and biochemical composition before reaching the intestinal epithelium. These dynamic and harsh conditions can increase the tendency of the NPs to agglomerate or dissolve and accordingly affect their bioavailability and toxicological properties (Lichtenstein *et al.* 2017; Sieg *et al.* 2017; McCracken *et al.* 2015; Böhmert *et al.* 2014; Murdock *et al.* 2008). Combining an *in vitro* digestion model, to simulate the GI tract conditions, with a cellular *in vitro* model of the intestinal barrier can provide more realistic insights in the fate of the NPs upon oral ingestion. Accordingly, in **chapter 3**, an *in vitro* model was used to simulate the physiological conditions within the human GI tract. This model was used to study the impact of these physiological conditions on the characteristics of the AgNPs. Subsequently, the transport of these digested NPs and their respective pristine NPs across an intestinal co-culture *in vitro* model of differentiated Caco-2/HT29-MTX cells simulating the intestinal barrier was assessed.

The co-culture epithelial cell model was exposed for 24 hr to pristine and *in vitro* digested (IVD) negatively charged 50 nm lipoic acid (LA) and citrate (Cit) coated AgNPs. The AgNPs size distribution, dissolution and particle concentration (mass- and number-based) were characterized in the apical, cell and basolateral compartments of the monolayer cultures, by using inductively coupled plasma mass spectrometry (ICP-MS) and single particle (sp) ICP-MS. It is of importance to highlight that the size detection limit of spICP-MS was 20 nm and accordingly any particles with sizes below this limit were included in the ionic silver (Ag^+) fraction. During *in vitro* digestion, a significant fraction of the AgNPs dissolved. The (LA) AgNPs dissolved to a significant higher extent (86 - 92%) during the digestion process than the (Cit) AgNPs (48 – 70%). Cellular exposure to increasing concentrations of pristine or IVD AgNPs

resulted in a concentration dependent increase of total Ag and AgNPs contents in the cellular fractions. The cellular concentrations were significantly lower following exposure to IVD AgNPs compared to the pristine AgNPs. Transport across the monolayer of intestinal cells either as total Ag or as AgNPs was limited (< 0.1%) following exposure to pristine and IVD AgNPs.

Interestingly, the presence of *de novo* formed AgNPs was observed during the *in vitro* digestion and in the cellular fractions upon exposure to both AgNPs and AgNO₃. The results clearly show that it is important to incorporate the intestinal digestive conditions into a model to assess the potential bioavailability of NPs. Based on the results obtained, it was concluded that systemic availability of NPs following oral ingestion is likely to occur albeit to a limited extent, which was in line with observations from sub-chronic rodent studies (van der Zande *et al.* 2012; Loeschner *et al.* 2011b).

It is very likely that suspending the AgNPs in protein-rich media or in the protein- and enzyme-rich GI fluids will result in the formation of a protein corona that might affect the cellular interactions of these AgNPs (Berardi and Baldelli Bombelli 2019; Ding *et al.* 2018). Although the protein corona of the AgNPs was not investigated in **chapter 3**, it is highly possible that the surface chemistry of the AgNPs could influence the composition of their protein corona as shown in **chapter 2** and consequently their uptake. Walczak *et al.* reported that pristine PSNPs of different surface chemistries were surrounded by protein coronas of different compositions while upon *in vitro* digestion lower protein amounts and different proteins were present in the protein coronas (Walczak *et al.* 2015). Additionally, following the changes in the protein corona formed, differences in the cellular uptake of the NPs were reported (Ding *et al.* 2018; Walczyk *et al.* 2010b). In the studies of Peng *et al.*, using poly(3-hydroxybutyrate-co-3-hydroxyhexanoate)-based cationic NPs (CNPs), the presence of pancreatin as part of the protein corona formed during digestion decreased Caco-2 cellular uptake of the CNPs. The authors concluded that the decreased cellular uptake could be ascribed to the presence of pancreatin in the protein corona formed during digestion (Peng *et al.* 2019). Given that pancreatin was also present in the digestive incubations of the AgNPs in the present thesis, these findings might also explain the decrease in the cellular uptake of IVD AgNPs compared to the pristine counterparts reported in **chapter 3**. Consequently, the effect

of the surface chemistry could be influencing the cellular uptake directly or in an indirect way via changing the protein corona around these AgNPs.

Toxicological potential of systemically available NPs

Since the results from **chapter 3** indicate that NPs can become systemically available after ingestion, other organs can be expected to be exposed as well. Therefore, in further studies presented in this thesis, three other *in vitro* bioassays were used in order to study the effects of the NPs on three other potential targets. In **chapter 4**, the potential of the AgNPs to pass the placental barrier was studied using the *in vitro* BeWo b30 placental transport model. This model was combined with the mouse embryonic stem cell test (EST) to obtain further insight in possible hazards for the developing foetus. While in **chapter 5** a liver *in vitro* model was evaluated to address its suitability to assess NPs related effects focusing on potential DNA damaging effects.

In **chapter 4**, the same AgNPs were used as in **chapter 3**, as well as the same ICP-MS and spICP-MS analytical techniques to characterize the presence of particulate or dissolved Ag in the samples. Given that the observations reported in **chapter 2**, indicated that the surface charge might influence transport of NPs, positively charged 50 nm branched polyethylenimine (BPEI) AgNPs were also included in the study as well as silver sulphide (Ag₂S) NPs representing the so-called “aged” AgNPs that can be (*de novo*) formed systemically and in the environment (He *et al.* 2019; Tripathi *et al.* 2017; Wang *et al.* 2017). Upon the exposure of the BeWo cell layer to the different types of AgNPs, a time-dependent increase of total Ag in the cellular compartments was observed. Similar to the intestinal cellular exposure, the surface chemistry of the AgNPs significantly affected the concentration of total Ag and AgNPs in the BeWo cellular compartment.

Comparing the spICP-MS results (*i.e.* Ag in its particulate form) with the total Ag measurements, it can be concluded that the cellular uptake of Ag was mainly as ionic Ag. Only limited transport of ionic and/or particulate Ag across the BeWo cell layers was observed which was dependent on the surface chemistry of the AgNPs. The surface chemistry of the AgNPs could also indirectly affect their cellular uptake and transport via influencing the protein corona composition which was reported in **chapter 2** using PSNPs. The Ag transport was mainly as particulate rather than ionic Ag and with higher AgNPs percentages in the

basolateral compartment than in the cellular compartment. The levels of AgNPs transported (1 – 8 %, as total Ag) were in line with levels that were reported to reach the foetus (1 – 8 %, as total Ag) upon injecting pregnant rats with AgNPs (Fennell *et al.* 2017).

The transported amount of Ag via the *in vitro* placental barrier (6 – 7 %) upon 24 hr exposure to (LA) and (Cit) AgNPs is significantly higher compared to the amount transported via the *in vitro* intestinal barrier (< 0.1 %) as described in **chapter 3**. This difference highlights the differences between different *in vitro* models of physiological barriers, in terms of barrier properties to NPs passage (Braakhuis *et al.* 2015; Schwab *et al.* 2015; van Thriel 2015).

The potential *in vitro* developmental toxicity of the AgNPs was subsequently investigated using the EST. In this assay, the potential to inhibit the differentiation of mouse embryonic stem cells (mESCs) into beating cardiomyocytes is used as an endpoint. Based on this study, the AgNPs did not induce *in vitro* developmental toxicity as the observed inhibition of differentiation of the mESCs were only detected at cytotoxic concentrations. The cytotoxicity inducing concentrations (*i.e.* IC₅₀ values) were higher than the concentrations that would be considered realistic based on the transport data obtained from the BeWo b30 transport experiments. Considering the oral route as one of the main exposure routes of the AgNPs, it is important to take into account also their very low transport across the intestinal barrier *in vitro* (**chapter 3**) which will consequently lower the concentrations of the AgNPs that might reach the foetus.

Several *in vivo* studies have shown that AgNPs (with different surface chemistries) are systemically available upon ingestion (Walker and Parsons 2014; Larese *et al.* 2009), subsequently reaching several organs including the liver (van der Zande *et al.* 2012; Loeschner *et al.* 2011a). The liver has been considered one of the most affected organs following AgNPs exposure (Wen *et al.* 2017; Hendrickson *et al.* 2016; Kim *et al.* 2008; Sung *et al.* 2008), resulting in various forms of toxicity, including genotoxicity (Kim *et al.* 2019).

Among several *in vitro* methods to measure the genotoxic potentials of substances, the γ -H₂AX assay has proven to be a sensitive and powerful alternative method to detect DNA-double strand breaks (DSBs) with a low false-positive rate (Heylmann and Kaina 2016; Nikolova *et al.* 2014; Khoury *et al.* 2013). Therefore, in **chapter 5**, the potential of the In Cell-Western (ICW)- γ -H₂AX assay was evaluated as an alternative *in vitro* assay to assess the

potential of AgNPs to induce phosphorylation of H₂AX in HepG2 liver cells following induction of DNA-DSBs. The pristine AgNPs with different surface chemistries and aged AgNPs that were used in this chapter were similar to ones used in the previous chapters of this thesis. It was found that, if AgNPs induced phosphorylation of γ -H₂AX in HepG2 cells, cytotoxic responses were also observed at the same concentrations. Based on the used setup in these experiments, apoptotic mediated false-positive responses cannot be excluded. Therefore, additional or modified endpoints need to be incorporated into the ICW- γ -H₂AX assay to use this assay as an *in vitro* test to predict the genotoxic potential of NPs (Nikolova *et al.* 2014).

Observation on aged and pristine AgNPs

It is of interest to note that the aged AgNPs (Ag₂S NPs) studied here, showed different biological behaviour compared to the pristine AgNPs (Liu *et al.* 2018; Yin *et al.* 2015). The dissolution and charge of the Ag₂S NPs were comparable to those of the pristine (LA) and (Cit) AgNPs. But the toxicity and transport of these aged NPs were significantly lower in different *in vitro* models used within this thesis.

FUTURE PERSPECTIVES

In the present thesis, we studied the impact of different physicochemical properties (*e.g.* size, surface charge, surface chemistry including corona formation and chemical composition) of the NPs on their biological interactions. This was investigated using combinations of different *in vitro* models (*e.g.* intestinal, placental, embryonic and liver) with support of advanced analytical techniques (*e.g.* single particle ICP-MS, LC-MS/MS and high content and confocal imaging). In this section, as emerging from the results of the present thesis, some other important aspects for future research of human safety assessment of NPs are discussed.

Advances in *in vitro* nanotoxicology research

One of the main aims of utilizing *in vitro* assays in toxicological safety assessments is to reduce the number of laboratory animals. It is promising to see that the use of such alternative methods is receiving much attention and that they are increasingly recommended as screening methods preceding commencing *in vivo* testing (EFSA Scientific Committee *et al.*

2018; Nel and Malloy 2017). For the continuity and progress of this approach, more advanced and complex *in vitro* models will be needed. These new models are bringing more realistic and physiologically relevant systems than the currently used 2D/monolayers models and include for example models that incorporate the gut-microbiome and organ on chip technologies which will be described briefly in this section.

Gut-microbiome

The gut-microbiome is a complex and dynamic system including a large number of microbial species and metabolic functions. The effects of the gut-microbiome on human health and disease and the effects of xenobiotics on the gut microbiota have gained increased attention in the last years (Behr *et al.* 2018; Waseem *et al.* 2018; Shvedova *et al.* 2016). The contribution of the gut-microbiome to toxicity and health is only beginning to be revealed (Kundu *et al.* 2017).

Studies on the interactions between the gut-microbiome and NPs and the impact of NPs on the metabolic capacity of the gut microbiome are limited (Bouwmeester *et al.* 2018; Fröhlich and Fröhlich 2016). The early stage results point toward varying effects of different NPs on the microbial community; for example, disturbance in the bacterial evenness in the colon of mice was detected upon 28 days ingestion of pristine AgNPs while no effects were detected upon ingestion the aged Ag₂S NPs (van den Brule *et al.* 2016). Also, it was found that upon 21 days oral exposure of rats to chitosan NPs loaded with copper sulphate, the cecal microbiota composition was affected and the production of the energy source butyrate was increased (Han *et al.* 2010).

Currently, the studies of NPs –gut-microbiome interactions are confronted with several challenges (Fadeel 2019; Bouwmeester *et al.* 2018; Hardy *et al.* 2018) including, but not limited to:

- 1) The complexity and dynamic composition of the gut-microbiome in addition to the effects of individual variations (*e.g.* lifestyle, gender, nutrition and physiology).
- 2) Most of the reported studies used rodent models which have a different microbiome than humans.
- 3) The bias in sampling method and location of the microbiota within the GI tract have a significant impact on the NPs-gut-microbiome interactions and their interpretation. For

example, the microbiota in the large intestine, where most of the samplings take place, is more complex than the microbiota in the small intestine.

Considering the few studies on possible NPs-gut-microbiome interactions and their limitations, more studies and developments are still required to assist in better understanding of these interactions.

Organ-on-chip technology

One of the new approaches in developing alternative *in vitro* methods are the organ-on-chip technologies, where biochemical, metabolic, genetic and functional characteristics of human organs are simulated using cell and tissue cultures in controlled microenvironments (Bhatia and Ingber 2014). The advances in the microfluidics and miniaturization fields are of importance in developing these technologies. Microfluidics provides a significant advantage to overcome the sedimentation issues that are sometimes observed with some high density NPs by incorporating fluid flow and mechanical forces to keep the NPs suspended which in return enhances the relevance of the *in vitro* testing to the *in vivo* situation (Valencia *et al.* 2012; Ziótkowska *et al.* 2011). For example, utilizing microfluidics in organ-on-chip technologies was successful in mimicking the physiological expansion–contraction motion of lungs due to breathing. Using this model, the lung epithelial and endothelial uptake and transport of SiO₂ NPs were enhanced which accentuated the toxic and inflammatory responses of the lung to SiO₂ NPs that were not detectable in the static models (Huh *et al.* 2010).

Furthermore, several single-organ-on-chip models have been developed for lung (Benam *et al.* 2016), liver (Knowlton and Tasoglu 2016; Ma *et al.* 2016), gut (Kulthong *et al.* 2018; Shah *et al.* 2016) *etc.*, in addition to multi-organ-on-chip-models where several organs are connected to each other on a single chip (Materne *et al.* 2015; Huh *et al.* 2013). The utilization of these models as alternative testing strategies to assess the hazards of NPs would provide a potential for real-time and high-throughput analysis and perhaps even long-term exposure, which together would provide the possibilities needed for adequate hazard assessment of NPs exposure.

Framework for hazard assessment of NPs

An adverse outcome pathway (AOP)

An AOP is a valuable framework where the molecular initiating events resulting from exposure to a substance are bridged with the associated adverse outcome of this substance (Ma *et al.* 2018). AOP is defined as “*a conceptual construct that portrays existing knowledge concerning the linkage between a direct molecular initiating event (MIE) and an adverse outcome (AO)*”, thereby capturing the sequential chain of causally-linked Key Events (KEs) at different levels of biological organisation (Brockmeier *et al.* 2017). Several attempts have been described in the literature to develop AOPs for different NPs. For example, applying the AOP framework to explore the mechanistic reproductive toxicity of AgNPs in zebrafish and their impact on human health (Ma *et al.* 2018). The AOP developed provided a framework for predictive linkage between the generation and accumulation of ROS (as MIE) and the induction of oxidative stress in the gonad tissue (as KE) upon five-weeks exposure of zebrafish to AgNPs.

Developing an AOP for NPs is still very challenging, considering the wide diversity of combinations of physicochemical properties of the NPs, the lack of proper *in situ* characterization of the NPs in many studies and varying exposure scenarios (Gerloff *et al.* 2017).

Omics technologies

Multi-omics-based approaches (*e.g.* genomics, transcriptomics and proteomics) combined with big data can be used to support the hazard identification and characterization of NPs and to develop biomarkers of exposure or effects (Paunovska *et al.* 2019; Fadeel *et al.* 2018). Omics technologies are defined as high content datasets of genes, proteins or metabolites which enable the assessment of thousands of genes and their products in a single sample. The capabilities of these techniques make them very promising to uncover the mechanisms behind cellular responses to NPs which will result in a significant leap in our understanding of the safety and biological interactions of the NPs. Additionally, integrating the omics datasets in the AOP approach is of added value in improving the understanding of toxicological effects of NPs (Brockmeier *et al.* 2017). The omics datasets may improve the description of the MIE and the selection of biomarkers of relevance in developing an AOP to assess the adverse or beneficial effects of NPs. For example, in a study on the reproductive

toxicity of AgNPs in the nematode *Caenorhabditis elegans* (*C. elegans*), transcriptomics analysis was used to identify oxidative stress as one of the MIEs or early KEs in the AOP of reproductive toxicity of AgNPs in *C. elegans* (Jeong *et al.* 2018).

Detection and characterization of NPs:

High quality toxicological studies with NPs require robust characterisation and detection methods of the NPs. Only then, the results of these studies can be used in the safety assessments of these NPs (Hammad and Bolt 2014). This approach was followed in the present thesis where state-of-the-art analytical techniques have been used to detect and characterise the NPs before and after testing them in different *in vitro* assays. In this section, several analytical challenges in characterization and quantification of NPs, required for their hazard assessment, are highlighted.

NPs characterization in complex matrices

Characterization of pristine NPs in simple and clean matrices is currently achievable using different analytical techniques with high sensitivity and accuracy. But the NPs in real life are present in very complex matrices such as food, biological fluids and tissues which makes it very difficult to characterize the NPs in such matrices. For example, in this thesis, dynamic light scattering (DLS) was not capable to provide reliable and accurate size measurement of the AgNPs suspended in the mixture of digestive solutions due to the signal disturbance by the proteins and salts present. By further diluting these suspensions of AgNPs and introducing gentle clean-up steps (*e.g.* centrifugation) to reduce the matrix effect and using the sensitive spICP-MS analysis, the characterization and quantification of AgNPs were possible. It should be considered however, to what extent these clean-up steps may affect the AgNPs characteristics.

Another point to consider is that engineered NPs (ENPs), NPs manufactured intentionally by humans, can be formed of elements that are naturally present in the environment (*e.g.* TiO₂, SiO₂ and CuO). The capability of analytical techniques to distinguish between the NPs of natural or engineered origin is limited. To tackle these challenges, several attempts are being made to develop improved techniques such as ICP-time-of-flight mass spectrometry (ICP-TOFMS) operated in single-particle mode assisted with machine learning.

This machine learning plays an important role in distinguishing and quantifying the naturally existing NPs and ENPs based on their unique elemental fingerprints (Mehrabi *et al.* 2019; Yang *et al.* 2019; Praetorius *et al.* 2017). Additionally, differentiation between the NPs and their ionic forms is of importance for hazard assessment of NPs. In this thesis, using the spICP-MS, a distinction could be made between particulate and ionic Ag. But it was not possible to identify and distinct whether these Ag particulates were AgNPs or Ag complexes (*e.g.* AgCl or Ag₂S) formed from ionic Ag. Theoretically that would be possible with ICP-TOFMS.

NPs can contain more than one metal forming multi-element NPs where the core of the NPs is made of a metal different from the metal forming the shell surround this core. These multi-element NPs are introducing new analytical challenges and opportunities to the current methods of measurement and characterization (Mehrabi *et al.* 2019). The spICP-TOFMS, mentioned early, is also proposed to be an analytical solution to measure the multi-element NPs. For example, using this technique, it was possible to estimate the size of Au-core/Ag-shell NPs, BiVO₄, (Bi_{0.5}Na_{0.5})TiO₃ and steel NPs (which contains Fe, Cr, Ni and Mo) (Naasz *et al.* 2018). Still, this technique is in the early stages and requires further development owing to its limitation of detecting only the NPs formed of two metals in addition to its lower accuracy of measuring steel NPs (Mehrabi *et al.* 2019; Naasz *et al.* 2018).

Protein corona

Several studies, including those in the present thesis, indicated the contribution of the protein corona to the biological effects of NPs (Cai *et al.* 2020; Afantitis *et al.* 2018; Hu *et al.* 2016; Vilanova *et al.* 2016; Docter *et al.* 2015; Hussain *et al.* 2015; Alkilany *et al.* 2013). For example, the amount of cellularly internalized NPs and the mechanism of their internalization differ with different protein corona composition (Francia *et al.* 2019). The protein corona is very dynamic where the amount and arrangements of proteins are constantly changing based on the physicochemical and biological interactions with the matrix in which the NPs are embedded.

There is no single ideal analytical technique to analyse the interaction of proteins with NPs and their corona. For this, complementary methods are required to compensate for the drawbacks of individual methods. For example, 1D and/or 2D polyacrylamide gel electrophoresis is an easy approach to visualize and qualitatively compare corona protein

patterns but it is low-throughput and lacks the possibility to quantify the corona constituents. Some of these limitations are overcome by combining the label-free LC-MS/MS analysis with these approaches (Docter *et al.* 2015). All these techniques for corona characterization are facing technical challenges such as losing part of the corona of low affinity proteins following the multiple washing and purification steps. The proteins in the corona are dynamic and change following changes in the surrounding medium, this results in identifying the proteins present at a certain moment with the proteins actually identified being also limited to the standard proteins used in the identification method (Nguyen and Lee 2017; Barrán-Berdón *et al.* 2013). All these aspects make it challenging to integrate the dynamic reactions of the protein corona in the risk assessment of NPs.

***In silico* computational models in nanotoxicology**

In silico methods that use computational models to generate data without a need for animal experiments can be used as a powerful approach in predictive nanotoxicology. The computational modelling in the nanotoxicology field is still in the early stages and in need of improved modelling tools, useful datasets, standardized methodologies and user-friendly interfaces. The endless diversity of variations of NPs makes it difficult to predict and characterize the hazard of these NPs. Currently, computational modelling is a useful approach to support the *in vitro* testing for example by identifying any potential hazardous property in the early development stage of the NPs in the process of safe-by-design NPs.

These approaches are facing several challenges such as the availability of sufficient and robust datasets of well-characterized NPs. Also, the development of rigorous decision-making procedures to derive reliable conclusion over the safety of NPs needs further progress. Additional parameters which are foreseen to improve the predictivity of the computational models include NPs corona formation and composition and the influence of the corona on the biological interaction and toxicokinetics of the NPs (*e.g.* biodistribution, bioprocessing and bioclearance). Computational models are used in several approaches, such as the use of dosimetry models to improve the interpretation of currently used *in vitro* models (Böhmert *et al.* 2018; Hinderliter *et al.* 2010). Computational models are also used to describe quantitative structure–activity relationships for NPs (QSARs) and grouping (or read across) approaches

(Villaverde *et al.* 2018). In this section, these models are described as promising examples of *in silico* models in nanotoxicology.

NPs dosimetry

In *in vitro* studies with NPs, the dosimetry is an important parameter affecting the interpretation of the toxicological effects of NPs. Cellular exposure to NPs is generally performed by exposure to NPs dispersed in a cell culture medium. NPs concentrations in the cell culture medium, however, are not necessarily reflecting the dosage of NPs that induces an effect or response in the cells upon interaction (delivered dose) (Chen *et al.* 2018). Diffusion, sedimentation and dissolution properties of NPs and thus the amount of NPs suspended in the cell culture medium that reaches the cells are affected by several NPs characteristics *e.g.* the size, density and agglomeration status of the NPs. NPs diffusion and sedimentation are also influenced by the density and viscosity of the medium (Thomas *et al.* 2018). Accordingly, the potency of certain NPs to induce adverse effects is misinterpreted. For this, a number of computational models have been developed to estimate the delivered dosage of NPs *e.g.* the *in vitro* sedimentation, diffusion and dosimetry (ISDD) model where the particokinetics (sedimentation and diffusion) of NPs in solutions are modelled (Böhmert *et al.* 2018; DeLoid *et al.* 2014; Hinderliter *et al.* 2010).

The ISDD model proved the importance of sedimentation in affecting the biological impact of NPs. For example, using the ISDD model, a study where A549 cells were exposed to 25 and 85 nm SiO₂ NPs showed that 20 -27% of the SiO₂ NPs sedimented resulting in underestimation of the amount of NPs that reached the cells and induced any possible effect (Peuschel *et al.* 2015). On the one hand, this model offers an applicable approach to estimate the delivered amount of NPs. On the other hand, this model is confronted with some limitations and difficulties, such as measuring the hydrodynamic size of NPs in protein rich medium where the light based techniques such as DLS and particle tracking analysis (PTA) do not offer reliable measurements due to protein interferences (Gollwitzer *et al.* 2016). Another difficulty is inapplicability of the ISDD model to the dissolving NPs where their sizes and density are changing. For this another model was developed to incorporate the dissolution effects called ISD3 (the *in vitro* sedimentation, diffusion, dissolution and dosimetry model) (Thomas

et al. 2018). The current usage of this latter model is still very limited although it has a promising potential to extend the application of dosimetry models to different types of NPs.

Read-across approaches

Many attempts and studies are done and still ongoing aiming to develop efficient approaches to assess the potential adverse effects of NPs. NPs read-across and grouping approaches can facilitate the prediction of potential adverse effects of non-tested NPs based on information collected from similar NPs that were tested and characterized (Lamon *et al.* 2019). The NPs could be grouped using diverse aspects *e.g.* exposure routes, physicochemical properties, type of biological interaction, *etc.* (Doganis *et al.* 2018). Quantitative structure-activity relationship (QSAR) models are theoretical models where the structure or physicochemical characteristics of compounds are related to their potential biological interactions (Pan *et al.* 2016). These models have achieved substantial progress for modelling bulk chemicals while the application of QSARs in the field of nanotoxicology is limited. This limitation could be attributed to the complexity of the characteristics of NPs and the lack of sufficient molecular descriptors appropriate for developing QSAR model for NPs. QSARs heavily rely on large and diverse datasets of high-quality experimental (*in vitro*) data (Richarz *et al.* 2015). Although the availability of such datasets is currently limiting the development and use of QSAR approaches for NPs, several web-based tools are already available to perform QSAR studies like OpenTox, eNanoMapper and OCHEM (Parthasarathi and Dhawan 2018; Chomenidis *et al.* 2017; Helma *et al.* 2017). An important aspect of usability of QSARs is the setting of the Applicability Domain (AD). The AD specifies the scope of each model with respect to the structural and physicochemical properties and response/effects information of the training dataset used to build the model. Some QSARs have shown a great potential in predicting the biological effects of different NPs (mainly metallic ones). For example, using two sets of data generated using *in vitro* models, a QSAR model was developed for NPs. The first dataset contained data (*e.g.* ATP content and mitochondrial membrane potential) of 51 different NPs with different metal core and surface chemistry tested in four different *in vitro* cell model. The second one contained cellular uptake data of different *in vitro* cell models of 109 NPs of the same metal core and surface chemistry. This model could establish statistically significant relationships between measured biological activity profiles of these NPs and their physical, chemical and geometrical properties. As the NPs that induced similar biological

responses were of similar metal cores, the similar cellular behaviour of NPs could be correlated to NPs of similar metal core and surface chemistry (Fourches *et al.* 2010). In another study, a QSAR model was successful in predicting the cytotoxicity of metal NPs solely from their physicochemical properties (*e.g.* molecular weight, mass, charge size and aggregate size) using previously generated *in vitro* cytotoxicity data of a group of several metal NPs to *E. coli* (17 NPs of different sizes) and HaCaT cells (18 NPs of different sizes). Among all the NPs physicochemical properties used in the QSARs, the initial and aggregate sizes were the most important (Pan *et al.* 2016).

The developed models have potential applications in improving the experimental design of safer NPs. Still, the usability of the QSAR approaches in nanotoxicology are challenged by complex and diverse NPs properties and the dependency on commercially available databases which lack standardisation of characterization of NPs (Villaverde *et al.* 2018; Burello 2017).

OVERALL CONCLUSION

The work presented in this thesis illustrated the added value of combining different *in vitro* methods with advanced analytical techniques as a screening strategy to study the toxicokinetics and toxicodynamics of NPs. This approach provides better understanding of the biological interactions of NPs. Additionally, the role of surface chemistry of NPs was shown as an important characteristic that influences the toxicological behaviour of NPs outweighing the size influence. Additionally, the status of the AgNPs as pristine or aged has a significant impact on the bioavailability and toxicity of the NPs. The ICP-MS and spICP-MS showed a great potential to become a high throughput testing technique for characterization and quantification of NPs. The *in vitro* data generated within this thesis could be further used for the optimization or development of QSAR models or AOPs for NPs. Despite the continuous efforts in standardizing the testing strategies to enable robust predictive *in silico* models, still case-by-case testing of NPs is required. Overall, the presented work in this thesis corroborated the value of the alternative *in vitro* models as a screening strategy for potential hazards that could be induced by NPs. This work also, once again, stressed the importance of the robust characterization of the NPs and its impact on the interpretation of the nanotoxicological studies.

REFERENCES

- Afantitis A, Melagraki G, Tsoumanis A, Valsami-Jones E, Lynch I. 2018. A nanoinformatics decision support tool for the virtual screening of gold nanoparticle cellular association using protein corona fingerprints. *Nanotoxicology* 12:1148-1165.
- Alkilany AM, Lohse SE, Murphy CJ. 2013. The Gold Standard: Gold Nanoparticle Libraries To Understand the Nano–Bio Interface. *Accounts of Chemical Research* 46:650-661.
- Arts JHE, Hadi M, Keene AM, Kreiling R, Lyon D, Maier M, Michel K, Petry T, Sauer UG, Warheit D, Wiench K, Landsiedel R. 2014. A critical appraisal of existing concepts for the grouping of nanomaterials. *Regulatory Toxicology and Pharmacology* 70:492-506.
- Barrán-Berdón AL, Pozzi D, Caracciolo G, Capriotti AL, Caruso G, Cavaliere C, Riccioli A, Palchetti S, Laganà A. 2013. Time Evolution of Nanoparticle–Protein Corona in Human Plasma: Relevance for Targeted Drug Delivery. *Langmuir* 29:6485-6494.
- Behr C, Ramírez-Hincapié S, Cameron HJ, Strauss V, Walk T, Herold M, Beekmann K, Rietjens IMCM, van Ravenzwaay B. 2018. Impact of lincosamides antibiotics on the composition of the rat gut microbiota and the metabolite profile of plasma and feces. *Toxicology Letters* 296:139-151.
- Benam KH, Novak R, Nawroth J, Hirano-Kobayashi M, Ferrante TC, Choe Y, Prantil-Baun R, Weaver JC, Bahinski A, Parker KK, Ingber DE. 2016. Matched-Comparative Modeling of Normal and Diseased Human Airway Responses Using a Microengineered Breathing Lung Chip. *Cell Systems* 3:456-466.e4.
- Berardi A, Baldelli Bombelli F. 2019. Oral delivery of nanoparticles - let's not forget about the protein corona. *Expert Opinion on Drug Delivery* 16:563-566.
- Bhatia SN, Ingber DE. 2014. Microfluidic organs-on-chips. *Nature Biotechnology* 32:760-772.
- Böhmert L, Girod M, Hansen U, Maul R, Knappe P, Niemann B, Weidner SM, Thünemann AF, Lampen A. 2014. Analytically monitored digestion of silver nanoparticles and their toxicity on human intestinal cells. *Nanotoxicology* 8:631-642.
- Böhmert L, König L, Sieg H, Lichtenstein D, Paul N, Braeuning A, Voigt A, Lampen A. 2018. In vitro nanoparticle dosimetry for adherent growing cell monolayers covering bottom and lateral walls. *Particle and Fibre Toxicology* 15:42.
- Bouwmeester H, van der Zande M, Jepson MA. 2018. Effects of food-borne nanomaterials on gastrointestinal tissues and microbiota. *WIREs Nanomedicine and Nanobiotechnology* 10:e1481.
- Braakhuis HM, Kloet SK, Kezic S, Kuper F, Park MVDZ, Bellmann S, van der Zande M, Le Gac S, Krystek P, Peters RJB, Rietjens IMCM, Bouwmeester H. 2015. Progress and future of in vitro models to study translocation of nanoparticles. *Archives of toxicology* 89:1469-1495.
- Brockmeier EK, Hodges G, Hutchinson TH, Butler E, Hecker M, Tollefsen KE, Garcia-Reyero N, Kille P, Becker D, Chipman K, Colbourne J, Collette TW, Cossins A, Cronin M, Graystock P, Gutsell S, Knapen D, Katsiadaki I, Lange A, Marshall S, Owen SF, Perkins EJ, Plaistow S, Schroeder A, Taylor D, Viant M, Ankley G, Falciani F. 2017. The Role of Omics in the Application of Adverse Outcome Pathways for Chemical Risk Assessment. *Toxicol Sci* 158:252-262.

- Burden N, Aschberger K, Chaudhry Q, Clift MJD, Fowler P, Johnston H, Landsiedel R, Rowland J, Stone V, Doak SH. 2017. Aligning nanotoxicology with the 3Rs: What is needed to realise the short, medium and long-term opportunities? *Regulatory Toxicology and Pharmacology* 91:257-266.
- Burello E. 2017. Review of (Q)SAR models for regulatory assessment of nanomaterials risks. *NanoImpact* 8:48-58.
- Cai R, Ren J, Ji Y, Wang Y, Liu Y, Chen Z, Farhadi Sabet Z, Wu X, Lynch I, Chen C. 2020. Corona of Thorns: The Surface Chemistry-Mediated Protein Corona Perturbs the Recognition and Immune Response of Macrophages. *ACS Applied Materials & Interfaces* 12:1997-2008.
- Cedervall T, Lynch I, Lindman S, Berggård T, Thulin E, Nilsson H, Dawson KA, Linse S. 2007. Understanding the nanoparticle-protein corona using methods to quantify exchange rates and affinities of proteins for nanoparticles. *Proceedings of the National Academy of Sciences* 104:2050-2055.
- Chen R, Qiao J, Bai R, Zhao Y, Chen C. 2018. Intelligent testing strategy and analytical techniques for the safety assessment of nanomaterials. *Analytical and Bioanalytical Chemistry* 410:6051-6066.
- Chomenidis C, Drakakis G, Tsiliki G, Anagnostopoulou E, Valsamis A, Doganis P, Sopasakis P, Sarimveis H. 2017. Jaqpot Quattro: A Novel Computational Web Platform for Modeling and Analysis in Nanoinformatics. *Journal of Chemical Information and Modeling* 57:2161-2172.
- DeLoid G, Cohen JM, Darrah T, Derk R, Rojanasakul L, Pyrgiotakis G, Wohlleben W, Demokritou P. 2014. Estimating the effective density of engineered nanomaterials for in vitro dosimetry. *Nature Communications* 5:3514.
- Ding L, Yao C, Yin X, Li C, Huang Y, Wu M, Wang B, Guo X, Wang Y, Wu M. 2018. Size, Shape, and Protein Corona Determine Cellular Uptake and Removal Mechanisms of Gold Nanoparticles. *Small* 14:1801451.
- Docter D, Westmeier D, Markiewicz M, Stolte S, Knauer SK, Stauber RH. 2015. The nanoparticle biomolecule corona: lessons learned – challenge accepted? *Chemical Society Reviews* 44:6094-6121.
- Doganis P, Tsiliki G, Drakakis G, Chomenidis C, Nymark P, Kohonen P, Grafström R, Abdelaziz A, Farcas L, Exner T, Hardy B, Sarimveis H. 2018. Chapter 11 Computational Modelling of Biological Responses to Engineered Nanomaterials. *Nanotoxicology: Experimental and Computational Perspectives*. The Royal Society of Chemistry, 276-303.
- EFSA Scientific Committee, Hardy A, Benford D, Halldorsson T, Jeger MJ, Knutsen HK, More S, Naegeli H, Noteborn H, Ockleford C, Ricci A, Rychen G, Schlatter JR, Silano V, Solecki R, Turck D, Younes M, Chaudhry Q, Cubadda F, Gott D, Oomen A, Weigel S, Karamitrou M, Schoonjans R, Mortensen A. 2018. Guidance on risk assessment of the application of nanoscience and nanotechnologies in the food and feed chain: Part 1, human and animal health. *EFSA Journal* 16:e05327.
- Fadeel B. 2019. The Right Stuff: On the Future of Nanotoxicology. *Frontiers in Toxicology* 1.
- Fadeel B, Farcas L, Hardy B, Vázquez-Campos S, Hristozov D, Marcomini A, Lynch I, Valsami-Jones E, Alenius H, Savolainen K. 2018. Advanced tools for the safety assessment of nanomaterials. *Nature Nanotechnology* 13:537-543.

- Fennell TR, Mortensen NP, Black SR, Snyder RW, Levine KE, Poitras E, Harrington JM, Wingard CJ, Holland NA, Pathmasiri W, Sumner SCJ. 2017. Disposition of intravenously or orally administered silver nanoparticles in pregnant rats and the effect on the biochemical profile in urine. *Journal of Applied Toxicology* 37:530-544.
- Fourches D, Pu D, Tassa C, Weissleder R, Shaw SY, Mumper RJ, Tropsha A. 2010. Quantitative nanostructure-activity relationship modeling. *ACS nano* 4:5703-5712.
- Francia V, Yang K, Deville S, Reker-Smit C, Nelissen I, Salvati A. 2019. Corona Composition Can Affect the Mechanisms Cells Use to Internalize Nanoparticles. *ACS nano* 13:11107-11121.
- Fröhlich E, Roblegg E. 2012. Models for oral uptake of nanoparticles in consumer products. *Toxicology* 291:10-17.
- Fröhlich E, Roblegg E. 2016. Oral uptake of nanoparticles: human relevance and the role of in vitro systems. *Archives of Toxicology* 90:2297-2314.
- Fröhlich EE, Fröhlich E. 2016. Cytotoxicity of Nanoparticles Contained in Food on Intestinal Cells and the Gut Microbiota. *International Journal of Molecular Sciences* 17:509.
- Gerloff K, Landesmann B, Worth A, Munn S, Palosaari T, Whelan M. 2017. The Adverse Outcome Pathway approach in nanotoxicology. *Computational Toxicology* 1:3-11.
- Gollwitzer C, Bartczak D, Goenaga-Infante H, Kestens V, Krumrey M, Minelli C, Pálmai M, Ramaye Y, Roebben G, Sikora A, Varga Z. 2016. A comparison of techniques for size measurement of nanoparticles in cell culture medium. *Analytical Methods* 8:5272-5282.
- Hammad S, Bolt HM. 2014. Current developments in nanosafety research. *Archives of Toxicology* 88:2089-2091.
- Han X-Y, Du W-L, Fan C-L, Xu Z-R. 2010. ORIGINAL ARTICLE: Changes in composition a metabolism of caecal microbiota in rats fed diets supplemented with copper-loaded chitosan nanoparticles. *Journal of Animal Physiology and Animal Nutrition* 94:e138-e144.
- Hardy A, Benford D, Halldorsson T, Jeger MJ, Knutsen HK, More S, Naegeli H, Noteborn H, Ockleford C, Ricci A, Rychen G, Schlatter JR, Silano V, Solecki R, Turck D, Younes M, Chaudhry Q, Cubadda F, Gott D, Oomen A, Weigel S, Karamitrou M, Schoonjans R, Mortensen A. 2018. Guidance on risk assessment of the application of nanoscience and nanotechnologies in the food and feed chain: Part 1, human and animal health. *EFSA Journal* 16:e05327.
- He D, Garg S, Wang Z, Li L, Rong H, Ma X, Li G, An T, Waite TD. 2019. Silver sulfide nanoparticles in aqueous environments: formation, transformation and toxicity. *Environmental Science: Nano* 6:1674-1687.
- Helma C, Rautenberg M, Gebele D. 2017. Nano-Lazar: Read across Predictions for Nanoparticle Toxicities with Calculated and Measured Properties. *Frontiers in Pharmacology* 8.
- Hendrickson OD, Klochkov SG, Novikova OV, Bravova IM, Shevtsova EF, Safenkova IV, Zherdev AV, Bachurin SO, Dzantiev BB. 2016. Toxicity of nanosilver in intragastric studies: Biodistribution and metabolic effects. *Toxicology Letters* 241:184-192.
- Heylmann D, Kaina B. 2016. The γ H2AX DNA damage assay from a drop of blood. *Scientific Reports* 6:22682.

- Hinderliter PM, Minard KR, Orr G, Chrisler WB, Thrall BD, Pounds JG, Teeguarden JG. 2010. ISDD: A computational model of particle sedimentation, diffusion and target cell dosimetry for in vitro toxicity studies. *Particle and Fibre Toxicology* 7:36.
- Hu X, Li D, Gao Y, Mu L, Zhou Q. 2016. Knowledge gaps between nanotoxicological research and nanomaterial safety. *Environment International* 94:8-23.
- Huh D, Kim HJ, Fraser JP, Shea DE, Khan M, Bahinski A, Hamilton GA, Ingber DE. 2013. Microfabrication of human organs-on-chips. *Nature Protocols* 8:2135-2157.
- Huh D, Matthews BD, Mammoto A, Montoya-Zavala M, Hsin HY, Ingber DE. 2010. Reconstituting Organ-Level Lung Functions on a Chip. *Science* 328:1662-1668.
- Hühn D, Kantner K, Geidel C, Brandholt S, De Cock I, Soenen SJH, Rivera_Gil P, Montenegro J-M, Braeckmans K, Müllen K, Nienhaus GU, Klapper M, Parak WJ. 2013. Polymer-Coated Nanoparticles Interacting with Proteins and Cells: Focusing on the Sign of the Net Charge. *ACS Nano* 7:3253-3263.
- Hussain SM, Warheit DB, Ng SP, Comfort KK, Grabinski CM, Braydich-Stolle LK. 2015. At the Crossroads of Nanotoxicology in vitro: Past Achievements and Current Challenges. *Toxicological Sciences* 147:5-16.
- Jeong J, Song T, Chatterjee N, Choi I, Cha YK, Choi J. 2018. Developing adverse outcome pathways on silver nanoparticle-induced reproductive toxicity via oxidative stress in the nematode *Caenorhabditis elegans* using a Bayesian network model. *Nanotoxicology* 12:1182-1197.
- Khoury L, Zalko D, Audebert M. 2013. Validation of high-throughput genotoxicity assay screening using γ H2AX in-cell western assay on HepG2 cells. *Environmental and Molecular Mutagenesis* 54:737-746.
- Kim JA, Salvati A, Åberg C, Dawson KA. 2014. Suppression of nanoparticle cytotoxicity approaching in vivo serum concentrations: limitations of in vitro testing for nanosafety. *Nanoscale* 6:14180-14184.
- Kim YJ, Rahman MM, Lee SM, Kim JM, Park K, Kang J-H, Seo YR. 2019. Assessment of in vivo genotoxicity of citrated-coated silver nanoparticles via transcriptomic analysis of rabbit liver tissue. *International journal of nanomedicine* 14:393-405.
- Kim YS, Kim JS, Cho HS, Rha DS, Kim JM, Park JD, Choi BS, Lim R, Chang HK, Chung YH, Kwon IH, Jeong J, Han BS, Yu IJ. 2008. Twenty-Eight-Day Oral Toxicity, Genotoxicity, and Gender-Related Tissue Distribution of Silver Nanoparticles in Sprague-Dawley Rats. *Inhalation Toxicology* 20:575-583.
- Knowlton S, Tasoglu S. 2016. A Bioprinted Liver-on-a-Chip for Drug Screening Applications. *Trends in Biotechnology* 34:681-682.
- Kroll A, Pillukat MH, Hahn D, Schnekenburger J. 2009. Current in vitro methods in nanoparticle risk assessment: Limitations and challenges. *European Journal of Pharmaceutics and Biopharmaceutics* 72:370-377.
- Krug HF, Wick P. 2011. Nanotoxicology: An Interdisciplinary Challenge. *Angewandte Chemie International Edition* 50:1260-1278.
- Kulthong K, Duivenvoorde L, Mizera BZ, Rijkers D, Dam Gt, Oegema G, Puzyn T, Bouwmeester H, van der Zande M. 2018. Implementation of a dynamic intestinal gut-on-a-chip barrier model for transport studies of lipophilic dioxin congeners. *RSC Advances* 8:32440-32453.

- Kundu P, Blacher E, Elinav E, Pettersson S. 2017. Our Gut Microbiome: The Evolving Inner Self. *Cell* 171:1481-1493.
- Lamon L, Aschberger K, Asturiol D, Richarz A, Worth A. 2019. Grouping of nanomaterials to read-across hazard endpoints: a review. *Nanotoxicology* 13:100-118.
- Larese FF, D'Agostin F, Crosera M, Adami G, Renzi N, Bovenzi M, Maina G. 2009. Human skin penetration of silver nanoparticles through intact and damaged skin. *Toxicology* 255:33-37.
- Lichtenstein D, Ebmeyer J, Meyer T, Behr A-C, Kästner C, Böhmert L, Juling S, Niemann B, Fahrenson C, Selve S, Thünemann AF, Meijer J, Estrela-Lopis I, Braeuning A, Lampen A. 2017. It takes more than a coating to get nanoparticles through the intestinal barrier in vitro. *European Journal of Pharmaceutics and Biopharmaceutics* 118:21-29.
- Liu S, Wang C, Hou J, Wang P, Miao L, Li T. 2018. Effects of silver sulfide nanoparticles on the microbial community structure and biological activity of freshwater biofilms. *Environmental Science: Nano* 5:2899-2908.
- Loeschner K, Hadrup N, Qvortrup K, Larsen A, Gao X, Vogel U, Mortensen A, Lam HR, Larsen EH. 2011a. Distribution of silver in rats following 28 days of repeated oral exposure to silver nanoparticles or silver acetate. *Particle and fibre toxicology* 8:18-18.
- Loeschner K, Hadrup N, Qvortrup K, Larsen A, Gao X, Vogel U, Mortensen A, Lam HR, Larsen EH. 2011b. Distribution of silver in rats following 28 days of repeated oral exposure to silver nanoparticles or silver acetate. *Particle and Fibre Toxicology* 8:18.
- Lundqvist M, Stigler J, Elia G, Lynch I, Cedervall T, Dawson KA. 2008. Nanoparticle size and surface properties determine the protein corona with possible implications for biological impacts. *Proc Natl Acad Sci USA* 105.
- Lynch I, Salvati A, Dawson KA. 2009. What does the cell see? *Nature Nanotechnology* 4:546-547.
- Lynch I, Weiss C, Valsami-Jones E. 2014. A strategy for grouping of nanomaterials based on key physico-chemical descriptors as a basis for safer-by-design NMs. *Nano Today* 9:266-270.
- Ma C, Zhao L, Zhou E-M, Xu J, Shen S, Wang J. 2016. On-Chip Construction of Liver Lobule-like Microtissue and Its Application for Adverse Drug Reaction Assay. *Analytical Chemistry* 88:1719-1727.
- Ma Y-B, Lu C-J, Junaid M, Jia P-P, Yang L, Zhang J-H, Pei D-S. 2018. Potential adverse outcome pathway (AOP) of silver nanoparticles mediated reproductive toxicity in zebrafish. *Chemosphere* 207:320-328.
- Materne E-M, Maschmeyer I, Lorenz AK, Horland R, Schimek KMS, Busek M, Sonntag F, Lauster R, Marx U. 2015. The multi-organ chip--a microfluidic platform for long-term multi-tissue coculture. *J Vis Exp*:e52526-e52526.
- McCracken C, Zane A, Knight DA, Hommel E, Dutta PK, Waldman WJ. 2015. Oxidative stress-mediated inhibition of intestinal epithelial cell proliferation by silver nanoparticles. *Toxicology in Vitro* 29:1793-1808.
- Mehrabi K, Günther D, Gundlach-Graham A. 2019. Single-particle ICP-TOFMS with online microdroplet calibration for the simultaneous quantification of diverse nanoparticles in complex matrices. *Environmental Science: Nano* 6:3349-3358.

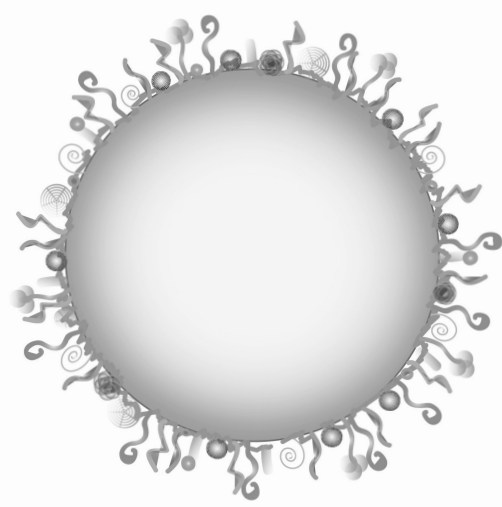
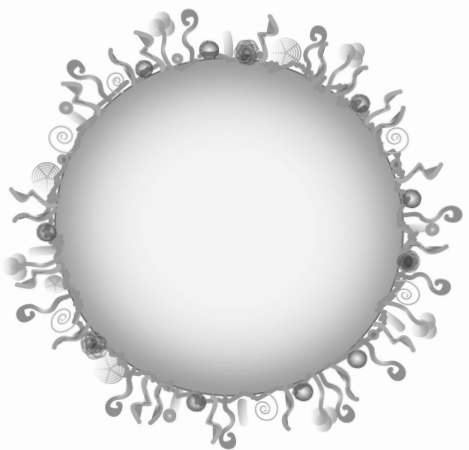
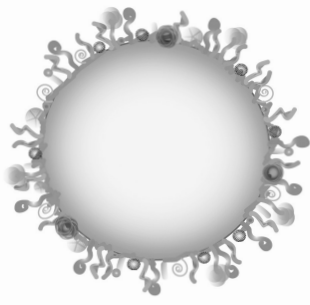
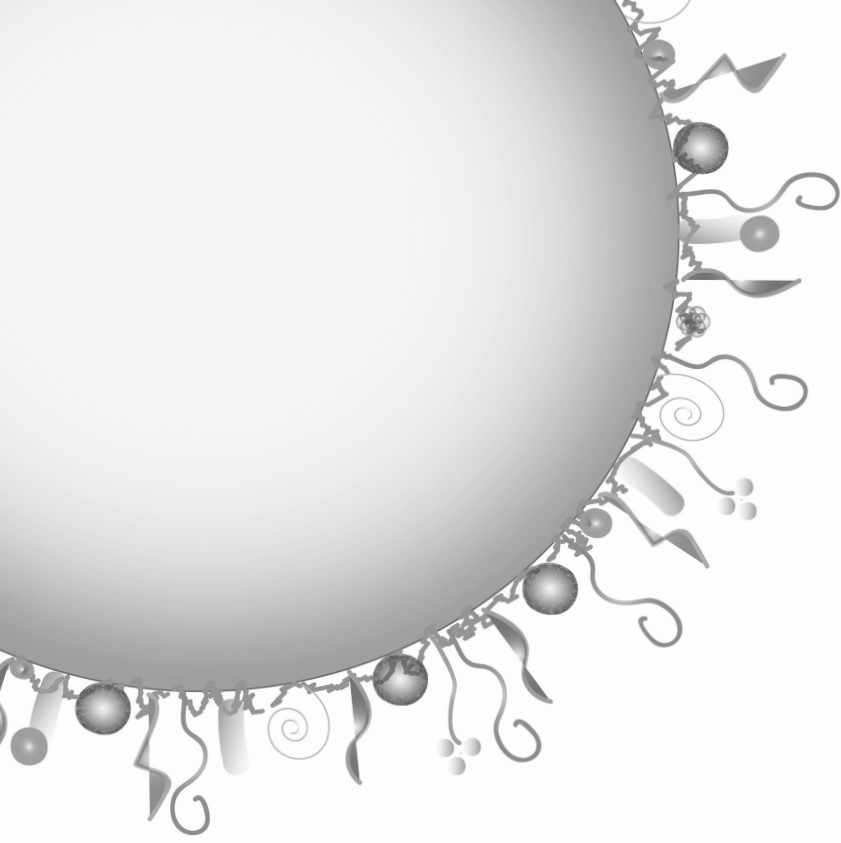
- Murdock RC, Braydich-Stolle L, Schrand AM, Schlager JJ, Hussain SM. 2008. Characterization of Nanomaterial Dispersion in Solution Prior to In Vitro Exposure Using Dynamic Light Scattering Technique. *Toxicological Sciences* 101:239-253.
- Naasz S, Weigel S, Borovinskaya O, Serva A, Cascio C, Undas AK, Simeone FC, Marvin HJP, Peters RJB. 2018. Multi-element analysis of single nanoparticles by ICP-MS using quadrupole and time-of-flight technologies. *Journal of Analytical Atomic Spectrometry* 33:835-845.
- Nel AE, Malloy TF. 2017. Policy reforms to update chemical safety testing. *Science* 355:1016-1018.
- Nguyen VH, Lee B-J. 2017. Protein corona: a new approach for nanomedicine design. *International journal of nanomedicine* 12:3137-3151.
- Nikolova T, Dvorak M, Jung F, Adam I, Krämer E, Gerhold-Ay A, Kaina B. 2014. The γ H2AX Assay for Genotoxic and Nongenotoxic Agents: Comparison of H2AX Phosphorylation with Cell Death Response. *Toxicological Sciences* 140:103-117.
- Oberdörster G, Maynard A, Donaldson K, Castranova V, Fitzpatrick J, Ausman K, Carter J, Karn B, Kreyling W, Lai D, Olin S, Monteiro-Riviere N, Warheit D, Yang H, Group ArftIRFRSINTSW. 2005a. Principles for characterizing the potential human health effects from exposure to nanomaterials: elements of a screening strategy. *Particle and Fibre Toxicology* 2:8.
- Oberdörster G, Oberdörster E, Oberdörster J. 2005b. Nanotoxicology: an emerging discipline evolving from studies of ultrafine particles. *Environ Health Perspect* 113:823-839.
- Pan Y, Li T, Cheng J, Telesca D, Zink JI, Jiang J. 2016. Nano-QSAR modeling for predicting the cytotoxicity of metal oxide nanoparticles using novel descriptors. *RSC Advances* 6:25766-25775.
- Parthasarathi R, Dhawan A. 2018. Chapter 5 - In Silico Approaches for Predictive Toxicology. In: Dhawan A, Kwon S, eds. *In Vitro Toxicology*. Academic Press, 91-109.
- Paunovska K, Loughrey D, Sago CD, Langer R, Dahlman JE. 2019. Using Large Datasets to Understand Nanotechnology. *Advanced Materials* 31:1902798.
- Peng Q, Liu J, Zhang T, Zhang T-X, Zhang C-L, Mu H. 2019. Digestive Enzyme Corona Formed in the Gastrointestinal Tract and Its Impact on Epithelial Cell Uptake of Nanoparticles. *Biomacromolecules* 20:1789-1797.
- Peters RJB, van Bommel G, Herrera-Rivera Z, Helsper HPFG, Marvin HJP, Weigel S, Tromp PC, Oomen AG, Rietveld AG, Bouwmeester H. 2014. Characterization of Titanium Dioxide Nanoparticles in Food Products: Analytical Methods To Define Nanoparticles. *Journal of Agricultural and Food Chemistry* 62:6285-6293.
- Peuschel H, Ruckelshausen T, Cavelius C, Kraegeloh A. 2015. Quantification of internalized silica nanoparticles via STED microscopy. *BioMed research international* 2015.
- Praetorius A, Gundlach-Graham A, Goldberg E, Fabienke W, Navratilova J, Gondikas A, Kaegi R, Günther D, Hofmann T, von der Kammer F. 2017. Single-particle multi-element fingerprinting (spMEF) using inductively-coupled plasma time-of-flight mass spectrometry (ICP-TOFMS) to identify engineered nanoparticles against the elevated natural background in soils. *Environmental Science: Nano* 4:307-314.
- Richarz A-N, Madden JC, Marchese Robinson RL, Lubiński Ł, Mokshina E, Urbaszek P, Kuz'min VE, Puzyn T, Cronin MTD. 2015. Development of computational models for the prediction of the toxicity of nanomaterials. *Perspectives in Science* 3:27-29.

- Riediker M, Zink D, Kreyling W, Oberdörster G, Elder A, Graham U, Lynch I, Duschl A, Ichihara G, Ichihara S, Kobayashi T, Hisanaga N, Umezawa M, Cheng T-J, Handy R, Gulumian M, Tinkle S, Cassee F. 2019. Particle toxicology and health - where are we? *Particle and Fibre Toxicology* 16:19.
- Ritz S, Schöttler S, Kotman N, Baier G, Musyanovych A, Kuharev J, Landfester K, Schild H, Jahn O, Tenzer S, Mailänder V. 2015. Protein Corona of Nanoparticles: Distinct Proteins Regulate the Cellular Uptake. *Biomacromolecules* 16:1311-1321.
- Schleh C, Semmler-Behnke M, Lipka J, Wenk A, Hirn S, Schäffler M, Schmid G, Simon U, Kreyling WG. 2012. Size and surface charge of gold nanoparticles determine absorption across intestinal barriers and accumulation in secondary target organs after oral administration. *Nanotoxicology* 6:36-46.
- Schwab F, Zhai G, Kern M, Turner A, Schnoor J, Wiesner M. 2015. Barriers, pathways and processes for uptake, translocation and accumulation of nanomaterials in plants – Critical review. *Nanotoxicology*.
- Shah P, Fritz JV, Glaab E, Desai MS, Greenhalgh K, Frachet A, Niegowska M, Estes M, Jäger C, Seguin-Devaux C, Zenhausern F, Wilmes P. 2016. A microfluidics-based in vitro model of the gastrointestinal human–microbe interface. *Nature Communications* 7:11535.
- Shvedova A, Pietroiusti A, Kagan V. 2016. Nanotoxicology ten years later: Lights and shadows. *Toxicology and Applied Pharmacology* 299:1-2.
- Sieg H, Kästner C, Krause B, Meyer T, Burel A, Böhmert L, Lichtenstein D, Jungnickel H, Tentschert J, Laux P, Braeuning A, Estrela-Lopis I, Gauffre F, Fessard V, Meijer J, Luch A, Thünemann AF, Lampen A. 2017. Impact of an Artificial Digestion Procedure on Aluminum-Containing Nanomaterials. *Langmuir* 33:10726-10735.
- Sierra MI, Valdés A, Fernández AF, Torrecillas R, Fraga MF. 2016. The effect of exposure to nanoparticles and nanomaterials on the mammalian epigenome. *International journal of nanomedicine* 11:6297-6306.
- Sung JH, Ji JH, Park JD, Yoon JU, Kim DS, Jeon KS, Song MY, Jeong J, Han BS, Han JH, Chung YH, Chang HK, Lee JH, Cho MH, Kelman BJ, Yu IJ. 2008. Subchronic Inhalation Toxicity of Silver Nanoparticles. *Toxicological Sciences* 108:452-461.
- Sutton SC, Nause R, Gandelman K. 2017. The impact of gastric pH, volume, and emptying on the food effect of ziprasidone oral absorption. *The AAPS Journal* 19:1084-1090.
- Tenzer S, Docter D, Kuharev J, Musyanovych A, Fetz V, Hecht R, Schlenk F, Fischer D, Kiouptsi K, Reinhardt C, Landfester K, Schild H, Maskos M, Knauer SK, Stauber RH. 2013. Rapid formation of plasma protein corona critically affects nanoparticle pathophysiology. *8:772-781*.
- Thomas DG, Smith JN, Thrall BD, Baer DR, Jolley H, Munusamy P, Kodali V, Demokritou P, Cohen J, Teeguarden JG. 2018. ISD3: a particokinetic model for predicting the combined effects of particle sedimentation, diffusion and dissolution on cellular dosimetry for in vitro systems. *Particle and Fibre Toxicology* 15:6.
- Tripathi DK, Tripathi A, Shweta, Singh S, Singh Y, Vishwakarma K, Yadav G, Sharma S, Singh VK, Mishra RK, Upadhyay RG, Dubey NK, Lee Y, Chauhan DK. 2017. Uptake, Accumulation and Toxicity of Silver Nanoparticle in Autotrophic Plants, and Heterotrophic Microbes: A Concentric Review. *Frontiers in Microbiology* 8.

- Valencia PM, Farokhzad OC, Karnik R, Langer R. 2012. Microfluidic technologies for accelerating the clinical translation of nanoparticles. *Nature nanotechnology* 7:623-629.
- van den Brule S, Ambroise J, Lecloux H, Levard C, Soulas R, De Temmerman P-J, Palmi-Pallag M, Marbaix E, Lison D. 2016. Dietary silver nanoparticles can disturb the gut microbiota in mice. *Particle and fibre toxicology* 13:38-38.
- van der Zande M, Vandebriel RJ, Van Doren E, Kramer E, Herrera Rivera Z, Serrano-Rojero CS, Gremmer ER, Mast J, Peters RJB, Hollman PCH, Hendriksen PJM, Marvin HJP, Peijnenburg AACM, Bouwmeester H. 2012. Distribution, Elimination, and Toxicity of Silver Nanoparticles and Silver Ions in Rats after 28-Day Oral Exposure. *ACS Nano* 6:7427-7442.
- van Thriel C. 2015. Highlight report: Translocation of nanoparticles through barriers. *Archives of Toxicology* 89:2469-2470.
- Vilanova O, Mittag JJ, Kelly PM, Milani S, Dawson KA, Rädler JO, Franzese G. 2016. Understanding the Kinetics of Protein-Nanoparticle Corona Formation. *ACS nano* 10:10842-10850.
- Villaverde JJ, Sevilla-Morán B, López-Goti C, Alonso-Prados JL, Sandín-España P. 2018. Considerations of nano-QSAR/QSPR models for nanopesticide risk assessment within the European legislative framework. *Science of The Total Environment* 634:1530-1539.
- Walczak AP, Kramer E, Hendriksen PJM, Helsdingen R, van der Zande M, Rietjens IMCM, Bouwmeester H. 2015. In vitro gastrointestinal digestion increases the translocation of polystyrene nanoparticles in an in vitro intestinal co-culture model. *Nanotoxicology* 9:886-894.
- Walczyk D, Bombelli FB, Monopoli MP, Lynch I, Dawson KA. 2010a. What the cell "sees" in bionanoscience. *J Am Chem Soc* 132.
- Walczyk D, Bombelli FB, Monopoli MP, Lynch I, Dawson KA. 2010b. What the Cell "Sees" in Bionanoscience. *Journal of the American Chemical Society* 132:5761-5768.
- Walker M, Parsons D. 2014. The biological fate of silver ions following the use of silver-containing wound care products – a review. *International Wound Journal* 11:496-504.
- Wang P, Lombi E, Sun S, Scheckel KG, Malysheva A, McKenna BA, Menzies NW, Zhao F-J, Kopittke PM. 2017. Characterizing the uptake, accumulation and toxicity of silver sulfide nanoparticles in plants. *Environmental Science: Nano* 4:448-460.
- Warheit DB, Sayes CM. 2015. Chapter 1.2 - Routes of Exposure to Nanoparticles: Hazard Tests Related to Portal Entries. In: Dolez PI, ed. *Nanoengineering*. Amsterdam: Elsevier, 41-54.
- Waseem H, Williams MR, Stedtfeld RD, Stedtfeld TM, Shanker R, Hashsham SA. 2018. Chapter 8 Organ-on-chip Systems: An Emerging Platform for Toxicity Screening of Chemicals, Pharmaceuticals, and Nanomaterials. *Nanotoxicology: Experimental and Computational Perspectives*. The Royal Society of Chemistry, 203-231.
- Wen H, Dan M, Yang Y, Lyu J, Shao A, Cheng X, Chen L, Xu L. 2017. Acute toxicity and genotoxicity of silver nanoparticle in rats. *PloS one* 12:e0185554-e0185554.
- Yang X, Liu X, Zhang A, Lu D, Li G, Zhang Q, Liu Q, Jiang G. 2019. Distinguishing the sources of silica nanoparticles by dual isotopic fingerprinting and machine learning. *Nature Communications* 10:1620.

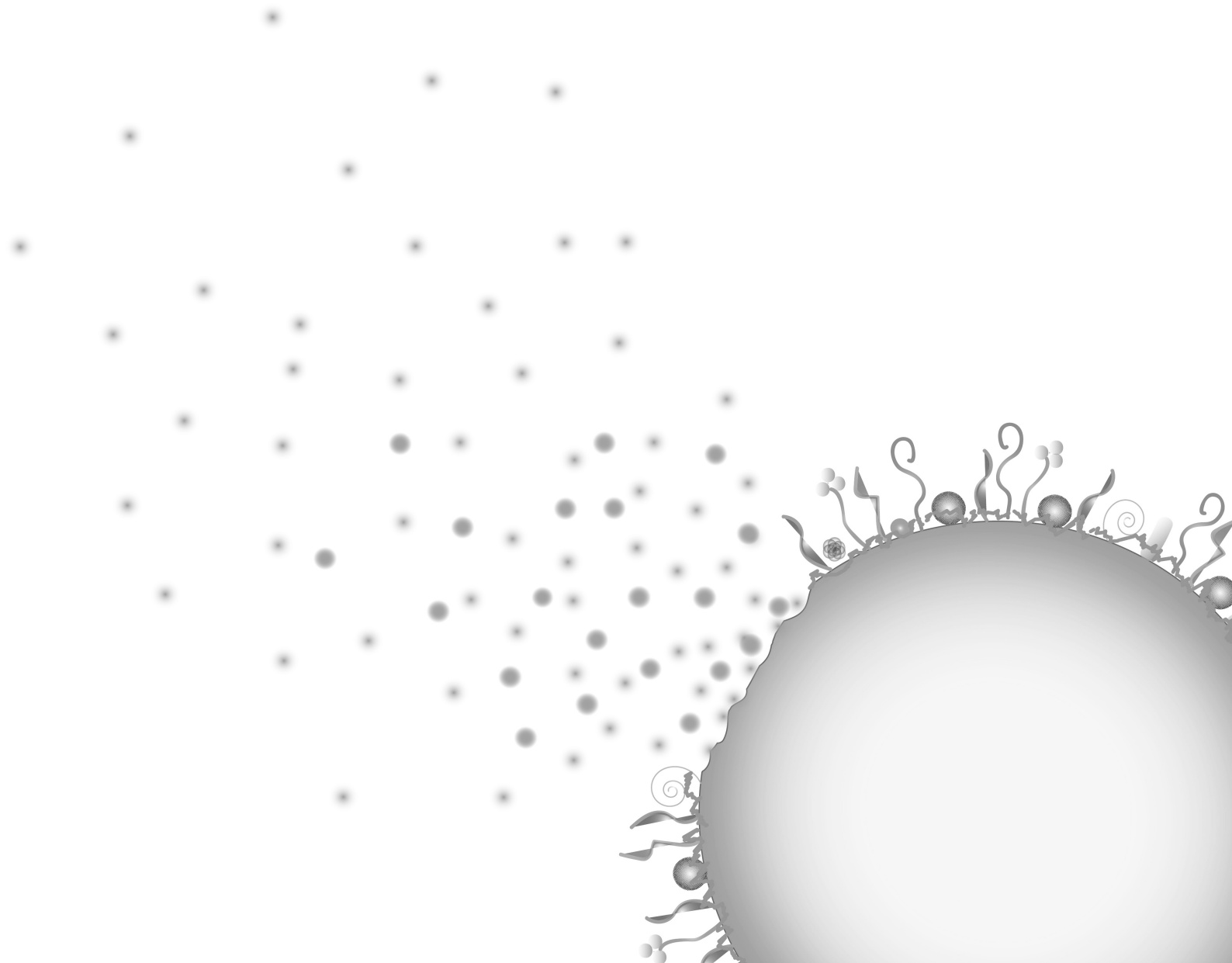
Yin Y, Yu S, Shen M, Liu J, Jiang G. 2015. Fate and Transport of Silver Nanoparticles in the Environment. In: Liu J, Jiang G, eds. Silver Nanoparticles in the Environment. Berlin, Heidelberg: Springer Berlin Heidelberg, 73-108.

Ziółkowska K, Kwapiszewski R, Brzózka Z. 2011. Microfluidic devices as tools for mimicking the in vivo environment. *New Journal of Chemistry* 35:979-990.



7

Summary





In **chapter 1** of this thesis, an overview of the main applications of NPs was provided and the main properties of NPs were briefly introduced. In addition, some of the key methods that are currently used in the toxicological safety assessment of NPs were presented. The aim of the thesis was introduced which was to investigate the potential of different *in vitro* methods combined with high-end analytical techniques as a testing strategy to study the toxicokinetic and toxicodynamic properties of silver (Ag) and polystyrene (PS) NPs and set priorities in their further safety testing. The current state of the art of the *in vitro* methods used in the studies in this thesis and the outline of the thesis were also presented.

In **chapter 2**, the influences of the size and surface chemistry of pristine PSNPs on the protein corona formation and subsequent uptake/association and transport of these NPs through a Caco-2 intestinal cell model were studied. Four negatively charged PSNPs of different sizes (50 and 200 nm) and with different surface chemistries (sulfone or carboxyl groups) were studied. The protein coronas of these PSNPs were analysed by LC-MS/MS which showed subtle differences in the protein composition of especially the two PSNPs with different surface chemistries. In further experiments, the impact of surface chemistry on the cellular uptake/association and transport was characterised using high-content imaging analysis. These experiments demonstrated that the PSNPs with sulfone surface groups were associated with the cells to a significantly higher extent than the PSNPs with carboxyl surface groups. No clear effect of the size of the PSNPs on the cellular uptake/association was noted. Also, the transport of the PSNPs with sulfone surface groups through the monolayer of cells was significantly higher than that of PSNPs with carboxyl surface groups.

The general conclusion was that the composition of the protein corona and the PSNPs surface chemistry influence the cellular NPs uptake/association and transport, with the effect of the NP surface chemistry outweighing the impact of NPs size on the cellular uptake/associations and transport. These results might be predictive of the intestinal transport of NPs. Still, further studies are required to identify which corona proteins affect the uptake and transport of NPs.

Chapter 3 described an investigation on the impact of the biochemical conditions within the human digestive tract on the intestinal fate of AgNPs with different surface chemistries. On top of that, the transport of these AgNPs across an intestinal *in vitro* model of Caco-

2/HT29-MTX cells was evaluated. An *in vitro* digestion model was used to simulate the human digestion processes. Two 50 nm negatively charged AgNPs with different surface chemistries were used, lipoic acid (LA) AgNPs and citrate (Cit) AgNPs next to silver nitrate (AgNO_3) as a source of ionic silver (Ag^+). The co-culture model was exposed to different concentrations of pristine and *in vitro* digested (IVD) AgNPs or AgNO_3 for 24 hr. Using ICP-MS and spICP-MS, the size distribution, dissolution, particle concentration (mass- and number-based) and total silver content of the AgNPs were characterized before and after digestion and in the apical, basolateral and cellular compartments of the Caco-2/HT29-MTX intestinal epithelial model. The surface chemistry of AgNPs had a significant influence on their dissolution and on their biological interactions with the Caco-2/HT29-MTX intestinal model. In general, a significant fraction of the AgNPs dissolved during the digestion up to 86 - 92% and 48 - 70% of the original amount of NPs for the (LA) and (Cit) AgNPs, respectively. Exposure of the monolayer of intestinal cells to increasing concentrations of pristine or IVD AgNPs resulted in a concentration dependent increase of total Ag and AgNPs content in the cellular fractions. The cellular concentrations were significantly lower following exposure to IVD AgNPs compared to the pristine AgNPs. The effect of the surface chemistry on the cellular concentration of Ag was only detected upon exposure to pristine AgNPs, while this difference disappeared upon exposure to IVD AgNPs.

Transport of Ag across the intestinal model layer, as either total Ag or AgNPs, was limited (< 0.1%) following exposure to pristine and IVD AgNPs. *De novo* formation of AgNPs was shown in the exposure suspensions of IVD AgNPs and AgNO_3 and in the cellular fractions, upon cellular exposure to pristine and IVD AgNO_3 . In conclusion, the surface chemistry of AgNPs and the biochemical conditions during *in vitro* digestion influences the dissolution and also influences the uptake/association within the Caco-2/HT29-MTX monolayer. This highlights the need to take *in vitro* digestion into account when studying nanoparticle toxicokinetics in an intestinal cellular *in vitro* model system. The observation that dissolution characteristics of NPs may change upon digestion could be of added value in the safe(r)-by-design NPs development.

Chapter 4 presented the outcomes from combining the BeWo b30 placental transport model and the embryonic stem cell test (EST) to investigate the capability of pristine AgNPs of different surface chemistries and aged AgNPs (Ag_2S NPs) to cross the placental barrier and

induce *in vitro* developmental toxicity. AgNO₃ was used as a source of Ag⁺. The pristine negatively charged AgNPs used in this study were similar to the ones used in **chapter 3** while in addition also positively charged 50 nm branched polyethylenimine (BPEI) AgNPs were included in the study. The size distribution, dissolution, particle concentration (mass- and number-based) and total Ag content of the AgNPs in the apical, basolateral and cellular compartments of the BeWo b30 placental transport model at different time points was characterized using ICP-MS and spICP-MS. The ability of the AgNPs to cross the BeWo b30 cell layer was limited and dependent on the surface chemistry of these AgNPs. The particles detected in the basolateral compartment could result from transport of the original AgNPs and/or from the *de novo* formed AgNPs in the basolateral compartment from Ag⁺ that was transported.

The *in vitro* developmental toxicity of the AgNPs was investigated by characterizing their potential to inhibit the differentiation of mouse embryonic stem cells (mESCs) into beating cardiomyocytes using the EST. The observed inhibitory effects of the AgNPs on differentiation of mESCs were most likely the result of cytotoxicity rather than specific effects related to developmental toxicity as the effects on differentiation of the mESCs were only detected at cytotoxic concentrations. Compared to the pristine AgNPs, the aged Ag₂S NPs were significantly less cytotoxic, transported less across the BeWo cell layer and did not induce *in vitro* developmental toxicity. In conclusion, the combination of the BeWo placental transport model with the mESCs differentiation assay appeared to provide a valuable alternative *in vitro* methodology for prenatal developmental toxicity testing and prioritization for further safety testing of AgNPs, with aged Ag₂S NPs appearing to present less of a hazard than pristine AgNPs.

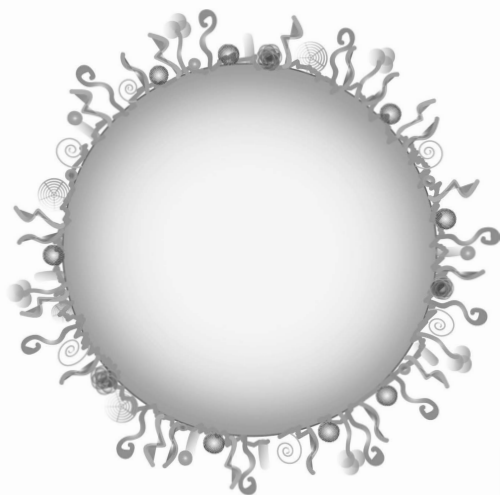
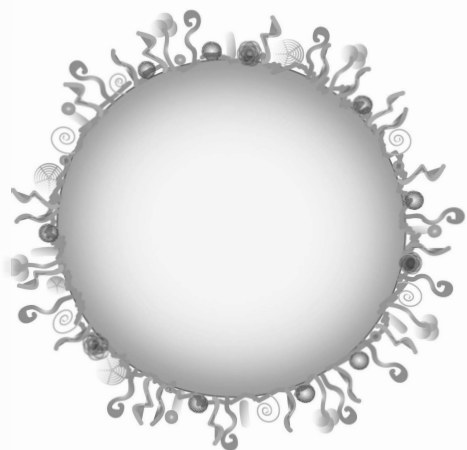
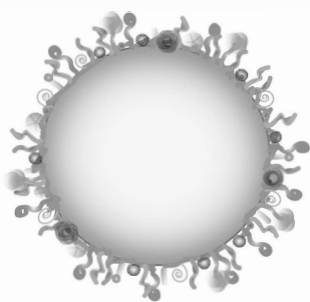
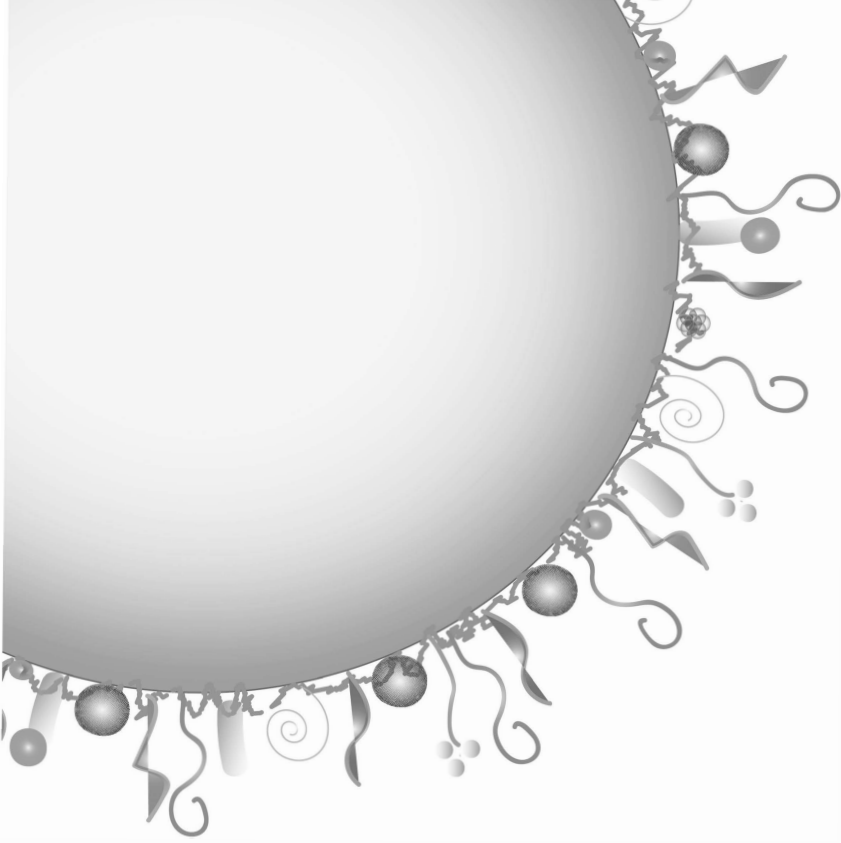
In **chapter 5**, the In-Cell Western (ICW)- γ -H₂AX assay was evaluated as an alternative *in vitro* assay to detect the potential of aged AgNPs and pristine AgNPs to induce phosphorylation of H₂AX in HepG2 liver cells. AgNO₃ was used as source of Ag⁺ to test the effects of Ag⁺ themselves. The γ -H₂AX induction detected was higher after 24 hr exposure compared to 4 hr and was accompanied by a significant cytotoxicity in the HepG2 cells. The increased induction of γ -H₂AX measured could be due to the cytotoxicity that occurred at the same concentrations which can result in DNA damage resulting in an increased induction of γ -H₂AX. This suggests potential false-positive confounders limiting the use of the ICW- γ -H₂AX

assay, in the form as applied in chapter 5, for evaluation of the genotoxicity of NPs. Additionally, the potential of the AgNPs to induce ROS production, as a potential underlying mechanism of induction of the cytotoxicity and/or DNA-DSBs, was assessed in HepG2 cells. No increase in ROS levels was measured upon exposure of the cells to the AgNPs for 4 or 24 hr and in the absence of cells, while an increase in ROS levels was detected upon AgNO₃ exposure of the cells and in the absence of cells.

In conclusion, the surface chemistry of AgNPs has a significant influence on their cytotoxic effects and the accompanying induction of γ -H₂AX levels in HepG2 cells. The aged Ag₂S NPs were biologically less active in inducing both cytotoxicity and γ -H₂AX levels, as these effects were absent in the dose range tested. The absence of cellular ROS generation upon exposure to all AgNPs indicates that the observed effects were not ROS-mediated. Additional tests, to rule out apoptotic mediated false-positive signals, need to be combined with the ICW- γ -H₂AX assay, to render this interesting assay into a robust screening method for the potential genotoxicity of NPs.

Chapter 6 of the present thesis included a general discussion of the results of the previous chapters and highlights on future perspectives for research in the field of *in vitro* nanotoxicology.

Overall, the work presented in this thesis illustrated the role of surface chemistry and the status of the NPs (pristine or aged and/or digested) on the toxicological behaviour of NPs. Besides, the combination of different *in vitro* models with high-end analytical techniques was shown to; 1) provide in-depth understanding of the biological behaviour of NPs, 2) assure the value of the alternative *in vitro* models as a testing strategy for potential hazards that could be induced by NPs and 3) assist in setting priorities for *in vivo* testing and contributing to reduction, refinement and replacement (3Rs) of animal testing required for the safety evaluation of NPs.



A

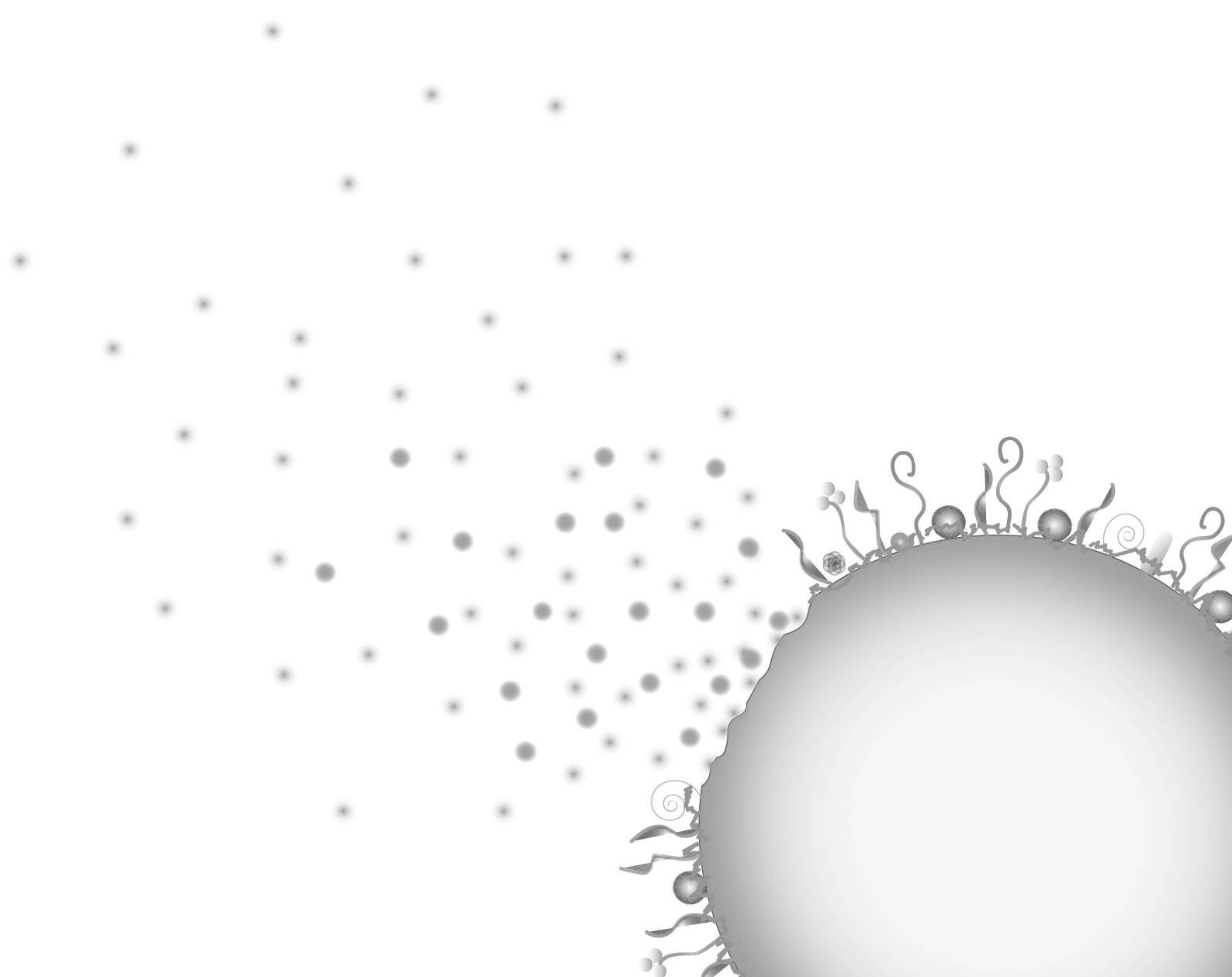
Appendices

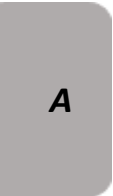
Acknowledgements

About the author

List of publications

Overview of completed training activities





Acknowledgements

I would like to express my gratitude and appreciation to many people who supported and encouraged me in the last years during my PhD journey, so that I can be who I am and where I am now. Without all of you, the outcomes of my work would not exist.

I want to thank my promotor Ivonne Rietjens whom I have learnt and gained, next to science, several key skills. During these 4 years I experienced your dedicated support, encouragement and guidance on how to be a good scientist, efficient and determined. Thank you for supporting this project to be a success story although the overwhelming difficulties it was confronted with. I appreciate your critical feedback during our discussions on the progress of this PhD project. I would like to thank you for your patience and dedication especially in the last moments of finalizing this thesis when you were abroad and still made time to respond swiftly with your feedback.

I would like to extend my gratitude to my co-promoters Hans Bouwmeester and Meike van der Zande. Our working relationship did not start with this PhD, it started when I did my MSc internship in one of your projects on nanotoxicology. Thank you for believing in me and putting effort and time in supporting my application for the grant that I was successfully awarded to start my PhD research. Although the difficulties accompanied this project, you tried as much as you could to bring it to a successful end.

Hans, it was a pleasure to work with you and have you as a co-promoter. Thank you for your dedication and continuous questioning during our discussions and challenging my scientific reasoning and ability to defend my opinion and decision. I really appreciate that your door was always open for quick questions (which ended many times into longer discussions!). Your relocation from WFSR to Wageningen university in the last year of my PhD was challenging and I appreciated that you listened and agreed to my opinion to finalize my PhD at WFSR without relocating to Wageningen university which made a big difference to me.

Meike, I really appreciated your friendly and easy-going attitude from my first day at WFSR (when it used to be called RIKILT) when you made my MSc internship interview comfortable and easy-going. Thank you for being approachable where we had many times

quick discussions at the end of the day while you are packing your stuff to go home without being bothered. Your input was always important. Especially when it comes to technical or lab related knowledge, our discussions were very useful to me. Your artistic talent was not only having an impact on your office that was decorated with your artwork, but also on the stunning graphical representations of results, which I have a few in my thesis. Thank you.

My lovely office mates, Kornphimol (Phim) and Milou. We started our PhDs almost at the same time. Within these years we shared a lot of good, crazy, difficult and hard times. Thank you for being supportive and collaborative whenever it is needed. Later, Loes and Nicole, you joined our office. I would like to thank you for being friendly and providing such a good atmosphere, especially in the last stressful days for myself, Phim and Milou on finalizing our PhDs. Although all my office mates were girls, I really appreciated that you all did not make the office very girly with pinkish stuff everywhere. You cannot imagine how relieved I was!

I want to thank all the colleagues at WFSR who I worked with and I was lucky to get their support without hesitation. Special thanks go to Anna Undas, my main coach for the ICP-MS. I owe most of what I knew about it to you. I am thankful for your support, friendliness and being approachable for questions and not judging even when I ask sometimes stupid questions (always saying there are no stupid questions!). You were always there to help me sorting out technical difficulties popped up with the ICP-MS when I almost started to freak out considering the enormous number of samples I analyse every time, thank you.

Greet and Sandra, it was a pleasure working with you and your endless support with ICP-MS measurements and especially with the enormous number of samples I measured every time. I really appreciated your flexibility and willingness to support my work wherever it is possible, especially when the lab was overly booked. Thank you for motivating me to practice my Dutch whenever I can without making me feel embarrassed for my imperfect pronunciation, hartelijk bedankt.

Ruud Peters, thank for your precious support, discussion and making time to discuss how to improve my ICP-MS measurements and shedding light on its possibilities and limitations.

I would like to extend my appreciation to Geert Stoppen, your support and guidance in the lab were precious. You liked to start your day very early before everyone. Even in the days when I had to start as soon as WFSR opened to perform some of my lengthy experiments, I found you there. It was difficult to compete with you in this matter. I have learnt a lot from you, thank you.

Astrid and Liza, thank you for your support and being approachable. I have enjoyed our casual talks and trying to practice my Dutch with you. Your office had always interesting gadgets and different creative things made by Astrid from lab supplies (colourful magnetic candies, cell culture flasks with m&m's cells). Ans Punt, you were supposed to be one of my co-promoters, but unfortunately it did not work as you moved with your career outside Wageningen university. But this did not stop you from continuing to work together on my first publication. I have learnt a lot from you. When you decided to join WFSR, I found your critical discussion and questions during my presentations of great help, thank you.

Valentina, Ningjing and Yajing, thank you for having such a good time and chats where we shared our thoughts, released our stress and most importantly supporting each other especially in long days where we were the last ones to leave the building. Marcia, thank you for your nice chatting, tips and advices not only from scientific perspective but also personal.

I would like to extend my thanks and gratitude to all my colleagues at WFSR for being supportive; Aafke, Ad, Deborah, Corina, Gerlof, Hannie, Henry, Jochem, Lonneke, Peter, Toine, Yamine and Yoran. Interconnect group, I have really enjoyed the time we spent together and participating in different activities from arranging international kitchen, chocolate making workshop, to Wadlopen. They were great times to socialize and know each other better, thank you.

I would like to thank all the co-authors of my articles (if I have not already mentioned them); your input and cooperation were vital to these publications.

Georgia, there are no words to express my appreciation and happiness of having you in my life. Thank you for being there and supporting me in the difficult days before the good ones. Ignacio, thanks for your tips and sharing your experience with me. Aziza, it was good to

have you as a friend and colleague. I liked our snap chats in the corridors of Toxicology and the nice time spent in different gatherings.

I would like to thank all the staff and PhD colleagues at Toxicology for both the scientific and personal interactions. Special thanks to office 4033, you were my host at Toxicology whenever I came for meetings or to perform experiments. Georgia, Ixchel Lu and Suparmi, thank you for your friendliness, I really enjoyed our casual talks and jokes a lot. Bert, thank you for the good times spent in teaching together, I enjoyed our chats a lot, you are a very bright and passionate person. Hans vd. Berg and Laura, thank you for your support and advices in the lab.

Thanks to Remco Fokkink for your support with my DLS and Zeta potential measurements. Arjen Bader, your support with confocal microscopy imaging is really appreciated. Annelies Bunschoten and Inge van der Stel, thank you for welcoming me in your lab and your support for my Odessey experimental measurements.

Big thanks to all my friends in the Netherlands who supported me and whom I spent great times with (Ali, Alaa, Elena, Elmansori, Karen, Louwrens, Majid, Marco, Marta, Monika, Tina and Wessam).

Georgia and Milou, thanks for being my paranymphs and helping me to prepare for my PhD defence, I am really grateful.

I want also to thank my family in Egypt who supported me endlessly in this journey. My mother and father (may his soul rest in peace) for your endless support and prayers, my brothers for standing by my side and for all the sacrifices you did. My niece and nephew whom I missed so much being away from them.

Also, I would like to thank my strength and persistence to finalise this work which resulted in this nice book.

Ashraf Abdelkhalig, 2020

أشرف عبد الخالق، ٢٠٢٠

About the author

Ashraf Abdelkhalig was born in March 1986 in Bahrain. After his secondary education in Alexandria - Egypt, he started his undergraduate studies in Food Science at Alexandria University in Egypt. After receiving his BSc degree in 2007, he was hired as a Teaching Assistant at Alexandria University. In 2012, he moved to the Netherlands to start his MSc studies in Applied Food Safety in Wageningen University.

During his MSc, Ashraf conducted his thesis on Nanotoxicology in the Division of Toxicology.

Followed by a 6-month internship in Nanotoxicology research at Wageningen Food Safety Research (WFSR,

Previously: RIKILT). After completing his MSc degree in 2014, he was hired as a Lecturer in at Alexandria University. In 2015, he started his PhD studies on the project presented in this thesis, which was a collaboration between the Division of Toxicology of Wageningen University and WFSR. During his PhD studies, Ashraf followed several courses from the Postgraduate Education in Toxicology program that will enable him to register as European Registered Toxicologist (ERT).



List of Publications

Abdelkhalig, A., van der Zande, M., Punt, A., Helsdingen, R., Boeren, S., Vervoort, J. J. M., Rietjens, I. M. C. M. and Bouwmeester, H. 2018. **Impact of Nanoparticle Surface Functionalization on the Protein Corona and Cellular Adhesion, Uptake and Transport.** Journal of Nanobiotechnology. 16:1:70. <https://doi.org/10.1186/s12951-018-0394-6>

Abdelkhalig, A., van der Zande, M., Undas, AK., Peters, RJB. and Bouwmeester, H. 2020. **Impact of *in vitro* digestion on gastrointestinal fate and uptake of silver nanoparticles with different surface modifications.** Nanotoxicology. 14:1, 111–126.

<https://doi.org/10.1080/17435390.2019.1675794>

Abdelkhalig, A., van der Zande, M., Peters, R.J.B. and Bouwmeester, H. 2020. **Combination of the BeWo b30 placental transport model and the embryonic stem cell test to assess the potential developmental toxicity of silver nanoparticles.** Particle and Fibre Toxicology. 17:11.

<https://doi.org/10.1186/s12989-020-00342-6>

Abdelkhalig, A., van der Zande, M. and Bouwmeester, H. 2020. **Induction of γ -H₂AX lesions and cytotoxicity in HepG2 cells by silver nanoparticles.** In preparation.

Overview of Completed Training Activities

Discipline specific activities

Cellular Toxicology, PET (Leiden University)	2016
Molecular Toxicology, PET (Vrije university of Amsterdam)	2016
Legal and Regulatory Toxicology, PET (National Institute for Public Health and the Environment (RIVM))	2016
Advanced Chemistry: Nanoparticle Science (Wageningen University)	2016
Organ Toxicology, PET (Radboud University Nijmegen)	2017
Occupational Toxicology, PET (Radboud UMC)	2018
Epidemiology, PET (Institute for Risk Assessment Sciences - Utrecht University)	2018
Pathobiology, PET (UMC Utrecht)	2019

General courses

VLAG PhD week (Wageningen University)	2016
Big data in the Life Sciences (Wageningen University)	2017
Risk Assessment, PET (Wageningen University, University)	2017
Philosophy and Ethics of Food Science and Technology (Wageningen University)	2018
Reviewing a scientific paper (Wageningen University)	2018
Brain friendly working and writing (Wageningen University)	2018
Searching and Organizing Literature (Wageningen University)	2018

Optional courses and other activities

Preparation of research proposal	2015
Weekly cluster meetings, (WFSR)	2015 - 2019
Environmental Toxicology, (Wageningen University)	2017
General Toxicology, (Wageningen University)	2018
Toxicology PhD trip to Japan	2018

Conferences and Meetings

Annual Meeting of Dutch Society of Toxicology (NVT), Netherlands (Oral presentation and poster)	2017
9 th International Conference on Nanotoxicology, Germany (Poster)	2018
JRC Summer School on Non-Animal Approaches in Science, Italy (Poster)	2019

The research described in this thesis was conducted within a collaborative project between Wageningen University and Wageningen Food Safety Research (WFSR).

This research was financially supported by the Netherlands Fellowship Programmes (NFP) grant to Ashraf Abdelkhalik. The research performed at WFSR was financially supported by the EU H2020 project NanoFASE (grant no. 646002).

Financial support from Wageningen University for printing this thesis is gratefully acknowledged.

Layout: Ashraf Abdelkhalik

Cover design: Georgia Papadi and Ashraf Abdelkhalik

Printing: ProefschriftMaken

Ashraf Abdelkhalik, 2020

